

## PUBLISHER :



Address of Publisher  
& Editor's Office :

GDAŃSK UNIVERSITY  
OF TECHNOLOGY  
Faculty  
of Ocean Engineering  
& Ship Technology

ul. Narutowicza 11/12  
80-952 Gdańsk, POLAND  
tel.: +48 58 347 13 66  
fax : +48 58 341 13 66  
e-mail : office.pmr@pg.gda.pl

Account number :  
**BANK ZACHODNI WBK S.A.**  
I Oddział w Gdańsku  
41 1090 1098 0000 0000 0901 5569

### Editorial Staff :

**Tadeusz Borzęcki** Editor in Chief  
e-mail : tadbtor@pg.gda.pl

**Przemysław Wierzchowski** Scientific Editor  
e-mail : e.wierzchowski@chello.pl

**Jan Michalski** Editor for review matters  
e-mail : janmi@pg.gda.pl

**Aleksander Kniat** Editor for international relations  
e-mail : olek@pg.gda.pl

**Kazimierz Kempa** Technical Editor  
e-mail : kkempa@pg.gda.pl

**Piotr Bzura** Managing Editor  
e-mail : pbzura@pg.gda.pl

**Cezary Spigarski** Computer Design  
e-mail : biuro@oficynamorska.pl

Domestic price :  
single issue : 20 zł

Prices for abroad :  
single issue :  
- in Europe EURO 15  
- overseas US\$ 20

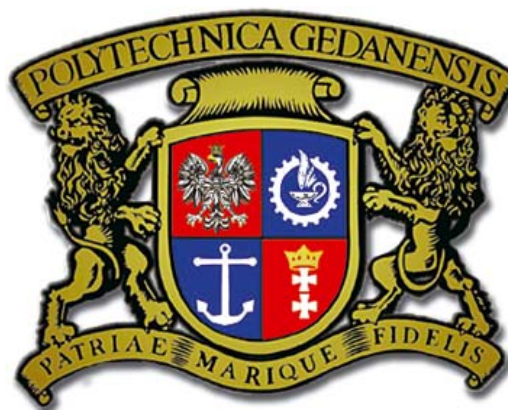
ISSN 1233-2585



**POLISH  
MARITIME  
RESEARCH**

*in internet*

[www.bg.pg.gda.pl/pmr/pmr.php](http://www.bg.pg.gda.pl/pmr/pmr.php)



## POLISH MARITIME RESEARCH

No 1(77) 2013 Vol 20

### CONTENTS

- 3 ZYGMUNT PASZOTA**  
*Losses and energy efficiency of drive motors and systems. Replacement of the Sankey diagram of power decrease in the direction of power flow by a diagram of power increase opposite to the direction of power flow opens a new perspective of research of drive motors and systems*
- 11 OLEKSANDR V. BONDARENKO, ANZHELA P. BOIKO, IRYNA R. SEROPYAN**  
*Determination of the main characteristics of the small waterplane area twin hull ships at the initial stage of design*
- 23 ZBIGNIEW KORCZEWSKI**  
*Analysing the potential for application of the phase shift method in endoscopic examination of marine engines*
- 31 ANDRZEJ ADAMKIEWICZ, JAN DRZEWIENIECKI**  
*Service and maintenance of marine steam turbogenerators with the assistance of vibration diagnostics*
- 39 LESZEK MATUSZEWSKI**  
*Multi-stage magnetic-fluid seals for operating in water - life test procedure, test stand and research results. Part II Results of life tests of multi-stage magnetic - fluid seal operating in water*
- 48 REMIGIUSZ IWAŃKOWICZ**  
*Application of multi-dimensional grouping to building steel stiffened shell structures*
- 59 MURAT OZKOK, I. HAKKI HELVACIOGLU**  
*Determination of the Effects of the Pre-Outfitting and Pre-Piping Assembly Operations on Shipyard Productivity*
- 70 ZENON ZWIERZEWICZ**  
*On the ship course-keeping control system design by using robust feedback linearization*
- 77 MAREK MOSZYŃSKI, ANDRZEJ CHYBICKI, MARCIN KULAWIAK, ZBIGNIEW LUBNIEWSKI**  
*A novel method for archiving multibeam sonar data with emphasis on efficient record size reduction and storage*
- 87 BOJAN BEŠKOVNIK**  
*Possibilities for Motorways of the Sea development in the eastern part of the Adriatic Sea*

# Editorial

---

POLISH MARITIME RESEARCH is a scientific journal of worldwide circulation. The journal appears as a quarterly four times a year. The first issue of it was published in September 1994. Its main aim is to present original, innovative scientific ideas and Research & Development achievements in the field of :

## **Engineering, Computing & Technology, Mechanical Engineering,**

which could find applications in the broad domain of maritime economy. Hence there are published papers which concern methods of the designing, manufacturing and operating processes of such technical objects and devices as : ships, port equipment, ocean engineering units, underwater vehicles and equipment as well as harbour facilities, with accounting for marine environment protection.

The Editors of POLISH MARITIME RESEARCH make also efforts to present problems dealing with education of engineers and scientific and teaching personnel. As a rule, the basic papers are supplemented by information on conferences , important scientific events as well as cooperation in carrying out international scientific research projects.

## Scientific Board

---

Chairman : Prof. **JERZY GIRTLEK** - Gdańsk University of Technology, Poland

Vice-chairman : Prof. **ANTONI JANKOWSKI** - Institute of Aeronautics, Poland

Vice-chairman : Prof. **MIROSLAW L. WYSZYŃSKI** - University of Birmingham, United Kingdom

---

Dr **POUL ANDERSEN**  
Technical University  
of Denmark  
Denmark

Prof. **WOLFGANG FRICKE**  
Technical University  
Hamburg-Harburg  
Germany

Prof. **YASUHIKO OHTA**  
Nagoya Institute of Technology  
Japan

Dr **MEHMET ATLAR**  
University of Newcastle  
United Kingdom

Prof. **STANISŁAW GUCMA**  
Maritime University of Szczecin  
Poland

Dr **YOSHIO SATO**  
National Traffic Safety  
and Environment Laboratory  
Japan

Prof. **GÖRAN BARK**  
Chalmers University  
of Technology  
Sweden

Prof. **ANTONI ISKRA**  
Poznań University  
of Technology  
Poland

Prof. **KLAUS SCHIER**  
University of Applied Sciences  
Germany

Prof. **SERGEY BARSUKOV**  
Army Institute of Odessa  
Ukraine

Prof. **JAN KICIŃSKI**  
Institute of Fluid-Flow Machinery  
of PASci  
Poland

Prof. **FREDERICK STERN**  
University of Iowa,  
IA, USA

Prof. **MUSTAFA BAYHAN**  
Süleyman Demirel University  
Turkey

Prof. **ZYGMUNT KITOWSKI**  
Naval University  
Poland

Prof. **JÓZEF SZALA**  
Bydgoszcz University  
of Technology and Agriculture  
Poland

Prof. **VINCENZO CRUPI**  
University of Messina  
Italy

Prof. **JAN KULCZYK**  
Wrocław University of Technology  
Poland

Prof. **TADEUSZ SZELANGIEWICZ**  
Technical University  
of Szczecin  
Poland

Prof. **MAREK DZIDA**  
Gdańsk University  
of Technology  
Poland

Prof. **NICOS LADOMMATOS**  
University College London  
United Kingdom

Prof. **WITALIJ SZCZAGIN**  
State Technical University  
of Kaliningrad  
Russia

Prof. **ODD M. FALTINSEN**  
Norwegian University  
of Science and Technology  
Norway

Prof. **JÓZEF LISOWSKI**  
Gdynia Maritime University  
Poland

Prof. **BORIS TIKHOMIROV**  
State Marine University  
of St. Petersburg  
Russia

Prof. **PATRICK V. FARRELL**  
University of Wisconsin  
Madison, WI  
USA

Prof. **JERZY MATUSIAK**  
Helsinki University  
of Technology  
Finland

Prof. **DRACOS VASSALOS**  
University of Glasgow  
and Strathclyde  
United Kingdom

Prof. **EUGEN NEGRUS**  
University of Bucharest  
Romania

# Losses and energy efficiency of drive motors and systems

## Replacement of the Sankey diagram of power decrease in the direction of power flow by a diagram of power increase opposite to the direction of power flow opens a new perspective of research of drive motors and systems

Zygmunt Paszota, Prof.  
Gdansk University of Technology, Poland

### ABSTRACT



*Losses and energy efficiency of every drive motor must be presented as functions of physical quantities independent of losses in the motor. Such quantities are speed and load required by the machine or device driven by the motor, changing in the drive operating field. Speed and load of the motor decide of the instantaneous useful power of the motor and also in a differentiated way of kinds and values of losses occurring in the motor. However, losses and energy efficiency of the hydrostatic drive motors and systems are evaluated by researchers and manufacturers as functions of parameters depending on the losses. The basic cause of such situation is the traditional, commonly accepted but erroneous, view of the power flow in the drive motors and systems represented by the Sankey diagram of power decrease in the direction of power flow. It is necessary to replace the Sankey diagram by the proposed diagram of increase of power in the motor and in the drive system in the direction opposite to the direction of power flow. The proposed view of losses and energy efficiency should be applied to all types of motor and drive systems. The aim of this paper is showing the resulting problems of the above postulates, exemplified by operation of a rotational displacement motor in a hydrostatic drive system. In order to make possible objective evaluation of the energy behaviour of different motor and system solutions and sizes, the losses and energy efficiency should be described and compared as dependent on the motor speed coefficient  $\bar{\omega}_M$  and load coefficient  $\bar{M}$  changing in the drive system operating field ( $0 \leq \bar{\omega}_M < \bar{\omega}_{Mmax}$ ,  $0 \leq \bar{M} < \bar{M}_{Mmax}$ ). The presented proposals open a new perspective of unavoidable research of drive motors and systems, making it possible to compare objectively the energy efficiency of different types of motors and drive systems.*

**Key words:** drive motors; drive systems; energy losses; energy efficiency; Sankey diagram; new research field

### INTRODUCTION

**Losses and energy efficiency of every drive motor must be presented as functions of physical quantities independent of losses in the motor. Such quantities are speed and load required by the machine or device driven by the motor, changing in the drive operating field. Speed and load of the motor decide of the instantaneous useful power of the motor and also in a differentiated way of kinds and values of losses occurring in the motor.**

However, losses and energy efficiency of the drive motors and systems are evaluated by researchers and manufacturers as functions of parameters depending on the losses. An example

of the wrong interpretation may be presentation of energy efficiencies of the hydrostatic rotational displacement motors as dependent on the flow intensity of the motor feeding liquid and on the pressure decrease of the motor.

Energy efficiency of turbines is presented in a similar way.

A cause of such situation is the traditional, commonly accepted but erroneous, view of the power flow in the drive motors and systems represented by the Sankey diagram of power decrease in the direction of power flow.

It is necessary to replace the Sankey diagram by the proposed diagram of increase of power in the motor and in the drive system in the direction opposite to the direction of power flow [1 ÷ 23].

**The proposed view of losses and energy efficiency should be applied to all types of motor and drive systems, for instance:**

- piston internal combustion motors,
- turbines,
- electric motors,
- hydrostatic displacement motors,
- ship screw propellers.

The aim of this paper is showing the resulting problems of the above postulates, exemplified by operation of a rotational displacement motor in a hydrostatic drive system.

In order to make possible objective evaluation of the energy behaviour of different motor and system solutions and sizes, the losses and energy efficiency should be described and compared as dependent on the motor speed coefficient  $\overline{\omega}_M$  and load coefficient  $\overline{M}_M$  changing in the drive system operating field ( $0 \leq \overline{\omega}_M < \overline{\omega}_{Mmax}$ ,  $0 \leq \overline{M}_M < \overline{M}_{Mmax}$ ).

**The presented proposals open a new perspective of unavoidable research of drive motors and systems, making it possible to compare objectively the energy efficiency of different types of motors and drive systems.**

## **INDEPENDENT AND DEPENDENT PARAMETERS OF A DRIVE MOTOR AND SYSTEM OPERATION, EXAMPLIFIED BY OPERATION OF A DISPLACEMENT MOTOR IN A HYDROSTATIC DRIVE SYSTEM**

The work of a rotational or linear hydraulic motor as an element of hydrostatic drive and control system, directly connected with the driven machine (device) must provide parameters required by the driven machine (angular speed  $\omega_M$  (rotational  $n_M$ ) of the shaft or linear speed  $v_M$  of the piston rod and shaft load (torque)  $M_M$  or piston rod load (force)  $F_M$ ) and also ensure the required machine movement direction.

The mechanical parameters of a motor (speed  $\omega_M$  ( $n_M$ ) or  $v_M$  and also load  $M_M$  or  $F_M$ ) change in the range from zero to maximum values  $\omega_{Mmax}$  ( $n_{Mmax}$ ) or  $v_{Mmax}$  and  $M_{Mmax}$  or  $F_{Mmax}$ .

**The required current speed  $\omega_M$  ( $n_M$ ) or  $v_M$  and required current load  $M_M$  or  $F_M$  of the driven machine are an effect of its work cycle and the work task. The current driven machine speed and load values are independent of the type and structure of that machine driving system control (e.g. an electrical or hydrostatic system).**

**The current speed and current load of a hydrostatic system driven machine have a direct or indirect impact on the mechanical, volumetric and pressure losses in the hydraulic motor, pump and other system elements, a system with determined motor speed control structure.** The losses are also an effect of the viscosity of the used working liquid (hydraulic oil).

**The current speed  $\omega_M$  ( $n_M$ ) or  $v_M$  and current load  $M_M$  or  $F_M$  of the driven machine influence, in consequence, the current hydraulic motor absorption capacity  $Q_M$  and pressure decrease  $\Delta p_M$  and also (depending on the used motor speed control structure) the current pump capacity  $Q_p$  and discharge pressure  $p_{p2}$ .**

If in effect of the increasing, required by the driven machine (device) hydraulic motor speed  $\omega_M$  ( $n_M$ ) or  $v_M$ , as well as in effect of the increasing, required by the driven machine motor load  $M_M$  or  $F_M$ , and also in effect of the mechanical, volumetric and pressure losses of the hydrostatic drive system elements, the maximum drive system capacity (determined by the maximum pump capacity  $Q_{pmax}$  or maximum pump discharge conduit

pressure  $p_{p2max}$  limited to the system nominal pressure  $p_n$ ) is fully used, then further increase of  $\omega_M$  ( $n_M$ ) or  $v_M$  as well as  $M_M$  or  $F_M$  will not be possible.

Maximum pump capacity  $Q_{pmax}$  is smaller than its theoretical capacity  $Q_{pt}$ . The pump theoretical capacity  $Q_{pt}$  is a product of the theoretical capacity  $q_{pt}$  per one pump shaft revolution and the no-load pump shaft speed  $n_{p0}$ . The pump  $Q_{pmax}$  capacity, however, results from the loaded pump speed  $n_p$ , lower than the speed  $n_{p0}$ , and from volumetric losses in the pump.

The system nominal pressure  $p_n$  is a maximum permissible continuous operation pressure  $p_{p2max}$  determined in the pump discharge.

**The maximum speed values  $\omega_{Mmax}$  ( $n_{Mmax}$ ) or  $v_{Mmax}$  as well as the maximum load values  $M_{Mmax}$  or  $F_{Mmax}$  of the hydraulic motor used in a hydrostatic drive system are limited by the maximum pump capacity  $Q_{pmax}$  or by the system (pump) nominal pressure  $p_n$  and also by the corresponding mechanical, volumetric and pressure losses in the remaining system elements, the losses being also an effect of viscosity of the working liquid used. Therefore, the  $\omega_{Mmax}$  ( $n_{Mmax}$ ) or  $v_{Mmax}$ ,  $M_{Mmax}$  or  $F_{Mmax}$  values are dependent variables.**

**The current mechanical operating parameters of the hydraulic motor used in a hydrostatic drive system (current motor speed  $\omega_M$  ( $n_M$ ) or  $v_M$  and current motor load  $M_M$  or  $F_M$ ) are independent values in the motor, deciding of the motor losses and of the hydraulic parameters (the current motor absorbing capacity  $Q_M$  and current pressure decrease  $\Delta p_M$  also depending on the motor mechanical, volumetric and pressure losses). The current motor absorbing capacity  $Q_M$  and current pressure decrease  $\Delta p_M$  are dependent variables in the motor.**

In the hydraulic motor (hydrostatic drive system) operating field ( $0 \leq \omega_M$  ( $n_M$ )  $< \omega_{Mmax}$  ( $n_{Mmax}$ ),  $0 \leq M_M < M_{Mmax}$ ) or ( $0 \leq v_M < v_{Mmax}$ ,  $0 \leq F_M < F_{Mmax}$ ), the pressure and flow intensities in the system and also the energy losses in the motor, in the pump and in the whole system, power of energy losses and energy efficiencies of the system elements should be considered the functions of the current speed  $\omega_M$  ( $n_M$ ) or  $v_M$  and the current load  $M_M$  or  $F_M$  required by the system driven machine (device). Also **the torque  $M_p$  that the pump loads the driving (electric or internal combustion) motor and the speed  $n_p$  that the motor drives the pump with should be considered the functions of the current speed and the current load required by the system driven machine.**

The decrease of speed  $n_p$  that the electric or internal combustion motor drives the pump with is connected with the increase of torque  $M_p$  that the pump loads the motor with. The decrease of speed depends on the operating characteristics of the motor, which is not a component of the hydrostatic drive system. Therefore, **the pump driving speed  $n_p$  should be treated as a parameter independent of the hydrostatic system (of the pump).**

## **NON-DIMENTIONAL COEFFICIENTS OF THE DISPLACEMENT MOTOR PARAMETERS, COEFFICIENTS OF ENERGY LOSSES IN THE HYDROSTATIC DRIVE ELEMENTS**

The energy efficiency of the hydrostatic drive system and its elements is described by mathematical models as functions of the hydraulic motor (hydrostatic drive system) speed coefficient  $\overline{\omega}_M$  and load coefficient  $\overline{M}_M$ .

**The current angular speed  $\omega_M$  (rotational speed  $n_M$ ) required of a rotational motor or the linear speed  $v_M$  required of a linear motor, operating in a hydrostatic drive system, are replaced in the energy efficiency mathematical**

models by the motor speed non-dimensional coefficient  $\bar{\omega}_M$ :

$$\bar{\omega}_M = \frac{\omega_M}{\omega_{Mt}} = \frac{n_M}{n_{Mt}} = \frac{\omega_M q_{Mt}}{2\Pi Q_{Pt}} = \frac{n_M q_{Mt}}{Q_{Pt}}$$

or

$$\bar{\omega}_M = \frac{v_M}{v_{Mt}} = \frac{v_M S_{M1}}{Q_{Pt}}$$

The rotational hydraulic motor speed coefficient  $\bar{\omega}_M$  is a ratio of the current angular speed  $\omega_M$  (rotational speed  $n_M$ ), required of the motor by driven machine, to

$$\text{theoretical angular speed } \omega_{Mt} = \frac{2\Pi Q_{Pt}}{q_{Mt}},$$

$$\text{(theoretical rotational speed } n_{Mt} = \frac{Q_{Pt}}{q_{Mt}}),$$

which would correspond with the theoretical capacity  $Q_{Pt}$  of the motor driving pump and with the theoretical motor absorbing capacity  $q_{Mt}$  per one shaft revolution. The speed  $\omega_{Mt}$  ( $n_{Mt}$ ) would be achievable on the condition, that there are no volumetric losses in the hydrostatic drive system (including the pump and the hydraulic motor) and the pump is driven by an (electric or internal combustion) motor operating with constant rotational speed  $n_p = n_{p0}$  independent of its load.

The theoretical angular speed  $\omega_{Mt}$  (rotational speed  $n_{Mt}$ ) of a rotational motor is treated as a constant reference value for the motor current angular speed  $\omega_M$  (rotational speed  $n_M$ ).

The linear hydraulic motor speed coefficient  $\bar{\omega}_M$  is a ratio of the current linear speed  $v_M$ , required of the motor by driven machine, to

$$\text{theoretical linear speed } v_{Mt} = \frac{Q_{Pt}}{S_{M1}},$$

which would correspond with the theoretical capacity  $Q_{Pt}$  of the motor driving pump and with effective area  $S_{M1}$  of the motor piston in the inlet chamber. The speed  $v_{Mt}$  would be achievable on the condition, that there are no volumetric losses in the hydrostatic drive system (including the pump and the hydraulic motor) and the pump is driven by an (electric or internal combustion) motor operating with constant rotational speed  $n_p = n_{p0}$  independent of its load.

The theoretical linear speed  $v_{Mt}$  of a linear motor is treated as a constant reference value for the current motor linear speed  $v_M$ .

The current torque  $M_M$  required of a rotational motor or current force  $F_M$  required of a linear motor, operating in a hydrostatic drive system, are replaced by the motor load non-dimensional coefficient  $\bar{M}_M$ :

$$\bar{M}_M = \frac{M_M}{M_{Mt}} = \frac{2\Pi M_M}{q_{Mt} p_n}$$

or

$$\bar{M}_M = \frac{F_M}{F_{Mt}} = \frac{F_M}{S_{M1} p_n}$$

The rotational hydraulic motor load coefficient  $\bar{M}_M$  is a ratio of the current torque  $M_M$ , required of the motor by driven machine, to

$$\text{theoretical torque } M_{Mt} = \frac{q_{Mt} p_n}{2\Pi},$$

which would correspond with the theoretical absorbing capacity  $q_{Mt}$  per one motor shaft revolution and with the hydrostatic system nominal pressure  $p_n$ . The torque  $M_{Mt}$  would

be achievable on the condition that there are no mechanical or pressure losses in the hydraulic motor and in the remaining system elements (except the pump) and the pressure  $p_{p2max}$  in the pump discharge conduit is equal to the system nominal pressure  $p_n$ .

The rotational motor theoretical torque  $M_{Mt}$  is treated as a constant reference value for the current motor torque  $M_M$ .

The linear hydraulic motor load coefficient  $\bar{M}_M$  is a ratio of the current force  $F_M$ , required of the motor by driven machine, to

$$\text{theoretical force } F_{Mt} = S_{M1} p_n,$$

which would correspond with the effective area  $S_{M1}$  of the motor piston in its inlet chamber and with the system nominal pressure  $p_n$ . The force  $F_{Mt}$  would be achievable on the condition that there are no mechanical or pressure losses in the hydraulic motor and in the remaining system elements (except the pump) and the pressure  $p_{p2max}$  in the pump discharge conduit is equal to the system nominal pressure  $p_n$ .

The linear motor theoretical force  $F_{Mt}$  is treated as a constant reference value for the current motor force  $F_M$ .

The mechanical, volumetric and pressure losses in a hydraulic motor, pump and in the remaining hydrostatic drive system elements are described in the mathematical models of the losses, power of losses and energy efficiency by the coefficients  $k_i$  – relations to the values connected with the values of the hydrostatic drive system characteristic parameters:

- theoretical capacity  $q_{Pt}$  per one pump shaft revolution,
- theoretical absorbing capacity  $q_{Mt}$  per one rotational hydraulic motor revolution or effective piston area  $S_{M1}$  in the linear motor inlet chamber,
- theoretical pump capacity  $Q_{Pt}$ ,
- system nominal pressure  $p_n$ .

The basis of energy evaluation of the particular design solutions and size of the volumetric machines is a catalogue of the coefficients  $k_i$  of energy losses in various types of pumps and hydraulic motors used in the hydrostatic drive systems, operating with different levels of pump theoretical capacity  $Q_{Pt}$  and system nominal pressure  $p_n$ , with the working liquid reference viscosity  $v_n$ .

## THE MOTOR OPERATING FIELD IN A DRIVE SYSTEM

Figure 1 presents the operating field of a rotational or linear displacement motor in a hydrostatic drive system. The operating field is determined in the plane of motor mechanical parameters, i.e. speed coefficient  $\bar{\omega}_M$  and load coefficient  $\bar{M}_M$ , independent of the motor and of the system.

The limit values  $\bar{\omega}_{Mmax} = f(\bar{M}_M)$  or  $\bar{M}_{Mmax} = f(\bar{\omega}_M)$  of the hydraulic motor operating field are determined by the maximum motor feed capability in the hydrostatic drive system. The values  $\bar{\omega}_{Mmax}$  and  $\bar{M}_{Mmax}$  are dependent on the motor and on the system losses.

The maximum motor absorbing capacity  $Q_{Mmax}$ , achieved in the system by the applied motor speed control structure, should be equal or close to the instantaneous maximum pump capacity  $Q_{pmax}$  (resulting from the theoretical capacity  $Q_{Pt}$ , decrease of the pump shaft rotational speed  $n_p$  and the intensity of pump volumetric losses  $Q_{pv}$ ).

The maximum possible motor pressure decrease  $\Delta p_{Mmax}$  should be equal or close to the system nominal pressure  $p_n$  determined in the pump discharge conduit, reduced by the pressure losses  $\Delta p_c$  in the system conduit. (In the motor series

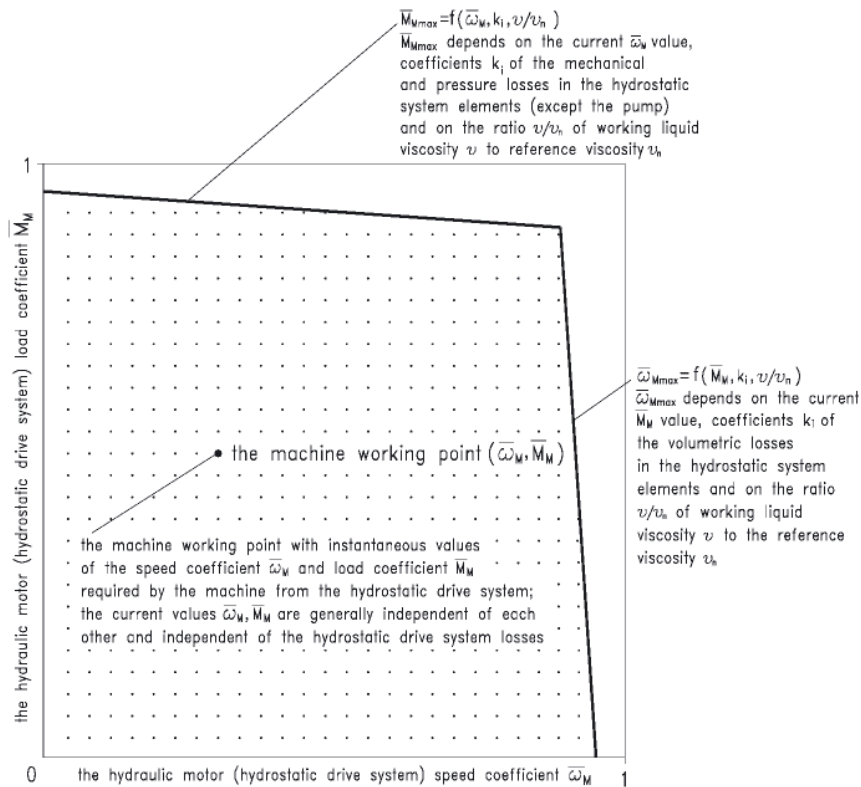


Fig. 1. The range of motor speed coefficient  $\bar{\omega}_M$  and load coefficient  $\bar{M}_M$  ( $0 \leq \bar{\omega}_M < \bar{\omega}_{Mmax}$ ,  $0 \leq \bar{M}_M < \bar{M}_{Mmax}$ ) in a hydrostatic drive system

throttling speed control structure, the maximum slot area of the throttling valve, proportional directional valve or servo-valve should allow to minimize the pressure decrease  $\Delta p_{DE|Q_{Mmax}}$  with the set  $Q_{Mmax} \approx Q_{pmax}$ .

Therefore the limit values  $\bar{\omega}_{Mmax}$  of the hydraulic motor speed coefficient are a function of the current motor load coefficient  $\bar{M}_M$ , coefficients  $k_i$  of the volumetric losses in the hydrostatic system elements (including coefficient  $k_2$  of the pump shaft rotational speed decrease  $\Delta n_p$ ) and a function of the ratio  $v/v_n$  of working liquid viscosity  $v$  to the reference viscosity  $v_n$ .

On the other hand, the limit values  $\bar{M}_{Mmax}$  of the hydraulic motor load coefficient are a function of the current motor speed coefficient  $\bar{\omega}_M$ , coefficients  $k_i$  of the mechanical and pressure losses in hydrostatic system elements and a function of the ratio  $v/v_n$  of working liquid viscosity  $v$  to the reference viscosity  $v_n$ .

### DIRECTION OF POWER INCREASE IN A DRIVE SYSTEM

The Sankey diagram is the fundamental cause of the incorrect evaluation of losses in a drive system.

The Sankey diagram connected with a drive system suggests an evaluation defining the output power of the system as a difference between the system input power and sum of the powers of losses occurring in the system. Therefore the energy losses in the system are evaluated as a function of parameters describing the input power.

In accordance with the proposed by the author diagram of power increase in a drive system opposite to the direction of power flow, **the system input power is a sum of the system output power and powers of losses occurring in the system. The energy losses in the system are evaluated as a function of parameters describing the system output power.**

Full picture of the energy losses in a drive system is a picture of power of energy losses in the system elements.

**Shaft power of the hydrostatic system feeding pump is equal to the sum of hydraulic motor shaft (or piston rod) power and powers of individual losses in the power flowing from the pump shaft to the hydraulic motor shaft (or piston rod).**

**The quantity of power increases, in order to overcome the power of energy losses, in the opposite direction to the direction of power flow.** Therefore, the image of power of energy losses in the system should be constructed in the direction from the hydraulic rotational motor shaft or from linear motor piston rod towards the system feeding pump shaft.

Power of the hydraulic motor, pump and of other system element losses (mechanical, volumetric, pressure losses) should be determined as functions of the parameters independent of those losses and influencing directly those losses.

Powers of energy losses in the system elements and also power of those elements must be precisely defined.

### DIAGRAM OF POWER INCREASE IN A ROTATIONAL DISPLACEMENT HYDRAULIC MOTOR, REPLACING THE SANKEY DIAGRAM

Figure 2 illustrates the diagram, proposed by the Author, of power increase in a rotational hydraulic motor opposite to the direction of power flow, replacing the Sankey diagram of power decrease in the direction of power flow.

The power  $P_{Mc}$  consumed by the hydraulic motor is a sum of motor shaft useful power  $P_{Mu}$  and powers of three different energy losses in the motor. The losses occur in series increasing power in the opposite direction to the direction of power flow. In effect, the power in the motor increases from the shaft useful power  $P_{Mu}$  to the working liquid power  $P_{Mc}$  consumed by the motor:

$$P_{Mc} = P_{Mu} + \Delta P_{Mm} + \Delta P_{Mv} + \Delta P_{Mp}$$

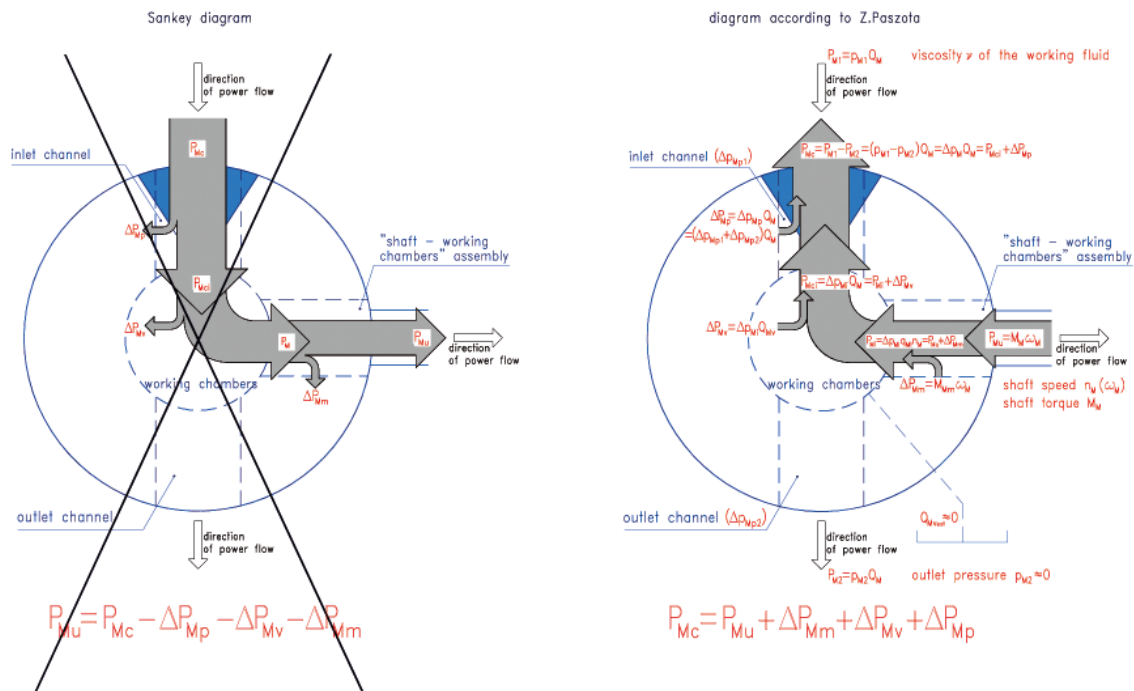


**Fig. 2.** Diagram of power increase in a rotational displacement hydraulic motor, opposite to the direction of power flow, replacing the Sankey diagram of power decrease in the direction of power flow (example of motor with theoretical (constant) capacity  $q_{Ml}$  ( $V_M$ ) per one shaft revolution)

Power increases from the motor useful power  $P_{Mu}$  required on the motor shaft by the driven machine (device) to power  $P_{Mc}$  consumed and required by the motor of the working liquid.

The increase of power is an effect of the powers of losses in the motor: power  $\Delta P_{Mm}$  of mechanical losses in the „shaft - working chambers” assembly, power  $\Delta P_{Mv}$  of volumetric losses in the working chambers and power  $\Delta P_{Mp}$  of pressure losses in the channels.

Powers  $\Delta P_{Mmp}$ ,  $\Delta P_{Mv}$  and  $\Delta P_{Mp}$  of the losses are functions of the output parameters of the motor assembly where the losses occur and diversified functions of the working liquid viscosity  $\nu$ : power  $\Delta P_{Mm}$  of mechanical losses is a function of torque  $M_{Mm}$  and shaft speed  $n_M$  ( $\omega_M$ ) required of the motor by the driven machine (device) and a function of the working liquid viscosity  $\nu$ , power  $\Delta P_{Mv}$  of volumetric losses is a function of the pressure decrease  $\Delta p_{Mi}$  indicated in working chambers (of torque  $M_{Mm}$  indicated in the chambers) and of the shaft rotational speed  $n_M$  as well as a function of the working liquid viscosity  $\nu$ , power  $\Delta P_{Mp}$  of pressure losses is a function of motor capacity  $Q_M$  and of the working liquid viscosity  $\nu$ .

Power  $P_{Mi}$  indicated in the working chambers:  $P_{Mi} = P_{Mu} + \Delta P_{Mm}$ , power  $P_{Mci}$  of the working liquid consumed in the working chambers:

$$P_{Mci} = P_{Mu} + \Delta P_{Mm} + \Delta P_{Mv} \quad \text{power } P_{Mc} \text{ of the working liquid consumed by the motor:}$$

$$P_{Mc} = P_{Mu} + \Delta P_{Mm} + \Delta P_{Mv} + \Delta P_{Mp}$$

The proposed diagram replaces the Sankey diagram of distribution of power in hydraulic motor causing incorrect loss evaluation during the hydraulic motor energy investigations.

Mechanical losses (and power  $\Delta P_{Mm}$  of mechanical losses) occur in the „shaft - working chambers” assembly.

Volumetric losses (and power  $\Delta P_{Mv}$  of volumetric losses) occur in the working chambers.

Pressure losses (and power  $\Delta P_{Mp}$  of pressure losses) occur in the channels.

### COMPLEX DEPENDENCE OF ENERGY LOSSES IN A ROTATIONAL DIPLACEMENT HYDRAULIC MOTOR ON THE SHAFT SPEED, ON THE SHAFT TORQUE, ON THE CAPACITY PER ONE SHAFT REVOLUTION AND ON THE WORKING LIQUID VISCOSITY

There exists a direct dependence of the torque  $M_{Mm}$  of mechanical losses in the „shaft - working chambers” assembly on the torque  $M_M$ , on the motor shaft rotational speed  $n_M$ , on the capacity  $q_{Mt}$  (or  $q_{Mgv}$ ) per one shaft revolution as well as on the working liquid viscosity  $\nu$ .

There is a complex dependence of the intensity  $Q_{Mv}$  of volumetric losses in the working chambers on the shaft loading torque  $M_M$  and on the torque  $M_{Mm}$  of mechanical losses in the „shaft - working chambers” assembly (decrease  $\Delta p_{Mi}$  of pressure indicated in the working chambers depends on  $M_M$  and  $M_{Mm}$ , on  $q_{Mt}$  (or  $q_{Mgv}$ ) and has direct impact on  $Q_{Mv}$ ) and also on the shaft speed  $n_M$  (influencing in a diversified way the torque

$M_{Mm}$  of mechanical losses and intensity  $Q_{Mv}$  of volumetric losses). The intensity  $Q_{Mv}$  of volumetric losses depends on a diversified impact of the working liquid viscosity  $\nu$ : indirectly by impact of  $\nu$  on the torque  $M_{Mm}$  of mechanical losses in the „shaft - working chambers” assembly and directly by impact of  $\nu$  on the intensity  $Q_{Mv}$  of losses in the working chambers.

It can be said, that it is a complex dependence of pressure losses  $\Delta p_{Mp}$  in the channels on the shaft rotational speed  $n_M$ , on the capacity  $q_{Mt}$  (or  $q_{Mgv}$ ) per one shaft revolution and on intensity  $Q_{Mv}$  of volumetric losses in the working chambers. The intensity  $Q_{Mv}$  of volumetric losses influences the motor capacity  $Q_M$  and at the same time  $Q_{Mv}$  depends in a complex way on the shaft loading torque  $M_M$  and on the torque  $M_{Mm}$  of mechanical losses in the „shaft - working chambers” assembly. Pressure losses  $\Delta p_{Mp}$  in the motor channels are also dependent on the diversified impact of the working liquid viscosity  $\nu$ : indirectly by impact of  $\nu$  on the torque  $M_{Mm}$  of mechanical losses in the „shaft - working chambers” assembly and by impact of  $\nu$  on the intensity  $Q_{Mv}$  of volumetric losses in the working chambers and directly by impact of  $\nu$  on the losses  $\Delta p_{Mp}$  of pressure in the channels.

Contrary to the commonly used, both by manufacturers and researchers, methods of evaluation of the rotational hydraulic motor losses, it is unacceptable to create a „sum” of the torque  $M_{Mm}$  of mechanical losses in the „shaft - working chambers” assembly and the „torque” of pressure losses  $\Delta p_{Mp}$  in the motor channels, and also such a „sum” must not be evaluated as

directly dependent on the same chosen parameters, because those losses are of different character and depend on different parameters:

$$M_{Mm} = f(M_M, n_M, q_{Mt}(q_{Mqv}), v)$$

$$\Delta p_{Mp} = f(Q_M, v)$$

**The impact of hydraulic oil viscosity  $v$  on the energy losses in a hydraulic motor, i.e. on:**

- torque  $M_{Mm}$  of mechanical losses in the „shaft - working chambers” assembly,
- intensity  $Q_{Mv}$  of volumetric losses in the working chambers,
- pressure losses  $\Delta p_{Mp}$  in the channels, is diversified.

Dependence of the motor losses on the hydraulic oil viscosity  $v$  should be presented in expressions describing also the dependence of those losses on other parameters which influence them directly:

$$M_{Mm} = f(M_M, n_M, q_{Mt}(q_{Mqv}), v)$$

$$Q_{Mv} = f(\Delta p_{Mi}, n_M, v)$$

$$\Delta p_{Mp} = f(Q_M, v)$$

**The motor overall efficiency  $\eta_M$** , as a function of  $M_M, n_M, q_{Mt}(q_{Mqv})$  and  $v$ , is a product of  $\eta_{Mm}, \eta_{Mv}$  and  $\eta_{Mp}$  efficiencies:

$$\begin{aligned} \eta_M &= f(M_M, n_M, q_{Mt}(q_{Mqv}), v) = \\ &= \frac{P_{Mu}}{P_{Mc}} = \frac{M_M \omega_M}{\Delta p_M Q_M} = \frac{2\Pi M_M n_M}{\Delta p_M Q_M} = \\ &= \eta_{Mm} \eta_{Mv} \eta_{Mp} \end{aligned}$$

where:

$P_{Mu}$  is the motor useful power,

$P_{Mc}$  is the motor consumed power.

Each of the three efficiencies, as a factor in the product describing the overall efficiency, is evaluated as a function of parameters directly influencing the respective losses and a function of parameter to which the losses are „added”:

- **motor mechanical efficiency  $\eta_{Mm}$** :

$$\begin{aligned} \eta_{Mm} &= \frac{P_{Mu}}{P_{Mi}} = \frac{M_M \omega_M}{(M_M + M_{Mm}) \omega_M} = \\ &= \frac{2\Pi M_M n_M}{2\Pi(M_M + M_{Mm}) n_M} = \\ &= \frac{M_M}{M_M + M_{Mm}} = f(M_M, n_M, q_{Mt}(q_{Mqv}), v) \end{aligned}$$

where:

$P_{Mi}$  is the power indicated in the motor working chambers:

$$\begin{aligned} P_{Mi} &= \Delta p_{Mi} q_{Mt}(q_{Mqv}) n_M = \\ &= (M_M + M_{Mm}) \omega_M = 2\Pi(M_M + M_{Mm}) n_M \end{aligned}$$

- **motor volumetric efficiency  $\eta_{Mv}$** :

$$\begin{aligned} \eta_{Mv} &= \frac{P_{Mi}}{P_{Mci}} = \frac{\Delta p_{Mi} q_{Mt}(q_{Mgv}) n_M}{\Delta p_{Mi} (q_{Mt}(q_{Mgv}) n_M + Q_{Mv})} = \\ &= \frac{\Delta p_{Mi} q_{Mt}(q_{Mgv}) n_M}{\Delta p_{Mi} Q_M} = \frac{q_{Mt}(q_{Mgv}) n_M}{q_{Mt}(q_{Mgv}) n_M + Q_{Mv}} \\ &= \frac{q_{Mt}(q_{Mgv}) n_M}{Q_M} = f(\Delta p_{Mi}, q_{Mt}(q_{Mgv}), n_M, v) \end{aligned}$$

where  $P_{Mci}$  is the power consumed in the motor working chambers:

$$P_{Mci} = \Delta p_{Mi} (q_{Mt}(q_{Mgv}) n_M + Q_{Mv}) = \Delta p_{Mi} Q_M$$

- **motor pressure efficiency  $\eta_{Mp}$** :

$$\begin{aligned} \eta_{Mp} &= \frac{P_{Mci}}{P_{Mc}} = \frac{\Delta p_{Mi} (q_{Mt}(q_{Mgv}) n_M + Q_{Mv})}{(\Delta p_{Mi} + \Delta p_{Mp}) (q_{Mt}(q_{Mgv}) n_M + Q_{Mv})} = \\ &= \frac{\Delta p_{Mi} Q_M}{\Delta p_M Q_M} = \frac{\Delta p_{Mi}}{\Delta p_{Mi} + \Delta p_{Mp}} \\ &= \frac{\Delta p_{Mi}}{\Delta p_M} = f(\Delta p_{Mi}, Q_M, v) \end{aligned}$$

In order to present the motor volumetric efficiency  $\eta_{Mv}$  as a factor in the  $\eta_{Mm} \eta_{Mv} \eta_{Mp}$  product describing  $\eta_M$ , i.e. to present  $\eta_{Mv}$  as a complex dependence on the  $(M_M, n_M, q_{Mt}(q_{Mgv}), v)$  parameters describing  $\eta_M$  and dependent on the mechanical losses, the intensity  $Q_{Mv} = f(\Delta p_{Mi}, n_M, q_{Mt}(q_{Mgv}), v)$  of volumetric losses in the working chambers should be determined with

$$\Delta p_{Mi} = \frac{2\Pi (M_M + M_{Mm})}{q_{Mt}(q_{Mgv})}$$

and with torque  $M_{Mm}$  of mechanical losses in the „shaft - working chambers” assembly as an  $M_{Mm} = f(M_M, n_M, q_{Mt}(q_{Mgv}), v)$  function.

In order to present the motor pressure efficiency  $\eta_{Mp}$  as a factor in the  $\eta_{Mm} \eta_{Mv} \eta_{Mp}$  product describing  $\eta_M$ , i.e. to present  $\eta_{Mp}$  as a complex dependence on the  $(M_M, n_M, q_{Mt}(q_{Mgv}), v)$  parameters describing  $\eta_M$  and dependent on the mechanical and volumetric losses in the motor, the pressure losses  $\Delta p_{Mp} = f(Q_M, v)$  in the channels must be determined with

$$Q_M = q_{Mt}(q_{Mgv}) n_M + Q_{Mv}$$

then intensity  $Q_{Mv} = f(\Delta p_{Mi}, n_M, v)$  of volumetric losses in the working chambers must be determined with

$$\Delta p_{Mi} = \frac{2\Pi (M_M + M_{Mm})}{q_{Mt}(q_{Mgv})}$$

and the torque  $M_{Mm}$  of mechanical losses in the „shaft - working chambers” assembly must be determined as an  $M_{Mm} = f(M_M, n_M, q_{Mt}(q_{Mgv}), v)$  function.

**The characteristic of the hydraulic motor overall efficiency  $\eta_M = f(M_M, n_M, q_{Mt}(q_{Mgv}), v)$  presents a complex**

**picture as a product  $\eta_{Mm}$   $\eta_{Mv}$   $\eta_{Mp}$  of three efficiencies correctly described by:**

- **mechanical efficiency  $\eta_{Mm} = f(M_M, n_M, q_{Mt}(q_{Mgv}), v)$ ,**
- **volumetric efficiency  $\eta_{Mv} = f(\Delta p_{Mi}, q_{Mi}(q_{Mgv}), n_M, v)$**
- **and pressure efficiency  $\eta_{Mp} = f(\Delta p_{Mi}, Q_M, v)$ .**

The picture of the hydraulic motor overall efficiency  $\eta_M = f(M_M, n_M, q_{Mt}(q_{Mgv}), v)$  must be supplemented by assessment of the **hydraulic motor operating field** ( $0 \leq \bar{\omega}_M < \bar{\omega}_{Mmax}$ ,  $0 \leq \bar{M}_M < \bar{M}_{Mmax}$ ) in the hydrostatic drive system, i.e. assessment of the range of  $n_M$  and  $M_M$  ( $\bar{\omega}_M$  and  $\bar{M}_M$ ) parameters.

In the motor (and the hydrostatic drive system) ( $0 \leq \bar{\omega}_M < \bar{\omega}_{Mmax}$ ,  $0 \leq \bar{M}_M < \bar{M}_{Mmax}$ ) operating field, its **current speed  $n_M$  ( $\bar{\omega}_M$ ) and load  $M_M$  ( $\bar{M}_M$ )** are an effect of the demand of the motor (system) driven machine (device) and are **independent of the losses in the hydraulic motor and in the motor driving hydrostatic system.**

However, the **hydraulic motor (system) operating field limit values  $n_{Mmax}$  ( $\bar{\omega}_{Mmax}$ ) and  $M_{Mmax}$  ( $\bar{M}_{Mmax}$ )** depend on the maximum capacity of the hydraulic motor driving system. The values  $n_{Mmax}$  ( $\bar{\omega}_{Mmax}$ ) and  $M_{Mmax}$  ( $\bar{M}_{Mmax}$ ) determine simultaneously the corresponding motor energy efficiency  $\eta_M$  and the overall system efficiency  $\eta$ .

The limit parameters of the hydrostatic drive system operation result from the pump theoretical capacity  $Q_{pt}$  and the system nominal working pressure  $p_n$  as well as from the actual energy losses in the hydraulic motor, conduits and pump and also losses in the motor speed throttling control assembly (if it is installed). Therefore, the limit values  $n_{Mmax}$  ( $\bar{\omega}_{Mmax}$ ) and  $M_{Mmax}$  ( $\bar{M}_{Mmax}$ ) are also dependent on the working liquid viscosity  $v$  changing in the  $v_{min} \leq v \leq v_{max}$  range. The hydrostatically driven hydraulic motor operating field is also influenced by the  $n_p = f(M_p)$  characteristic of the (electric or internal combustion) motor in the pump driving system.

## **NECESSITY OF USE OF THE ENERGY LOSS MATHEMATICAL MODELS WITH THE LOSS COEFFICIENTS IN DISPLACEMENT MOTOR AND IN A HYDROSTATIC DRIVE SYSTEM**

**Evaluation of the hydraulic motor overall efficiency  $\eta_M = f(M_M, n_M, q_{Mt}(q_{Mgv}), v)$  as a product  $\eta_{Mm}$   $\eta_{Mv}$   $\eta_{Mp}$  of three motor efficiencies can be performed only by means of the mathematical models of losses and efficiencies, where the defined coefficients  $k_i$  of energy losses in the motor and in the motor drive system are used.**

Evaluation of the hydraulic motor energy efficiency is performed together with evaluation of the efficiency of a hydrostatic drive system where the hydraulic motor is used (including also the energy efficiency of pump, conduits and the hydraulic motor speed throttling control assembly (if it is used)).

In the proposed method, based on the mathematical models of losses, each kind of energy losses is a function of parameters directly influencing the losses and independent of those losses.

Evaluated are the values of the  $k_i$  coefficients of energy losses, relating the mechanical, volumetric and pressure losses in the hydraulic motor, pump and other system elements to the reference values of driving system: nominal pressure  $p_n$  of the system, theoretical capacity  $Q_{pt}$  of the system driving pump, theoretical torque  $M_{pt}$  of the pump shaft as well as theoretical torque  $M_{Mt}$  of the hydraulic motor shaft. **The  $k_i$  coefficients are determined at the hydraulic oil reference viscosity  $v_n$ .** At the

same time the impact is determined of the viscosity ratio  $v/v_n$  in the  $v_{min} \leq v \leq v_{max}$  range on each kind of energy losses.

The method allows to evaluate the values and proportions of mechanical, volumetric and pressure losses in the hydraulic motor, pump, conduits and in the throttling assembly (if installed), as well as the dependence on the hydraulic oil viscosity  $v$ .

**The energy investigations of a pump and hydraulic motor as independent displacement machines are limited to determination of the  $k_i$  coefficients of losses in them. The energy efficiency characteristics of those machines are determined in parallel with efficiency evaluation of the hydrostatic drive system where they are used.**

The knowledge of  $k_i$  coefficients of the mechanical, volumetric and pressure losses in the drive system elements allows to obtain, with the numerical method, the characteristics of the hydrostatic drive system overall efficiency, pump efficiency, hydraulic motor efficiency, conduit efficiency and the motor speed throttling control assembly (if it is used) structural efficiency in the motor (system) ( $0 \leq \bar{\omega}_M < \bar{\omega}_{Mmax}$ ,  $0 \leq \bar{M}_M < \bar{M}_{Mmax}$ ) operating field at a selected ratio  $v/v_n$  of the hydraulic oil viscosity  $v$  to the reference viscosity  $v_n$ .

Characteristics of the overall efficiency of elements used in a hydrostatic drive system: pump  $\eta_p$ , hydraulic motor  $\eta_M$ , conduits  $\eta_c$  and throttling control assembly (if it is used) structural efficiency  $\eta_{st}$  are defined as functions of the hydraulic motor (system) speed coefficient  $\bar{\omega}_M$  and load coefficient  $\bar{M}_M$  and the hydraulic oil viscosity ratio  $v/v_n$ .

At the same time the hydraulic motor ( $0 \leq \bar{\omega}_M < \bar{\omega}_{Mmax}$ ,  $0 \leq \bar{M}_M < \bar{M}_{Mmax}$ ) operating field in the hydrostatic drive system is determined at the selected ratio  $v/v_n$  of the hydraulic oil viscosity to the reference viscosity.

Characteristics of energy efficiency of the pump and hydraulic motor with the determined constant coefficients  $k_i$  of losses and also of efficiency of the conduits are different in hydrostatic systems with different motor speed control structures.

The method is precise by definition and simple in use. It simplifies the laboratory investigation of pumps, hydraulic motors and hydrostatic drive systems. It allows to seek for energy saving solutions of pumps and hydraulic motors. It allows also to evaluate the overall energy efficiency of the drive and to find energy saving hydrostatic drive system structures.

## **CONCLUSIONS**

1. Losses and energy efficiency of every drive motor and system must be presented as functions of physical quantities independent of losses in the motor and system. Such quantities are speed and load required by the machine or device driven by the motor, changing in the ( $0 \leq \bar{\omega}_M < \bar{\omega}_{Mmax}$ ,  $0 \leq \bar{M}_M < \bar{M}_{Mmax}$ ) drive operating field. Speed and load of the motor decide of the instantaneous useful power of the motor and also in a differentiated way of kinds and values of losses occurring in the motor.
2. In energy considerations of a motor and a drive system, it is necessary to replace the Sankey diagram by the proposed diagram of power increase in the direction opposite to power flow.
3. It is necessary to determine the motor operating field in its drive system, i.e. to determine the motor speed coefficient  $\bar{\omega}_M$  and load coefficient  $\bar{M}_M$  dependent on and independent of losses in the motor and in the system.
4. The example of operation of a rotational displacement motor in a hydrostatic drive system shows a complex relation of

energy losses in the motor and in the system to the motor shaft speed and load, to the capacity per one shaft revolution and to the working liquid viscosity. Evaluation of the motor overall efficiency  $\eta_M$  as a product of mechanical efficiency  $\eta_{Mm}$ , volumetric efficiency  $\eta_{Mv}$  and pressure efficiency  $\eta_{Mp}$  can be performed only by means of mathematical models of losses and efficiencies with the use of defined coefficients of losses in the motor and in the motor driving system.

**5. The presented proposals open a new perspective of unavoidable research of drive motors and systems, making it possible to compare objectively the energy efficiency of different types of motors and drive systems.**

**BIBLIOGRAPHY**

1. Paszota Z.: *Graphical presentation of the power of energy losses and power developed in the elements of hydrostatic drive and control system. Part I – Rotational hydraulic motor speed series throttling control systems.* Chapter in the monograph: „*Research, design, production and operation of hydraulic systems*” (in Polish), Adam Klich, Edward Palczak and Andrzej Meder editors. „Cylinder” Library. Komag Mining Mechanisation Centre, Gliwice 2008
2. Paszota Z.: *Graphical presentation of the power of energy losses and power developed in the elements of hydrostatic drive and control system. Part II – Rotational hydraulic motor speed parallel throttling control and volumetric control systems.* Chapter in the monograph: „*Research, design, production and operation of hydraulic systems*” (in Polish), Adam Klich, Edward Palczak and Andrzej Meder editors. „Cylinder” Library. Komag Mining Mechanisation Centre, Gliwice 2008
3. Paszota Z.: *Direction of increase of power stream in the hydrostatic drive and control system. Graphical presentation of the power of energy losses and power developed in the elements of hydrostatic drive and control system. Part I – Rotational hydraulic motor speed series throttling control systems* (in Polish), Napędy i sterowanie, scientific monthly, No 10 (114), October 2008
4. Paszota Z.: *Direction of increase of power stream in the hydrostatic drive and control system. Graphical presentation of the power of energy losses and power developed in the elements of hydrostatic drive and control system. Part II – Rotational hydraulic motor speed parallel throttling control and volumetric control systems* (in Polish), Napędy i sterowanie, scientific monthly, No 11 (115), November 2008
5. Paszota Z.: *Graphical presentation of the power of energy losses and power developed in the elements of hydrostatic drive and control system. Part I – Rotational hydraulic motor speed series throttling control systems.* Polish Maritime Research 3 (57) 2008, Vol. 15
6. Paszota Z.: *Graphical presentation of the power of energy losses and power developed in the elements of hydrostatic drive and control system. Part II – Rotational hydraulic motor speed parallel throttling control and volumetric control systems.* Polish Maritime Research 4 (58) 2008, Vol. 15
7. Paszota Z.: *The operating field of a hydrostatic drive system.* Chapter in the monograph: „*Research, design, production and operation of hydraulic systems*” (in Polish), Adam Klich, Antoni Kozieł and Edward Palczak editors. „Cylinder” Library. Komag Mining Mechanisation Centre, Gliwice 2009
8. Paszota Z.: *Parameters of the energy efficiency investigations of pumps and hydraulic motors. The operating field of a hydrostatic drive system* (in Polish), Napędy i sterowanie, scientific monthly, No 11 (127), November 2009
9. Paszota Z.: *The operating field of a hydrostatic drive system parameters of the energy efficiency investigations of pumps and hydraulic motors.* Polish Maritime Research 4 (62) 2009, Vol. 16
10. Paszota Z.: *Energy losses in a rotational hydraulic motor – definitions and relations for evaluation of the efficiency of motor and hydrostatic drive.* Chapter in the monograph: „*Research, design, production and operation of hydraulic systems*” (in Polish), Adam Klich, Antoni Kozieł and Edward Palczak editors. „Cylinder” Library. Komag Mining Mechanisation Centre, Gliwice 2010
11. Paszota Z.: *Theoretical and mathematical models of the torque of mechanical losses in a hydraulic rotational motor for hydrostatic drive.* Chapter in the monograph: „*Research, design, production and operation of hydraulic systems*” (in Polish), Adam Klich, Antoni Kozieł and Edward Palczak editors. „Cylinder” Library. Komag Mining Mechanisation Centre, Gliwice 2010
12. Paszota Z.: *Energy losses in a rotational hydraulic motor – definitions and relations for evaluation of the efficiency of motor and hydrostatic drive* (in Polish), Napędy i sterowanie, scientific monthly, No 10 (138), October 2010
13. Paszota Z.: *Theoretical and mathematical models of the torque of mechanical losses in a hydraulic rotational motor for hydrostatic drive* (in Polish), Napędy i sterowanie, scientific monthly, No 11(139), November 2010
14. Paszota Z.: *Energy losses in the hydraulic rotational motor – definitions and relations for evaluation of the efficiency of motor and hydrostatic drive.* Polish Maritime Research 2 (65) 2010, Vol. 17
15. Paszota Z.: *Theoretical and mathematical models of the torque of mechanical losses in a hydraulic rotational motor for hydrostatic drive.* Polish Maritime Research 3 (66) 2010, Vol. 17
16. Paszota Z.: *Hydrostatic drives as safe and energy saving machines* (in Polish), Napędy i sterowanie, scientific monthly, No 1(141), January 2011
17. Paszota Z.: *Hydrostatic drives as safe and energy saving machines* (in Polish), Proceedings of the „*Innovative machines and Technologies - Safety*” conference, Szczyrk 03 – 04 February 2011
18. Paszota Z.: *Hydrostatic drives as safe and energy saving machines. The drive investigation method compatible with the diagram of power increase opposite to the direction of power flow.* Polish Maritime Research 1(68) 2011, Vol. 18
19. Paszota Z.: *Theoretical and mathematical models of the torque of mechanical losses in the pump used in a hydrostatic drive.* Polish Maritime Research 4(71) 2011, Vol. 18,
20. Paszota Z.: *Effect of the working liquid compressibility on the picture of volumetric and mechanical losses in a high pressure displacement pump used in a hydrostatic drive. Part I Energy losses in a drive system, volumetric losses in a pump.* International Scientific-Technical Conference Hydraulics and Pneumatics, Wrocław, 16 – 18 May 2012. Ośrodek Doskonalenia Kadr SIMP - Wrocław: ODK SIMP Wrocław, 2012,
21. Paszota Z.: *Effect of the working liquid compressibility on the picture of volumetric and mechanical losses in a high pressure displacement pump used in a hydrostatic drive. Part II Mechanical losses in a pump /International Scientific-Technical Conference Hydraulics and Pneumatics, Wrocław, 16 – 18 May 2012 / Ośrodek Doskonalenia Kadr SIMP - Wrocław: ODK SIMP Wrocław, 2012,*
22. Paszota Z.: *Effect of the working liquid compressibility on the picture of volumetric and mechanical losses in a high pressure displacement pump used in a hydrostatic drive. Part I Energy losses in a drive system, volumetric losses in a pump.* Polish Maritime Research 2(73), 2012, Vol.19,
23. Paszota Z.: *Effect of the working liquid compressibility on the picture of volumetric and mechanical losses in a high pressure displacement pump used in a hydrostatic drive. Part II Mechanical losses in a pump.* Polish Maritime Research 3(75), 2012, Vol.19.

**CONTACT WITH THE AUTHOR**

Prof. Zygmunt Paszota  
 Faculty of Ocean Engineering  
 and Ship Technology  
 Gdansk University of Technology  
 Narutowicza 11/12  
 80-233 Gdansk, POLAND  
 e-mail: zpaszota@pg.gda.pl

# Determination of the main characteristics of the small waterplane area twin hull ships at the initial stage of design

**Oleksandr V. Bondarenko**, Assoc. Prof.  
**Anzhela P. Boiko**, Assoc. Prof.  
**Iryna R. Seropyan**, Engineer second class  
Admiral Makarov National University of Shipbuilding, Mykolayiv, Ukraine

## ABSTRACT

*The basic selecting peculiarities of the optimal project characteristics of the small waterplane area twin hull ships compared to conventional ships are considered. The description of the mathematical model and the ship operating model is given. The choice of the optimization method is justified.*

**Keywords:** small waterplane area twin hull ship; mathematical model; constraints; objective function; optimization

## INTRODUCTION

Small waterplane area twin hull (SWATH) ships have excellent seaworthiness and are used as pilot, research, passenger, patrol, pleasure yachts due to the peculiarities of their hull form. Because of novelty and lack of its quantity, the design experience of such type of ships is little. Besides, an engineer has to solve a lot of problems that are not inherent for the traditional types of ships when choosing the project characteristics of SWATH ship.

It should also be considered that in case of intense competition in a very short period there must be designed the best ship variant that will be much better than the competing projects. Using the traditional design methods by the original or the variation method gives an opportunity to get the project of SWATH ship that meets the task requirements but doesn't guarantee its high efficiency. The way out of such situation is to move to an optimization design. But the application of the optimization approach requires special knowledge and skills of the engineers, especially in the design of such complex objects as small waterplane area twin hull ships. Therefore, the problem of improving the decisions quality at the initial designing stages of small waterplane area twin hull ships is rather important.

Review of domestic and foreign publications has shown that there are few papers devoted to the application of the optimization approach for the SWATH ship design, for example [1-6]. The analysis of these studies gives grounds for the authors to conclude following issues that require further study:

1. In most models the determine problem is considered that doesn't allow take into account the effect of uncertainty of the initial information on the project efficiency.
2. At the initial design stage the comfort requirements of passengers are hardly set and the reliability factor is ignored.

The aim of the article is to consider the basic selecting peculiarities of the optimal project characteristics of the small waterplane area twin hull ships including the uncertainty of the initial information.

## BASIC MODEL

### *Design problems*

The basis for the project design is a technical task (C vector) containing the SWATH ship specifications set by the owner. Vector C is as follows:

- required service speed (kN);
- number of passengers;
- endurance (day);
- hull material (steel, aluminum Alloy, glass-reinforced plastic);
- superstructure material (steel, aluminum Alloy, glass-reinforced plastic);
- number of struts (single, tandem);
- type of machinery (medium speed diesel, high speed diesel, diesel electric, gas turbine).

Tab. 1. Design variables and parameters of SWATH ship

Variable	Symbol	Description	$x_i^{\min}$	$x_i^{\max}$
$x_1$	$l_H$	relative length of lower hull $L_H/D_H$	10	20
$x_2$	$l_S$	slenderness coefficient of strut $L_S/t_S$	15	35
$x_3$	$C_{WPS}$	waterplane area strut coefficient	0.6	0.9
$x_4$	$k_W$	relative waterplane area $A_{WPS}/\nabla^{2/3}$	0.5	1.5
$x_5$	$h_c$	ratio of the distance between lower hull center-line to the length of the ship $B_S/L_H$	0.3	0.6
$x_6$	$l_d$	ratio of the ship draft to the lower hull diameter $d/D_H$	1.0	2.0
$x_7$	$b_h$	ratio of the lower hull beam to its depth $B_H/H_H$	1.0	2.0
$x_8$	$C_{PH}$	lower hull prismatic coefficient	0.5	0.9
$x_9$	$n_f$	factor of the lower hull nose shape	2	4
$x_{10}$	$n_a$	factor of the lower hull tail shape	2	4
$x_{11}$	$n_h$	factor of the lower hull cross section shape	2	8
$x_{12}$	$n_s$	strut nose and tail shape factor	2	4
$x_{13}$	$l_{NH}$	hull nose length to lower hull ratio $L_{NH}/L_H$	0.2	0.5
$x_{14}$	$l_{NS}$	strut nose length to strut length ratio $L_{NS}/L_S$	0.2	0.5
$x_{15}$	$\eta_p$	payload coefficient $W_p/\Delta$	0.05	0.30
$x_{16}$	$s_b$	strut setback $S_b/L_H$	-0.1	0.1

Let's denote the vector of independent variables through  $X = (x_1, x_2, \dots, x_n)$ . The  $X$  vector includes the design variables and parameters of SWATH ship (Table 1).

The optimization problem of SWATH ship at the initial stage of design is formally stated as follows:

Minimize or maximize objective function:

$$f(X, C) \rightarrow \min(\max) \quad (1)$$

Subject to the bound constraints:

$$x_i^{\min} \leq x_i \leq x_i^{\max}; i = 1, \dots, n \quad (2)$$

and functional constraints:

$$g_j(X) \geq 0; j = 1, \dots, m \quad (3)$$

where:

- $m$  – total number of constraints;
- $x_i^{\min}, x_i^{\max}$  – lower and upper bounds on the independent variable (see Table 1);
- $n$  – number of independent variables.

The functional constraints of the  $g_j(X) \geq 0$  task include inequalities that define the ship performance requirements. The following constraints include:

- requirements for intact stability (High Speed Craft Code);
- rolling period;
- equality between weight and displacement;
- minimum value of lower hull diameter;
- maximum value of draft;
- maximum value of breadth;
- minimum and maximum values of strut tail length;
- minimum and maximum values of strut tail length;
- minimum and maximum values of lower hull tail length;
- motion sickness indexes (MSI) and etc.

All of these constraints are got on the basis of the analysis of technical requirements to the ship characteristics. There is a possibility to regulate the feasible search space by enabling/disabling of certain constraints.

The objective function or criterion optimization (1) represents the expected value of efficiency indexes [7]. This criterion seeks the maximization of expected (average) profit or the minimization of expected operational cost:

$$f(X, C) = M\{EI\} \text{Prob} \rightarrow \max \quad (4)$$

$$f(X, C) = M\{EI\}(1 - \text{Prob}) \rightarrow \min$$

where:

- $EI$  – efficiency indexes;
- $M\{\dots\}$  – average.

The data of the problem assumes that the payoff (or cost) associated with each decision alternative is probabilistic.

Also there is a choice of another criterion form: aspiration level criterion, utility function.

In this formulation the optimization problem is usually nonlinear and conditionally divided into two parts. The first part deals with the ship mathematical model development, the second one provides the selection of the optimal solution search method.

These parts for each type of ship have their own peculiarities that effect the whole process of the problem solution. Particularly for SWATH ship it is possible to point further features.

The first SWATH ship feature as an optimization object is the technical solutions variety used while creating in the part of principle project and constructive layouts and their possible combinations. The studies gave an opportunity to reveal the significant changes in the relationship nature between the main structural elements of SWATH ship and well-known monohull ship. For example, the twin hull construction means the increasing of the dependence of the design characteristics on the size and configuration of the hulls and struts, much changing of the external load effect nature (forces and moments that act in cross direction become the most important), the value changing of the total resistance components, and, as a result, the constructive measures for its decrease.

Possible relationship variants of the hull and strut sizes, shape parameters are so variable that while their proving it is necessary to make much research work. Even small changes of the hull form parameters while displacement increasing or decreasing influence the required propulsion power and the weight. The same way they influence the SWATH ship seakeeping performance. Thus, according to the study [5], for the pilot ship with a small waterplane area at the stage of preliminary design it was necessary to make 120 steps of design, each of them included the calculation of resistance and seakeeping control. Such number of variant elaborations can be done only with the help of special software. Besides, the hull shape, got by computer-aided design, must be adapted for the machinery layout and rudders.

The second SWATH ships feature is that the process of their optimal design is much complicated than in the traditional monohull ships and catamarans with simple hull configuration. It is known that all the performance of monohull ships are mainly defined by their principle dimensions (length, beam, draft and depth), block coefficient. To the catamarans with simple hull configuration the separation of demi-hulls and vertical clearance (Table 2) are added. And in case of SWATH ship it is important to consider the geometrical characteristics and shape parameters not only of each single hull, but also the struts, and, in addition, hydrodynamic interference effect of hulls and struts (Fig. 1) [2].

Besides, when designing SWATH ship it is important to consider the fact that external forces are defined not only by the geometrical hull, strut and their connections characteristics but also their positional relationships.

Tab. 2. Number of design variables and combinations

Ship type	L	B	D	d	C <sub>b</sub>	Number of variables	Number of combinations
Monohull	1	1	1	1	1	5	3 <sup>5</sup> = 243
Catamaran	1	3	2	1	1	8	3 <sup>8</sup> = 6561
SWATH	3	4	3	1	1	12	3 <sup>12</sup> = 531441

The next feature is the lack of sufficient design and construction experience, and a small amount of built ships which can be used as the prototypes. Nowadays approximately 80 ships are built, and only 20 of them are for passengers.

While the SWATH ship project design there should be a justification of those characteristics that are not included into the design task, but at the same time have strong influence on the SWATH ship efficiency, notably:

- the selection of constructive and arranging type: mono, catamaran, trimaran, and other variants, number of struts;
- the selection of constructive materials with an opportunity to combine variants that are different for the hull and superstructure: steel, aluminum, glass-reinforced plastic;
- justification of the spectrum of the comfort level with the arranging the passengers according to the categories, as well as according to the decks and cabins along the length of the ship;

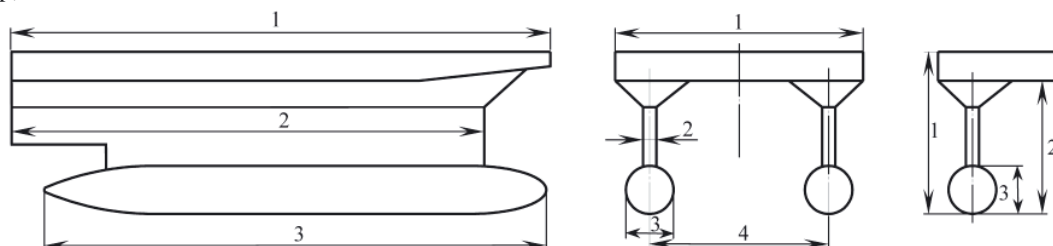


Fig. 1. SWATH ship design variables scheme

- justification of the spectrum of the cruising range and seakeeping levels in combination with the maximal and operational speed.

The development of the general arrangement of the ship also needs special attention because great area of the SWATH ship decks provides completely new ship space structure and presents almost unlimited possibilities in the inhabited area organization.

When solving the optimization problem there should be considered the existence and trustworthiness of the initial economical information used when estimating the ship efficiency. It is very difficult at the initial design stage to set the price of fuel, crew expenditures, port charges etc. These characteristics change during a season, not mentioning the operation time of 15-25 years. That's why consideration of the economic situation instability is rational to carry out by moving to the stochastic formulation of the optimization problem.

According to the information above there was developed a program complex (PC) SWATH Ship in order to find the best elements of the ship.

The basis of the PC mathematical support consists of the mathematical model of the ship as an engineering building and operational model.

### Mathematical model of SWATH ship

The SWATH ship mathematical model contains analytical dependences that allow to define (Fig. 2): geometrical ship characteristics; lightship weight and deadweight; capacity (required areas for passengers and areas of service, public and sanitary rooms); intact stability and the stability (GZ) curve; geometrical characteristics of the fins; ship seakeeping performances; building cost.

The mathematical model is realized into two units: «SWATH\_model» and «Resist».

The «SWATH\_model» unit contains the algorithm for calculation the basic SWATH ship characteristics.

The initial data for calculation are the start values of the independent variables, the parameters noted in the design task and extra data.

The selection of the main dimensions begins with the calculation of the ship payload:

$$W_p = (P_{Pas} + N_{Endr} \cdot P_{Fr.w} + P_{Prov}) \cdot N_{Pas} / 1000; [t] \quad (5)$$

where:

- $P_{Pas}$  – one passenger mass, [kg];
- $P_{Fr.w}$  – fresh water for a passenger per day, [kg];
- $P_{Prov}$  – provision for a passenger per day, [kg];
- $N_{Pas}$  – number of passengers;
- $N_{Endr}$  – endurance, [day].

Then the ship design displacement is estimated:

$$\Delta = W_p / \eta_p; [t] \quad (6)$$

where:

- $\eta_p$  – payload coefficient.

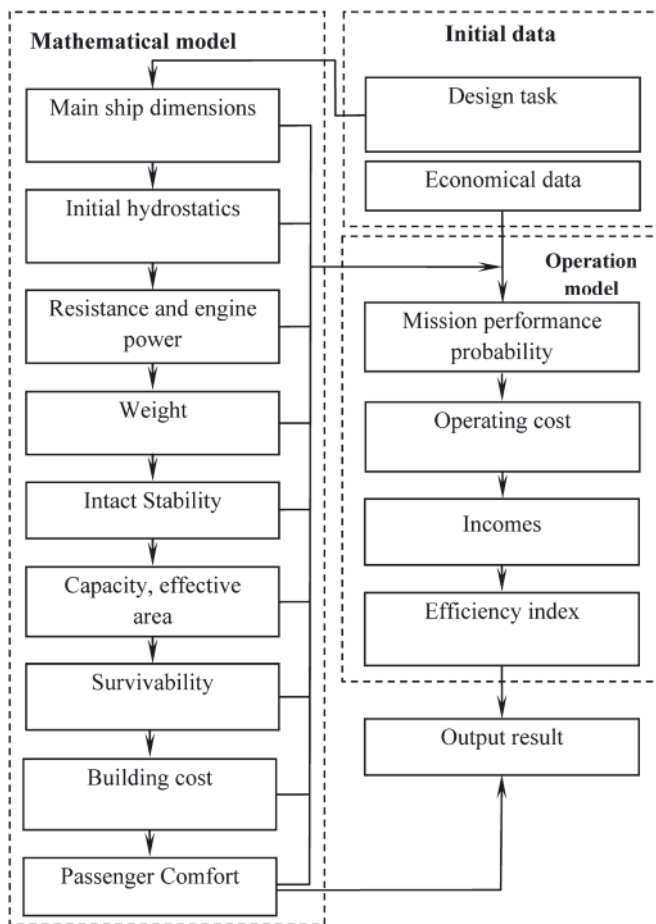


Fig. 2. Block diagram of the SWATH ship mathematical model and operational model

At the next stage the calculation of the basic SWATH ship geometrical characteristics is performed. Some of dependences are listed in the Table 3.

The formulas shown in Table 3 are obtained under the assumption that the lower hull forebody is elliptical, the stern is parabolic, the strut nose and tail are parabolic.

The values of the geometric SWATH ship characteristics are used to generate the hull surface, as well as to calculate the propulsive performance of the ship, weight and seakeeping.

Determination of the lightship weight and deadweight mass is performed by solving the weight equation:

$$\Delta = W_{LS} + DW \quad (7)$$

where:

$W_{LS}$  – lightship weight, t;

$DW$  – deadweight, t.

At the early stage of design the calculation of the SWATH ship lightship weight is reasonable to perform in the following groups:

$$W_{LS} = W_{Hull} + W_{Sup} + W_M + W_{Out} + W_{SM} \quad (8)$$

where:

$W_{Hull}$  – hull weight, [t];

$W_{Sup}$  – superstructure weight, [t];

$W_M$  – machinery weight, [t];

$W_{Out}$  – outfit weight, [t];

$W_{SM}$  – design margin, [t].

The biggest difficulty in calculation is the hull weight because of the lack of information about the prototype weight and statistic dependences. In PC in order to define the hull

weight there was taken a basic approach. According to this approach [2] SWATH ship hull weight is estimated through the structural part thickness taking into account the operation load and requirements of the Ship-Classification Society:

$$W_{Hull} = (1 + C_0) \sum_i (1 + C_i) W_{si} \quad (9)$$

where:

$C_0 = 0.085$  – coefficient that takes into account the weight of additional components (painting, welding material and margin);

$C_i$  – coefficient that takes into account the weight of other than the plate (stiffeners);

$W_{si}$  – plate weight of the main SWATH ship structural part: lower hulls, struts, sponsons, box, inside decks and platforms, longitudinal and transverse bulkheads.

The plate weight of the SWATH ship hull structural parts is defined according to the following dependence:

$$W_{si} = 0.001 \sum_{i=1}^n S_i t_i q_i; [t] \quad (10)$$

where:

$S_i, t_i, q_i$  – area [m<sup>2</sup>], thickness [m] and density of the material [kg/m<sup>3</sup>] of the  $i$  hull part appropriately.

The surface area  $S_i$  of the structural parts of the SWATH hull is determined using the parametrical model and is directly connected with independent variables.

For the ships with glass-reinforced plastic hulls the similar coefficients are difficult to obtain. That's why according to the calculations for several small waterplane area twin hull ships made of glass-reinforced plastic there was obtained the following dependence between the hull weight and ship displacement:

$$W_{hull} = 0.2168\Delta + 4.6129 \quad (11)$$

The superstructure at the first approximation is calculated depending on the material by the formula:

$$W_{Str} = g_{Str} V_{Sup}; [t] \quad (12)$$

where:

$g_{Str}$  – the superstructure volume density, [t/m<sup>3</sup>];

$V_{Sup}$  – the superstructure volume with regard for the wheelhouse, [m<sup>3</sup>].

The other lightship weight groups with some changing and improvements are defined by formulas that are used at the designing of the high speed passenger catamarans.

Providing of the passenger SWATH ship capacity is performed by calculating necessary areas:

$$A_{\Sigma} = \sum_{i=1}^n A_{r_i}; [m^2] \quad (13)$$

where:

$A_{r_i}$  – required room area, [m<sup>2</sup>];

$n$  – number of rooms on the ship.

When calculating the cost of ship building at the initial stage design the following expression was used:

$$C_S = (1 + k_1)(C_M + C_O + C_W) \quad (14)$$

where:

$k_1$  – coefficient of the commercial expenditures and planned contributions, includes the value-added tax and the profit of the shipbuilding plant;

Tab. 3. Calculation of the SWATH ship geometrical characteristics

Item	Symbol	Formula
Waterplane area, [m <sup>2</sup> ]	$A_{WPS}$	$A_{WPS} = \nabla^{2/3} k_W$
Fore waterplane area coefficient of the strut	$C_{WL\_F}$	$C_{WL\_F} = n_s / (1 + n_s)$
Aft waterplane area coefficient of the strut	$C_{WL\_A}$	$C_{WL\_A} = n_s / (1 + n_s)$
Strut length, [m]	$L_S$	$L_S = \sqrt{\frac{A_{WPS} L_S}{2 C_{WPS}}}$
Strut thickness, [m]	$t_s$	$t_s = l_s / L_S$
Midship section coefficient of the lower hull	$C_{MH}$	$C_{MH} = \frac{\sqrt{\pi} \cdot \Gamma\left(\frac{1}{n_h}\right)}{2^{\frac{2}{n_h}} \cdot n_h \cdot \Gamma\left(\frac{1}{2} + \frac{1}{n_h}\right)}$
Block coefficient of the lower hull	$C_{BH}$	$C_{BH} = C_{MH} C_{PH}$
Lower hull beam, [m]	$B_H$	from the equation solution $\frac{2 C_{BH} l_H B_H^3}{b_H^{3/2}} + \frac{A_{WPS} (l_d - 1) B_H}{b_H} - \nabla = 0$
Lower hull depth, [m]	$H_H$	$H_H = B_H / b_H$
Lower hull diameter, [m]	$D_H$	$D_H = \sqrt{H_H B_H}$
Lower hull length	$L_H$	$L_H = l_H D_H$
Ship draft, [m]	$d$	$d = l_d H_H$
Midship area of the lower hull, [m <sup>2</sup> ]	$A_{MH}$	$A_{MH} = C_{MH} H_H B_H$
One lower hull displacement volume, [m <sup>3</sup> ]	$\nabla_H$	$\nabla_H = C_{PH} A_{MH} L_H$
Strut submerged depth, [m]	$H_{SS}$	$H_{SS} = d - H_H$
Strut submerged volume, [m <sup>3</sup> ]	$\nabla_S$	$\nabla_S = (A_{WPS} H_{SS}) / 2$
Strut setback, [m]	$S_b$	$S_b = s_- b L_H$
Length overall, [m]	$L_{OA}$	$L_{OA} = \max(L_S + S_b; L_H)$
Box length, [m]	$L_{Box}$	$L_{Box} = \min(L_S + S_b; L_{OA})$
Vertical (box) clearance, [m]	$H_{DK}$	$H_{DK} = \max(0.75 h_{3\%}; 0.625 \sqrt{B_H H_H})$
Strut depth, [m]	$h_s$	$h_s = H_{SS} + H_{DK}$
Distance between lower hull center line, [m]	$B_S$	$B_S = h_c L_H$
Box beam, [m]	$B_{Box}$	$B_{Box} = B_S + B_H$
Depth of cross structure box, [m]	$H_{DB}$	$H_{DB} = (B_{Box} - 2B_H) / 7.5$
Depth up to the [m]ain deck, [m]	$D$	$D = H_H + h_s + H_{DB}$

$C_M$  – material cost, [US \$];  
 $C_O$  – equipment cost, [US \$];  
 $C_W$  – the labour cost, [US \$].

Cost of labour is calculated as follows:

$$C_W = (1 + k_O) \sum_{i=1}^N c_{pi} L_{pi} \quad (15)$$

where:

$c_{pi}$  – unit hourly wage, [US \$/man-hours];  
 $L_{pi}$  – labour man hours [8];  
 $N$  – number of parts;  
 $k_O$  – coefficient that takes into account the overhead cost.

Hull material cost:

$$C_M = (1 + k_2) \sum_{i=1}^N c_i W_{si} \quad (16)$$

where:

$k_2$  – coefficient that takes into account the material losses;  
 $c_i$  – specific is the cost of 1 ton material, [US \$/t].

Equipment cost:

$$C_O = \sum_{j=1}^K c_j W_j \quad (17)$$

where:

$W_j$  – weight of unit, [t];  
 $c_j$  – cost of outfit per unit weight or power.

The «Resist» unit implements the resistance calculation method  $R_T$  and the propulsion engine power  $P$ . For defining the  $R_T$  there was the following formula:

$$R_T = R_F + R_W + R_{SP} + R_{AP} + R_{AA} \quad (18)$$

where:

$R_F, R_{AP}, R_{AA}$  – frictional, appendages and aerodynamic resistance;  
 $R_W, R_{SP}$  – wave and spray resistance.

The calculation of frictional, appendages and aerodynamic resistance is performed by the known dependences of the ship theory considering the SWATH ship construction peculiarities [3, 9].

Spray resistance calculation is based on the results of the model tests, as described in [10].

The wave resistance of the small waterplane area twin hull ship is defined according to the formula, kN:

$$R_W = \sum_i R_{Wi} + \sum_i \sum_j \Delta R_{Wij} \quad (19)$$

where:

$\sum_i R_{Wi}$  – individual wave resistance of every body that is a part of the SWATH ship, [kN];  
 $\sum_i \sum_j \Delta R_{Wij}$  – additional wave resistance as a result of the wave systems interference, [kN]. The wave resistance is defined for those bodies such as underwater hull, fore and aft struts. There is also an opportunity to calculate the resistance for the Slice type ships and single-hull SWATH ship.

In order to calculate the components of the SWATH ship wave resistance there was used the Michell integral:

$$R_W = \frac{4\rho g^4}{\pi U^6} \int_0^{\pi/2} (I^2 + J^2) w^2 \sec^5 \theta d\theta \quad (20)$$

where:

$$J(\theta) = - \int_{-\frac{L}{2}}^{\frac{L}{2}} \int_{-T}^0 Y(x, z) \exp(k_0 z \sec^2 \theta) \cos(k_0 x \sec \theta) dx dz;$$

$\theta$  – integration variable;

$k_0 = g/U^2$  – wave number, [1/m];

$w = 2 \cos(k_0 b \sec^2 \theta \sin \theta)$ ;

$$I(\theta) = - \int_{-\frac{L}{2}}^{\frac{L}{2}} \int_{-T}^0 Y(x, z) \exp(k_0 z \sec^2 \theta) \sin(k_0 x \sec \theta) dx dz;$$

$2b$  – distance between center line of the hull, [m];

$\rho$  – fluid density, [t/m<sup>3</sup>];

$U$  – ship speed, [m/s];

$Y(x, z)$  – SWATH ship lower hull or strut offsets, m.  
 When calculating the wave integral, the original integration procedure according to the Filon rule was used.

Then the main engines power is defined:

$$P = \frac{P_E}{\eta_s \eta_D} (SM + 1), [kW] \quad (21)$$

where:

$\eta_s$  – propulsive coefficient;

$SM$  – sea margin power;

$P_E = R_T U$  – effective power, [kW].

In the program there provided the power curve output or the output of the resistance curve, that visually show the dependence of total and other types of resistance from the ship speed.

### Operational problems

The operational costs and the SWATH ship economic efficiency indexes are defined by the economic analysis in operational model. *Operational model* allows examining the ship dynamic operation being effected by chance factors. The chance factors under the environmental effect are generally defined by the hydrometeorological conditions, that typical for the examined operational area, as well as by the initial uncertain data, that are used in calculation of the operational economic indexes.

The operational model of the ship that makes regular scheduled cruises between two points is realized in the «Simulation» unit and contains three blocks: «Meteo», «Voyage», «Statistic». Before the ship setting out on a voyage there is a check of being ready to do that. In case of storm the ship voyage is canceled during the storm. Its value is generated in the «Meteo» block. In other cases the ship voyage between the departure point and destination is being modeled. While voyage there were calculated the coefficient of ship loading, the average cruise speed taking into account the wave height and wind speed, MSI and other operation indexes. In the port the passengers loading and unloading is being modeled. The process is repeated till the simulation time ends. Then the control is given to the «Statistic» block, where the statistic processing of the simulation results is performed and one of the economic efficiency indexes is calculated.

The program provides an opportunity to simulation the operation of one, two and three ships on the line according to the following shape of service: a ship that returns and doesn't return to the destination point on the same day; a ship that makes several trip per day; two or three ships that make series trip; two or three ships that make opposite trips. The voyages can be made every day or special days.

The economic analysis provides the calculation of one of chosen ship efficiency indexes: net present value (NPV), required freight rates (RFR), payback period (PP), net income (NI) and profitability index (PI).

The operation costs are defined as the sum of the following components:

$$C_O = C_{Fix} + C_{Var} \quad (22)$$

where:

$C_{Fix}$  – fixed cost;

$C_{Var}$  – voyage cost.

*Fixed operation cost* depends on the crew number, ship building cost and is calculated by:

$$C_{Fix} = C_{Crew} + C_R + C_{IS} + C_D + C_{Of} \quad (23)$$

where:

$C_{Crew}$  – crew costs;

$C_R$  – repair and maintenance;

$C_{IS}$  – insurance;

$C_D$  – depreciation;

$C_{Of}$  – administration.

*Voyage costs* include the following components:

$$C_{Var} = C_P + C_F + C_{Oil} \quad (24)$$

where:

$C_P$  – port charges;

$C_F$  – fuel;

$C_{Oil}$  – lubrication oil.

The SWATH ship economic efficiency analysis is performed with a glance of the risk factor and the factor of probability of the mission performance during the whole life cycle. For the passenger ships that perform scheduled voyages the probability of the mission performance can be estimated as following:

$$\text{Prob} = P_1 P_2 P_3 P_4 \quad (25)$$

where:

- $P_1$  – probability of the voyage performance;
- $P_2$  – probability of keeping the given average speed during the trip;
- $P_3$  – economic risks (probability of the nonnegative profit receiving);
- $P_4$  – reliability meaning the probability of the constructions and equipment accident – free operation.

The values of the probability of the mission performance and the parameters of the optimization criterion distribution law are defined via the simulation modeling of the ship trip elements.

The simulation modeling [11] is based on the computer reproduction of the extensive ship operation process with

a glance of external environment interaction. The SWATH ship operation process is presented as serial manual of the ship operation process between the departure and destination point, load/unload it in ports, etc., taking into account the hydro- and meteorological conditions. As a result of such modeling certain events and conditions are fixed that allows to define the system efficiency characteristics.

The main stages of simulation modeling:

- Accumulation and statistical data manipulation in order to determine the distribution law;
- random numbers generation with given distribution laws using random numbers generators;
- construction and realization of the ship operation model;
- carrying out of the simulation experiment;
- statistical manipulation of the modeling results.

The block diagram of the simulation modeling procedure is shown in the Fig. 3.

The second part of the problem is solved with the optimization method depending on the design variables vector length, availability constraints, non-linear criterion and constraints. According to the analysis results the genetic

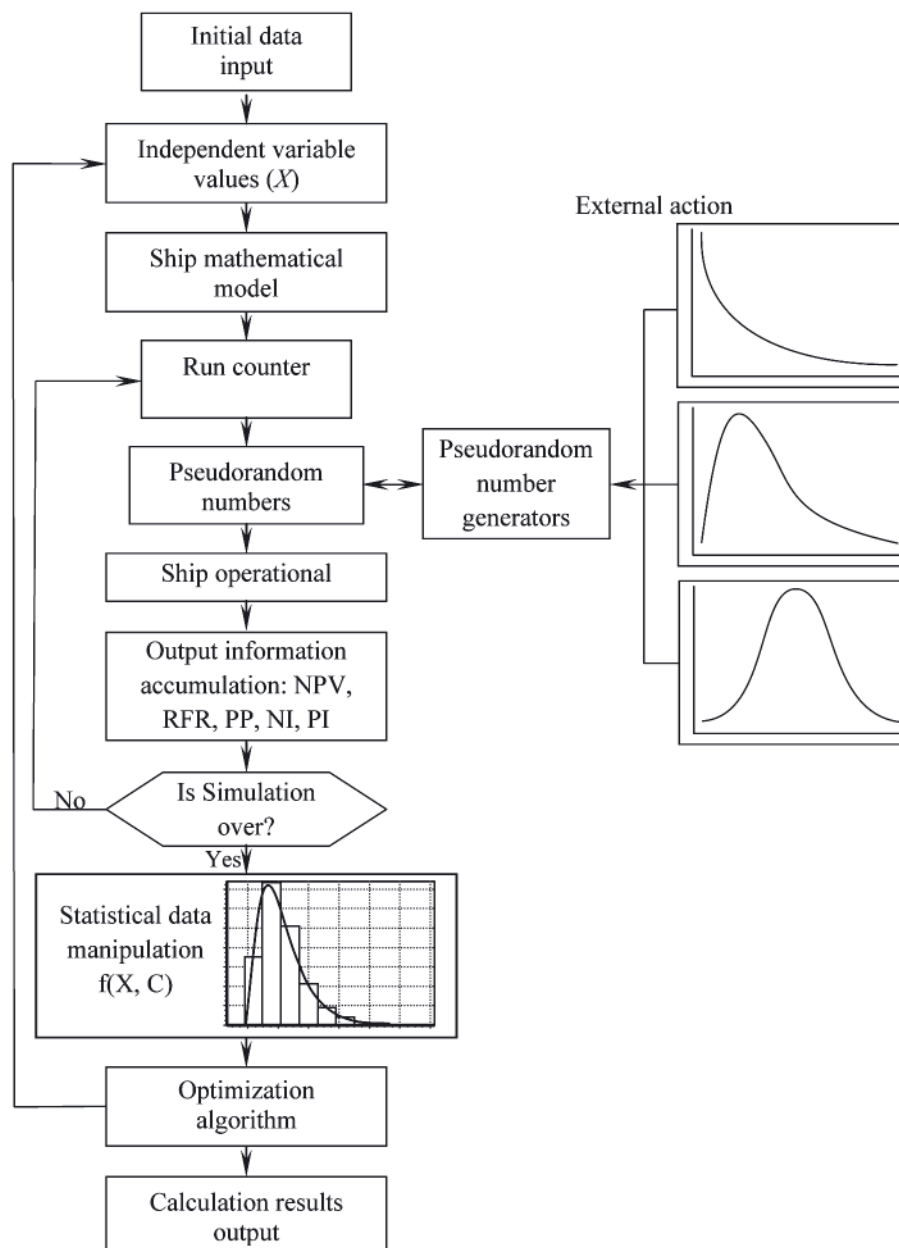


Fig. 3. Block diagram of the simulation modeling

algorithm (GA) is suggested to use while solving the problem. GA is a simple evolution model in natural world that is realized as a computer program [12-14]. In the genetic algorithm, the analogues of natural genetics and natural selection are used. In general, the GA search strategy is described by the following cycle. At the first iteration the initial «population» is formed (the whole set of the project solutions). Then for each «individual» (problem solutions) the fitness function values are calculated, that helps to identify the best «individual». After that GA generates a new «population» with the genetic operators of selection, crossover, mutation and elitism strategy. For the new «population» the estimation of the fitness function value, etc. The process is repeated till one of the stopping criteria is performed.

The optimal solution search method with the application of genetic algorithm is realized in the «GeneticAlg» units.

Apart from the given units that realize the SWATH ship design methods, computer program contains the interface units that provide the operational comfort for the system user. The computer program interface allows to input the initial data, to choose the objective function type and economic efficiency indexes, to set the initial conditions of simulation, the parameters of the genetic algorithm and the determined and stochastic economic data, to output the calculation results in the graphical or tabular style.

The *SWATH Ship* program complex is designed in the Borland Delphi Professional 7.0 programming system and can be used in the Windows 98/XP/Vista operation systems.

The program complex can be used in the following range of characteristics: passenger carrying capacity – 20...450 persons; service speed – 20...40 knot; endurance – 100...500 miles; ship length – 20...50 m. Besides, using the *SWATH Ship* it's possible to carry out different experiments dealing with the check of the models validity, sensitivity etc.

### Results and verification

In order to verify the calculations using the developed methodology and based on it programs complex, the series of the SWATH model towing tests (Fig. 4) were carried out in the towing tank of the National University of Shipbuilding.

The towing tests of the models were carried out at speeds of 0.5 to 3.0 m/s, that correspond to the Froude numbers in

the length from 0.17 to 1.07. The experiment was carried out in two stages. At the first stage the model with two struts on each hull was tested. After the first stage ended the space between the struts was sewn. And then the SWATH one-strut model was tested.

The results of the model testing were recalculated for the 32 m long full-size ship. Then with the help of the developed program the impedance values were obtained. Recalculation from the model to the full-size ship and the results of theoretical

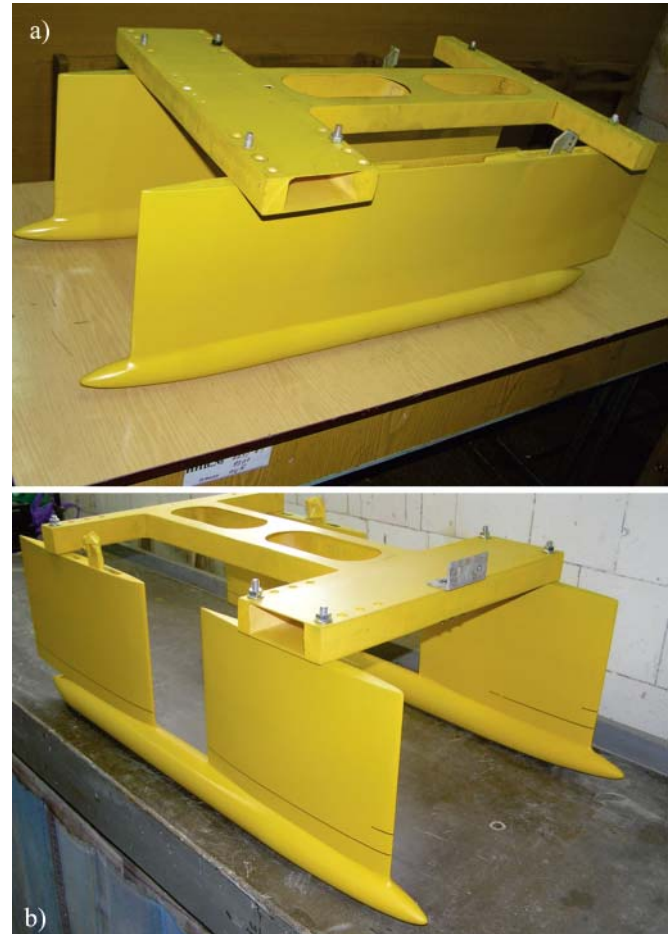


Fig. 4. SWATH models: a) single strut; b) tandem strut

Tab. 4. Estimation of total ship resistance from model experiment and SWATH Ship program

$U_M$ , [m/s]	Fr	$R_p$ , [kN]		Error, [%]
		from model experiment	Theory by program	
0.625	0.2231	13.21	12.97	1.83
0.875	0.3124	46.44	45.907	1.15
0.882	0.3149	44.27	45.79	3.45
1.000	0.3570	31.72	33.654	6.10
1.250	0.4463	71.38	72.071	0.97
1.500	0.5355	104.25	107.933	3.53
1.750	0.6248	114.93	122.994	7.02
2.000	0.7140	123.48	135.932	10.08
2.25	0.8033	148.03	151.919	2.63
2.5	0.8926	173.12	172.172	0.55
2.75	0.9818	209.78	197.94	5.64

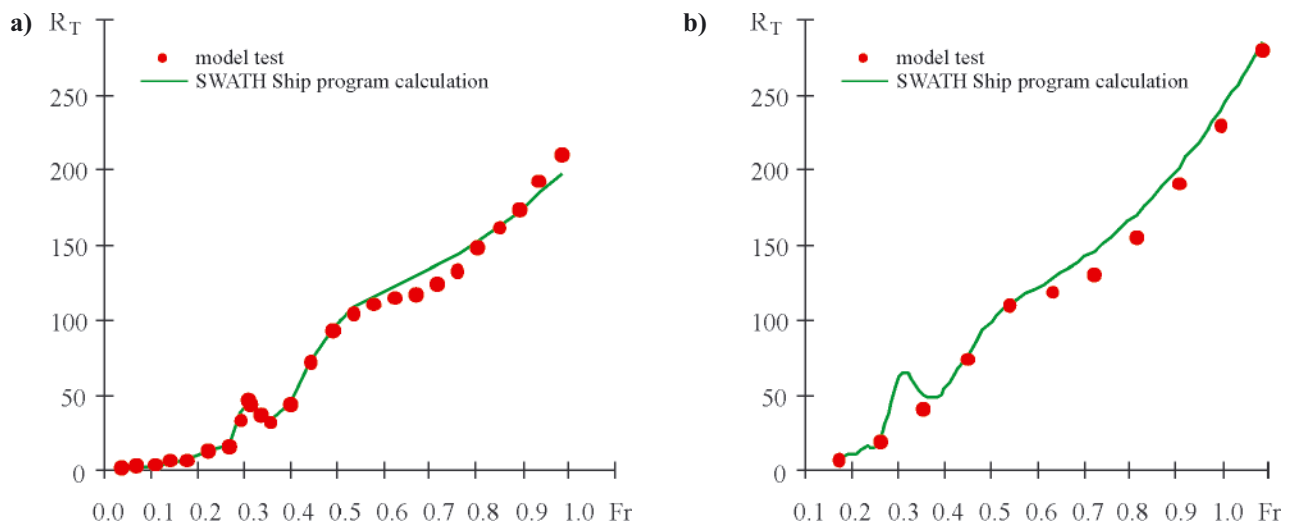


Fig. 5. Comparison of measured and calculated total ship resistance: a) Single strut SWATH ship, b) Tandem strut SWATH ship

Tab. 5. The SWATH optimal performance for the Odessa – Varna route

Description	Hull/Superstructure material		
	Steel /Steel	Aluminum Alloy /Aluminum Alloy	Steel /Aluminum Alloy
Lower hull length, [m]	25.755	25.123	25.808
Lower hull beam, [m]	2.472	1.786	2.295
Lower hull depth, [m]	1.9	1.635	1.928
Hull nose length, [m]	3.863	3.768	3.871
Hull tail length, [m]	3.963	9.731	5.887
Strut length, [m]	26.024	20.888	23.734
Strut thickness, [m]	1.156	1.049	0.973
Strut height, [m]	2.885	2.752	2.817
Strut nose length, [m]	6.506	5.222	5.934
Strut tail length, [m]	10.852	6.672	8.994
Waterplane area strut coefficient	0.849	0.873	0.853
Box clearance, [m]	2.092	1.743	2.005
Distance between lower hull center line, [m]	10.507	9.628	10.328
Ship draft, [m]	2.693	2.643	2.740
Depth up to the [m]ain deck, [m]	5.79	5.367	5.749
Length overall, [m]	26.378	25.123	25.808
Box length, [m]	26.378	25.123	25.808
Box beam, [m]	12.979	11.413	12.623
Depth of cross structure box, [m]	1.004	0.98	1.004
Displacement, [t]	250	150	225
Deadweight, [t]	39.26	34.75	37.95
Main Engines, [number × kW]	2 × 3460	2 × 2300	2 × 3460
Generator, [kW]	190	190	190
Crew	5	5	5
Cost of ship, thousand [US \$]	4857	3752	4767
Payback period, [year]	9.3	5.9	8.4
Net Present Value, thousand [US \$]	2390	4357	2427

calculation of the one-strut SWATH towing resistance are shown in the Table 4. Similar results were obtained for the two-strut SWATH.

According to the tests and calculated data using the developed program, the diagrams of the towing resistance and Froude number dependence for the one- (Fig. 5a) and two-strut (Fig. 5b) SWATH were constructed.

The results, obtained with the help of theoretical calculation using the developed program, quite accurately match the test data of the small size models.

The technique's working efficiency is shown by the example of solving the problem of choosing the best performance of the passenger SWATH for the Odessa – Varna route. The time schedule of the Krymskaya Strela catamaran is used in the calculation. During the calculating of capital investment in the ship construction it is supposed that the buyer's own funds are 20%, and the rest 80% of investment is the bank loan for 8 years under the 6...10 % interest rate per year. The ship operational lifetime is 15 years. The net present value is used as an economical efficiency factor. The SWATH optimal performance values for the passenger Odessa – Varna shipping, obtained after the work of optimization program, are listed in the Table 5.

In order to define the main SWATH characteristics the genetic algorithm with the following parameters was used as an optimization method: population number – 50 chromosomes, gene capacity – 32 bit, crossover probability – 0.9, mutation probability – 0.1, inversion probability – 0.05, initial penalty – 0.5, extreme achieving accuracy – 0.000001. The elitism strategy was used during the optimization. These parameters are set experimentally as a result of multiple test runs of the program.

The calculation results have shown that the most economically efficient SWATH model is the one that is made of aluminum because it brings the highest return at the lowest expenditures and has less payback period.

## CONCLUSIONS

1. The SWATH ship is more complicated for the optimization research than the conventional monohull ships and catamarans with traditional hull shape. First of all it's connected with the variability of the used technical solutions in the project and construction arrangement and their possible combinations. It's also connected with the difficult optimization process and lack of design and construction experience.
2. The general problem statement of the SWATH ship optimal design is characterized such complexity factors as large number of independent variables, presence of constraints, necessity to account the stochastic and uncertainty external agencies. The solving process of such problem provides the use of the penalty function approach (for the constraints account), genetic algorithm (for the direct optimum search) and simulation modeling (for the accounting of the data uncertainty).

Further research work is advisable to direct for improvement of the algorithm calculation of the propulsive coefficient, seakeeping performance and for enlargement of the model for other types of small waterplane area twin hull ship.

## Appendix A

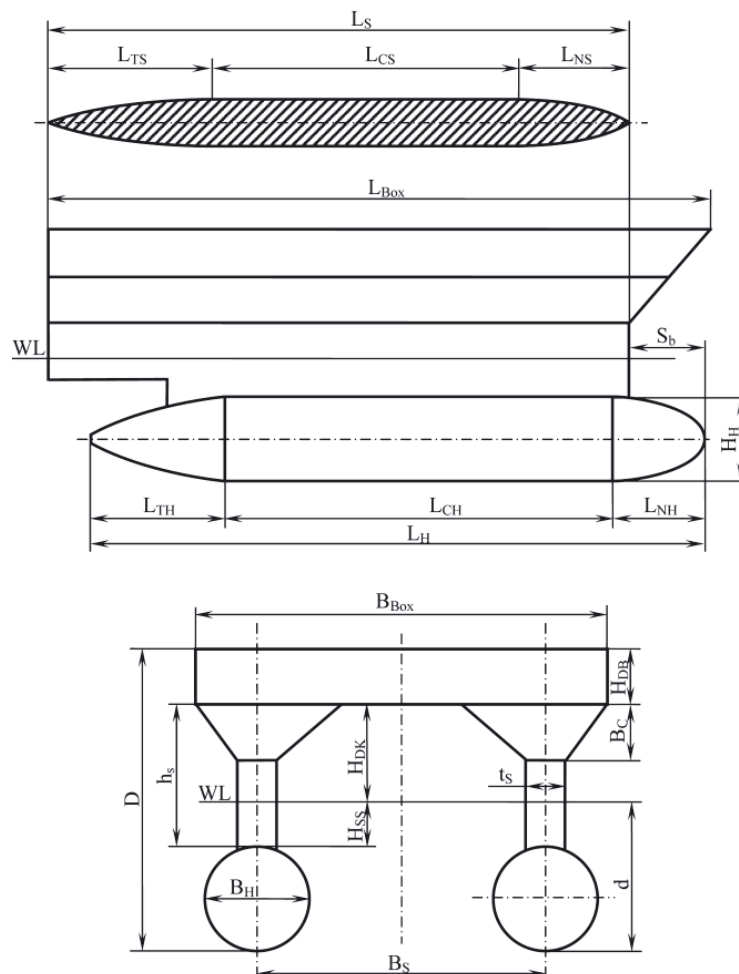


Fig. A.1. Hull form parameters

## NOMENCLATURE

$A_{MH}$	–	midship area of the lower hull, [m <sup>2</sup> ]	$n_s$	–	strut nose and tail shape factor
$A_{r_i}$	–	required room area, [m <sup>2</sup> ]	$N_{Pas}$	–	number of passengers
$A_{WPS}$	–	waterplane area, [m <sup>2</sup> ]	$N_{Endr}$	–	endurance, [day]
$b_H$	–	ratio of the lower hull beam to its depth	$P$	–	engine power, [kW]
$B$	–	breadth of the ship, [m]	$P_E$	–	effective power, [kW]
$B_{Box}$	–	box beam, [m]	$P_{Fr.w}$	–	fresh water for a passenger per day, [kg]
$B_H$	–	lower hull beam, [m]	$P_{Pas}$	–	one passenger mass, [kg]
$B_S$	–	distance between lower hull center line, [m]	Prob	–	probability of the mission performance
$C$	–	vector of technical task	$P_{Prov}$	–	provision for a passenger per day, [kg]
$C_B$	–	block coefficient	$P_1$	–	probability of the voyage performance
$C_{BH}$	–	block coefficient of the lower hull	$P_2$	–	probability of keeping the given average speed during the trip
$C_{Crew}$	–	crew costs, [US \$]	$P_3$	–	economic risks (probability of the nonnegative profit receiving)
$C_D$	–	depreciation cost, [US \$]	$P_4$	–	reliability [m]eaning the probability of the constructions and equipment accident-free operation
$C_F$	–	fuel cost, [US \$]	$q_i$	–	density of the [m]aterial hull part [kg/m <sup>3</sup> ]
$C_{Fix}$	–	fixed cost, [US \$]	$R_{AA}$	–	aerodynamic resistance, [kN]
$C_i$	–	coefficient that takes into account the weight of other than the plate	$R_{AP}$	–	appendages resistance, [kN]
$C_{IS}$	–	insurance cost, [US \$]	$R_F$	–	frictional resistance, [kN]
$C_M$	–	material cost, [US \$]	$R_{SP}$	–	spray resistance, [kN]
$C_{MH}$	–	midship section coefficient of the lower hull	$R_T$	–	total resistance, [kN]
$C_O$	–	equipment cost, [US \$]	$R_W$	–	wave resistance, [kN]
$C_{Of}$	–	administration cost, [US \$]	$s_b$	–	strut setback
$C_{Oil}$	–	lubrication oil cost, [US \$]	$S_b$	–	strut setback, [m]
$C_p$	–	cost of port charges, [US \$]	$S_i$	–	area of the $i$ hull part [m <sup>2</sup> ]
$C_{PH}$	–	lower hull prismatic coefficient	SM	–	sea margin power
$C_R$	–	repair and maintenance cost, [US \$]	$t_i$	–	thickness of hull part [m]
$C_S$	–	cost of ship, [US \$]	$t_s$	–	strut thickness, [m]
$C_{Var}$	–	voyage cost, [US \$]	$U$	–	ship speed, [m/s]
$C_W$	–	the cost of the work of the shipbuilding plant, [US \$]	$U_M$	–	model speed, [m/s]
$C_{WL\_A}$	–	aft waterplane area coefficient of the strut	$V_{Sup}$	–	superstructure volume, [m <sup>3</sup> ]
$C_{WL\_F}$	–	fore waterplane area coefficient of the strut	$W_{Hull}$	–	hull weight, [t]
$C_{WPS}$	–	waterplane area strut coefficient	$W_{LS}$	–	lightship weight, [t]
$C_0$	–	coefficient that takes into account the weight of additional components (painting, welding material and margin)	$W_{Out}$	–	outfit weight, [t]
$d$	–	ship draft, [m]	$W_p$	–	payload, [t]
$D$	–	depth up to the main deck, [m]	$W_M$	–	machinery weight, [t]
$D_H$	–	lower hull diameter, [m]	$W_{si}$	–	plate weight of the main SWATH ship structural part: lower hulls, struts, sponsons, box, inside decks and platforms, longitudinal and transverse bulkheads
$D_W$	–	deadweight, [t]	$W_{SM}$	–	design margin, [t]
$f(X, C)$	–	efficiency criterion	$W_{sup}$	–	superstructure weight, [t]
Fr	–	Froude number	$x_i^{min}$	–	minimum value of independent variable
$g_j(X)$	–	ship performance requirements	$x_i^{max}$	–	maximum value of independent variable
$g_{Str}$	–	the superstructure volume density, [t/m <sup>3</sup> ]	$X$	–	vector of independent variables
$h_c$	–	ratio of the distance between lower hull center-line to the length of the ship	$Y(x, z)$	–	SWATH ship lower hull or strut offsets, [m]
$h_s$	–	strut depth, [m]	$2b$	–	distance between center line of the hull, [m]
$h_{3\%}$	–	wave height of 3% probability	$\Gamma$	–	gamma-function
$H_{DB}$	–	depth of cross structure box, [m]	$\Delta$	–	displacement, [t]
$H_{DK}$	–	vertical (box) clearance, [m]	$\eta_p$	–	payload coefficient
$H_H$	–	lower hull depth, [m]	$\eta_s$	–	propulsive coefficient
$H_{SS}$	–	strut submerged depth, [m]	$\rho$	–	fluid density, [t/m <sup>3</sup> ]
$k_W$	–	relative waterplane area	$\sum_i R_{wi}$	–	individual wave resistance of every body that is a part of the SWATH ship, [kN]
$k_0$	–	wave number, [1/M]	$\sum_i \sum_j \Delta R_{wij}$	–	additional wave resistance as a result of the wave systems interference, [kN]
$k_1$	–	coefficient of the commercial expenditures and planned contributions, includes the value-added tax and the profit of the shipbuilding plant	$\nabla$	–	volume displacement, [m <sup>3</sup> ]
$l_d$	–	ratio of the ship draft to the lower hull diameter	$\nabla_H$	–	one lower hull displacement volume, [m <sup>3</sup> ]
$l_H$	–	relative length of lower hull	$\nabla_s$	–	strut submerged volume, [m <sup>3</sup> ]
$l_{NH}$	–	hull nose length to lower hull ratio			
$l_{NS}$	–	strut nose length to strut length ratio			
$l_s$	–	slenderness coefficient of strut			
$L$	–	length of the ship, [m]			
$L_{OA}$	–	length overall, [m]			
$L_{Box}$	–	box length, [m]			
$L_H$	–	lower hull length, [m]			
$L_S$	–	strut length, [m]			
MSI	–	motion sickness indexes			
$n_a$	–	factor of the lower hull tail shape			
$n_f$	–	factor of the lower hull nose shape			
$n_h$	–	factor of the lower hull cross section shape			

## REFERENCES

1. Dubrovskiy, V. A.; Matveev, K.; Sutulo, S.: *Small Waterplane Area Ships*. Fair Lawn, Backbone Publishing Co., 2007.
2. Lee, K. Y.; Lee, D. K.; Kim, Y. D.: *A Computer-Based Design Model for Coastal Passenger SWATH Ships*. Journal of Ship Technology Research, № 2 (36), pp. 72–83, 1989.
3. Nethercote, W. C.; Schmitke, R. T.: *A Concept Exploration Model for SWATH Ships*. The Naval Architect Journal, vol. 124, № 5, pp. 113–130, 1982.

4. Pal, P.K.: *Computer-aided Design of Swath Passenger Ferries*. Pacific 2006 International Maritime Conference. Sydney, pp. 460–469, 2006.
5. Spethmann, K.: *A realised SWATH-Application as an Example for Naval Purposes*. Jahrbuch der Schiffbautechnischen Gesellschaft. Band 95., pp. 213–221, 2001.
6. Tantsjura, A.G.: *Mathematical model of a small waterplane area twin hull (SWATH) ship for optimization of its characteristics*. Collected papers of NKI, Nikolaev, Vol. 154, pp. 44–53, 1979.
7. Taha, H.A.: *Operations Research: An Introduction*. Eighth Edition. New Jersey: Pearson Education, 2006.
8. Miroyannis, A.: *Estimation of ship construction costs*. Massachusetts Institute of Technology, 2006
9. Bertram, V.: *SWATH Ship Design Formulae Based on Artificial Neural Nets*. Journal of Ship Technology, vol. 3, № 1, pp. 1–9, 2007.
10. Chapman, R.B.: *Spray drag of surface piercing struts*. AIAA/SNAME Advanced Vehicles Conference, Annapolis, July, 1972.
11. Law, A.M.; Kelton, W.D.: *Simulation Modeling and Analysis*. Third Edition. New York: McGraw-Hill, 2000.
12. Back, T.: *Evolutionary Algorithms in Theory and Practice*. New York: Oxford University Press, 1996.
13. Davis, L.: *Handbook of Genetic Algorithms*. New York: Van Nostrand, 1991.
14. Michalewicz, Z.: *Genetic Algorithms + Data Structures = Evolution Programs*. Berlin-Heidelberg: Springer-Verlag, 1996.

#### CONTACT WITH THE AUTHORS

Oleksandr V. Bondarenko, Assoc. Prof.  
 Anzhela P. Boiko, Assoc. Prof.  
 Iryna R. Seropyan, Engineer second class  
 Admiral Makarov National University of Shipbuilding,  
 Mykolayiv  
 Faculty of Naval Architecture  
 9 Geroi Stalingrada Ave, Mykolayiv, Ukraine, 54025  
 e-mail: Oleksandr.Bondarenko@nuos.edu.ua  
 e-mail: Angboyko@mail.ru  
 e-mail: Iryna.seropyan@nuos.edu.ua

# Analysing the potential for application of the phase shift method in endoscopic examination of marine engines

Zbigniew Korczewski, Prof.  
Gdansk University of Technology, Poland

## ABSTRACT



*The article presents theoretical principles of image processing in digital endoscopy which makes use of a miniaturised spectral scanner “PhaseProbe” designed by General Inspection Technologies LP, the producer of the measuring videoendoscope Everest XLG3. The technology of optoelectronic 3D mapping of the examined surface, which consists in measuring the phase shift between the emitted and reflected light waves, is briefly described. The efficiency of the “PhaseProbe” based method of endoscope measurements is compared with the earlier developed methods, such as “ShadowProbe” and “LaserDots”, which were used by the author in real conditions of diagnostic investigations of engines in operation in marine power plants. The processed results of the endoscope analysis of the broken gas turbine engine rotor blades which were earlier dimensioned using the inspection probes of “StereoProbe”, “ShadowProbe” and “LaserDots” type and now are examined by the author with the aid of the phase shift method make a valuable complement and synthesis of the discussion presented in the article.*

**Key words:** endoscopic diagnostics; phase shift method; marine engines

## INTRODUCTION

Despite rapid technological development in measuring methods used in industrial endoscopy, precise measurement of the dimensions of the detected surface defects is still a challenging problem. New opportunities in this area have been brought by various 3D scanning techniques which consist in converting the real three-dimensional shape of the examined surface into a digital form. The theoretical principles of the phenomena of light wave diffraction and interference which accompany this mapping were worked out over 200 years ago by Thomas Young<sup>1)</sup>, but only as recently as in 2010 the most modern optoelectronic devices for light emission and detection made it possible to design the measuring videoendoscope Everest XLG3 by General Inspection Technologies LP. This videoendoscope makes use of the spectral scanner miniaturised to the overall dimension of the inspection probe head of an order of 6 mm [4, 5, 6]. Moreover, a method has been developed which uses the results of the light wave phase shift

measurement<sup>2)</sup> to create a digital 3D model of the examined surface being a precise mapping of its real geometric shape and dimensions<sup>3)</sup>.

## PHASE SHIFT METHOD – 3D MEASUREMENT

A key element in the design of the inspection probe of the measuring videoendoscope Everest XLG3 in the “PhaseProbe” option is the diffraction lens mounted in the inspection probe head – Fig. 1. The design of the lens bases on a pair of symmetrically fixed diffraction gratings (2) which generate a static interference pattern having the form of halftone screens with known parameters, (i.e. gratings of dark and bright interference fringes with certain density) on the examined surface. The part of the halftone screen which is within the visual field of the image processing optics (1) is recorded on the matrix of the CCD camera as a cloud of points, the X, Y, Z coordinates of which are known. Then this

<sup>1)</sup> Thomas Young (1773-1829) – an English physicist and physiologist. Initiated the wave theory of light by stating that the light waves are transverse waves. In 1801 he discovered diffraction and interference of light waves (Young’s experiment). A detailed description of these phenomena was issued by him in 1807.

<sup>2)</sup> United States Patent No.: US 7,821,649 B2.

<sup>3)</sup> In the promotional materials issued by Everest VIT in Polish, the light wave phase shift measurement method is more briefly referred to as the “3D phase method”.

pattern is analysed and converted, in the triangulation process done by the central unit of the videoendoscope, to a grid of triangles which transform the virtual image of the examined surface into its 3D equivalent. A complementary element of the "PhaseProbe" lens is the window of the standard illumination system fed with a 75-watt high-intensity discharge arc lamp (HID) having the luminous flux equal to 4300 lumen, as the measure of its brightness [3]. The resultant colour temperature of the light source<sup>4)</sup> is approximately equal to 5000 K.

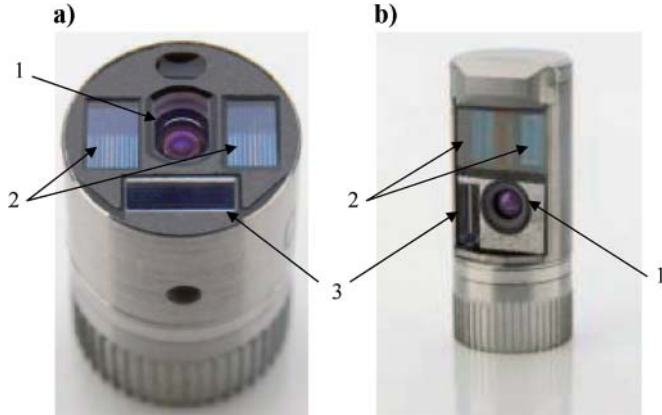


**Fig. 1.** Diffraction lens for measuring the phase shift with the aid of "PhaseProbe" of the videoendoscope Everest XLG3 [4]. **a)** straight-ahead direction of observation (field of vision angle "FOV" – 105°, depth of field "DOF" – 8-250 mm, **b)** side direction of observation ("FOV" – 105°, "DOF" – 7-250 mm). 1) image processing optics – CCD camera, 2) diffraction grating, 3) window of standard illumination system.

The standard illumination system of the videoendoscope works in the continuous mode only during routine observation of the examined surfaces. During the measurement the standard illumination system is automatically switched off to reach the maximal possible resolution of the interference fringe pattern generated by the diffraction gratings, which are illuminated in this time by electro-luminescence diodes (LED) radiating the precisely defined light wave length.

When the distance of the "PhaseProbe" lens from the examined surface changes, the halftone screens of diffraction fringes also undergo relevant changes, according to the schematic diagram shown in Fig. 2. Therefore based on the records and analyses of the deformation pattern of particular diffraction fringes we can conclude about qualitative and quantitative surface deformations of the examined object. Since the observed dimensions of the surface defects are not only the function of their real dimensions but also of the distance of the inspection head lens from the examined surface, its precise determination is a basic metrological problem in 3D measurements. For this purpose we can apply the phase shift method, initially described by Thomas Young – Fig. 3. Monochromatic, incoherent light waves (revealing the same length but different and time-dependent phase shifts) are emitted in a sequence by the light sources LED1, LED2, LED3. These light waves undergo double diffraction: initially on the gaps which equalize the vibration phases, and then, as the monochromatic coherent waves, on the diffraction grating gaps, thus creating a pattern of bright and dark interference fringes of the same intensity on the examined body surface. The bright fringes (maxima of interference) are

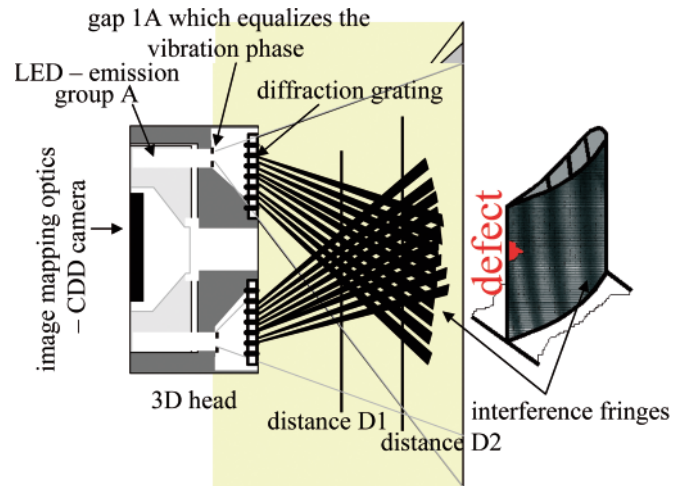


**Fig. 2.** Schematic diagram of the method of 3D measurement with the aid of the "PhaseProbe" inspection probe diffraction lens

situated in places of highest superposition of the two interfering light waves of the same length, while the dark fringes (minima of interference) – in the place of their highest difference. We can talk about so-called constructive interference, for which the condition of the equality of the light wave optical path length difference (phase difference) and a multiple of the wave length is met, or destructive interference – when the optical path length difference of the light waves is the odd multiple of the half of the light wave length. Using the nomenclature for macroscopic quantities shown in Fig. 3, and taking into account that the distance D of the inspection head lens from the examined surface is much longer than the diffraction grating constant d ( $D \gg d$ ) we can assume that the line segment AC is almost perpendicular to the optical paths  $r_1$  and  $r_2$ . That means that the angle ABC is almost equal to the angle PRO (denoted as  $\alpha$ ). Hence the optical path length difference between the interfering light waves (being the effect of the phase shift) can be given by the following formula:

$$BC = \Delta r = d \cdot \sin \alpha \quad (1)$$

Thus the condition for the appearance of the bright interference fringe on the examined surface is identical with the constructive interference condition:

$$d \cdot \sin \alpha = n \cdot \lambda \quad (2)$$

where:

$n = 1, 2, 3, \dots$  - is the order of the successive interference fringe.

For point P in Fig. 3, the phase difference of the emitted light waves is equal to their four lengths.

The condition for the appearance of the static dark fringe in interference pattern is identical with the destructive interference condition:

$$d \cdot \sin \alpha = (2n + 1) \cdot \lambda / 2 \quad (3)$$

where:

$n = 1, 2, 3, \dots$  - is the order of the successive interference fringe.

<sup>4)</sup> The colour temperature is the method of visible light evaluation used in illumination, photography and filming. The colour temperature of the source of light is assessed by comparing its chromaticity to that of the perfectly black body. The colour temperature is usually measured in Kelvin degrees, and it is the temperature to which the perfectly black body is to be heated to obtain the given colour. Contrary to a common sense, a higher colour temperature (above 5000K), means "cool" (green-blue) colours, while a lower colour temperature (2700-3000K) means "warm" (yellow-red) colours. The "cool" light is considered better in case of tasks which need concentration [www.ModernHome.pl].

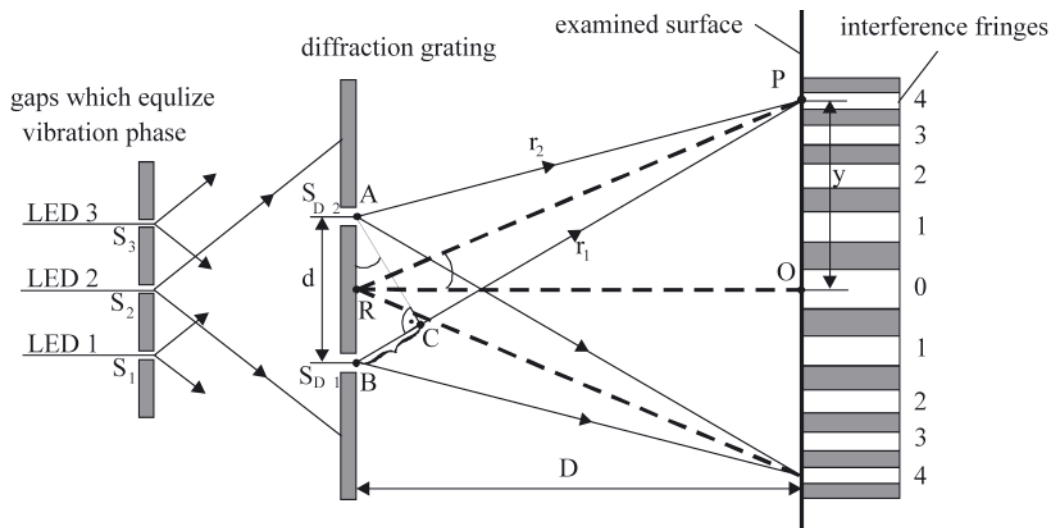


**Fig. 3.** Method of calculating the distance between the inspection head and the examined surface in the phase shift method.  $S_1, S_2, S_3$  – gaps which equalize the vibration phase,  $S_{D1}, S_{D2}, \dots, S_{Dn}$  – diffraction grating gaps (for clarity of the picture, their structure is presented in part only and is over-enlarged),  $r_1, r_2$  – optical paths of the light waves,  $d$  – diffraction grating constant (distance between two neighbouring gaps, diaphragm width),  $D$  – distance of the inspection head lens from the examined surface,  $y$  – distance of the interference fringe of a given order from the zero-order fringe,  $0, 1, 2, 3, 4 \dots n$  – order of the successive interference fringe

If the dark interference fringe was expected to appear at point P in Fig. 4, the phase difference between the emitted light waves should be equal to the odd multiple of the half of the wave length, i.e. four and half of the wave length.

Since the light beam deflection angle  $\alpha$  at which the bright fringes are created increases for each successive interference number, the value of the deflection angle sine function increases as well, thus determining the distance between particular fringes in the interference pattern. The first-order fringe is always situated opposite the diaphragm, between the gaps  $d$  and is the symmetry axis of the interference pattern.

If we manage to create a stable and sharp pattern of widely distributed interference fringes on the examined surface as a result of light wave diffraction and interference, we can measure with high precision their distances from the zero-order fringe and then, having known the length  $\lambda$  of the emitted light wave and the diffraction grating constant  $d$ , calculate the distance of the videoendoscope inspection head lens from the examined surface  $D$  using the following formula:

$$d \cdot \frac{y}{\sqrt{D^2 + y^2}} = n \cdot \lambda \quad (4)$$

Hence:

$$D = y \cdot \sqrt{\left(\frac{d}{n \cdot \lambda}\right)^2 - 1} \quad (5)$$

Of high importance, from the technological point of view, in the production of the probe lens of the “PhaseProbe” videoendoscope is precise incision of two diffraction gratings, consisting of parallel and equidistant grooves having minimal dimensions of an order of 1-2 mm, on two glass plates using a diamond cutting edge. These grooves compose the diffraction grating diaphragms which separate its optical gaps. The width of the gap is to be approximately equal to the width of the groove and, simultaneously, to the light wave length.

The sine qua non condition for obtaining a stable pattern of the interference fringes from the diffraction grating is securing a monochromatic and coherent light source<sup>5)</sup>. The light waves emitted by the LED diodes are monochromatic, which means that they have the same wave length  $\lambda$ , but they are not coherent, i.e. the sinusoidal waves of the light beam do not vibrate with the same amplitude, frequency and phase, or time-independent phase difference. To solve this problem, the incoherent source of LED light generates the waves on the diffraction gratings of the “PhaseProbe” head lens via additional gaps which equalize their phases (according to the Huygens principle<sup>6)</sup>, the waves which leave the diffraction grating gaps are generated by vibrating points situated on the same wave front, which means the presence of a constant phase difference between them).

To provide opportunities for complete and accurate 3D mapping of the examined surface, the phase shift method makes use of a system of two diffraction gratings, each of which is fed from three LED emission groups which emit, in a sequence, sinusoidal light waves mutually shifted by a phase angle equal to  $120^\circ$  (this solution secures high sharpness of the static interference pattern) – Fig. 4.

This way a rapidly changing projection and recording of two patterns (half-tone screens) of interference fringes with known density take place on the examined surface. These fringes are deformed adequately to the scale of surface deformation (they deflect left when the material has piled up and right in case of material decrement). The pattern of the light reflected from the examined surface is recorded on the CCD camera matrix.

The videoendoscope processor system (CPU) identifies and localises particular fringes. Then it performs a comparison analysis of the phase shift between the known emitted light and the reflected light. The results of the calculations, performed taking additionally into account parameters of camera calibration and the angle between the direction of the projection and that of the halftone screen recording, have the

<sup>5)</sup> This condition can be only met by laser light sources.

<sup>6)</sup> Christiaan Huygens (1629 -1695) – Dutch mathematician, physicist and astronomer. In the area of physics, he performed a number of works on optics. He formulated the Huygens principle, which says about the wave propagation in the vicinity of obstacles. His experiments confirmed the theory on the wave nature of light. He also examined the phenomenon of light refraction in various materials.

form of X, Y, Z coordinates for each camera pixel. The cloud of points created in the above manner, the number of which results from the resolution of the applied camera, makes the basis for dimensioning the detected surface defects.

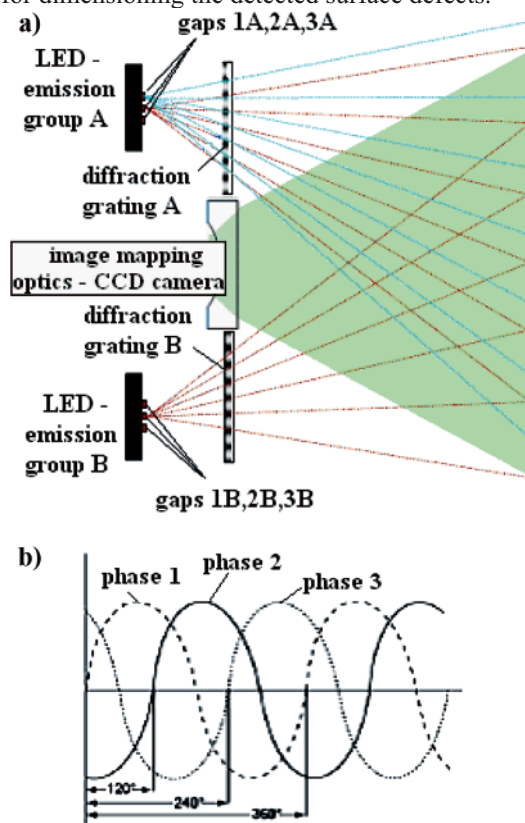


Fig. 4. Phase shift in the 3D measurement method [6]. a) interference pattern generated by the inspection head lens, b) phase shift pattern of the sinusoidal light waves emitted by three emitting groups LED 1, 2 and 3 and the diffraction gratings „A” and „B”.

## ADVANTAGES AND DISADVANTAGES OF THE 3D MEASUREMENT METHOD

The videoendoscope Everest XLG3 is equipped with a 3D measurement probe bearing the name of “PhaseProbe” which is a „flexible three-dimensional eye” of the operator. These borescopes reveal numerous advantages, which are the reason why they are in more and more frequent use. The basic advantage of the 3D measurement technology with respect to older measuring methods, such as “StereoProbe”, “ShadowProbe”, and “LaserDots” for instance, is its ergonomics. Switching from the standard (qualitative) measurement mode to the measuring (quantitative) mode does not require withdrawing the inspection probe from the inside of the examined object and changing the optic lens. Apart from complicated manual work to be done to change the lens, a big problem in those cases was finding again the earlier detected surface defect, the more so that the measuring lens reveal, as a rule, low quality of image processing of the examined surface observed from a larger distance. For instance, the depth of field for “ShadowProbe” lens is within 7-30 mm, while for “PhaseProbe” it ranges between 7-250 mm!

On the other hand, “PhaseProbe” is very sensitive to image movements (vibration) and light reflection from highly reflective surfaces. The measurement cannot be performed, in practice, when the operator does not manage to keep the tip of a flexible and a number of meters long probe still and situated at a proper angle for at least two seconds. It is extremely difficult to reach this state, even if a special probe rigidiser with a tube gripper is used for this purpose [2, 3]. From the practical point

of view it is a serious disadvantage of the “PhaseProbe” based 3D measurement method and it should be eliminated in the future by its inventors.

Taking into account high cost of purchase of the measuring set, which, despite the decreasing trend, still remains at the level of 40-50 thousand Euro, each time a decision about its purchase should have strong rational background.

When discussing possible areas of application of the measuring videoendoscope with “PhaseProbe” in marine engine diagnostics, working spaces should be mentioned for which surface wear is decisive for the efficiency of the energy conversion processes taking place in the engine. Tasks to be done in those cases include precise determination of parameters characterising the roughness of the surfaces composing the borders of the working space. This should be done over a relatively large area, which from the point of view of endoscope diagnostics requires its full numerical mapping and dimensioning. In those cases the quantitative measure of wear of the examined surface is the arithmetic mean deviation of its profile from the average line determined along a normalised elementary line segment, or the roughness height calculated using ten points of this profile.

The research experience gained in the past by the author suggests that the phase shift method can be efficiently used for diagnosing the following constructional elements:

1. For working spaces of piston engines:
  - a) cylinder bearing surface – honing grooves,
  - b) valve seats – valve set faces, wear thresholds on valve heads,
  - c) air and exhaust gas flow ducts – shape and geometric dimensions, active flow sections, condition of inner surfaces,
  - d) turbo compressor rotor assembly - shape and geometric dimensions of blades, condition of blade profile surfaces and inter-blade passages;
2. For flow parts of turbine engines:
  - a) rotor assemblies of compressors and turbines – shape and geometric dimensions of stator and rotor blades, condition of blade profile surfaces and inter-blade passages,
  - b) combustion chamber - shape and geometric dimensions of blade systems in flame tube swirl vanes, condition of inner and outer surfaces of flame tubes.

The measuring methods of “Stereo”, “Shadow” and/or “LaserDots” type provide opportunities for digital processing of stereoscope effects, which makes it possible to dimension the observed objects in such a way that they give an impression of quasi three-dimensionality with its depth, massiveness and mutual distribution. Unfortunately, their application to full (sufficiently detailed), three-dimensional mapping of larger surfaces is very limited for the following reasons:

1. The “Stereo” method: the 3D measurement bases on precise correlation of two identical characteristic points of the left and right view of the dispersed stereoscope image [4]. A problem can arise when no clear characteristic points can be found on the examined surface. The second limitation is remarkable labour consumption of the measurement which results from small angles of the visual field and depths of field of the used “Stereo” type lens, which are equal to: „FOV” – 45÷60°, „DOF” - 2÷80 mm. This prolongs the time of the measurements necessary for full three-dimensional mapping of the entire examined surface. For these reasons the “Stereo” method is more efficient in cases when only a limited number of surface points is required for measuring basic dimensions of the detected defects.

2. The “LaserDots” method: the 3D measurement consists in projecting a matrix of markers composed of a number (49, for instance) of laser beam points on the examined surface and numerical recording of their shift to the left or right of the screen as the result of surface profile changes [2]. Since the areas situated between the matrix markers cannot be interpolated in this way, any surface changes taking place in these areas cannot be dimensioned either. As a consequence, the 3D mapping of the examined surface is only limited to laser marker points, which does not secure the required resolution of the measurement.
3. The “Shadow” method has a form of single-fringe scanning and brings useful three-dimensional information only with respect to one plane of the examined surface profile within a very limited area, as a result of optical limitations of the applied “Shadow” type lens („FOV” – 50°, „DOF” – 7÷30 mm). An additional difficulty in the realisation of the 3D measurement with the aid of the “Shadow” method is the need for very precise linear positioning of the fringe with respect to the examined surface, which requires some experience. If the surface is not ideally flat, or the inspection probe lens is not directed perpendicularly, then a relatively large error can be recorded in the measurements which require referring the baseline to the points situated off the line, the line-point distance measurement for instance. For these reasons, and bearing in mind the fact that, like in the “Stereo” method, a huge-capacity processor is to be installed in the videoendoscope to solve equations of the mathematical model describing the 3D profile of the examined surface in this technique, the application of the “Shadow” method is rather limited to only dimensioning the detected surface defects [2].

### 3D MEASUREMENT TECHNOLOGY

The endoscopic examination of inner spaces of the engine using the “PhaseProbe” of the videoendoscope Everest XLG3<sup>7)</sup> can be realised in the standard mode or the measuring mode without change of inspection head lens. The standard examination is oriented on general qualitative evaluation of

the technical state of a constructional element in the engine, along with the search for and identification of failures of surface defects. If any change in the constructional structure of the examined elements is identified, an attempt is to be made to evaluate it in quantitative way using the measuring mode for this purpose. As already mentioned, it does not require any additional actions concerning the operation of the inspection probe, except moving its lens as close as possible to the examined surface, while preserving at the same time a sufficiently large depth of field (like in the measurements performed in the “ShadowProbe” and “StereoProbe” options) and an optimal visual angle (45° is the recommended angle in case of the examination of shining or spotty surfaces). A remarkable advantage of the software of the videoendoscope equipped with “PhaseProbe” is continuous analysis and adjustment of the distance between the measuring lens and the examined surface. During the measurement of the phase shift, a range-finder strip is displayed on the LCD monitor of the video-probe handset (1 in Fig. 6a). Exceeding the measuring range is signalled by a single red strip, which means that we should not make attempt to measure. When the distance of the lens from the examined surface decreases, it results in the increasing number of the displayed strips, which, what is more, change the colour to green, which means that the measurement can be done. Scanning, started by pressing the push-button *Enter* on the manual panel, initiates the process of fast (lasting about 1-2 seconds) and multiple recording of the digital image. This is the crucial action of the technology of 3D measurement (as mentioned above), which lasts until the message “Processing” is displayed on the monitor screen. After the measurement is completed, the distance of the lens from the examined surface (at the point of the active cursor) is displayed on the monitor as the MTD (Maximum Target Distance) index. Unlike the “StereoProbe” and “ShadowProbe” methods, the phase shift method does not require additional correction of the measurement depending on this distance (“Accuracy Index”). Further processing of the recorded image is done using a specialist software, GE Inspection Manager v.06<sup>8)</sup>, see Fig. 5, after completing the endoscope examination.

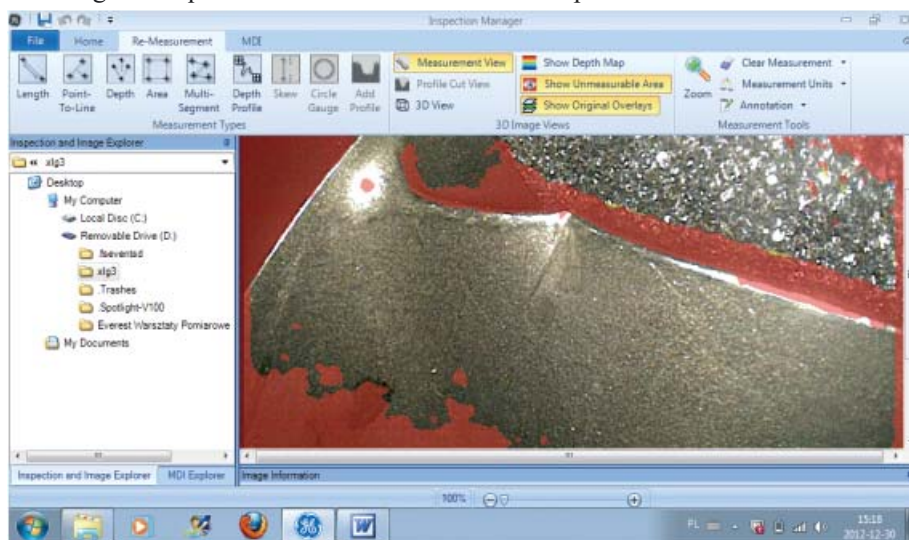


*Fig. 5. View of the computer screen after starting the programme GE Inspection Manager v.06 in the “Measurement area” mode (image parts which are not accessible for measurement as excessively distant, dark or screened by light reflection are marked red)*

- 7) Due to volume limitations of the present article, it does not include detailed constructional and parametric characteristics of the videoendoscope Everest XLG3. This information can be found on internet pages of General Inspection Technologies LP and dealers of Everest VIT endoscope equipment. Moreover, detailed descriptions of the methodology of the endoscope based diagnostic investigations of marine engines, which are also omitted here, can be found in numerous earlier publications by the author.
- 8) By courtesy of “Everest VIT GmbH Poland”.

In the “PhaseProbe” method the following measuring options are available:

- length,
- multi-segment length, length of a broken line (perimeter),
- distance of a point from the straight basic line,
- depth (convexity),
- diameter of the area marked by a circular rule,

- profile and profile map of the examined surface, as well as the 3D view of the cloud of the measuring points which map the examined surface, with options of its rotation with respect to X, Y and Z axis.

Figures 6 and 7 show the processed results of the endoscope examination of the turbine engine rotor blades using “PhaseProbe” and the phase shift method. The surface defects

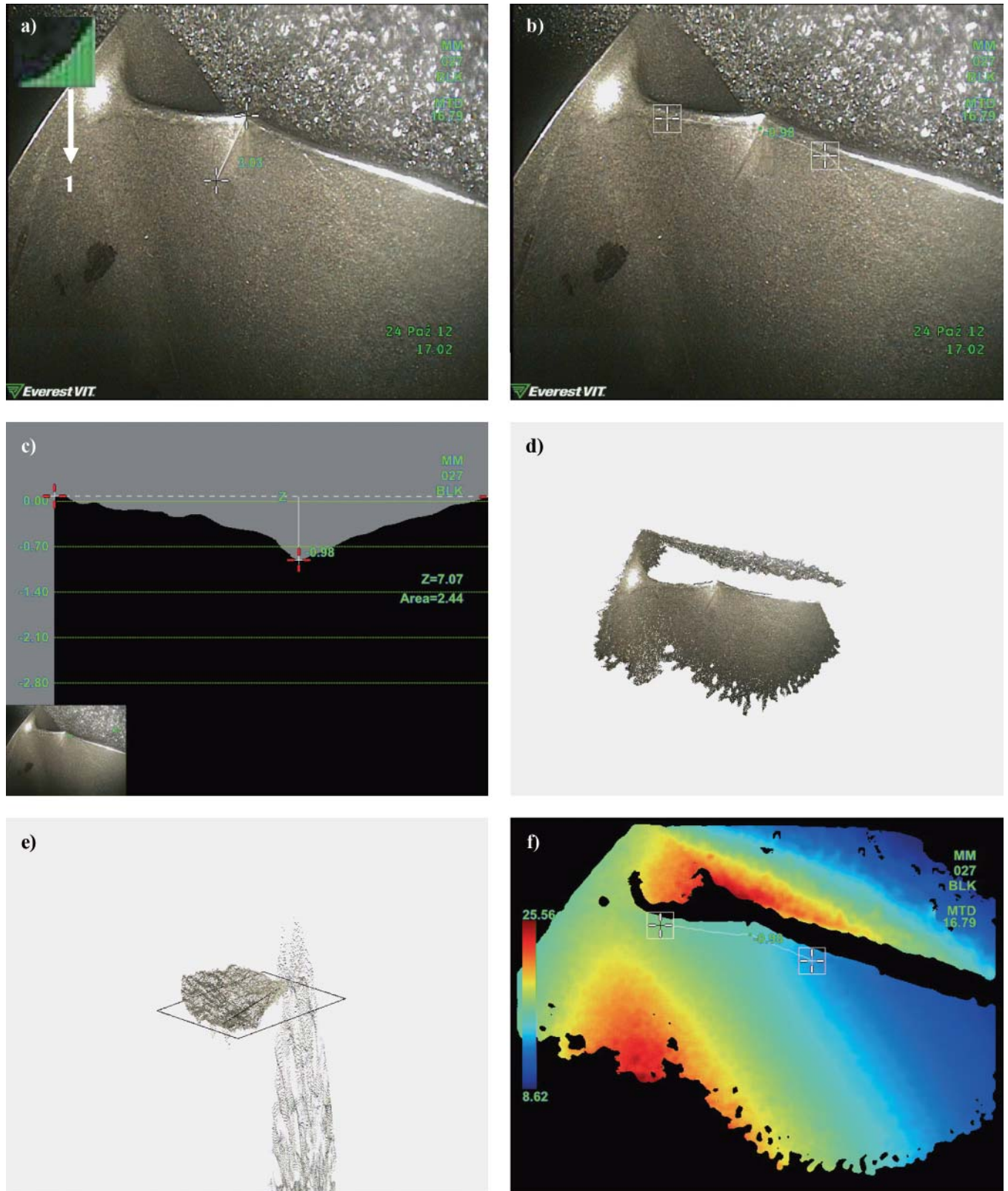


**Fig. 6.** Results of the 3D measurement of the indentation on the turbine engine rotor blade trailing edge performed with the aid of the phase shift method. *a)* 1D measurement of indentation length – 3.03 mm, at MTD index – 16.79 mm, *b)* measurement of indentation profile – 0.98 mm, at MTD index – 16.79 mm, *c)* indentation profile sector – 0.98 mm, at MTD index – 16.79 mm, distance between cursors  $Z=7.07$  mm, *d)* 3D view of the cloud of measuring points, *e)* 3D view of the cloud of points with the reference plane, *f)* dimensioned map of surface deformation profile

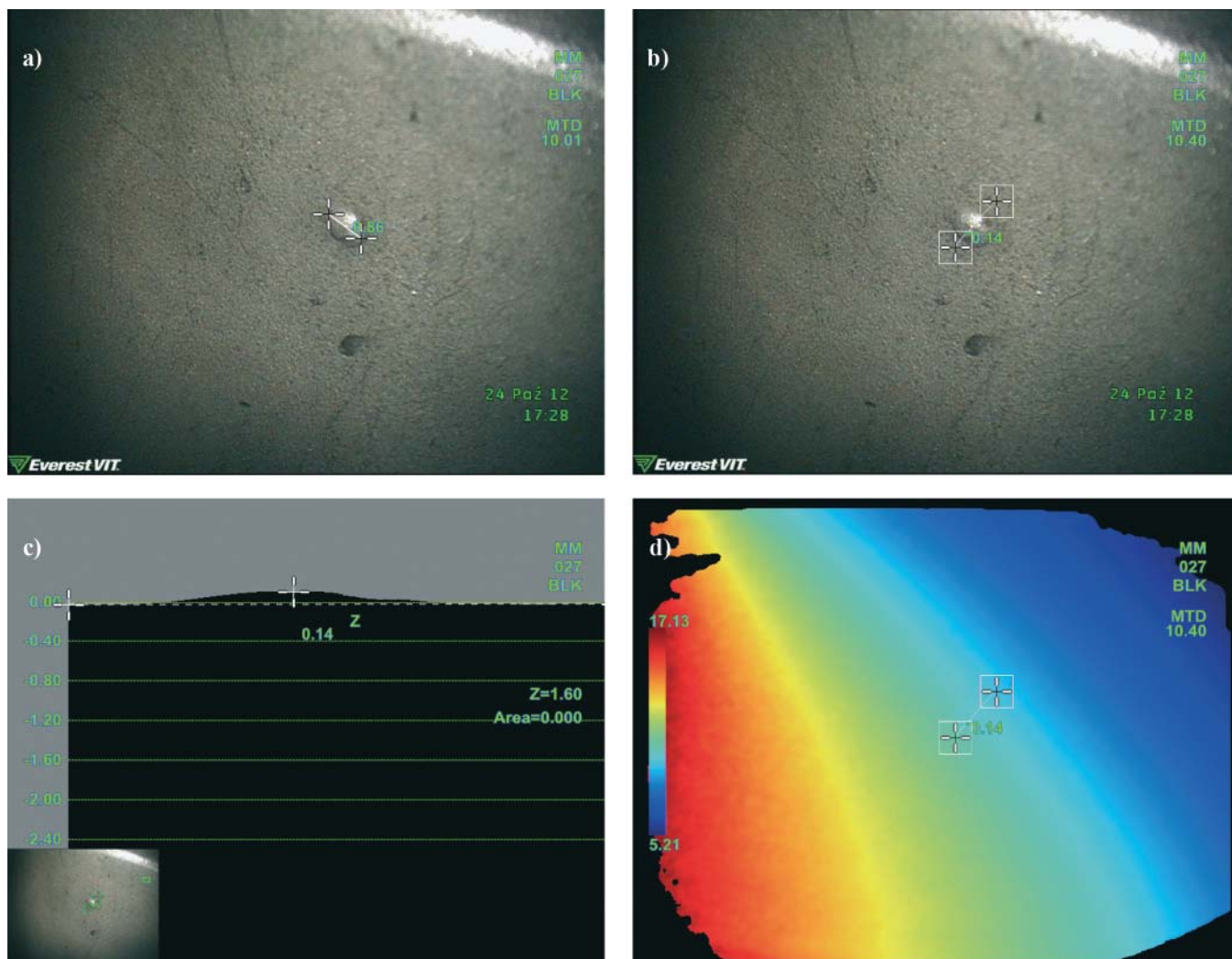


**Fig. 7.** Results of the 3D measurement of local material deposit ("eczema") in the turbine engine rotor blade trough performed with the aid of the phase shift method. **a)** 1D measurement of deposit diameter – 0.86 mm, at MTD index – 10.01 mm, **b)** measurement of deposit profile – 0.14 mm, at MTD index – 10.40 mm, **c)** deposit profile sector, distance between cursors  $Z=1.60$  mm, **d)** dimensioned map of surface deformation profile

selected for 3D processing and dimensional analysis of the recorded numerical images had been earlier examined with the aid of the measuring probes "StereoProbe", "ShadowProbe" and "LaserDots" [2]. Figures 6a and 7a show the results of standard dimensioning of, respectively, the length of indentation and point material deposit on the examined turbine blade. The examination was performed at rather large values of the MTD index: 16,79 mm and 10,01 mm. These results are very similar to those obtained in the past using other measuring methods. But completely new metrological capabilities have been brought by the 2D measurement of surface deformation profile, Figs. 6b, 6c, 7b and 7c, the three-dimensional cloud of measuring points, Figs 6d and 6e, and the dimensional map of surface deformation profile, Figs. 6f and 7d. A possibility to rotate the digital model of the examined surface which precisely models its real shape and geometrical dimensions makes the process of diagnostic inference easier and more efficient, and remarkably increases the reliability of the formulated diagnosis.

## FINAL REMARKS AND CONCLUSIONS

A basic condition for formulating a reliable endoscope diagnosis of the technical state of working surfaces in a marine engine is an opportunity to perform not only qualitative but also quantitative assessment of the detected

surface defects. New perspectives in this area are brought by digital endoscopy. Numerical image analysers cooperating with the measuring heads of "StereoProbe", "ShadowProbe", "LaserDots" and here described "PhaseProbe" type provide opportunities for numerical processing of stereoscopic effects which in turn makes it possible to dimension the observed images in such a way that they give an impression of quasi three-dimensionality, with its depth, massiveness, and mutual distribution.

Recent years show that further development of the endoscopic diagnostics of marine engines is absolutely determined by increasing technical capabilities of the more and more perfect and faultless measuring equipment. Precise and ergonomically designed digital endoscopes open new prospects for developing the diagnostic knowledge on the kinetics of working space wear in engines in operation, leaving less and less space for traditionally used optical endoscopes [1]. However, there is one *sine qua non* condition: the diagnostician should study in detail technical capabilities of the owned measuring videoendoscope and be able to use them effectively in the environmental conditions in which the diagnostic examination is performed. He also should avoid operating mistakes which would lead not only to the decrease of the life time and reliability of the very expensive measuring endoscope equipment, but also to worsened reliability of the diagnosis of the examined engine.

## REFERENCES

1. Hlebowicz J.: *Industrial endoscopy* (in Polish). Biuro Gamma. Warsaw 2000.
2. Korczewski Z.: *Endoscopy of marine engines* (in Polish). AMW, Gdynia 2008.
3. Korczewski Z.: *Analysing the ability to identify the technical and energetic state of a marine main engine piston-crankshaft system during its operation taking into account diagnostic parameters measured with the aid of methods used in endoscopic diagnostics* (in Polish). Report prepared within the framework of the research project financed by z MNiSW No N509 494638 and entitled : „Decision making based control of operation of piston-crankshaft systems in marine main engines of sea-going vessels performed with the aid of technical diagnostics and taking into account the safety and environment protection.” Gdansk University of Technology, 2010.
4. General Electric Company Inspection Technologies. *The Everest XLG3 VideoProbe System*. Operation Instruction. USA 2011.
5. General Electric Company Inspection Technologies. *The Everest XLG3 VideoProbe System*. Manual Guide. USA 2011.
6. VideoProbe System – GE Measurement & Control. USA 2011.

---

## CONTACT WITH THE AUTHOR

Zbigniew Korczewski, Prof.  
Faculty of Ocean Engineering  
and Ship Technology  
Chair of Marine and Land Power Plants  
Gdansk University of Technology  
Narutowicza 11/12  
80-233 Gdansk, POLAND  
e-mail: sek4oce@pg.gda.pl  
phone/fax: +48 58 347 21 81

# Service and maintenance of marine steam turbogenerators with the assistance of vibration diagnostics

Andrzej Adamkiewicz, Assoc. Prof.  
Jan Drzewieniecki, Ph.D.  
Maritime University of Szczecin, Poland

## ABSTRACT

*The paper discusses the problem of maintenance of the marine steam turbogenerator sets used in power systems on VLCC type oil tankers. The analysis of operation, monitoring and applied diagnostic methods of a selected turbogenerator working in the AT series waste energy system produced by Mitsubishi is presented. The analysis focuses on the applied maintenance method and its credibility and effectiveness in terms of technical assessment. The results of the performed maintenance actions and applied operational procedures making use of technical diagnostics and supported by a wider range of measurement capabilities of external service are presented and evaluated. The range of the study includes the readiness, reliability and safety of the use of turbogenerators being the result of the maintenance performed in accordance with the applied strategy of operation.*

**Keywords:** turbogenerator; vibration diagnostic; service; maintenance; condition monitoring; signal analysis

## INTRODUCTION

Steam turbines in auxiliary power units of ship power systems usually perform the function of power generators used during a sea-passage as the main source of electrical energy and cargo pump drive. They are mainly used on vessels specialising in handling, storage and transport of crude oil, such as FPSO (Floating Production, Storage and Offloading) units for instance, and in waste energy recovery systems for VLCC (Very Large Crude Oil Carrier) tankers. They are produced by such manufactures as, inter alia: Mitsubishi Heavy Industries Ltd, Peter Brotherhood Ltd., Shinko Ind. Ltd [2].

During the operation of the marine steam turbogenerators, the processes of their intensive use resulting in the production of the required electric power take place, accompanied by directly related processes of maintenance and monitoring of technical state and suitability to perform tasks, as well as functional, technical and operational readiness, while preserving technical and economic efficiency under given restrictions and disturbances. These processes include:

- identification/determination and preservation of the required technical state,
- technical/maintenance, prevention, and control services, complemented by periodical repairs [5, 9].

The above defined maintenance of steam turbines in marine power generation sets includes control methods, measures and systems used for controlling their functional and task-oriented

readiness for rational and efficient use at an expected level in given conditions and time, according to their specifications. Here, of high importance is the diagnostics performed with the use of integrated and stand-alone systems and methods of technical diagnostics. It is performed in direct contact with the turbine and plays the superior role in maintenance, with the identification and analysis of its results allowing to control the turbine operation process.

The maintenance strategy is adopted taking into account the existing conditions and resource supplies. For tankers, it is most common to use the planned maintenance strategy (PMS – Planned Maintenance System) which bases on the time-schedule (TBO – Time Base Overhauling) making use of the preventive maintenance (PM – Preventive Maintenance) and elements of technical diagnostics. At present, monitoring the correctness of turbogenerator operation consists in disassembly-free control of working processes, done via the evaluation of the generated diagnostic signals, including selected representative vibration signals, and their comparison with the reference values. The scope and credibility of the control depend largely on the used measurement equipment and qualifications of the personnel [1].

The aim of the article is to validate the proposed method of steam turbine maintenance with the modification of the set of parameters needed for monitoring the correctness of turbogenerator operation, and justify the need for monitoring the trend of changes of the parameters carrying the highest information capacity.

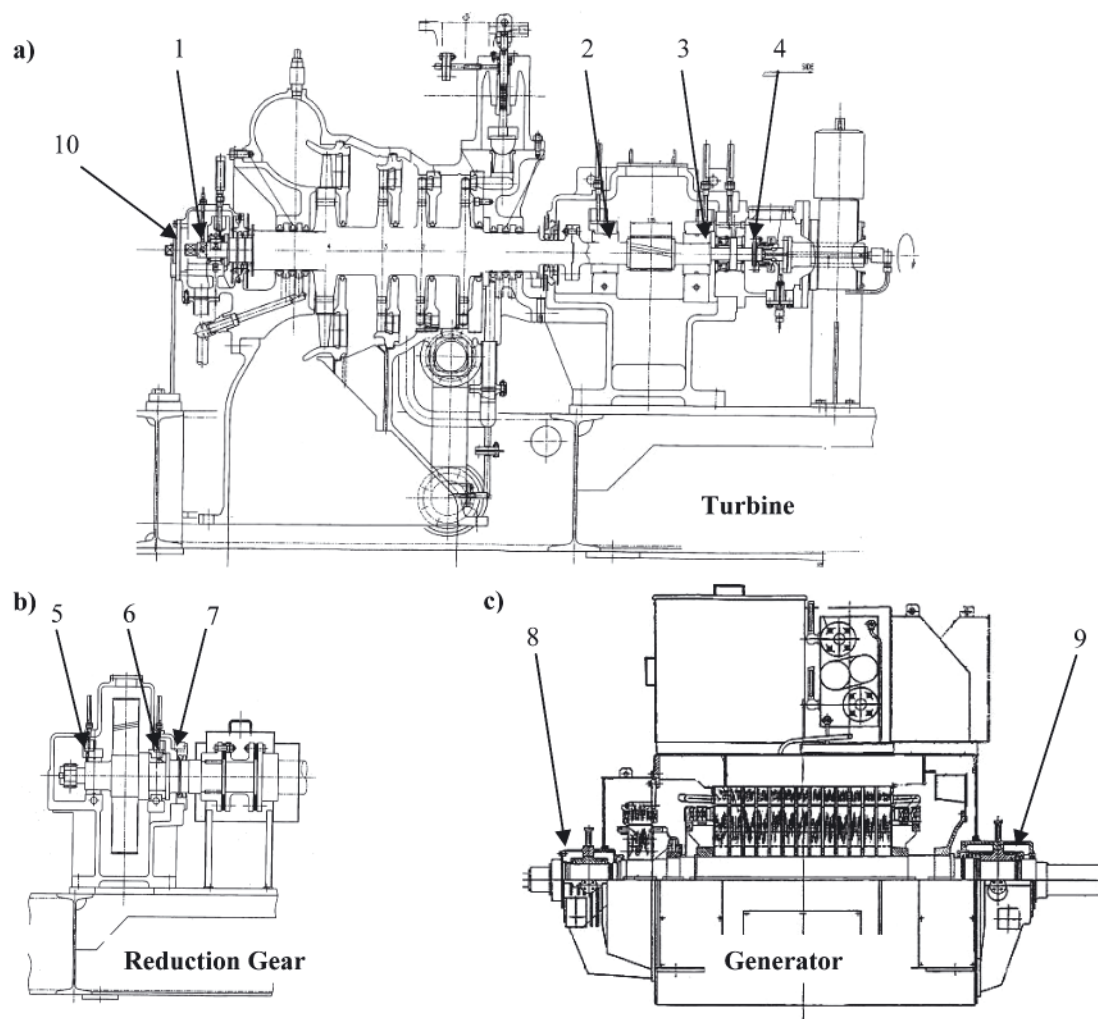


**Fig. 1.** Longitudinal sections of the turbine (a), reduction gear (b) and generator (c) with the distribution of rotor's relative vibration sensor 10 and identification of bearings in the steam turbogenerator: 1) turbine rotor bearing, 2) pinion bearing turbine side, 3) pinion bearing generator side, 4) turbine thrust bearing, 5) gear wheel bearing turbine side, 6) gear wheel bearing generator side, 7) gear thrust bearing, 8) generator bearing turbine side, 9) generator bearing free end side

## THE RESEARCH OBJECT

The procedures concerning the operation and diagnosis of ship steam turbines have been examined based on a turbogenerator with a 1100 kW horizontal, four-stage condensation steam turbine AT42M produced by Mitsubishi Heavy Industry Ltd, which drives a synchronous generator via a reduction gear. These turbogenerators are installed in the waste heat recovery systems of a VLCC tankers and work with the exhaust gas boiler co-operating in some operating states with the auxiliary boiler. Leaving the turbine, the superheated steam from the exhaust boiler flows to a vacuum condenser cooled with the seawater. The cross sections of the turbogenerator with its basic components, their bearings and the distribution of the measurement points monitored during its operation are shown in Fig. 1 [3].

As a rule, the turbogenerator is equipped with a monitoring and control system consisting of thermometers measuring local temperatures of the bearings, see Fig. 1: points 1-9, and PTR-M type thermocouples (thermo-resistance bulbs) for their remote monitoring. Thermal and flow parameters of the working media are controlled by thermometers, thermocouples and pressure gauges.

Moreover, the list of elements of the control and measurement system includes: pressure switches with the autostart of the second generator at low live steam pressure,

thermostats controlling the oil temperature with the auto start of an independent oil pump in case of low oil pressure, and turbogenerator limit controllers (safety systems) with the emergency stop in case of: oil pressure drop below the lower limit, abnormal/excessive vibrations, high vapour pressure at the inlet to the condenser, and/or an excessive turbine speed (overspeed trip), doubled by the manual emergency "stop".

The turbogenerator is also equipped with a system to measure the turbine rotor shaft vibration in relation to its bearings (relative rotor/ bearing vibration), which is the VM-5G model, produced by Shinkawa, with an eddy-current sensor shown in Fig. 1 (Section 10). The model can be, at customer's request, extended by an additional sensor. This system allows a remote visualization of displacements (vibrations) and is connected to the general marine power plant monitoring system, with the alarm set at 50 microns, as a standard, and the stop function activated when the limit of 80 microns is exceeded [3].

## OPERATIONAL SERVICE AND MAINTENANCE OF TURBOGENERATORS

The service and maintenance of marine steam turbogenerators during ship operation has the form of continuous (semi-automatic) monitoring process, with the maintenance resulting from working hours. This process consists in simultaneous

Tab. 1. Sample working parameters of steam turbogenerator working at 750 kW load

State parameter values of working media		Measured	Alarm/ limits	Emergency stop
Steam pressure [MPa]	Main	1.1	0.5	-
	1 stage	0.07	-	-
	Gland	0.01	-	-
	Exhaust [MPa]	0.101	0.087	0.04
Steam temp. [°C]	Main	326	-	-
	Exhaust	130	-	-
Lube oil pressure [MPa]	Bearings	0.46	0.29	0.04
Lube oil temp. [°C]	System	48	60	-
Medium temp. in cooler [°C]	LO IN	48	-	-
	LO OUT	40	-	-
	Water IN	43	-	-
	Water OUT	47	-	-
Bearing temp. [°C]	Turbine (1)	59	75	90
Gear bearing temp. [°C]	Pinion gear (2)	59	75	90
	Pinion gear (3)	56	75	90
	Wheel gear (5)	56	75	90
	Wheel gear (6)	58	75	90
Thrust bearing temp. [°C]	Turbine (4)	59	75	90
	Gear (7)	58	75	90
Generator bearings temp. [°C] at side of	Turbine (8)	59	75	90
	Free end (9)	59	75	90
RMS rotor's relative vibration [µm]	Turbine (10)	27	50	80

control, recording and archiving of operating parameters and working process parameters. The list of monitored measures with sample values registered at turbogenerator load of 750 kW and nominal speed of 1800 rev/min, after a total of 57,200 hours from the last overhaul (including safety thresholds for alarms and emergency stops) is given in Tab. 1.

As a rule, most parameters are recorded every four hours and archived automatically by the power plant monitoring system. This rule, however, does not include vibration measurements. In the unmanned engine room, some parameters are entered in the engine room log once a day. A comprehensive report with turbogenerator parameters is analyzed in the technical department of the ship-owner once a month. This report also includes turbogenerator working/maintenance hours, and results of the lube oil analysis. Selected elements of such a report are presented in Tab. 1.

The only element of vibration diagnostics which is part of the standard equipment of the turbogenerator is the measuring system of the bearing related displacement – the relative turbine rotor/bearing vibration. It aims at a continuous control of RMS vibration level of the running turbogenerator, with a possibility to switch the alarm on when the permissible values are exceeded, and stop the turbogenerator in case of exceeding the absolute limits. However, it is not possible to register vibration level changes as a function of time, with further trend analysis.

## OPERATIONAL OBSERVATIONS AND MEASUREMENTS

In the turbogenerator operation process, an increase of relative vibrations from 20 to 30 microns, i.e. by about 50% compared to those observed in the previous period have been recorded. This fact inspired checking the vibration levels in

full range of turbogenerator - TG load. The registered vibration levels confronted with the limits are shown graphically in Fig. 2.

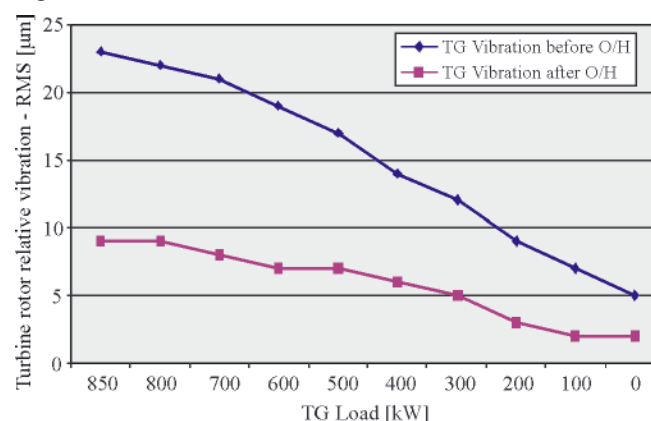


Fig. 2. RMS value changes of turbine rotor's relative vibration signal in the turbogenerator working at 1800 rev/min, for two technical states: before and after overhaul o/h

The RMS values of the turbine rotor vibrations as a function of load changes at constant nominal rotational speed increases throughout the entire load range.

The vibrations at smaller rotor speeds than the designed/nominal value were also inspected, see Fig. 3 for a quasi-static realisation of the turbogenerator start-up process. The RMS values of the turbine rotor vibrations as a function of rotational speed when the turbogenerator worked in the off-load mode also increased throughout the full speed range, which is particularly noticeable in the critical speed range of 800-1100 rev/min.

Comparing the results in the two presented cases with the data from earlier trials/delivery measurements and with the results with similar measurements done later after

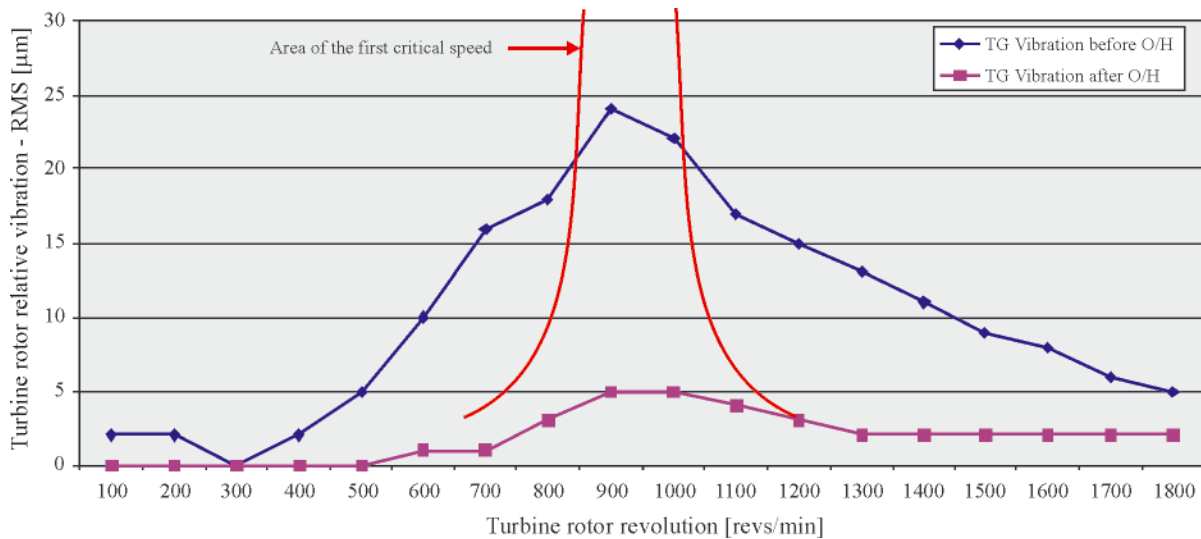


Fig. 3. RMS value changes of turbine rotor's relative vibration signal in the turbogenerator idling at various revolutions – for two technical states: before and after overhaul o/h, with the indicated area of the first critical speed

turbogenerator overhaul (see Fig. 2 and 3), a significant increase of the vibration level is observed, which suggests worsening of the technical/dynamic state of the turbogenerator. Despite the elimination of external disturbances caused by different states of ship load, hydro-meteorological conditions and/or the work of other engines and equipment, repeated measurements confirmed the increased unserviceability of the turbogenerator. Unfortunately, it was not possible to determine its location and source. Taking into consideration the location of the measuring transducer and the nature of the wear observed in the turbogenerator bearings it was assumed that a very likely reason of the noticeable increase of the vibration level was the increased clearance in the turbine bearing (Fig. 1a, point. 1).

The operating experience gained so far [8] suggests that the currently used operational methods and procedures are inadequate and insufficient. Their effectiveness and credibility depend on a proper assessment done by a human operator and his/her ability to use the archived information.

The lack of the fault development trend analysis limits the diagnosis of the turbogenerator operation to a two-state form: good condition - the state of fitness/technical ability, or poor condition - the state of unfitness/technical inability. Such an approach makes it impossible to assess the time of nearing the state of unfitness even if there is only a partial state of fitness.

Therefore the scope of the diagnosis performed for maintenance purposes needs to be extended by a trend-based

diagnostic inference making use of an additional apparatus for measuring characteristic parameters of turbogenerator vibration [4, 6].

### ASSESSING THE TECHNICAL STATE OF THE TURBOGENERATOR WITH THE AID OF VIBRATION DIAGNOSTICS

Since the manufacturing and installation technology was believed to be correct with respect to the examined turbogenerator, further research was oriented on searching for operating reasons of the observed changes of turbogenerator's dynamic state which manifested themselves by elevated bearing vibration amplitudes. The intensity and nature of such vibrations depend on, among other factors, unbalanced mass inertia, quality of the alignment, thermal deformations, and/or bearing operation conditions [6].

In this situation it was decided to perform additional measurements of turbogenerator dynamics. It was done by an external service team with the aid of the Schenk apparatus and the measuring instrument Yibroport with the module for RMS velocity measurement [7]. The absolute vibrations were measured using a piezoelectric velocity transducer with a magnetic base mounted on a flat surface of the machine bearing housing, see the diagram in Fig. 4. The measurements were done in the vertical (V), horizontal (H) and axial (A) directions.

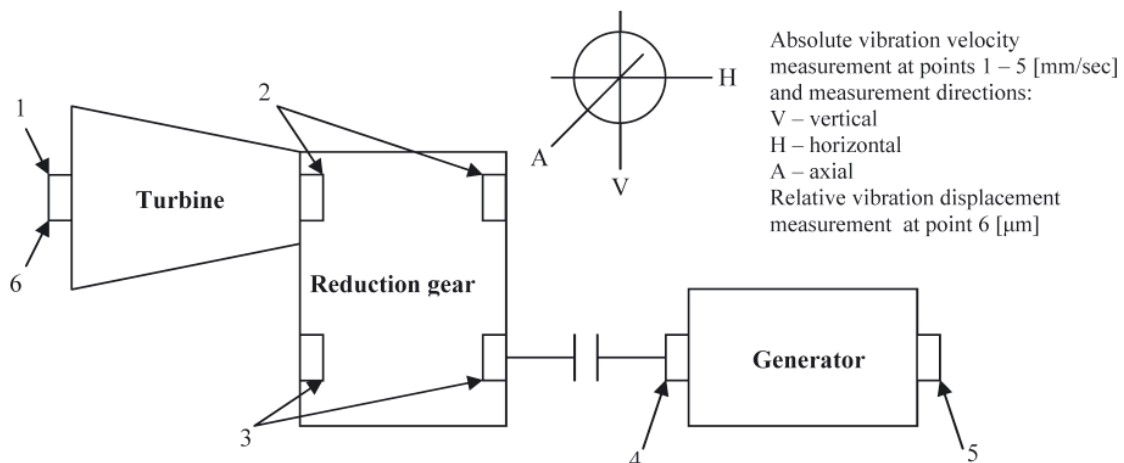


Fig. 4. Schematic distribution of vibration signal measurement points in steam turbogenerator: 1) and 6) turbine rotor bearing, 2) reduction gear pinion bearings, 3) reduction gear wheel bearings, 4) generator bearing turbine side, 5) generator bearing free end side

**Tab. 2.** RMS values of absolute bearing house vibration velocities, measuring points 1-5, and relative turbine rotor/bearing vibration, point 6, for various turbogenerator loads and nominal speed 1800 rev/min

kW	1			2			3			4			5			6
	V	H	A	V	H	A	V	H	A	V	H	A	V	H	A	V
0	0.72	1.69	1.25	0.84	1.44	0.87	0.89	1.31	0.85	0.93	0.88	1.50	1.55	0.61	1.29	5
180	0.69	1.49	1.64	0.88	1.02	1.18	0.94	1.16	1.24	1.05	0.91	1.50	1.92	0.63	1.71	9
530	0.86	1.44	1.66	0.65	1.18	1.01	0.86	1.18	0.85	0.97	0.72	0.99	1.31	0.64	1.15	17
880	2.11	1.52	<b>2.74</b>	0.90	1.07	0.93	0.99	1.21	0.76	0.86	0.66	0.90	1.20	0.68	1.03	<b>27</b>

The measured RMS values of the absolute bearing house vibration velocities, the measuring points 1-5, and of the relative turbine rotor/bearing vibration, point 6, are collected in Tab. 2 for different turbogenerator loads and the rated speed of 1800 rev/min [7].

Tab. 3 collects the reference criteria for assessing the dynamic state a turbogenerator taking into account the acceptable and limited RMS velocity values [4, 5, 6]. These criteria make the basis for creating a set of quantities being comparison classifiers. The obtained results were compared with the measured reference values from Tab. 3. The all specified measuring vibration levels were within the acceptable range, below 3 mm/s, and their values increased with the increasing turbogenerator load. However, the observed vibration levels were slightly higher than those recorded by other indications for the turbine bearings, especially in the axial direction of 2.74 mm/s. This trend was also reflected in the results of the measurements of the relative turbine rotor/bearing housing vibrations – 27 microns, recorded using a standard eddy-current displacement transducer installed by the producer. The results of the measurements have proved that the turbogenerator was in state of partial fitness with the reduced technical performance of the turbine bearing of concern. It was the reason why the verification of its technical state with the suggested need to replace the bearings was included to the scope of the incoming

overhauling after utilization of the resource hours (TBO – Time Base Overhauling).

In order to enhance the results of the diagnostic inference, the measured vibration signals were analyzed using spectral analysis and the fast Fourier transform FFT [9]. The results of the analysis of the 1<sup>st</sup> and 2<sup>nd</sup> order harmonics for various turbogenerator loads are shown in Tab. 4 [7].

The values and amplitudes of the 1<sup>st</sup> and 2<sup>nd</sup> order harmonics of particular frequencies measured at points 1-5 reveal the similar nature as in the time domain, with the elevated vibrations indicated by higher 1<sup>st</sup> order harmonics for the turbine bearing, at the 2<sup>nd</sup> order harmonics close to zero. This may indicate an increased bearing clearance - point 1, Tab. 4 and Fig. 5 a-c. On the other hand, at point 2 Tab. 4 the harmonic components of the 1<sup>st</sup> and 2<sup>nd</sup> order do not reveal increased values and do not indicate changes in the dynamic state of the turbogenerator at this measuring point.

The analysis of the harmonic amplitudes of vibration signals measured at points 3 and 4 Tab. 4 shows the increased 2<sup>nd</sup> order harmonics which may indicate a slight (permissible) unbalance of the turbine rotor. However, by comparing the frequency of the vibration amplitude waveform at the measuring point 6, Tab. 4 and Fig. 6 we can notice that there are increased values for both the 1<sup>st</sup> and 2<sup>nd</sup> order harmonics which may be associated with a slight (permissible) alignment deviation.

**Tab. 3.** Ranges of absolute vibration velocity RMS values which classify the dynamic state of turbogenerator [mm]

0 – 2.8	Small vibration. Low wear of bearing. Low noise level. State of operational suitability/technical efficiency. Good condition, no disability.
2.8 – 7.1	Noticeable vibration, often caused by increased wear of bearings. Increased noise level. Needs to find a reason, plan inspection/repair in the near future. The need for additional measurements and observations. Status of partial/incomplete technical efficiency. Sufficient state, small/partial damage. Plan the repair.
7.1 – 18	High level of noise and vibration. Too high temperature of bearings. Loss of oil film. Wear. Need to stop and perform inspection/repair. State of unfitness/technical malfunction. The state of need for improvement, dangerous damage. Do the repair.
> 18	Very high level of noise and vibration. Damage to the machine, emergency stop. The need for repair. State of unfitness/technical malfunction. Unacceptable state, catastrophic damage. Immediately stop the engine. Turbogenerator should be stopped automatically by safety systems.

**Tab. 4.** 1<sup>st</sup> and 2<sup>nd</sup> order harmonics of the absolute vibration velocity signals recorded at measuring points 1-5 for different turbogenerator loads and revolutions 1800 rev/min

kW	H	1			2			3			4			5		
		V	H	A	V	H	A	V	H	A	V	H	A	V	H	A
0	1N	0.13	0.13	0.37	0.23	0.27	0.10	0.13	0.37	0.10	0.71	0.29	0.54	0.34	0.20	0.47
	2N	0.10	0.02	0.03	0.01	0.03	0.01	0.17	0.61	0.34	1.15	0.37	0.78	0.81	0.34	0.68
180	1N	0.37	0.27	0.82	0.37	0.27	0.06	0.30	0.34	0.30	0.20	0.17	0.78	0.27	0.06	0.41
	2N	0.03	0.03	0.06	0.03	0.03	0.03	0.47	0.47	0.54	0.34	0.27	1.26	0.47	0.13	0.47
530	1N	0.55	0.40	0.88	0.26	0.14	0.20	0.47	0.39	0.60	0.55	0.2	0.13	0.89	0.13	0.57
	2N	0.1	0.01	0.01	0.01	0.01	0.01	0.10	0.58	0.13	0.2	0.27	0.4	0.15	0.08	0.08
880	1N	1.4	0.52	1.9	0.46	0.28	0.32	0.48	0.50	0.46	0.64	0.33	0.42	0.78	0.32	0.39
	2N	0.01	0.01	0.01	0.01	0.01	0.01	0.07	0.43	0.05	0.05	0.17	0.04	0.11	0.08	0.09

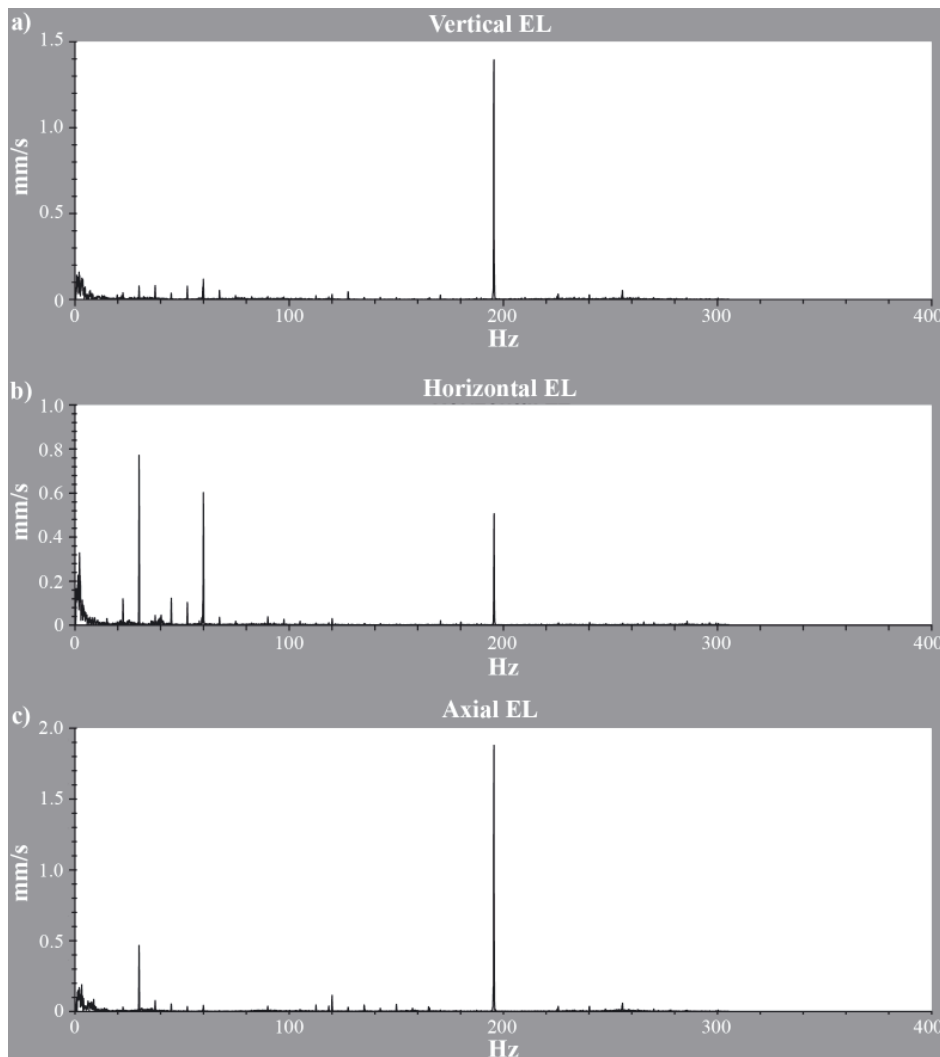


Fig. 5. Harmonic analysis of vibration signals measured in turbine rotor bearing at 880 KW: a) vertical direction (V), b) horizontal direction (H), c) axial direction (A)

The spectral analysis of the waveforms and the 1<sup>st</sup> and 2<sup>nd</sup> order harmonic components confirm the conclusion formulated after time domain analysis about the technical state of the turbogenerator, in particular the state of the turbine rotor bearing, and the need for its overhaul. It also made it possible to infer about the dynamic state of other bearing nodes – other measuring points. The formulated conclusions and operational decisions were verified during turbogenerator overhaul in a shipyard.

## TURBOGENERATOR REPAIR INSPECTION

During the verification, traces of normal/operational wear were observed on both active and passive reduction gear wheels and in their bearings, and also in the generator bearing on the turbine side and in the turbine and gear thrust bearings. The results of relevant clearance measurements done in these

bearings are given in Tab. 5, entries 2-8, the presented values are within the design ranges [3]. However, significant traces of wear were observed on the lower shell in the turbine rotor bearing, see Fig. 7a, which was confirmed by visual/organoleptic inspection and measurement of bearing clearance, see Tab. 5, position 1. These results slightly exceeded the acceptable values. In the generator bearing, traces of wear were observed on the edges of the outer working surface of the upper shell on the free end of the shaft, see Fig. 7b. This may indicate a slight misalignment between the generator and reduction gear shafts on the side of the passive wheel, as a possible consequence of relatively low precision of assembly. The measured values of the bearing clearance were equal to the design dimensions given in Tab. 5, position 9. Fig. 7 shows the observed traces of operational wear on the working surfaces of the turbogenerator bearing shells which were replaced with new ones during the dry-dock overhaul.

Tab. 5. Design clearances and clearance measurements in AT42M type turbogenerator journal bearings

Bearing name	Design clearances [mm]		Measured clearances [mm]	
	Turbine side	Generator side	Turbine side	Generator side
Turbine rotor bearing (1)	0.100 – 0.166		0.175	
Pinion bearings (2 and 3) Reduction gear	0.328 – 0.365		0.330	0.290
Wheel bearings (5 and 6) Reduction gear	0.125 – 0.175		0.160	0.175
Generator bearings (8 and 9)	0.175		0.170	0.175
Thrust bearings (4 and 7)	0.250 – 0.300	0.300 – 0.524	0.300	0.340

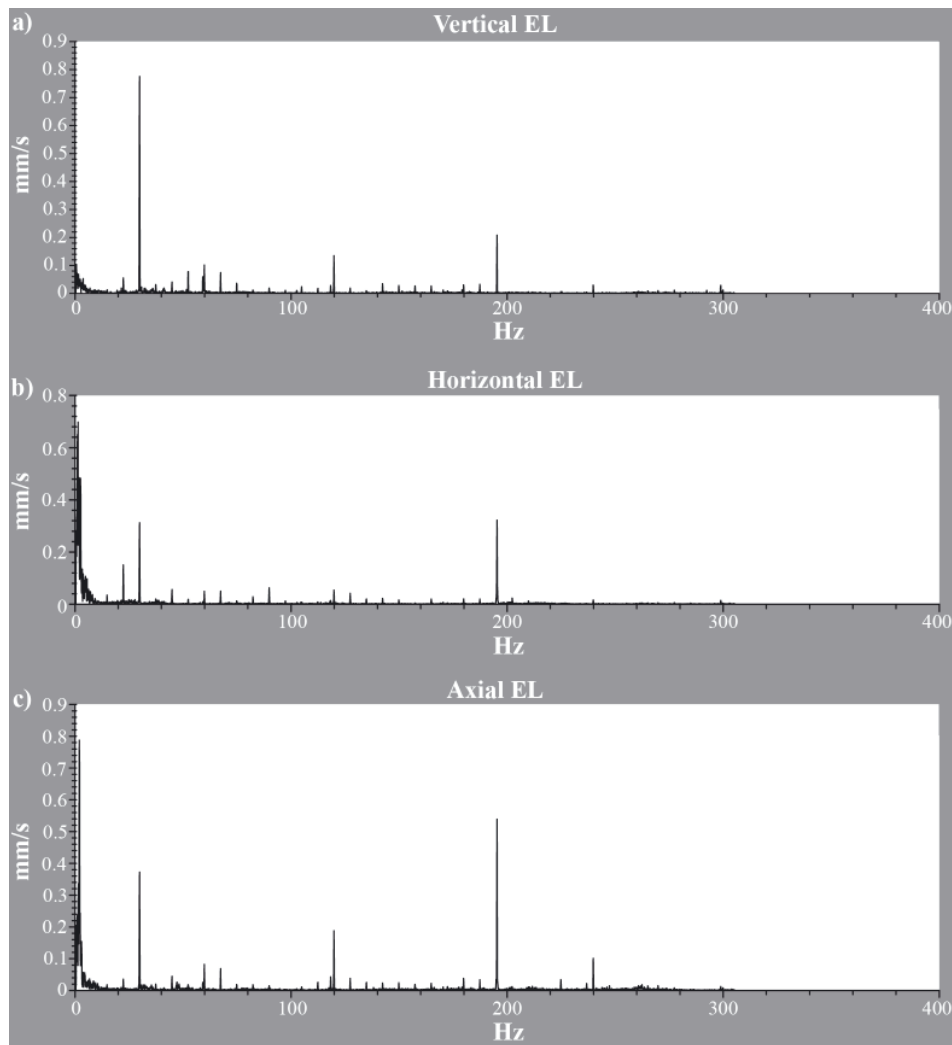


**Fig. 6.** Harmonic analysis of vibration signals measured in generator free end bearing at 880 KW:  
*a)* vertical direction (*V*), *b)* horizontal direction (*H*), *c)* axial direction (*A*)

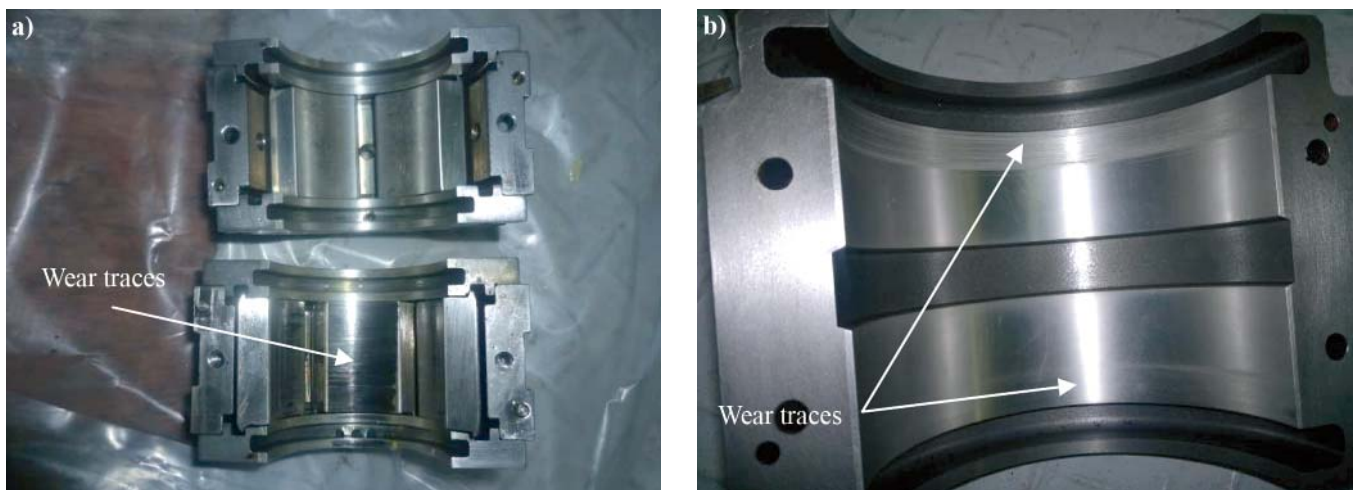


**Fig. 7.** Operational wear traces in turbogenerator type AT42M bearings: *a)* turbine rotor bearing 1 steam exhaust side; *b)* bottom half of generator free end bearing 5

Taking into account the values of the recorded clearances (Tab. 5 position 1 and 9), the state of the bearings 1 and 5 (Fig. 4), was classified as partially fit and conditionally accepted for further use/operation. However, due to the specific nature of the whole turbogenerator as the “critical equipment” for readiness task in a safe and trouble-free operation of the ship, and also the bearing themselves as critical spare parts on board, a decision was made to replace these bearings with new ones.

Within the framework of comprehensive evaluation of the technical state of turbogenerator components, the measurements of turbine shaft runout in specific control planes were done. The measurements showed slight deviation of the measured values from zero, of an order of  $\pm 0.02$  mm, thus proving the absence of shaft deflection due to thermal deformation. The measurements of the turbine rotor unbalance which were done at the dynamic balancer indicated the unbalance values not

exceeding 10 grams: 8.0 grams in the turbine bearing support area, and 6.4 grams for the reduction gear of the active wheel bearing. These values were reduced to less than 1 gram, i.e. 990 mg and 239, respectively [7].

## CONCLUSIONS

- The confrontation of the results of technical state verification of the examined turbogenerator with the analysis of the vibration measurements shows that they are compatible. This justifies the opinion about correctness of the diagnostic inference based on the measured vibration signals in both the time and frequency domains. Moreover, the vibration diagnostics turned out to be a useful and reliable source of information on the dynamic state of the turbogenerator and its components.
- This conclusion was confirmed by further measurements performed after completing the overhaul and assembling the turbogenerator and its components, including the coaxial connection of gear and generator shafts - checking of coupling alignment, which showed a significant decrease in the relative turbine shaft/bearing vibrations (the RMS change curves after overhaul in Fig. 2 and 3). Absolute vibration measurements after repairs were not performed – this decision was made based on the results of the overhaul and subsequent turbogenerator operational performance reports.
- The presented method of turbogenerator service and maintenance indicates that it is advisable to include the trend analysis of changes of its technical components as an important tool in decision-making processes. This would require supplementing the method by predictive maintenance models of turbogenerator operation.

## BIBLIOGRAPHY

1. Adamkiewicz A., Rutkowski J.: *Operational evaluation of informational capacity of the operational supervision system of the auxiliary steam turbine on a FPSO type vessel* (in Polish). *Postępy Nauki i Techniki* nr 11, Lublin 2011.
2. Adamkiewicz A., Michalski R., Zeńczak W: *Selected problems of energy conversion in marine power systems* (in Polish). Wydawnictwo KAPRINT, Lublin 2012.
3. *Instruction Book for Main Turbogenerator Turbine type AT42M*. Mitsubishi Heavy Industry Ltd., Nagasaki 15.09.2004.
4. Kozak M.: *Steam turbine structure and maintenance control methods* (in Polish). Wydawnictwo KAPRINT, Lublin 2008.
5. Niziński S., Michalski R.: *Maintenance of vehicles and machines* (in Polish). Wydawnictwo Instytutu Technologii Eksploatacji, Radom 2007.
6. Orłowski Z.: *Diagnostics in steam turbines' life* (in Polish). Wydawnictwo Naukowo-Techniczne, Warszawa 2001.
7. *Service and Dynamic Balancing Reports*. Viking Engineering Ltd., Singapore 13.06.2012.
8. *Summary of Marine Engine Trouble Cases, Auxiliary Turbine Engine 01.1989 – 12.2003*. All Japan Seaman's Union, Tokyo 2004.
9. Żółtowski B.: *Machine dynamics investigations* (in Polish). Akademia Techniczno-Rolnicza, Bydgoszcz 2002.

## CONTACT WITH THE AUTHORS

Andrzej Adamkiewicz, Assoc. Prof.  
Jan Drzewieniecki, Ph.D.  
Department of Condition Monitoring & Maintenance  
of Machinery  
Maritime University of Szczecin  
ul. Podgórna 52/53,  
70-205 Szczecin, POLAND  
tel.: +48 91 4338123, fax: +48 91 4318542  
e-mail: a.adamkiewicz@am.szczecin.pl  
e-mail: j.drzewieniecki@am.szczecin.pl

# Multi-stage magnetic-fluid seals for operating in water – life test procedure, test stand and research results

## Part II

### Results of life tests of multi-stage magnetic - fluid seal operating in water

Leszek Matuszewski, Ph.D.  
Gdansk University of Technology, Poland

#### ABSTRACT



*The edge criteria for magnetic-fluid seals durability research were described in previous article [24] and now the tests results are presented. The tests were made with three magnetic fluids using various magnets quantity in magnetic assemblies. If values obtained in the repeated test deviated by more than 10 % from results of the first test an additional control test was made for final characteristics. The characteristics are: critical pressure, critical motion velocity and working life of the seal. The test stands were prepared for particular seals dimensions and results of tests are presented in the form of tables, cross section draws and diagrams. In conclusion one can see that multi-stage magnetic-fluid seals could be efficiently used in water for rotating shaft seals in a limited range of motion velocity and cycles quantity. Nevertheless a particular applications can be provided by magnetic-fluid seals only.*

**Keywords:** shaft sealing; magnetic fluid; utility water; seal durability; critical pressure; critical motion velocity

#### INTRODUCTION

This paper presents the most significant results of the research projects performed in the years 2009÷2012. All the projects were carried out on the test stands located at the Faculty of Mechanical Engineering and Robotics, Mining and Metallurgy Academy (AGH), Cracow, Poland.

As described in the first part of the paper [24] the research methodology of the performed projects ensured determination of static penetration pressure and limiting working speed of the seal for each of its tested versions. Each of the tests introduced important information which made it possible to draw seal life curve and determine the largest motion speed at which failure-free operation (lack of leakage) is possible up to the basic number of cycles (equal to 1 million rotations), assumed for the seal.

This author conducted the research projects on the application of magnetic fluid (MF) seals operating in utility water in collaboration with the Laboratory of Seals and Application of Magnetic Fluids, AGH, [12, 13, 14]. The tests performed on the research stand adjusted to operation of seal in liquids [15] showed that application of some commercial magnetic fluids to MF seals being in direct contact with water in operational conditions typical for ocean engineering, mainly to driving systems, is possible. In the tests which had an utilitarian character, multi-stage MF seals representing models of real MF

seals were used and their operational conditions were limited to the selected technical task. In this paper, due to a limitation of its volume, only some example diagrams are presented.

#### 1. RUN OF THE TESTS

In the tests in question the MASTL1 – V2 test stand was used. The stand contains a special test head intended for realizing the assumed research aims, driving system composed of an electric motor and its controller, as well as a measurement system composed of gauges and transducers for measuring pressure, motor's torque and operational temperature. The stand is fitted with multi-channel measuring instruments for measurement data acquisition, processing and recording. Their detailed description was given in the first part of the paper [24].

##### 1.1. Tests of seal critical pressure

The tests of seal static critical pressure were performed in compliance with the procedure described in the paper titled “Multi-stage magnetic-fluid seals for operating in water – life test procedure, test stand and research results, Part 1.” [24]. The pressure in the test chamber was gradually increasing up to occurrence of penetration of MF seal. The sealed medium was pure utility water. Value of seal static critical pressure is

the basis for determining pressure values to be set to obtain the appropriate values of the relative pressure  $p_r/p_{krl} = 0.8, 1.6, 2.4$ , complying with the test programme. The tests were conducted for three magnetic fluids: FLS 040.040, FLA 002.25, FLA 003.45, with using 14 magnets in the magnetic system, and additionally with 10 and 18 magnets for the fluid FLA003.45. In all the tests the nominal gap height for magnetic fluid was equal to 0,1 mm at 100µl magnetic fluid dosage applied to each of the sealing stages. Each test was repeated. If values obtained in the repeated test deviated by more than 10 % from results of the first test an additional control test was made.

In Fig. 1.1 the example diagram of pressure run during determination of statical critical pressure is presented.

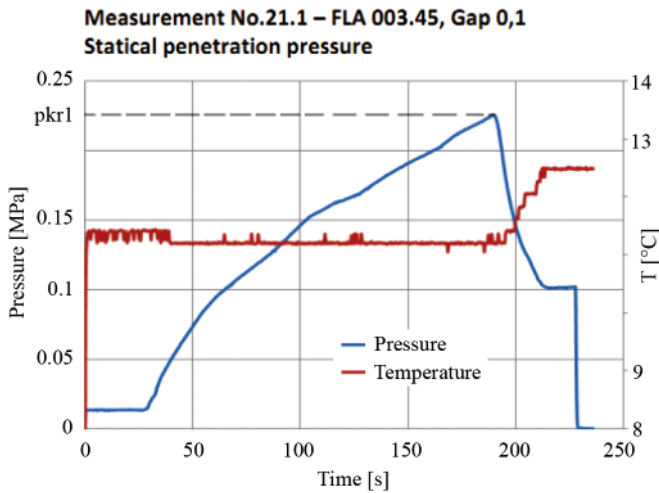


Fig. 1.1. The example diagram of determination of statical penetration pressure for the fluid FLA 003.45 at 0.1 mm gap height and three-stage sleeve: the pressure curve peak value represents the value of the statical penetration pressure (for the whole three-stage seal)

### 1.2. Tests of critical motion speed of MF seal

The tests of MF seal critical motion speed were performed to determine the lowest value of motion speed at which loss of sealing capability of a seal occurs “immediately”. Information on critical motion speed value makes performing seal life test easier. The tests were conducted with gradually increasing speed in compliance with the procedure described in the first part of the paper, for the magnetic fluids: FLS 040.040, FLA 002.25, FLA 003.45, and with the use of the seals of 0.1 mm nominal gap height and 100 µl dosage of magnetic fluid applied to each sealing stage. According to the test programme relative pressure values were used. Each measurement was repeated to eliminate random results.

For FLA003.45 fluid additional measurements were made at the relative pressure values  $p_w = p_r/p_{krl} = 0.8, 1.6, 2.4$  and 10 and 18 permanent magnets used in the magnetic system.

In Fig. 1.2 is presented the example diagram of run of determination of limiting penetration speed recorded during the tests.

### 1.3. Life tests of MF seal

The MF seal life tests were carried out to determine the seal motion speed at which MF seal life for the assumed seal operating conditions and gap geometry would be equal to 1mln cycles (number of rotations). To determine one-million-cycle life it was necessary to perform series of measurements at constant, but lower and lower for each successive measurement, seal motion speed. The series of measurements were started from a motion speed equal or close to a seal critical motion speed specific to a seal under the test. The tests were conducted

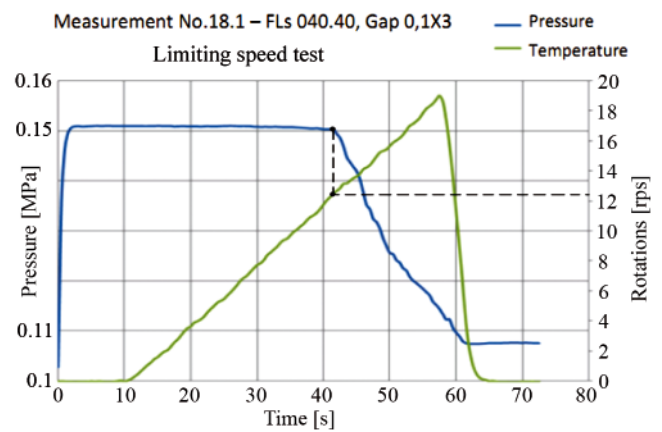


Fig. 1.2. The example diagram of determination of the seal critical speed for the fluid FLS 040.40 at 0.1 mm gap height and three-stage sleeve. The instance of exceeding the critical speed is signalled by sudden drop of pressure

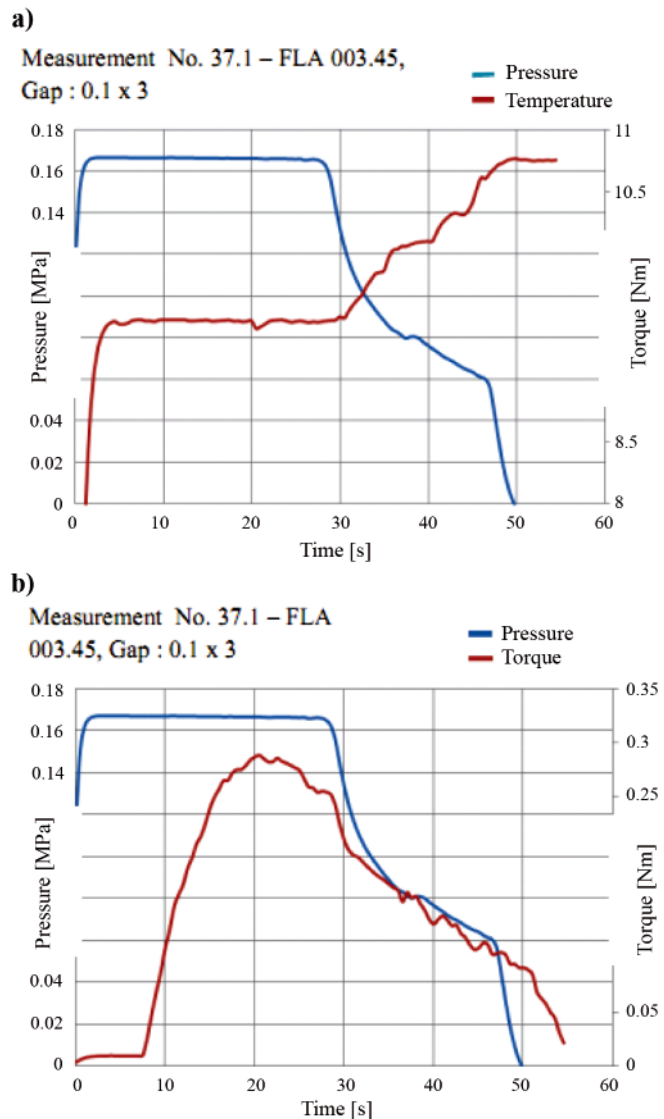


Fig. 1.3. The example diagram of pressure and temperature runs in function of duration time counted from the instant of disclosure of a leakage. The MF seal with FLA 003.45 magnetic fluid at 10 rps; the relative pressure of 2.4, the gap height of 0.1 mm with 3 edges; a) temperature change of the seal during its leakage, b) change of drag- to-motion moment of the seal during its leakage.

for three magnetic fluids: FLA 002.25, FLS 040.040, FLA 003.45, and with the use of the seals of 0.1 mm nominal gap height and 100 µl dosage of magnetic fluid applied to each

sealing stage. The relative pressure values  $p_w = p_r/p_{kri} = 0.8, 1.6, 2.4$  were used. For FLA003.45 fluid additional measurements were performed with 10 and 18 permanent magnets used in the magnetic system in accordance with a respective programme.

The life criterion will be satisfied if during the test at an assumed shaft rotational speed no leakage is observed after one million of cycles, then the test is stopped and the speed is considered to be corresponding to one-million-cycle life. In Fig. 1.3 the example diagrams of run of MF seal life test, is presented. In Fig. 1.3a is shown an increase of temperature at the instant of leakage, caused probably by penetration of water of a higher temperature into cooled zone of the seal. In Fig. 1.3b is shown a drop of moment of drag to motion of the seal at the instant of leakage, caused by loss of the magnetic fluid from the seal. During this test the leakage was very intensive.

## 2. RESULTS OF THE TESTS

The test results are collected in the form of tables, curves and diagrams. In the tables are given values of test parameters and measurement results obtained during the tests, and on the curves and diagrams are shown values of the achieved results in function of the parameters of the tested seals or of test running time.

The test results for three kinds of the tested magnetic fluids are elaborated separately for each of the standard research tests:

- total statical critical pressure of a seal,
- critical motion speed of a seal,
- long-term operation speed of a seal.

On the curves and diagrams are presented the obtained values in function of particular testing factors, as well as in the form of comparisons of various parameters of the tests.

All the tests were conducted with the use of the same sleeve with three sealing stages, at 0.1 mm gap and 100  $\mu$ l dosage of magnetic fluid applied to each of the gap. A variable design parameter was number of permanent magnets in the magnetic system: 14 magnets were used for three kinds of the tested magnetic fluids, and additionally 10 and 18 magnets in the tests with FLA 003.45 magnetic fluid.

### 2.1. Test results of total statical critical pressure of the seal

In Fig. 2.1 are shown the penetration pressure values for the seal with three sealing stages, obtained from the tests with three tested magnetic fluids. The penetration pressure measurements were made after one hour of fluid stabilization in the seal.

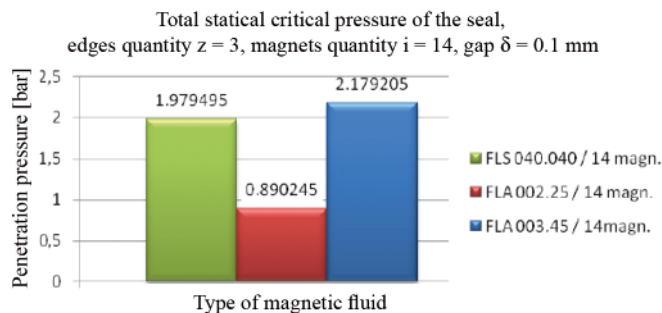


Fig. 2.1. Comparison of values of the total statical critical pressure for three tested magnetic fluids

In the successive series of the tests were determined penetration pressure values for the seal of three sealing stages,

obtained for FLA 003.45 magnetic fluid from the testing with the use of different number of permanent magnets in the sealing system. In all the tests 100  $\mu$ l dosage of magnetic fluid was applied to each sealing stage.

### 2.2. Test results of critical speed of the seal

In Tab. 1 are collected the critical speed test results at different values of relative pressure for three magnetic fluids and 14 magnets used in the magnetic system of the seal.

Tab. 1. Test results of critical speed for MF seal. Number of permanent magnets in the magnetic system: 14

Relative pressure $p_r/p_{kri}$	FLA 00.2.25	FLA 003.45	FLS 040.040
	Critical speed [rps]		
0.8	> 100	> 100	90
1.6	80	83	47
2.4	76	10	12

In Fig. 2.2 are shown the results of limiting speed tests for three magnetic fluids at the relative pressure  $p_w = p_r/p_{kri} = 0.8$ , with 14 permanent magnets.

Critical speed values for three magnetic fluids. Relative pressure  $p_r/p_{kri} = 0.8$ , edges quantity  $z = 3$ , magnets quantity  $i = 14$ , gap  $\delta = 0.1$  mm, liquid volume  $v = 100$   $\mu$ l

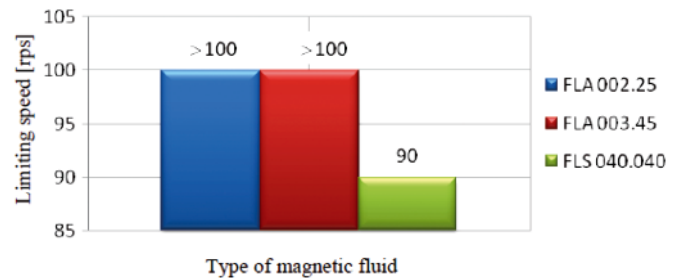


Fig. 2.2. Comparison of limiting speed values for the tested magnetic fluids at the relative pressure  $p_w = p_r/p_{kri} = 0.8$ , and with 14 permanent magnets used in the sealing system

In the case of two magnetic fluids the critical speed exceeded the value of 100 rps at the relative pressure  $p_w = p_r/p_{kri} = 0.8$ . Because of mechanical limitations in operation of the test stand it was not possible to increase the rotational speed of the seal in question. In the successive test series were obtained measurement results of critical speed for three magnetic fluids at the relative pressure  $p_w = p_r/p_{kri} = 1.6$  and 14 magnets used in the sealing system, and the critical speed values of the tested fluids were compared to each other at the relative pressure  $p_w = p_r/p_{kri} = 2.4$  and 14 magnets.

When comparing the critical speed values obtained for the magnetic fluids at the relative pressure  $p_w = p_r/p_{kri} = 2.4$  attention should be paid to significant differences between real pressure values set in the test chamber. During the tests with FLA 003.45 and FLS 040.040 fluids the pressure in the test chamber was over twice higher than that assumed in the tests with FLA 002.25 fluid. It indicates significant influence of absolute pressure value on operational efficiency of MF seals working in water. Influence of magnetic field on limiting speed for FLA 03.45 fluid was tested additionally at the relative pressure  $p_w = p_r/p_{kri} = 1.6$  and different number of magnets in the magnetic system of the seal. It was demonstrated that along with increasing number of magnets installed in the test head (i.e. increasing magnetic field intensity) critical speed value for FLA 003.45 fluid also increases.

Tab. 2. Results of seal life tests in function of seal motion speed for FLA 002.25 magnetic fluid

Stabilization time: 1h	Kind of magnetic fluid	Statical critical pressure of the seal: total value /value per one stage. $p_{krIII}/p_{krl}$ [MPa]	Number of magnets in the sealing system
Nominal gap height: 0.1 mm	FLA 002.25	0.0890245/0.0296748	14
Relative pressure (set pressure) $p_w = p_r/p_{krl}$ ( $p_r$ ) [MPa]	Critical speed [rps]	Rotational speed [rps]	Number of rotations to leakage (time of operation [h])
0.8 (0.023)	over 100	100	1700 (0.00472)
		80	1840 (0.00639)
		60	99936 (0.4627)
		45	2251800 (13.9) No leakage. exceeded 1mln rotations
1.6 (0.047)	80	80	80 (0.05383)
		70	2450 (0.00972)
		50	171780 (0.2071139)
		30	257040 (2.38)
		20	388800 (5.4)
		10	648000 (18)
		5	100000 (55.6) No leakage. exceeded 1mln rotations
2.4 (0.071)	76	76	356 (0.02583)
		70	3000 (0.01389)
		30	5400 (0.05)
		5	34200 (1.9)

Notations which appear on the below presented drawings, are explained on the example of Fig. 2.3:

FLA 002.25 - symbol of the tested magnetic fluid

$z = 3$  - number of stages of the test sleeve

$\delta = 0,1$  - height of the test gap, [mm]

$p_r = 0.023$  - value of the set operational pressure, [Mpa]

$p_r/p_{krl} = 0.8$  - the relative pressure equal to 0.8, the ratio of the set operational pressure  $p_r$  and the statical critical pressure per one stage,  $p_{krl}$ , (in the case of three-stage sleeve: 1/3 of the total penetration pressure)

353532.6 - full distance passed by the seal up to leakage occurrence, [m].

### 2.3. Life test results of the seal with the basic number of permanent magnets in the magnetic system (equal to 14 pieces)

In Tab. 2 are collected the life test results of the seal with FLA 002.25 magnetic fluid and 14 magnets installed in the head. Number of rotations to leakage constitutes a seal life measure.

In Fig. 2.3 is presented the diagram of number of rotations to leakage in function of motion speed of the seal with FLA 002.25 magnetic fluid at the relative pressure  $p_w = p_r/p_{krl} = 0.8$ . On the diagram is shown the trend line in the form of the function:

$$y = -6.47\ln(x) + 137.7$$

In Fig. 2.4 is presented the diagram of number of rotations to leakage in function of motion speed of the seal with FLA 002.25 magnetic fluid at the relative pressure  $p_w = p_r/p_{krl} = 1.6$ . On the diagram is shown the trend line in the form of the function:

$$y = -7.88\ln(x) + 123.7$$

In Fig. 2.5 is shown the diagram of number of rotations to leakage in function of motion speed of the seal with FLA 002.25

magnetic fluid at the relative pressure  $p_w = p_r/p_{krl} = 2.4$ . On the diagram the trend line is given in the form of the function:

$$y = -22.94\ln(x) + 241.39$$

The successive series of tests were conducted for different kinds of magnetic fluids, i.e. the FLA 003.45 and FLS 040.040, as well as with different numbers of magnets located circumferentially: 10, 14 and 18. Relevant tables and diagrams are not included in the paper due to limitation of its volume.

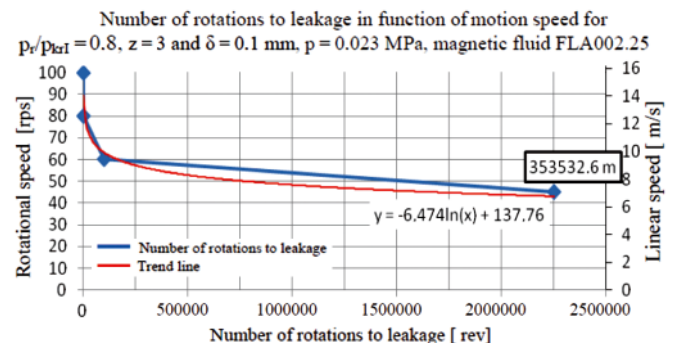


Fig.2.3. Number of rotations to leakage in function of motion speed of the seal with FLA 002.25 magnetic fluid at the set operational parameters

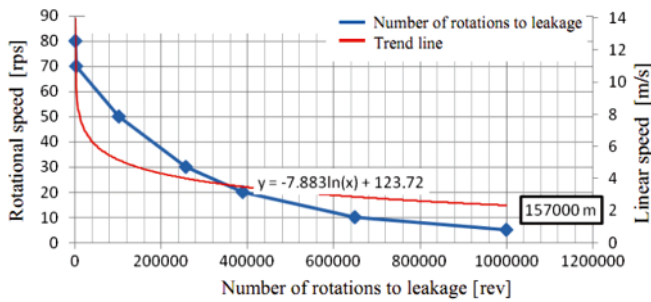


Fig. 2.4. Number of rotations to leakage in function of motion speed of the seal with FLA 002.25 magnetic fluid at the set operational parameters

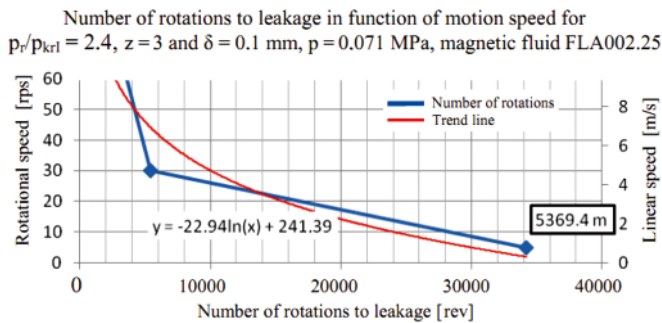


Fig. 2.5. Number of rotations to leakage in function of motion speed of the seal with FLA 002.25 magnetic fluid at the set operational parameters

### 3. COMPARISON OF TEST RESULTS

Series of the tests aimed at determination of MF seal life in function of magnetic field intensity, external pressure and kind of magnetic fluid, were performed.

#### 3.1. Seal life in function of magnetic field intensity in the system

In Fig. 3.1 are presented the diagrams of number of rotations to leakage in function of rotational speed of the seal for different values of magnetic field intensity in the gap filled with magnetic fluid, dependent on number of magnets applied in the magnetic system of the seal. Results of the tests for FLA 003.45 magnetic fluid at the relative pressure  $p_w = p_r/p_{krl} = 1.6$  and with 10, 14 and 18 permanent magnets used in the sealing system, were compared to each other.

Number of rotations to leakage in function of motion speed at different number of permanent magnets in the sealing system for  $p_r/p_{krl} = 1.6$ ,  $z = 3$  and  $\delta = 0.1$  mm, magnetic fluid FLA003.045

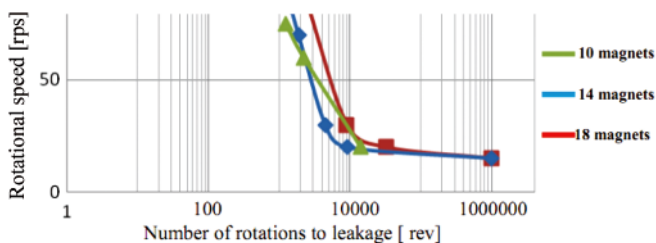


Fig. 3.1. Influence of change in magnetic field intensity on number of rotations to leakage in the seal

#### 3.2. Seal life in function of set value of relative pressure

In Fig. 3.2 are presented the diagrams of number of rotations to leakage in function of rotational speed for different values of relative pressure set in the tests with FLA 002.25 magnetic fluid. The tests were carried out at the relative pressure values  $p_w = p_r/p_{krl} = 0.8, 1.6, 2.4$  and the same number of magnets equal to 14.

In Fig. 3.3 are presented the diagrams of number of rotations to leakage in function of rotational speed for different values of relative pressure set in the tests with FLA 003.45 magnetic fluid. The tests were carried out at the relative pressure values  $p_w = p_r/p_{krl} = 0.8, 1.6, 2.4$  and the same number of magnets equal to 14.

Number of rotations to leakage in function of rotational speed at different relative pressure values  $p_r/p_{krl} = 0.8, 1.6, 2.4$   $z = 3$  and  $\delta = 0.1$  mm, magnetic fluid FLA002.25

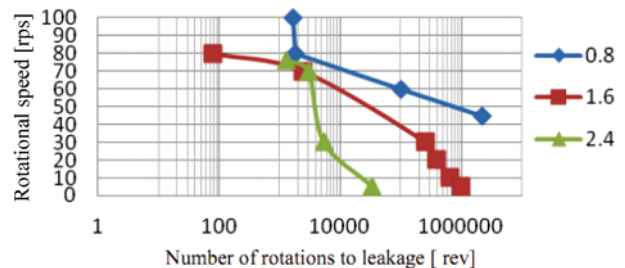


Fig. 3.2. Number of rotations to leakage in function of rotational speed at different relative pressure values for FLA 002.25 magnetic fluid

Number of rotations to leakage in function of motion speed at different relative pressure values in the sealing system for  $p_r/p_{krl} = 0.8, 1.6, 2.4$   $z = 3$  and  $\delta = 0.1$  mm, magnetic fluid FLA003.045

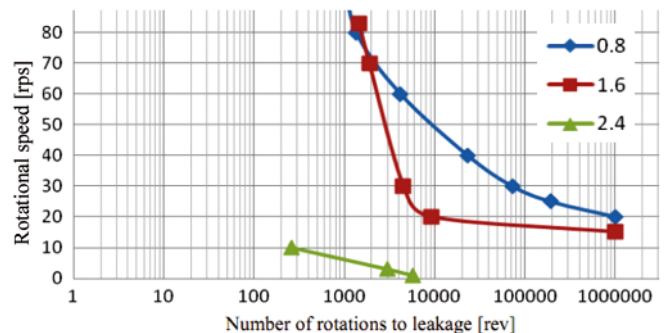


Fig. 3.3. Number of rotations to leakage in function of rotational speed at different relative pressure values for FLA 003.45 magnetic fluid

In addition, were investigated and determined numbers of rotations to leakage in the seal in function of rotational speed for different values of relative pressure set in the tests with FLA 040.040 magnetic fluid, i.e. at the relative pressure values  $p_w = p_r/p_{krl} = 0.8, 1.6, 2.4$ , and the same number of magnets equal to 14. The tests were repeated for different values of relative pressure set in the tests with another magnetic fluid, i.e. FLA 003.45, and 10 magnets applied in the magnetic system. The tests were carried out at the relative pressure values  $p_w = p_r/p_{krl} = 0.8, 1.6, 2.4$ .

#### 3.3. Seal life in function of kind of magnetic fluid

In Fig. 3.4 are presented the diagrams of number of rotations to leakage in function of rotational speed for three magnetic fluids: FLA 002.25, FLA 003.45 i FLS 040.040, at the set relative pressure value  $p_w = p_r/p_{krl} = 0.8$ . The tests were carried out in the magnetic system with 14 magnets.

Moreover, were investigated and determined numbers of rotations to leakage in the seal in function of rotational speed for three magnetic fluids: FLA 002.25, FLA 003.45 i FLS at the relative pressure value  $p_w = p_r/p_{krl} = 1.6$  and with 14 magnets used in the magnetic system.

The tests were repeated and numbers of rotations to leakage in function of rotational speed were determined also for three magnetic fluids: FLA 002.25, FLA 003.45 i FLS 040.040 but at the set relative pressure value  $p_w = p_r/p_{krl} = 2.4$ . The tests were carried out in the magnetic system of 14 magnets.

Number of rotations to leakage in function of rotational speed for different magnetic fluids and the relative pressure value  $p_r/p_{krl} = 0.8$ . Number of magnets 14,  $z = 3$  and  $\delta = 0.1$  mm.

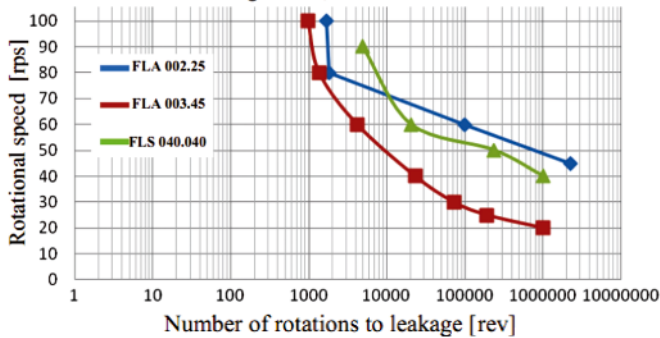


Fig. 3.4. Number of rotations to leakage in function of rotational speed for different magnetic fluids and relative pressure value equal to 0.8

### 3.4. Rotational speed for seal life of one million number of rotations

In Tab. 3 are presented the rotational speed values at which, during testing the seals, one million number of rotations was exceeded. The table contains results obtained for three magnetic fluids at different numbers of magnets, i.e. 10, 14, 18, in the magnetic system and different relative pressure values  $p_w = p_r/p_{krl} = 0.8, 1.6, 2.4$ .

Tab. 3. The rotational speed values at which one million number of rotations was exceeded, in function of number of magnets in the magnetic system, for three magnetic fluids and different relative pressure values  $p_w = p_r/p_{krl} = 0.8, 1.6, 2.4$

Number of magnets	Kind of magnetic fluid	Rotational speed values [rps]		
		Relative pressure $p_w = p_r/p_{krl}$		
		0.8	1.6	2.4
14	FLA 002.25	45	5	below 5
14	FLA 003.45	20	15	below 1
14	FLS 040.040	40	10	2
10	FLA 003.45	20	below 20	10
18	FLA 003.45	not tested	not tested	not tested

In Fig. 3.5 is presented a comparison of rotational speed values for three tested fluids, at which one million number of rotations was reached at the relative pressure  $p_w = p_r/p_{krl} = 0.8$ .

Rotational speed corresponding to seal life of 1 million number of rotations, Relative pressure  $p_r/p_{krl} = 0.8$

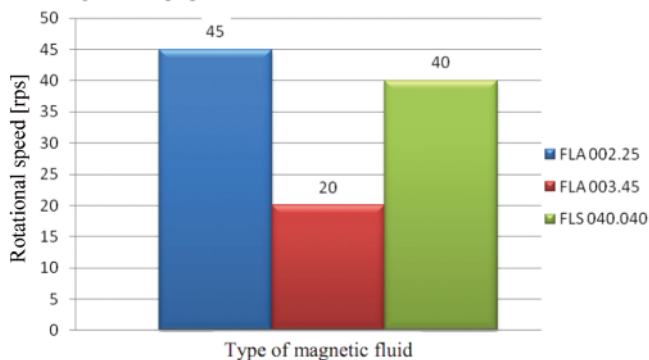


Fig. 3.5. Comparison of rotational speed values at which one million number of rotations was reached for three tested fluids at the relative pressure  $p_w = p_r/p_{krl} = 0.8$

The tests were repeated for the tested fluids at the relative pressure values  $p_w = p_r/p_{krl} = 1.6$  and  $2.4$ , respectively.

Fig. 3.6 is shown a comparison of rotational speed values at which the condition of reaching 1 mln number of rotations was fulfilled for particular fluid FLA002.25 at three relative pressure values  $p_w = p_r/p_{krl} = 0.8, 1.6, 2.4$ .

Rotational speed values corresponding to seal life of 1 million of rotations, fluid FLA002.25, relative pressure  $p_r/p_{krl} = 0.8, 1.6, 2.4$

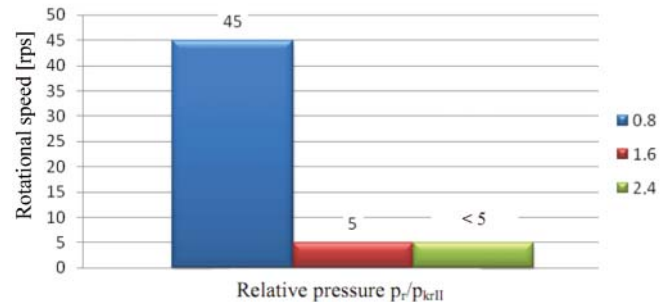


Fig. 3.6. Comparison of rotational speed values at which one million number of rotations was reached for FLA 002.25 fluid at the relative pressure values  $p_w = p_r/p_{krl} = 0.8, 1.6, 2.4$

The tests were repeated for the magnetic fluids: FLA 003.45 and FLS 040.040, at the relative pressure values  $p_w = p_r/p_{krl} = 0.8, 1.6, 2.4$  and in configurations with 10, 14 and 18 magnets.

In Fig. 3.7 is presented an example comparison of rotational speed values at which the condition of reaching 1 mln number of rotations was fulfilled for FLA 002.25 magnetic fluid at three relative pressure values  $p_w = p_r/p_{krl} = 0.8, 1.6, 2.4$  and with decreased number of magnets in the sealing system, i.e. 10 pieces.

Rotational speed values corresponding to seal life of 1 million number of rotations, fluid FLA003.45, relative pressure  $p_r/p_{krl} = 0.8, 1.6, 2.4$ , magnets quantity  $z = 10$

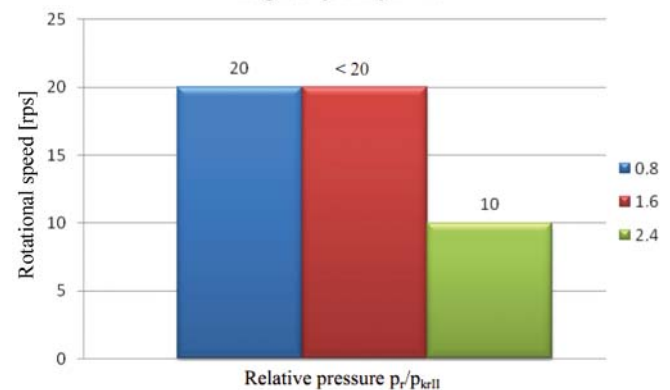


Fig. 3.7. Comparison of rotational speed values at which one million number of rotations was reached for FLA 002.25 fluid at the relative pressure values  $p_w = p_r/p_{krl} = 0.8, 1.6, 2.4$  and with decreased number of magnets in the sealing system, i.e. 10 pieces

## 4. DISCUSSION OF TEST RESULTS

In the frame of the conducted experimental projects on the MF seal with three sealing stages operating in water, three kinds of magnetic fluid were tested in conditions of different values of factors which influence operational effectiveness of the seal. The three effectiveness measures were applied:

- critical pressure of the seal (penetration pressure),
- critical motion speed („immediate” penetration motion speed),
- motion speed for a limited seal life (motion speed for one-million-cycles life).

The two external factors and one design factor affecting seal operation were taken into account:

- external factors:
  - water pressure in the test chamber,
  - seal motion speed,
- design factor:
  - number of magnets in magnetic system of the seal.

To estimate influence of the factors on the seal, 120 test runs lasting from about 1 hour up to over 30 hours, were performed.

The test results were elaborated separately for each kind of the performed tests (critical pressure, critical speed, long-term operation speed), and then they were compared mutually to make it possible to assess operational features of the seals working with different magnetic fluids and in different external conditions.

#### 4.1. Critical pressure tests of the seal

Results of the tests are presented in Fig. 2.1 and 2.2. In each case the total critical pressure  $p_{kri}$  of the seal with three sealing stages was tested by using 100 $\mu$ l magnetic fluid dosage per one stage.

In the tests of the seals with 14 magnets the highest critical pressure value equal to 0.217 MPa was achieved for FLA 003.45 magnetic fluid of the saturation magnetization  $M_s = 45$  kA/m [17]. A little lower value equal to 0,198 MPa was obtained for FLS 040.040 magnetic fluid for which the value of  $M_s = (40 \div 50)$  kA/m was specified by its producer [17]. It seems that for the tested fluid the value of  $M_s \approx 40$  kA/m is more realistic. For FLA 002.25 magnetic fluid of the saturation magnetization  $M_s = 25$  kA/m the critical pressure value equal to 0,089 MPa was obtained.

The tests on FLA 003.45 magnetic fluid with the use of 10 and 18 permanent magnets show that either at this smaller or greater number of magnets used in the magnetic system the critical pressure value was lower than that obtained for 14 magnets.

#### 4.2. Critical speed tests of the seal

The critical pressure is defined as the smallest value of rotational speed at which – at given constant values of parameters – a leakage occurs during continuous increasing the rotational speed from 0 to its maximum value of 100 rps. As the maximum value of rotational speed was limited by torque meter characteristics in some cases it was not possible to determine this value because it exceeded the 100 rps - limit. The critical speed was tested at each of three relative pressure values, for each of the magnetic fluids. For FLA 003.45 magnetic fluid the tests were also performed with the use of different number of permanent magnets (in configurations of 10, 14, and 18 magnets).

The test results are collected in Tab. 1 and presented in Fig. 2.3 through 2.6. In the tests, at the relative pressure values  $p_w = p_r/p_{kri} = 0,8$  and  $p_w = p_r/p_{kri} = 1.6$  the greatest limiting speed values were observed for FLA 002.25 and FLA 003.45 magnetic fluids. In the tests at the relative pressure  $p_w = p_r/p_{kri} = 0.8$  the 100 rps speed value was exceeded for both the fluids, whereas at the relative pressure  $p_w = p_r/p_{kri} = 1.6$  the speed values amounted to 80 and 83 rps, respectively. However the magnetic fluids in question produced on the basis of the same primary liquid - SILOXAN, greatly differ to each other in saturation magnetization value:  $M_s = 25$  kA/m and  $M_s = 45$  kA/m, respectively. And, smaller limiting speed values were obtained

in the tests with the use of FLS 040.040 magnetic fluid produced on the basis of silicon liquids.

In the tests at the relative pressure  $p_w = p_r/p_{kri} = 2.4$  the greatest limiting speed value equal to 76 rps was achieved in the tests with the use of FLA 002.25 fluid of the smallest saturation magnetization value. The limiting speed values for the remaining fluids are about six times smaller despite their almost twice greater saturation magnetization. It should be taken into consideration that absolute pressure values set in the tests with FLS 040.040 and FLA 003.45 fluids were significantly greater than that used in the tests with FLA 002.25 fluid. The value resulted from the assumed test concept according to which absolute pressure values are derived from relative pressure values:  $p_w = p_r/p_{kri}$ . Since great differences appeared between statical penetration values for the magnetic fluids in question, pressure values set in the tests with FLA 002.25 magnetic fluid were consequently much lower than those set in the tests with the remaining fluids.

In the limiting speed tests at the number of magnets: 10, 14, 18, performed with the use of FLA 003.45 magnetic fluid at the relative pressure value  $p_w = p_r/p_{kri} = 1.6$  (Fig.2.6) the greatest limiting speed value of 91 rps was obtained for 18 magnets, and the smallest value of 75 rps for 10 magnets in number.

#### 4.3. Life tests of the seal

Life of MF seals was the most thoroughly investigated issue in this research project. In most of the tests the number of cycles (number of rotations) performed by a seal up to leakage was taken as its life criterion. Full sets of the tests with 14 permanent magnets in the magnetic system and at the relative pressure values  $p_w = p_r/p_{kri} = 0.8, 1.6,$  and  $2.4$  were performed for three kinds of magnetic fluids described in article [24]. The tests were aimed at checking relation between number of performed cycles and rotational speed set in test.

For FLA 003.45 magnetic fluid were additionally performed tests with 10 and 18 magnets installed in the test head. One million rotations of the seal were assumed to be the basic number of cycles. For so defined basic number of cycles was determined the largest motion speed at which no leakage was observed in the tested seal. The quantity was called one-million-cycle life. It should be stressed that in some tests for the above mention speed a greater number of cycles without leakage was achieved, whereas in other tests it was decided not to continue running up to the basic number of 1 mln cycles as it would require to do long-lasting tests not planned in the project in question.

The results of the seal life tests are collected in Tab. 2 through 6 and shown on the diagrams in Fig. 2.7 through 3.6

The seal life diagrams for three kinds of magnetic fluids tested at three relative pressure values  $p_w = p_r/p_{kri} = 0.8, 1.6,$  and  $2.4$  indicate large differences in values of the speed for which number of cycles to leakage, corresponding to them, was obtained. The differences appear both if to compare the tests for particular fluids at different relative pressure values and if they concern comparison of the results obtained from the tests of different kinds of fluids.

The largest speed for long-term operation was reached in the test with FLA 002.25 fluid at the relative pressure value  $p_w = p_r/p_{kri} = 0.8$ . It was equal to 45 rps, and in the test the basic number of 1 mln cycles was exceeded. The smallest speed for long-term operation was reached in the test with FLA 003.45 fluid at the relative pressure value  $p_w = p_r/p_{kri} = 2.4$ .

It was equal to 1 rps, and in the test the basic number of cycles was not reached. However it should be stressed that in the test with FLA 002.25 fluid in which the largest long-term

operation speed was obtained the pressure set in the test was equal to 0.0232 MPa, whereas in the test with FLA 003.45 fluid, in which the smallest motion speed was obtained, the set pressure was equal to 0.1824 MPa. The experimental data obtained from all the tests were approximated by logarithmic trend lines of different coefficients depending on a given test.

The seal tests under different magnetic field intensity (different numbers of permanent magnets in the magnetic system of the seal) were performed for FLA 003.45 magnetic fluid at the relative pressure value  $p_w = p_r/p_{kri} = 1.6$ . Comparison of results of the tests indicates that the largest limiting speed of 91 rps was obtained in the test with the use of the magnetic system of the highest magnetic field intensity (18 permanent magnets). And, the values of operational speed for the basic number of 1 mln cycles without leakage were close to each other. From the comparison of the results the value of about 15 rps was achieved.

## 5. RECAPITULATION AND CONCLUSIONS

According to the applied testing methodology it was decided, for each tested version of the seal, to determine the following:

- statical penetration pressure of the seal,
- limiting operational speed of the seal.

Each of the measurements introduced important information which made it possible to reach the research aim as follows:

- to determine seal life curve and the highest motion speed for which it is possible to achieve, without leakage, the basic number of cycles (rotations) equal to 1 mln as assumed for the tests in question.

In the tests water pressure value set in the measurement chamber was a crucial factor. The factor was accounted for in the form of the relative pressure defined as the ratio of the set pressure and the critical pressure i.e. the seal penetration pressure per one sealing stage, determined in the statical test, ( $p_w = p_r/p_{kri}$ ).

The using such concept of setting the testing pressure of water made it possible to simply account for influence of the factor on seal life for particular magnetic fluids, but in the same time it made comparing life values of different fluids more difficult because of large differences in set testing pressures resulting from highly different values of the statical penetration pressure of the tested magnetic fluids. For instance the highest long-term operational speed equal to 45 rps was reached in the tests with FLA 002.25 magnetic fluid at the set pressure value of 0,0237 MPa ( $p_w = p_r/p_{kri} = 0.8$ ) resulting from its low penetration pressure value equal to 0,0297 MPa per one sealing stage. As in the analogous test at the value  $p_w = p_r/p_{kri} = 0.8$  for FLA 003.045 fluid (of the penetration pressure per one sealing stage equal to 0.072 MPa) it was required to set the water pressure of 0.058 MPa, the long-term operation speed of the seal with the fluid in question amounted to 20 rps only. The results show that the pressure greatly influences life of MF seal operating in water.

The limiting operational speed of seal constitutes an important testing information as it makes it possible to estimate speed value from which determining seal life curve should be started - and consequently - determining the seal life for the basic number of cycles equal to 1 mln. However this parameter is not very important from practical point of view.

The tests with various numbers of magnets in the sealing system revealed influence of magnetic field intensity on limiting speed of magnetic fluids, but they did not confirm a significant

influence of the factor on life of MF seals operating in water.

Results of the life tests for majority of the tested magnetic fluids and seals show similar picture on the diagrams. At higher rotational speed values a short period of operation to leakage (small number of cycles) is observed. At lower motion speed values failure-free operation period is much longer and distinctly tends to the speed value which could be taken as that for long-term operation. Such character of seal life curve could be best described by a logarithmic trend line.

The performed tests make it possible to offer the following conclusions:

1. The tests confirmed correctness of the assumed testing methods.
2. The test stand design is appropriate and allows to carry out the tests correctly.
3. The tested magnetic fluids produced on the basis of liquids with strong hydrophobic properties (silicon liquid, siloxan) may be applied to rotational seals operating in water, however only in a limited range of motion speed.
4. The tests confirmed that the assumed research hypotheses were right:
  - Motion speed influences life of MF seal operating in water: at lower speed values a significant increase of seal life is observed.
  - Water pressure influences MF seal life: at higher pressure values set in the tests a significant decrease of MF seal life is observed.
5. For each of the tested fluids it was possible to determine a motion speed value at which the assumed life of 1 mln cycles (number of rotations) was reached without any leakage from the seal.
6. The seal life diagrams for different motion speed values indicate that for each of the fluids can be observed a range of speed values below which a significant extension of failure - free operation period of the seal occurs. The process is probably associated with Kelvin - Helmholtz phenomenon of instability [2, 3, 11].
7. Value of statical penetration pressure depends on the saturation magnetization intensity of magnetic fluid,  $M_s$ .
8. Magnetic field intensity in the seal system only slightly influences the increasing of statical penetration pressure values of the seal. In the tests with the use of 18 permanent magnets, only a small decrease of the penetration pressure was observed in comparison with that obtained in the tests with 14 permanent magnets.
9. Magnetic field intensity has a low influence on a rotational speed value at which the basic value of seal life equal to 1 mln rotations is obtained.

## BIBLIOGRAPHY

1. Szydło Z., Zachara B., Ochoński W.: *Ferro-magnetic fluids and their application in machinery engineering* (in Polish). 1<sup>st</sup> Conference on Automation of Machines, Devices and Processes, Krynica, 1999.
2. Rosensweig R.E.: *Ferrohydrodynamics*. Dover Publications, Inc. Mineola, New York, 1997.
3. Rinaldi C., Chaves A., Elborai S., He X., Zahn M.: *Magnetic fluid rheology and flows*. Current Opinion in Colloid & Interface Science, Vol.10, Issue 3-4, October, 2005.
4. Orlov D. B., et al.: *Eksperimentalnoe issledovanie resursa magnitoidkostnykh uplotnenij pri germetizacii zidkikh sred*. Magnitnaya Gidrodinamika, No. 4, pp.127-130, 1989.
5. Kurfess J., Muller H. K.: *Sealing liquids with magnetic fluids*. Journal of Magnetism and Magnetic Materials, 85, 1990
6. Viherala J., et al.: *Sealing of Liquids with Magnetic Fluid Seals*. Proc. of 6<sup>th</sup> Nordic Symposium on Tribology, NORDTRIB'94, Uppsala, Sweden, 12-15 June 1994.

7. Kim Y. S., Nakatsuka K., Fujita T., Atarashi T.: *Application of hydrophilic magnetic fluid to oil seal*. Journal of Magnetism and Magnetic Materials, 201 (1999), pp. 361-363.
8. Liu T., Cheng Y., Yang Z.: *Design optimization of seal structure for sealing liquid by magnetic fluids*. Journal of Magnetism and Magnetic Materials, Vol. 289, Complete, March, 2005.
9. Guo C., Feng S.: *Sealing mechanism of magnetic fluids*. Journal of Shanghai University (English edition), 2006, 10(6), pp.522-525.
10. Chorney Alvan F.; Mraz Will.: *Hermetic Sealing with Magnetic Fluids*. Machine Design; May 7, 1992, 64, 9, ProQuest Science Journals p. 79.
11. Mitamura Y., Arioka S., Sakota K., Azegami M.: *Application of a magnetic fluid seal to rotary blood pumps.*, *J Phys Condens Matter*. 2008 May 21;20(20):204145. doi: 10.1088/0953-8984/20/20/204145. Epub 2008 May 1.
12. Szydło Z., Matuszewski L.: *Experimental research on effectiveness of the magnetic fluid seals for rotary shafts working in water*. Polish Maritime Research, 2007, vol. 14, No. 4, pp. 53–58.
13. Szydło Z., Matuszewski L.: *Ring thruster – a preliminary optimisation study of ferrofluid seal and propeller*. Polish Maritime Research, 2007, Spec. issue S1, pp. 71-74.
14. Szydło Z., Matuszewski L.: *The application of magnetic fluids in sealing nodes designed for operation in difficult conditions and in machines used in sea environment*. Polish Maritime Research, 2008, Vol. 15, No. 3, pp. 49-58.
15. Szydło Z., Ochoński W., Zachara B.(inventors): *A measurement head for testing parameters of seals with ferro-magnetic fluid* (in Polish). Patent specification No. PL 377598 A1, submitted on 2005-10-12 by Mining and Metallurgy Academy, Cracow, published in Bulletin of Polish Patent Office, 2007, No. 8, p. 22
16. Bonvouloir, J.: *Experimental Study of High Speed Sealing Capability of Single stage Ferrofluidic Seal*. ASME Transactions, Journal of Tribology, Vol.119, July 1997
17. Ferrolabs, Inc. Sterling, VA United States, <http://www.ferrolabs.com/> 2010
18. Szydło Z., Matuszewski L.: *Life tests of a rotary single-stage magnetic-fluid seal for shipbuilding applications*. Polish Maritime Research. 2011, Vol. 18, No. 2, pp. 51-59.
19. Szydło Z.: *High speed magnetic fluid seal operating in water environment*. 17<sup>th</sup> International Colloquium on Tribology, 19-21 January 2010, Book of synopses 2010/(Ed.) Wilfried J. Bartz Ostfildern: Technische Akademie Esslingen, 2010.
20. Szydło Z.: *Determination of tribological characteristics and limiting operational conditions of ferro-magnetic seals* (in Polish). Report on realization of the KBN research project No. 7T07B 02412. Publ. by Mining and Metallurgy Academy, Cracow, 2000.
21. Jibin Zou, B, Jiming Zou, and Jianhui Hu.: *Design and pressure control of high pressure differential magnetic fluid seals*. IEEE Transactions on Magnetics, Vol. 39, No. 5, September 2003
22. P.P.H.U. "ENES" Ltd, Paweł Zientek, products performance list, Warszawa, [www.magnesy.pl/](http://www.magnesy.pl/) 2010
23. PZ HTL Ltd, Manufacturer's datasheet
24. Matuszewski L.: *Multi-stage magnetic-fluid seals for operating in water; life test procedure, test stand and research results Part I: Life test procedure, test stand and instrumentation*, Polish Maritime Research. 2012 Vol 19; pp. 62-70

---

#### CONTACT WITH THE AUTHOR

Leszek Matuszewski, Ph.D.  
 Faculty of Ocean Engineering  
 and Ship Technology  
 Gdansk University of Technology  
 Narutowicza 11/12  
 80-233 Gdansk, POLAND  
 e-mail: [leszekma@pg.gda.pl](mailto:leszekma@pg.gda.pl)

# Application of multi-dimensional grouping to building steel stiffened shell structures

Remigiusz Iwańkiewicz, Ph.D.

The West Pomeranian University of Technology, Szczecin, Poland

## ABSTRACT



*In this paper the present state of grouping technology theory is discussed. Attention is paid to lack of publications on grouping methods based on linear operators instead of classical incidence matrices. A computation algorithm for generating three-dimensional groups has been proposed. Every group contains joined structures, working cells and final (output) structures. Operation of the algorithm has been compared with results gained from literature sources dealing with binary grouping. And, calculations based on real assembly sequencing of a set of ship hull sections, have been performed.*

**Keywords:** group technology; assembly sequencing; steel structures manufacturing

## 1. INTRODUCTION

Hulls of typical merchant ships belong to a group of steel stiffened shell structures (3S). Such structures can be found also in very large tanks, bridge elements, offshore units etc. Because of their dimensions and necessity to expand working frontage, production of 3S structures is usually carried out in accordance with the so called prefabrication subdivision. It means that final product is composed of many simultaneously produced prefabricated units (subassemblies). They usually are further subdivided into lower stage units. Consequently, a multistage assembly sequencing is formed. Number of stages depends on structure geometry and manufacturing conditions of a producer (a. o. – cranes at his disposal). 3S structures are as a rule produced in a few pieces or short series, that forces enterprises such as shipyards to keep agile production organisation and makes designing and production preparation work more labour consuming. The problem of a degree of producing in series is tightly connected with the notion of technological similarity of products. Products even if different visually and functionally may require similar production processes and – from the enterprise point of view – belong to one common series.

One of the cardinal tasks of design office is to act in accordance with the principle of „design for production” by applying as much standardization of design solutions as possible, including assortment of rolled profiles and shapes of cut details. Such actions are of a low degree of structural complexity.

A successive action aimed at minimization of unitary production character of 3S structures is searching for such

division planes for their assembly as to obtain the effect of a greater degree of serial production at least in early stages of assembly process. Two 3S structures may differ from each other in technology, for instance: by accessibility for automotive welders, shapes of curvatures, assembling sequence and possibility of being manoeuvred. Simultaneously, their structurally simpler subassemblies may be very similar stiffened panels as regards their technology.

The theory which makes it possible, on the level of models, to:

- measure technological similarity,
- state when a given product can be qualified to be an element of greater series, as well as
- so design a given production system as it could realize production in a way as repeatable as possible

is the classical theory of group technologies (GT). Its main aim is to distinguish, in the set of resources used in the process or set of products, some subsets called groups. In the literature [2, 3, 4, 5, 13] only working cells of different kinds or, simply, machines are usually distinguished as grouped resources. In the case of grouping the products we aim at maximization of their repeatability and reduction of design and production preparation processes [11]. Due to having at hand certain groups of products, designers of prototypes have at their disposal hints helping to maintain high producibility.

Among profits resulting from application of group technologies to organizing production cells the following are numbered [9]:

- widened standardization of working cells, applied instrumentation, set-ups of working parameters,

- reduction of interoperative transport as a result of relocation of work objects within production cells,
- facilitated scheduling of production,
- shortened cycles of production,
- lessened buffer stores and lowered freeze level of current assets,
- elevated motivation of employees and simplified procedures of worktime estimating.

The grouping is performed with use of:

- visual assessment of elements of a set – on the basis of a subjective validation by experts,
- classification and coding – on the basis of an assumed coding system of features (in the case of products: their geometry and production technology),
- analysis of technological routes realized by products.

The method of analyzing technological routes is advantageous as it makes it possible to group simultaneously a set of resources and products. Here the groups of the set of resources are called input ones.

Identification of input and output groups permits also to design the so called production cells where each of them constitutes the pair (group of resources; group of products). Such pairs are called two-dimensional. Algorithms for two-dimensional grouping have been developed for a few dozen years [6, 1, 16].

The grouping of factors by using the method of analyzing technological routes is realized according to the following scheme [16]:

1. The formulating of relations between resources and products by using the so called incidence matrix – to each of the resources an appropriate row of the matrix is assigned, and to each of the products – a column of it (or *vice versa* – it is a question of convention).
2. The determining of mutual technological similarities between resources as well as between products. Consequently, two matrices of technological similarities are built – separately for each of the analyzed sets.
3. The setting of a threshold for technological similarity, above which it has to be considered that two elements of the set in question should be assigned to the same group.

The two-dimensional grouping makes it possible to respond quickly to the question: how to organize production cells in the system if planned assortment of products and engineering techniques available to producer, are known? It is easy to reach the effect if the incidence matrix unambiguously describes relations between given products and working cells. However in practice the forming of such incidence matrix is very labour-consuming and demanding comprehensive knowledge on technologies used in a given enterprise.

An extension of the classical two-dimensional grouping method is the proposal of distinguishing, in the set of used resources, two separable subsets. As a result, we have to do with three sets and perform analysis of similarity between products on the basis of their incidence with the first and second set of resources. In both the sets of resources we analyze similarity independently, on the basis of incidence with the second subset of resources as well as the set of products. From the analysis result three-dimensional groups, i.e. the ordered threes: (1<sup>st</sup> group of resources, 2<sup>nd</sup> group of resources, group of products). The first concepts of the kind belong to Min and Shin [17]. Their proposals deal with analysis of technological similarities in the two subsets of resources: machines and operators as well as in the set of products. Successive elaborations have been a natural generalization towards *n*-dimensional models [14, 15, 18].

## 2. CONCEPT OF THREE-DIMENSIONAL GROUPING IN MANUFACTURING 3S STRUCTURES

### 2.1. Input data, standardizing and scaling

The three-dimensional grouping is proposed for application in manufacturing 3S structures with taking into account an ordered set of various working cells in which joining process of structures into higher stage structural units, is performed.

The following notions are introduced:

- $S = \{s_1, \dots, s_m\}$  – working cells,
- $C^{in} = \{c_1^{in}, \dots, c_n^{in}\}$  – joined structures (put in the cells),
- $C^{out} = \{c_1^{out}, \dots, c_p^{out}\}$  – produced structures (put out the cells).

The structures differ to each other as regards their geometry. And, it is not essential where butting contacts of plate sheets are placed, nor other features of technological importance (e.g. form of cut-outs and gasket plates). Only the functional features are taken into account, namely: arrangement of shells, stiffeners and brackets, ways of ensuring continuity of girders etc. Structures of various complexity degrees are considered. It may be single details or large-size spatial structures, e.g. hull block sections or even entire ship hull.

To every output structure can be assigned elements of the set *S* and  $C^{in}$  which take part in its production. To every working cell can be assigned structures which are delivered to it. It leads to formulation of three matrices of incidence between relevant sets. The concepts have been published so far are based on binary matrices. However production of 3S structures is associated with a rather low diversity of cells. And, differences between structures amount to labour consumption of processes as well as quantity of lower-stage subassemblies of which the structures are formed. Practical implementation of grouping technologies into production of 3S structures faces the problem of an insufficient informing force of binary incidence matrices. For instance, structures which greatly differ to each other as regards requirements for equipment of working cells, can be built of identical subassemblies and with the use of identical welding methods. In this case, application of the binary grouping methods may lead to erroneous placing technologically different products into the very same cells. As a result low specialized production cells are obtained, that contradicts their essence.

As a solution for the above mentioned problems it is proposed to apply a grouping model based on continuous incidence matrices. For every pair of sets of the input factors *X* and output factors *Y* the following matrix is determined:  $A^{X-Y} \in M(|X| \times |Y|, \mathbb{R}^+ \cup \{0\})$ , where  $a_{ij}^{X-Y} > 0$ , if production of *j*-th element of the set *Y* requires to engage *i*-th element of the set *X*, if not:  $a_{ij}^{X-Y} = 0$ . Values of the non-zero coefficients  $a_{ij}^{X-Y}$  are standards of consumption of input factors per production unit of appropriate output factors. In the case of working cells the consumption standards usually represent the following:

- amount of working time of a cell during production of unit of a structure,
- amount of a concrete effect of work of a cell, generated during production of unit of a structure (e.g. one meter of welded joint, one square meter of painted surface etc).

The continuous incidence matrix is a linear operator acting, in this case, between vector spaces of production factors [12]. Such operators find wide application to a.o. operational research, and they may find much wider use in solving the grouping problems in enterprise.

## 2.2. Measure of grouping quality

Three-dimensional grouping the sets  $S$ ,  $C^{in}$  and  $C^{out}$  is an optimization problem and amounts to searching for the division  $\Gamma$  of the Cartesian product  $S \times C^{in} \times C^{out}$  into  $\gamma$  subsets:

$$\Gamma = \Gamma(S \times C^{in} \times C^{out}, \gamma) = \left\{ \Gamma_i = (S_i, C_i^{in}, C_i^{out}) \in S \times C^{in} \times C^{out} : (i=1, \dots, \gamma), \bigcap_{i=1}^{\gamma} S_i = \bigcap_{i=1}^{\gamma} C_i^{in} = \bigcap_{i=1}^{\gamma} C_i^{out} = \emptyset \right\} \quad (2.1)$$

The groups  $\Gamma_i$  are really sums of the subsets  $S_i$ ,  $C_i^{in}$  and  $C_i^{out}$ , however they are written in the form of ordered threes, that facilitates to identify elements of each of the group.

The division  $\Gamma$  can be assessed as regards its quality. In 1986 Chandrasekharan and Rajagopalan [7] proposed to apply a criterion for the two-dimensional grouping of binary incidence matrix. This is maximization of a weighted sum of densities of submatrices and their neighborhood. And, the density is meant to be number of unities related to whole number of elements of the matrix in question. In 2007 Li [15] extended the criterion, for the multi-dimensional case, by assigning weights to particular incidence matrices.

In the case of continuous matrices, differences in values of the elements should be accounted for additionally apart from the fact of occurrence of non-zero elements of incidence matrices in the space of groups and outside it.

Let the weights of particular incidence matrices be equal to:  $\omega_{S-C^{in}}$ ,  $\omega_{S-C^{out}}$ ,  $\omega_{C^{in}-C^{out}}$  respectively. Then it is proposed to take, as a quality measure for  $\Gamma$  division, the following criterion:

$$E(\Gamma) = \frac{\omega_{S-C^{in}} \cdot W(A^{S-C^{in}}, \Gamma) + \omega_{S-C^{out}} \cdot W(A^{S-C^{out}}, \Gamma) + \omega_{C^{in}-C^{out}} \cdot W(A^{C^{in}-C^{out}}, \Gamma)}{\omega_{S-C^{in}} + \omega_{S-C^{out}} + \omega_{C^{in}-C^{out}}} \rightarrow \max \quad (2.2)$$

where:

$W(A^{X-Y})$  – grouping quality index for continuous matrix of incidence between the set  $X$  and  $Y$ .

Let the set of indices of elements of the set  $X$  belonging to  $k$ -th group is marked  $I_k^X$ . Then the following is defined:

$$W(A^{X-Y}, \Gamma) = q \cdot \eta_1(A^{X-Y}, \Gamma) + (1-q) \cdot \eta_0(A^{X-Y}, \Gamma) \quad (2.3)$$

where:

- $\eta_1(A^{X-Y}, \Gamma)$  – sum of values of elements of the matrix  $A^{X-Y}$  belonging to all groups, related to their total number,
- $\eta_0(A^{X-Y}, \Gamma)$  – sum of values of elements of the matrix  $A^{X-Y}$  not belonging to any of the groups, related to their total number,
- $q$  – weight of membership of elements in groups in relation to their possible being left outside the groups. In the literature  $q = 0.5$  is often assumed [15].

$$\eta_1(A^{X-Y}, \Gamma) = \frac{\sum_{k=1}^{\gamma} \sum_{i \in I_k^X} \sum_{j \in I_k^Y} a_{ij}^{X-Y}}{\sum_{k=1}^{\gamma} |I_k^X| \cdot |I_k^Y|} \quad (2.4)$$

$$\eta_0(A^{X-Y}, \Gamma) = \frac{\sum_k \sum_{l \neq k} \sum_{i \in I_k^X} \sum_{j \in I_l^Y} a_{ij}^{X-Y}}{\sum_k \sum_{l \neq k} |I_k^X| \cdot |I_l^Y|} \quad (2.5)$$

The quantity  $\eta_1(A^{X-Y}, \Gamma)$  is the mean value of all elements within groups, and  $\eta_0(A^{X-Y}, \Gamma)$  is the mean value of elements outside the groups. As the elements  $a_{ij}^{X-Y}$  are normalized within the range  $[0,1]$ , both the quantities are also contained in this interval, consequently, the inequalities:  $0 \leq W(A^{X-Y}, \Gamma) \leq 1$ ,  $0 \leq E(\Gamma) \leq 1$  are also satisfied.

Additionally, every group is assumed to be consisted of sequence of non-empty sets. For instance, to the groups cannot be assigned only a set of output structures and cells without a set of input structures. The assumption is aimed at preventing against natural grouping input structures into one group, cells into second group and output structures into third group.

## 2.3. Algorithm of the three-dimensional grouping for continuous incidence matrices

The algorithm of multi-dimensional grouping was presented by Li in 2003 [14]. However this proposal is limited to binary incidence matrices. As a result it does not make use of cluster analysis methods but is the author's solution strongly based on the binary description of elements of sets.

Below are presented principal steps of the proposed algorithm. It is of a recurrential character. The grouping is realized by determining centres of groups having assumed number of elements and assigning to them the closest elements according to a selected measure.

The requirement of that every group should contain elements from all the grouped sets is satisfied in Step 2.5, in which one element of each of the sets is assigned to each of the groups and only in the next step unlimited assignment of remaining elements takes place.

As already mentioned, it is worth normalizing the continuous incidence matrices within a selected interval.

### Start-up of the algorithm

#### Step 1:

Having at our disposal normalized continuous matrices of incidence between the sets:  $S$ ,  $C^{in}$  and  $C^{out}$  we form the following integrated matrix:

$$A = \begin{pmatrix} \mathbf{0} & A^{S-C^{in}} & A^{S-C^{out}} \\ (A^{S-C^{in}})^T & \mathbf{0} & A^{C^{in}-C^{out}} \\ (A^{S-C^{out}})^T & (A^{C^{in}-C^{out}})^T & \mathbf{0} \end{pmatrix}_{(m+n+p) \times (m+n+p)} \quad (2.6)$$

Further proceeding consists in solving the problem of two-dimensional grouping, where the cells and input and output structures are considered jointly as the so called set of elements:

$$F = S \cup C^{in} \cup C^{out} = \{f_1, \dots, f_{m+n+p}\} \quad (2.7)$$

The elements numbered from 1 to  $m$  represent working cells, the elements of numbers from  $m + 1$  to  $m + n$  - input structures and the elements of numbers from  $m + n + 1$  to  $m + n + p$  - output structures. Therefore we have:

$$\begin{aligned} f_1 &= s_1, \dots, f_m = s_m, \\ f_{m+1} &= c_1^{in}, \dots, f_{m+n} = c_n^{in}, \\ f_{m+n+1} &= c_1^{out}, \dots, f_{m+n+p} = c_p^{out} \end{aligned} \quad (2.8)$$

#### Step 2:

The division  $K$  of a set of elements  $F$  into clusters (one-dimensional groups) such that one working cell, one input structure and one output structure is present in each of them:

$$K(F) = \{K_i \subset F : i = 1, \dots, \min\{|S|, |C^{in}|, |C^{out}|\}\}, \quad (2.9)$$

$$\forall_i \{K_i \cap S \neq \emptyset, K_i \cap C^{in} \neq \emptyset, K_i \cap C^{out} \neq \emptyset\}$$

The division  $K$  should be performed for the following number of clusters:

$$\gamma = 2, \dots, \min\{|S|, |C^{in}|, |C^{out}|\} \quad (2.10)$$

Such division for a given  $\gamma$  is marked  $K^\gamma$ . Successive steps of the algorithm should be made for each of the variant of  $\gamma$  value.

The division into clusters can be realized by using one of the division-based algorithms. Here a modified c-means method is implemented. The method in its classical form has been described a.o. by Hartigan in 1975 [10] as well as Tan, Steinbach and Kumar in 2005 [19]. The proposed modification is aimed at ensuring occurrence, in each of the clusters, at least one element out of each of the sets:  $S$ ,  $C^{in}$  and  $C^{out}$ .

#### Step 2.1:

The forming of the cluster division matrix  $\Lambda^\gamma = (\Lambda_{ij}^\gamma)$ , where  $q = m + n + p$  is total number of factors.

In its successive steps the algorithm assigns value 1 (unity) to components of the division matrix at intersection of cluster columns and rows of relevant factors. The initial division is made in accordance with the following algorithm:

$$\begin{aligned} r &\leftarrow \left\lfloor \frac{\min\{m, n, p\}}{\gamma} \right\rfloor; && // \text{rounding down} \\ \text{for } [j = 1, 2, \dots, \gamma - 1]: \\ &\text{for } [i = 1 + (j - 1) \cdot r, \dots, j \cdot r]: \Lambda_{ij}^\gamma \leftarrow 1; \\ &\text{for } [i = m + 1 + (j - 1) \cdot r, \dots, m + j \cdot r]: \Lambda_{ij}^\gamma \leftarrow 1; \quad (2.11) \\ &\text{for } [i = m + n + 1 + (j - 1) \cdot r, \dots, m + n + j \cdot r]: \Lambda_{ij}^\gamma \leftarrow 1; \\ \text{for } [i = 1 + (\gamma - 1) \cdot r, \dots, m]: \Lambda_{ij}^\gamma \leftarrow 1; \\ \text{for } [i = m + 1 + (\gamma - 1) \cdot r, \dots, m + n]: \Lambda_{ij}^\gamma \leftarrow 1; \\ \text{for } [i = m + n + 1 + (\gamma - 1) \cdot r, \dots, q]: \Lambda_{ij}^\gamma \leftarrow 1; \\ \text{return } \Lambda^\gamma; \end{aligned}$$

#### Step 2.2:

The determining of the matrix of cluster centres,  $(\alpha_{ij})_{q \times \gamma}$ :

$$\forall_{j=1, \dots, \gamma} \alpha^{(j)} = \frac{\sum_{i=1}^q A^{(i)} \cdot \Lambda_{ij}^\gamma}{\sum_{i=1}^q \Lambda_{ij}^\gamma} \quad (2.12)$$

#### Step 2.3:

The determining of the matrix of distances between elements and cluster centres.

For every  $i$ -th element and  $j$ -th group,  $D_{ij}$  value is determined. Here, it is possible to assume an arbitrary measure, not necessarily metric one. The following variants are proposed to be considered:

- angular measure (scalar product of vectors):

$$\forall_{i=1, \dots, q} \forall_{j=1, \dots, \gamma} D_{ij} = \frac{A^{(i)T} \cdot \alpha^{(j)}}{\sqrt{\sum_{k=1}^q A_{ki}^2} \cdot \sqrt{\sum_{k=1}^q \alpha_{kj}^2}} \quad (2.13)$$

- Manhattan measure:

$$\forall_{i=1, \dots, q} \forall_{j=1, \dots, \gamma} D_{ij} = |A^{(i)}_1 - \alpha^{(j)}_1| + \dots + |A^{(i)}_q - \alpha^{(j)}_q| \quad (2.14)$$

- Euclidean measure:

$$\forall_{i=1, \dots, q} \forall_{j=1, \dots, \gamma} D_{ij} = \sqrt{(A^{(i)}_1 - \alpha^{(j)}_1)^2 + \dots + (A^{(i)}_q - \alpha^{(j)}_q)^2} \quad (2.15)$$

- Chebyshev measure:

$$\forall_{i=1, \dots, q} \forall_{j=1, \dots, \gamma} D_{ij} = \max_{k=1, \dots, q} \{ |A^{(i)}_k - \alpha^{(j)}_k| \} \quad (2.16)$$

- Mahalanobis measure:

$$\forall_{i=1, \dots, q} \forall_{j=1, \dots, \gamma} D_{ij} = \sqrt{(A^{(i)} - \alpha^{(j)})^T \cdot V^{-1} \cdot (A^{(i)} - \alpha^{(j)})} \quad (2.17)$$

$$V = \text{diag}(\sigma_1^2, \dots, \sigma_q^2)$$

In the below presented exemplary calculations the above specified measures have been mutually compared as regards their effectiveness.

**Step 2.4:**

The saving of the cluster division matrix after introducing a new variable:  $\hat{\Lambda} = \Lambda^\gamma$ .  
The zeroing of the cluster division matrix:  $\Lambda^\gamma = (0)_{q \times \gamma}$ .

**Step 2.5:**

The assigning of one factor from each of the three subsets to every cluster. This way three-element clusters  $\gamma$  in number were built. Below is presented the algorithm of assigning the factors numbered from 1 to  $m$ , i.e. these belonging to the subset of cells:

$$\begin{aligned}
 & \mathbf{for} [i = 1, 2, \dots, m]: \\
 & \quad \mathbf{for} [j = 1, 2, \dots, \gamma]: \Delta_{ij} \leftarrow D_{ij}; \quad //\text{forming local matrix of distances} \\
 & \quad \mathbf{for} [l = 1, 2, \dots, \gamma]: \\
 & \quad \quad \left. \begin{aligned}
 & d = \min_{\substack{i=1, \dots, m \\ j=1, \dots, \gamma}} \{ \Delta_{ij} \}; \\
 & \mathbf{for} [i = 1, 2, \dots, m]: \\
 & \quad \mathbf{for} [j = 1, 2, \dots, \gamma]: \\
 & \quad \quad \mathbf{if} [ \Delta_{ij} = d ]: \\
 & \quad \quad \quad \Lambda_{ij}^\gamma \leftarrow 1; \quad //\text{assigning object to cluster} \\
 & \quad \quad \quad \Delta^{(j)} \leftarrow (\max \{ \Delta \} + 1)_{m \times 1}; \quad //\text{local blocking } j\text{-th cluster (column)} \\
 & \quad \quad \quad \Delta^{T(i)} \leftarrow (\max \{ \Delta \} + 1)_{\gamma \times 1}; \quad //\text{local blocking } i\text{-th object (row)} \\
 & \quad \quad \quad D^{T(i)} \leftarrow (\max \{ D \} + 1)_{\gamma \times 1}; \quad //\text{global blocking } i\text{-th object (row)}
 \end{aligned} \right\} \\
 & \quad \mathbf{return} \Lambda^\gamma;
 \end{aligned} \tag{2.18}$$

For the two successive subsets the procedure runs analogously. Changes deal only with the range of variability of factor's number in the loops  $\mathbf{for}[i = \dots]$ .

**Step 2.6:**

In the preceding step it was ensured that in each of the  $\gamma$  clusters one working cell, one input structure and one output structure was placed. Now it is possible to assign factors, without any limitations, by taking into account only the criterion of minimization of distances from the cluster centres  $\alpha^{(j)}$ :

$$\begin{aligned}
 & \mathbf{for} [i = 1, 2, \dots, q]: \\
 & \quad \mathbf{for} [j = 1, 2, \dots, \gamma]: \\
 & \quad \quad \mathbf{if} [ D_{ij} = \min_{j=1, \dots, \gamma} \{ D^{T(i)} \} ]: \Lambda_{ij}^\gamma = 1; \tag{2.19} \\
 & \quad \mathbf{return} \Lambda^\gamma;
 \end{aligned}$$

**Step 2.7:**

Comparison between the obtained cluster division matrix and the solution reached from the preceding loop. Here Frobenius norm is applied to difference between the compared matrices:

$$\left\| \Lambda^\gamma - \hat{\Lambda} \right\|_F = \sqrt{\sum_{i=1}^q \sum_{j=1}^{\gamma} (\lambda_{ij}^\gamma - \hat{\lambda}_{ij})^2} \tag{2.20}$$

Further action is dependent on assessment of value of the norm. The assessment is made by comparing its result with the assumed limit value  $\delta$  experimentally determined for a given case.

$$\begin{aligned}
 & \mathbf{if} \left[ \left\| \Lambda^\gamma - \hat{\Lambda} \right\|_F \leq \delta \right]: \mathbf{go to step 3}; \\
 & \mathbf{otherwise}: \mathbf{go to step 2.2};
 \end{aligned} \tag{2.21}$$

**Step 3:**

For the determined  $\gamma$  the cluster division matrix  $\Lambda^\gamma$  is known. The clusters  $K_1^\gamma, \dots, K_\gamma^\gamma$  are also given in the form of sets of the factors to which correspond unity values in respective columns of the matrix  $\Lambda^\gamma$ . As a result the division  $\Gamma$  into three-dimensional groups is obtained:

$$\forall_{i=1, \dots, \gamma} \Gamma_i = (K_i^\gamma \cap S, K_i^\gamma \cap C^{in}, K_i^\gamma \cap C^{out}) \tag{2.22}$$

**Step 4:**

Comparison of variants of number of clusters and applied distance measures is performed by determining the division which maximizes value of the objective function:

$$\Gamma^* = \Gamma: E(\Gamma) \rightarrow \max \tag{2.23}$$

**The end of the algorithm**

The investigating of many variants of number of clusters may seem time-consuming. However it should be taken into

account that in practical building 3S structures we deal with a total number of different working cells, which amounts to a few dozen only. This is much less than that of possible variants of input and output structures.

The algorithm makes it possible to search for similarities between produced 3S structures, working cells and structures which are joined together in the cells. As a result, is obtained information which deals with the following:

- structure of working cells, i.e. which operations have to be realized by the cells and how many working cells should realize given operations,
- kinds of the structures which will be most often delivered to the cells to be joined together there, which is connected with ensuring appropriate transport means, as well as with possible location of the cells and manufacturers of subassemblies in close neighbourhood,
- indication of a cell which has to be responsible for production of a given structure in the case when the structure is qualified to belong to one of the groups.

The described problem may seem to be solvable by independent realization of the two two-dimensional grouping: output structures – cells, input structures – cells. However it should be observed that possibility of building a given output structure by a production cell is strictly dependent on a degree of complexity of input structures which have to be joined together. Two cells may produce the same structure, however one of them may be specialized in assembling complex subassemblies whereas the other may realize the process of assembling single details to form simple structural units. Therefore the output structure will be assigned to three-dimensional group only if it itself shows technological similarity and also the input structures and working cells coincidental with it do the same.

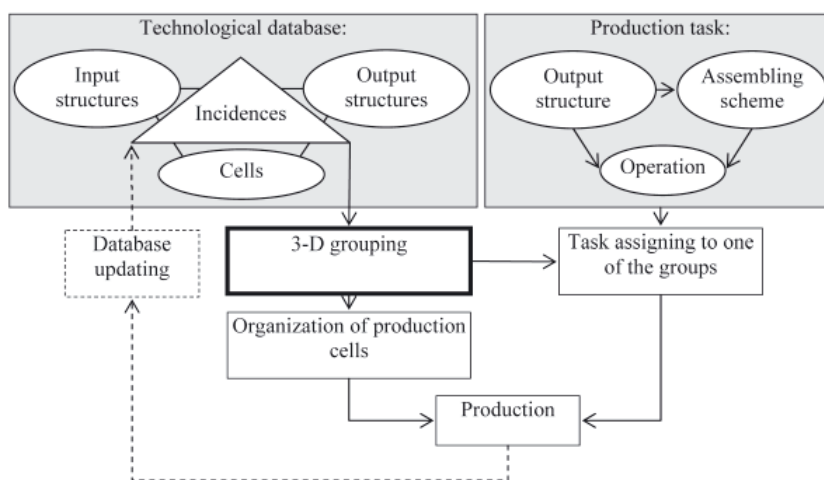


Fig. 2.1. Location of the proposed algorithm into production planning process of 3S structures

### 3. EXEMPLARY CALCULATIONS

#### 3.1. Example 1 – the binary problem proposed by Li

In 2007 Li [15] considered the following 3-D binary problem (let's call it: „Li” problem):

$$A^{M-P} = \begin{matrix} & p_1 & p_2 & p_3 & p_4 \\ m_1 & \begin{pmatrix} 1 & 1 \\ & 1 \end{pmatrix} \\ m_2 & \begin{pmatrix} & 1 & 1 & 1 \\ & & 1 & 1 \end{pmatrix} \\ m_3 & \begin{pmatrix} & & 1 \\ & & & 1 \end{pmatrix} \\ m_4 & \begin{pmatrix} & & & 1 \\ & & & & 1 \end{pmatrix} \end{matrix}, A^{M-O} = \begin{matrix} & o_1 & o_2 & o_3 & o_4 & o_5 \\ m_1 & \begin{pmatrix} 1 & 1 \\ & 1 \end{pmatrix} \\ m_2 & \begin{pmatrix} 1 & 1 & 1 \\ & 1 & 1 \end{pmatrix} \\ m_3 & \begin{pmatrix} 1 & 1 \\ & 1 \end{pmatrix} \\ m_4 & \begin{pmatrix} 1 \\ & 1 \end{pmatrix} \end{matrix}, A^{P-O} = \begin{matrix} & o_1 & o_2 & o_3 & o_4 & o_5 \\ p_1 & \begin{pmatrix} 1 & 1 & 1 \\ & 1 & 1 & 1 \\ & 1 & 1 & 1 \end{pmatrix} \\ p_2 & \begin{pmatrix} & 1 & 1 & 1 \\ & & 1 & 1 & 1 \end{pmatrix} \\ p_3 & \begin{pmatrix} & & 1 & 1 & 1 \\ & & & 1 & 1 & 1 \end{pmatrix} \\ p_4 & \begin{pmatrix} & & & 1 & 1 & 1 \end{pmatrix} \end{matrix}$$

and formulated its pseudo-optimum solution in the form of division into the two groups:

$$\Gamma_1 = (\{m_2, m_4\}, \{p_2, p_4\}, \{o_1, o_3, o_5\})$$

$$\Gamma_2 = (\{m_1, m_3\}, \{p_1, p_3\}, \{o_2, o_4\})$$

The grouping can be represented by the sorted incidence matrices with the distinguished submatrices of groups as follows:

$$A_{sort}^{M-P} = \begin{matrix} & p_2 & p_4 & p_1 & p_3 \\ m_2 & \begin{pmatrix} 1 & 1 \\ & 1 \end{pmatrix} & & & 1 \\ m_4 & \begin{pmatrix} 1 & 1 \\ & 1 \end{pmatrix} & & & \\ m_1 & & & \begin{pmatrix} 1 & 1 \\ & 1 \end{pmatrix} & \\ m_3 & & & & \begin{pmatrix} 1 \\ & 1 \end{pmatrix} \end{matrix}, A_{sort}^{M-O} = \begin{matrix} & o_1 & o_3 & o_5 & o_2 & o_4 \\ m_2 & \begin{pmatrix} 1 & 1 & 1 \\ & 1 & 1 \end{pmatrix} & & & & \\ m_1 & & & & \begin{pmatrix} 1 & 1 \\ & 1 \end{pmatrix} & \\ m_3 & & & & \begin{pmatrix} 1 & 1 \\ & 1 \end{pmatrix} & \end{matrix}, A_{sort}^{P-O} = \begin{matrix} & o_1 & o_3 & o_5 & o_2 & o_4 \\ p_2 & & \begin{pmatrix} 1 & 1 & 1 \\ & 1 & 1 & 1 \end{pmatrix} & & & \\ p_4 & & \begin{pmatrix} 1 & 1 & 1 \\ & 1 & 1 & 1 \end{pmatrix} & & & \\ p_1 & \begin{pmatrix} 1 & 1 & 1 \\ & 1 & 1 & 1 \end{pmatrix} & & & & \\ p_3 & \begin{pmatrix} 1 & 1 & 1 \\ & 1 & 1 & 1 \end{pmatrix} & & & & \end{matrix}$$

The quality index of the above mentioned grouping, under assumption of the weights  $q = 0.5$  and  $\omega_1 = \omega_2 = \omega_3$ , amounts to:  $E(\Gamma^{Li}) = 1/3(0.875 + 0.95 + 0.05) = 0.625$ .

The Li's solution is compared now with the results obtained by means of the proposed algorithm and distance measures described by Eqs. through. As can be observed in this case the division can be done into 2, 3 or 4 groups. Tab. 3.1 presents the divisions which provide the best values of the quality indices for particular measures.

Tab. 3.1. Results of solving the problem „Li”

Measure	Division	Quality index
Manhattan	$\Gamma_1 = (\{m_1\}, \{p_4\}, \{o_1\}),$ $\Gamma_2 = (\{m_2\}, \{p_3\}, \{o_4\}),$ $\Gamma_3 = (\{m_3\}, \{p_2\}, \{o_3, o_5\}),$ $\Gamma_4 = (\{m_4\}, \{p_1\}, \{o_2\})$	0.267
Euclidean, Mahalanobis	$\Gamma_1 = (\{m_2\}, \{p_1, p_2, p_3\}, \{o_1\}),$ $\Gamma_2 = (\{m_1, m_3, m_4\}, \{p_4\}, \{o_2, o_3, o_4, o_5\})$	0.511
Angular	$\Gamma_1 = (\{m_1\}, \{p_1\}, \{o_1\}),$ $\Gamma_2 = (\{m_2\}, \{p_2\}, \{o_4\}),$ $\Gamma_3 = (\{m_3\}, \{p_3\}, \{o_3\}),$ $\Gamma_4 = (\{m_4\}, \{p_4\}, \{o_2, o_5\})$	0.567
Chebyshev	$\Gamma_1 = (\{m_1, m_2, m_4\}, \{p_1, p_2, p_3\}, \{o_1, o_3, o_5\}),$ $\Gamma_2 = (\{m_3\}, \{p_4\}, \{o_2, o_4\})$	<b>0.668</b>

As can be observed, the Chebyshev measure provides the division of the quality index higher than the solution obtained by Li. The division can be represented by the following sorting of incidence matrices:

$$A_{sort}^{M-P} = \begin{matrix} & p_1 & p_2 & p_3 & p_4 \\ \begin{matrix} m_1 \\ m_2 \\ m_4 \\ m_3 \end{matrix} & \begin{pmatrix} 1 & & & \\ & 1 & & \\ & & 1 & \\ & & & 1 \end{pmatrix} & & & 
 \end{matrix}, 
 A_{sort}^{M-O} = \begin{matrix} & o_1 & o_3 & o_5 & o_2 & o_4 \\ \begin{matrix} m_1 \\ m_2 \\ m_4 \\ m_3 \end{matrix} & \begin{pmatrix} & & & & & \\ & & & & 1 & 1 \\ & 1 & 1 & 1 & & \\ & & & & & \\ & & & & 1 & 1 \end{pmatrix} & & & 
 \end{matrix}, 
 A_{sort}^{P-O} = \begin{matrix} & p_1 & & & & \\ \begin{matrix} o_1 & o_3 & o_5 & o_2 & o_4 \end{matrix} & \begin{pmatrix} 1 & 1 & 1 & & \\ & & & 1 & 1 \\ & & & & \\ & 1 & 1 & 1 & \\ & & & & 1 & 1 \end{pmatrix} & & & 
 \end{matrix}$$

It can be hence stated that the proposed algorithm is potentially useful to grouping the sets whose incidences are expressed by binary variables. Certainly, quality of obtained results depends on assumed weights. Let's observe that the increasing of the weight  $q$  would cause the increasing of superiority of the solution obtained with Chebyshev measure over the result of Li. Simultaneously, the decreasing of the weight  $\omega_3$  would result in improving the solution of Li and decreasing the quality of our solution.

### Example 2 – extension of the binary problem of Li

In order to present action of the grouping algorithm in the case of continuous incidence matrices the binary problem discussed in Example 1 will be modified. It is done by assigning random values from the interval (0,1] to non-zero elements of incidence matrices. As a result the following problem is obtained:

$$A^{M-P} = \begin{matrix} & p_1 & p_2 & p_3 & p_4 \\ \begin{matrix} m_1 \\ m_2 \\ m_3 \\ m_4 \end{matrix} & \begin{pmatrix} 0.1 & & & \\ & 0.5 & & \\ & & 0.2 & 1 & 0.9 \\ & & & 0.6 & \\ & 0.5 & & & 0.3 \end{pmatrix} & & & 
 \end{matrix}, 
 A^{M-O} = \begin{matrix} & o_1 & o_2 & o_3 & o_4 & o_5 \\ \begin{matrix} m_1 \\ m_2 \\ m_3 \\ m_4 \end{matrix} & \begin{pmatrix} & & 0.2 & & 0.3 \\ & 1 & & 0.7 & 0.5 \\ & & 0.3 & & 0.1 \\ & 0.6 & & & \end{pmatrix} & & & 
 \end{matrix}, 
 A^{P-O} = \begin{matrix} & p_1 & & & & \\ \begin{matrix} o_1 & o_2 & o_3 & o_4 & o_5 \end{matrix} & \begin{pmatrix} 0.2 & & 0.1 & & 1 \\ & 0.9 & & 0.3 & 0.8 \\ & & 0.5 & 0.7 & 0.6 \\ & 0.9 & & 0.4 & \end{pmatrix} & & & 
 \end{matrix}$$

Tab. 3.2 presents the best results obtained with the use of the grouping algorithm.

Tab. 3.2. Results of solving the problem „Li” extended to continuous form

Measure	Division	Quality index
Angular	$\Gamma_1 = (\{m_1\}, \{p_4\}, \{o_1\})$ , $\Gamma_2 = (\{m_2\}, \{p_1\}, \{o_2, o_4\})$ , $\Gamma_3 = (\{m_3\}, \{p_3\}, \{o_3\})$ , $\Gamma_4 = (\{m_4\}, \{p_2\}, \{o_5\})$	0.379
Euclidean	$\Gamma_1 = (\{m_1\}, \{p_1\}, \{o_1\})$ , $\Gamma_2 = (\{m_2\}, \{p_2\}, \{o_2\})$ , $\Gamma_3 = (\{m_3\}, \{p_3\}, \{o_3\})$ , $\Gamma_4 = (\{m_4\}, \{p_4\}, \{o_4, o_5\})$	0.381
Manhattan	$\Gamma_1 = (\{m_1\}, \{p_1, p_3\}, \{o_1, o_3\})$ , $\Gamma_2 = (\{m_2, m_4\}, \{p_2\}, \{o_2\})$ , $\Gamma_3 = (\{m_3\}, \{p_4\}, \{o_4, o_5\})$	0.383
Mahalanobis	$\Gamma_1 = (\{m_3\}, \{p_1\}, \{o_1, o_3\})$ , $\Gamma_2 = (\{m_2, m_4\}, \{p_2\}, \{o_2\})$ , $\Gamma_3 = (\{m_1\}, \{p_3, p_4\}, \{o_4, o_5\})$	0.406
Chebyshev	$\Gamma_1 = (\{m_1\}, \{p_2\}, \{o_2\})$ , $\Gamma_2 = (\{m_4\}, \{p_1\}, \{o_4\})$ , $\Gamma_3 = (\{m_2\}, \{p_3\}, \{o_1\})$ , $\Gamma_4 = (\{m_3\}, \{p_4\}, \{o_3, o_5\})$	<b>0.536</b>

Also in this case the Chebyshev measure turns out to be most effective in grouping the elements. This time the division into four specialized groups is the best. In matrix form it can be presented as follows:

$$A^{M-P} = \begin{matrix} & p_2 & p_1 & p_3 & p_4 \\ m_1 & \boxed{\phantom{0.1}} & 0.1 & 0.5 & \\ m_4 & 0.5 & \boxed{\phantom{0.1}} & & 0.3 \\ m_2 & 0.2 & & \boxed{1} & 0.9 \\ m_3 & & & 0.6 & \boxed{\phantom{0.1}} \end{matrix},$$

$$A^{M-O} = \begin{matrix} & o_2 & o_4 & o_1 & o_3 & o_5 \\ m_1 & \boxed{0.2} & 0.3 & & & \\ m_4 & & \boxed{\phantom{0.1}} & 0.6 & & \\ m_2 & & & \boxed{1} & 0.7 & 0.5 \\ m_3 & 0.3 & 0.1 & & \boxed{\phantom{0.1}} & \end{matrix},$$

$$A^{P-O} = \begin{matrix} & o_2 & o_4 & o_1 & o_3 & o_5 \\ p_2 & \boxed{0.9} & 0.3 & & & 0.8 \\ p_1 & & \boxed{\phantom{0.1}} & 0.2 & 0.1 & 1 \\ p_3 & & & \boxed{0.5} & 0.7 & 0.6 \\ p_4 & 0.9 & 0.4 & & \boxed{\phantom{0.1}} & \end{matrix}$$

### 3.2. Example 3 – practical problem – the welding of steel structures

#### 3.2.1. Problem description

Let an example of building five kinds of input structures shown in Fig. 3.1, be considered. The structures have been not subjected to any analysis of possible, at least partial, unification of their sets of lower-stage subassemblies. Intentionally, real rough data are considered.

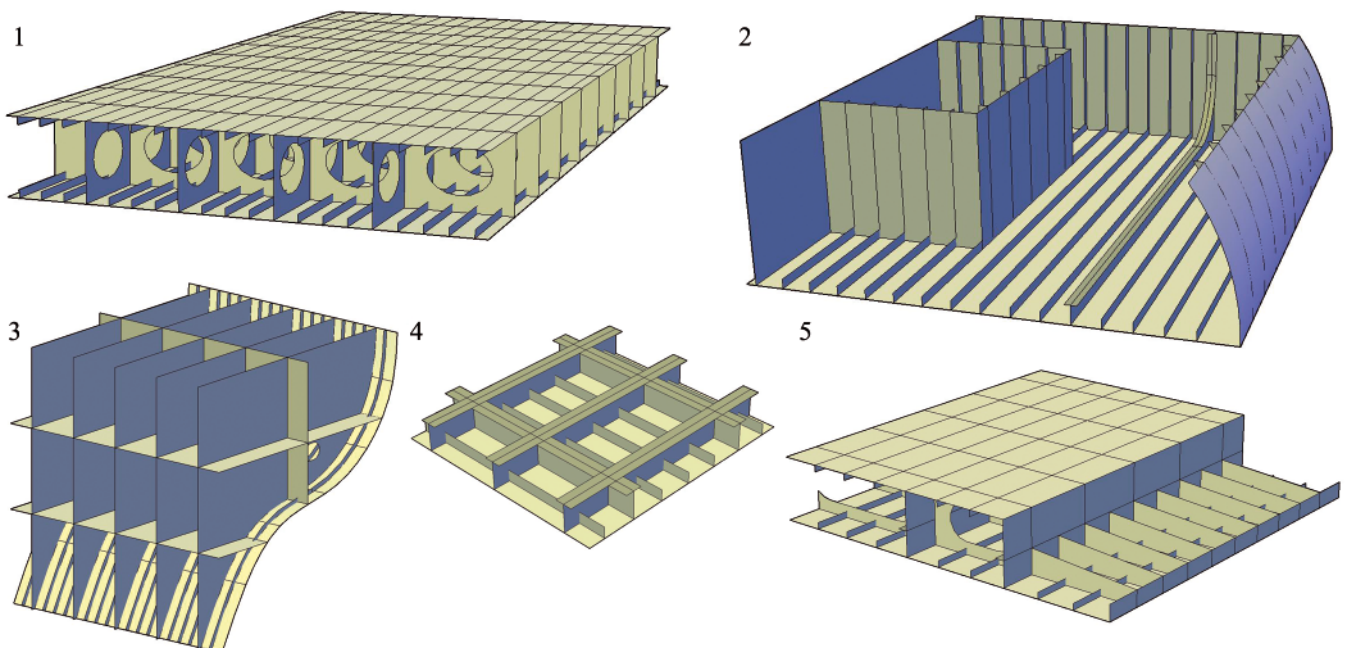


Fig. 3.1. Considered output structures



$$A^{S-C^{out}} = \begin{matrix} & \begin{matrix} c_1^{out} & & & & c_5^{out} \end{matrix} \\ \begin{matrix} s_1 \\ \\ \\ \\ \\ \\ \\ s_8 \end{matrix} & \begin{pmatrix} 0 & 0 & 0.17 & 0 & 0 \\ 0 & 0.02 & & & \\ 0 & & 1 & & \\ 0.29 & 0.04 & & 0.01 & 0.08 \\ 0 & & 0.06 & & \\ 0.41 & & 0.2 & & 0.13 \\ 0.41 & 0.1 & & 0.04 & 0.2 \\ 0 & & & 0.004 & \end{pmatrix} \end{matrix}$$

### 3.2.2. Results of the grouping

With the use of the algorithm described in Chapter 2.3 the divisions into 2, 3, 4 and 5 three-dimensional groups were obtained according to the condition. The following values of weighing coefficients:  $q = 0.5$ ,  $\omega_{S-C^{in}} = \omega_{S-C^{out}} = \omega_{C^{in}-C^{out}} = 1$  were assumed.

Five measures of distance between elements were tested, i.e. the angular, Manhattan, Euclidean, Chebyshev and Mahalanobis one. For four numbers of groups and five distance measures, twenty divisions and quality indices corresponding to them, were obtained – Fig. 3.3.

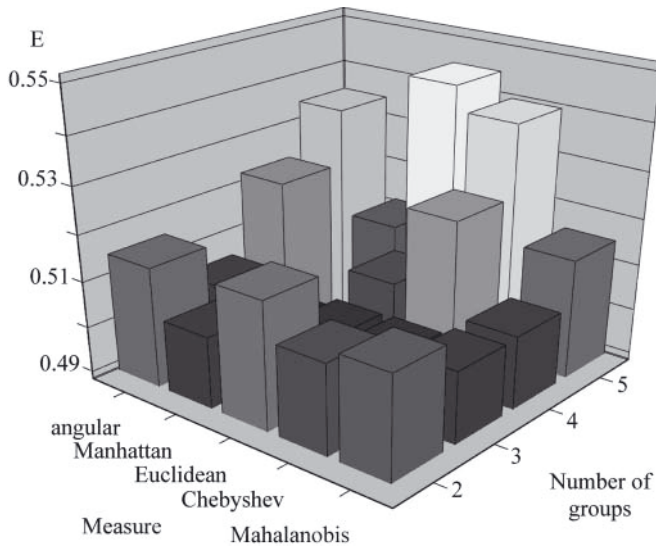


Fig. 3.3. Quality indices of divisions for different numbers of groups and distance measures

The best solution was obtained for the division into five groups by using Euclidean measure:  $(E(\Gamma) = 0.545)$ . The groups are as follows:

$$\begin{aligned} \Gamma_1 &= (\{s_5\}, \{c_5^{in}, c_6^{in}, c_{31}^{in}\}, \{c_5^{out}\}) \\ \Gamma_2 &= (\{s_8\}, \{c_1^{in}, c_2^{in}, c_3^{in}, c_7^{in}, \dots, c_{13}^{in}, c_{18}^{in}, c_{19}^{in}, \\ &\quad c_{21}^{in}, \dots, c_{30}^{in}, c_{32}^{in}, \dots, c_{37}^{in}\}, \{c_4^{out}\}) \\ \Gamma_3 &= (\{s_1, s_3\}, \{c_{17}^{in}\}, \{c_3^{out}\}) \\ \Gamma_4 &= (\{s_4, s_6, s_7\}, \{c_4^{in}\}, \{c_1^{out}\}) \\ \Gamma_5 &= (\{s_2\}, \{c_{14}^{in}, c_{15}^{in}, c_{16}^{in}, c_{20}^{in}\}, \{c_2^{out}\}) \end{aligned}$$

If the grouping between pairs of the sets are taken into account then it can be observed that the greatest mean value in the groups (Eq. ) is always reached for the division into five groups. However effectiveness of the measures shows different values for different pairs, e.g. for:

- S-C<sup>in</sup> – angular measure is the best,  $(\eta_1(A^{S-C^{in}}, \Gamma) = 0.0515)$
- S-C<sup>in</sup> – Euclidean measure is the best  $(\eta_1(A^{S-C^{out}}, \Gamma) = 0.2857)$ ,
- C<sup>in</sup>-C<sup>out</sup> – Chebyshev measure is the best  $(\eta_1(A^{C^{in}-C^{out}}, \Gamma) = 0.1131)$ .

As can be observed, during analyzing we are forced to take into account various measures, since their effectiveness depends on values of co-ordinates of grouped elements.

In the above discussed example can be observed a tendency for breaking up the division into as many groups as possible. It results from a low density of incidence matrices which constitute input data. And, such density directly results from the breaking-up of the set of input structures. Reduction in size of the set C<sup>in</sup> is possible by standardizing the input structures. Influence of such approach on results of grouping will be discussed in a separate publication.

## CONCLUSIONS

In this paper has been presented the algorithm which on the basis of three assumed sets, groups their elements in such a way as locate at least one element out of each set into each of the group. In the algorithm the method of cluster analysis of k-means as well as five different measures of distance between multi-dimensional space points, was applied. It was elaborated with the aim of its applications to organization of production of 3S structures. To this end, were distinguished three sets of elements occurring in enterprises which produce structures of the kind. The sets as well as continuous matrices of incidence between them form input data for the proposed grouping algorithm. These are: set of working cells, set of input structures (subassemblies) and set of output structures.

The grouping division obtained this way can find application during designing production cells. Certainly, the above determined groups are only an indication as to mutual location of working cells and their equipment. Three-dimensional group can be interpreted as an indication for very close location of:

- working cells for production of concrete input structures (or points of delivery of the structures from outside of the enterprise),
- working cells for joining the structures into larger objects (output structures) as well as
- working cells which use the output structures for further joining them, or possible cleaning, painting, fitting, launching or also loading and dispatching.

Full modification of a non-optimum spatial organization of working cells may be impossible. It is hard to expect that because of results of grouping whole workshop buildings would be moved. However enterprise logistic system is much more adaptable in this respect.

The group may be hence interpreted also as an indication for elevation of enterprise investment priorities in certain areas.

It can be:

- extension of internal roads between selected cells;
- purchase of transport means dedicated to certain structures, acc. their mass, gabarites, shapes;
- ordering, to subcontractors, some workings which especially disturb determined production flows within enterprise.

A general conclusion which can be drawn on the basis of the performed calculations is that the problem of designing group technologies becomes greatly complicated in the moment of relating it to real production problems. Theoretical methods in this area have been developed for tens of years however reality seriously challenges both theoreticians and engineers aimed at implementing the methods into practice.

## BIBLIOGRAPHY

1. Ballakur A., Steudel H.J.: *A within-cell utilization based heuristic for designing cellular manufacturing systems*. International Journal of Production Research, 25, 1987, 639–665.
2. Ben-Arieh D., Sreenivasav R.: *Information analysis in a distributed dynamic group technology method*. International Journal of Production Economics 60–61, 1999, 427–432.
3. Bhat M.V., Haupt A.: *An efficient clustering algorithm*. IEEE transactions on systems. Man and Cybernetics SMC-6 (1), 1976, 61–64.
4. Boctor F.F.: *A linear formulation of the machine-part cell formation problem*. International Journal of Production Research, 29 (2), 1991, 343–356.
5. Boe W.J., Cheng C.H.: *A close neighbor algorithm for designing a cellular manufacturing system*. International Journal of Production Research, 29 (10), 1991, 2097–2116.
6. Chan H.M., Milner D.A.: *Direct clustering algorithm for group formation in cellular manufacture*. Journal of Manufacturing Systems, 1 (1), 1982, 65–75.
7. Chandrasekharan M.P., Rajagopalan R.: *An ideal seed non-hierarchical clustering algorithm for cellular manufacturing*. International Journal of Production Research, 24 (2), 1986, 451–464.
8. Cho K.-K., Sun J.-G., Oh J.-S.: *An automated welding operation planning system for block assembly in shipbuilding*. International Journal of Production Economics 60-61 (1), 1999, 203-209.
9. Groover M.P.: *Fundamentals of modern manufacturing: materials, processes and systems*. 4th ed., John Wiley&Sons, 2010.
10. Hartigan J. A.: *Clustering Algorithms*. John Wiley & Sons Inc., 1975.
11. Hassan M.M.D.: *Layout design in group technology manufacturing*. International Journal of Production Economics, 38, 1995, 173-188.
12. Iwańkiewicz R.: *Object-matrix model of complex manufacturing technology*. Industrial Management & Data Systems, 108 (8), 2008, 1131-1148.
13. Kitaoka M., Nakamura, R., Serizawa, S., Usuki, J.: *Multivariate analysis model for machine-part cell formation problem in group technology*. International Journal of Production Economics, 60–61, 1999, 433–438.
14. Li M.-L.: *The algorithm for integrating all incidence matrices in multi-dimensional group technology*. International Journal of Production Economics, 86, 2003, 121-131.
15. Li M.-L.: *Efficiency measurement for multi-dimensional group technology*. International Journal of Advanced Manufacturing Technology, 35, 2007, 621-632.
16. Li M.-L., Parkin R.E.: *Group technology revisited: a simple and robust algorithm with enhanced capability*. International Journal of Production Research, 35 (7), 1997, 1969-1992.
17. Min H., Shin D.: *Simultaneous formation of machine and human cells in group technology: A multiple objective approach*. International Journal of Production Research, 31 (1), 1993, 2307–2318.
18. Parkin R.E., Li M.-L.: *The multi-dimensional aspects of a group technology algorithm*. International Journal of Production Research, 35 (8), 1997, 2345–2358.
19. Tan P.-N., Steinbach M., Kumar V.: *Introduction to Data Mining*. Addison Wesley, 2005, 496-515.

---

## CONTACT WITH THE AUTHOR

Remigiusz Iwańkiewicz, Ph.D.  
 West Pomeranian University of Technology, Szczecin  
 Faculty of Marine Technology and Transport  
 Al. Piastów 41  
 71-065 Szczecin, POLAND  
 e-mail: iwankow@zut.edu.pl

# Determination of the Effects of the Pre-Outfitting and Pre-Piping Assembly Operations on Shipyard Productivity

**Murat Ozkok**, Assist. Prof.  
Karadeniz Technical University, Turkey  
**I. Hakki Helvacioğlu**, Assoc. Prof.  
Istanbul Technical University, Turkey

## ABSTRACT

*The process improvement operations are very significant in shipbuilding industry as the other industries. In recent years, the shipyards attempt to improve their processes by examining their current production system and to reduce the cycle time of the interim product so that they can keep their competitive power. If the cycle time of the interim products is decrease, that may cause to increase the annual production capacity and market share of the shipyard. In order to do this, the shipyards have to analyse their own production system and carry out some improvements on it. In this study, the effects of carrying out the outfitting and piping assembly operations in earlier work stations were investigated by using a methodology presented here. The steps in the methodology were applied to a double bottom block of a container ship. It was shown that if the outfitting and the piping assembly operations are carried out in earlier stations instead of the block assembly station, this may increase the throughput by 33%. The results of the study were discussed in the final section.*

**Key words:** Pre-outfitting assembly; pre-piping assembly; simulation; ship production

## INTRODUCTION

Shipbuilding is a global industry competing in the world extent [1]. In recent years, the shipyards attempt to improve their production processes in order to yield advantages against their competitors by manufacturing the ship as soon as possible. Geoje Samsung Shipyard is able to manufacture 40 ships per year in South Korea and it is also known as one of the most efficient shipyards in the world [2]. As compared with the other shipyards, Samsung shipyard has a great competitive advantage against its competitors. So, the point is that the shipyards have to investigate their production system and do some improvements in order to keep the competitive power.

One of the latest trend in manufacturing process is to reduce the cycle time of the product. In order to reduce the cycle time, it is needed to make process improvements on the current production system. Eker [3] reported some improvement suggestions with regard to the processes in the painting shops of the Sedef Shipyard and Schalekamp Shipyard. In the study [4], the format of the design drawings coming from design department was changed and the cutting process was carried out in shorter time and in more effective way. The process improvement operations was also applied on the scaffold area and material stock area [5] and the layout of the work stations [6] and [7]. In Todd Pacific Shipyard, as a result of improvement process, the moving distances of the forklifts were shortened in the rate of 50% and the oil wastes occurring during the operations of the forklifts were also reduced [8]. As can be seen

from the above works, the process improvement applications are able to be applied in many fields in shipyard.

The effects of the improvements on the production system can be seen by simulation. Simulation has a great importance for the production companies. In the competition environment, the changes on the production system and the effects of these changes are very significant in terms of the company performance. Simulation has been applied in many industry for years as it provides a great advantage for the planner. In shipbuilding industry, it has a great deal of application fields such as layout, production processes and so on. In the study that has been still going on by Michigan University and Seoul University, it is aimed to simulate all the activities in shipyard and to see the effects of the changes on the production system [9]. In the other study, the stations forming the sub assembly line were modelled by using simulation and after the system was simulated, a robot was settled in the production line and the rate of productivity was determined [10]. Shin [11] aimed to settle the work stations of the shipyard in the optimum way. That's a layout application of simulation. Alkaner [12] considered a profile cutting station and the processes of the profile cutting station were determined. Then, these processes were modelled in a simulation program and the effects of changing the resources were investigated. In the study [13], the panel production station was considered as a bottleneck station. Processes were determined and modelled in simulation program. Then, by doing some changes on the processes, the completion time of the panel cutting station was tried to be

optimized. In this study, Arena simulation program [14] was used for modelling the work flows between stations as the modules of it are very appropriate for modelling the production activities. The activities can also be modelled easily by using the modules.

In many shipyards in Turkey, the whole assembly operations with regard to outfitting and piping are carried out in the block assembly area. In the block assembly area, after the steel assembly operations of the block are over, the outfitting and piping assembly operations are carried out. Therefore, the work load of the block assembly area is very high and this may cause to a new bottleneck in the production system. In this study, the outfitting and piping assembly operations of the block will be carried out in earlier work stations and some changes will be applied on the current production line. As a result, the effects of all these changes on the current production system will be determined. The phases of the methodology are followed one by one and the effects of the pre-outfitting and pre-piping activities on the entire production system are seen.

In literature, the papers with regard to pre-outfitting are very limited. In the papers, the modular outfitting concept is mentioned. Fafandjel [15] mentioned that the ship is manufactured in shorter time by using modular outfitting concept. Yu and Ishida [16] searched how to determine the effectiveness of the modular outfitting concept. Baade et al. [17] mentioned the advantages of the modular outfitting in his paper.

## METHODOLOGY

Fig. 1 presented the methodology implemented in this study. The methodology consists of nine steps. In the first step of the model, the product, which is produced in shipyard production line, is defined. Then, the workstations, that are involved in product fabrication, are described. In the step 3, detailed process analysis of current production system is performed. After comprehensive process analysis, simulation model of the current production system is modelled in ARENA simulation software (in step 4). In step 5, simulation model is run along a specific period and production quantity (throughput) of the production system is achieved. Then, some suggestions on current production system are made in step 6. After that, these suggestions are applied on current simulation model in step 7 and the new production case is obtained. In step 8, the effects of the changes are discussed and evaluated. Finally, in the last step (step 9), comparison of the current and new production cases is performed.

## APPLICATION

### *Defining of product (Step 1)*

Ships are fabricated in blocks which constitute ship structure. There are various sort of blocks such as bow, aft, side, bulkhead and double bottom block. In this study, a double bottom block of a container ship is illustrated as an example. Double bottom block is one of the main interim products in shipbuilding. The reason of considering the double bottom block in this study is that almost all of the work stations are involved in its production activities.

As the structure of a double bottom block is examined, it can be seen that it has different production phases, which are called as production stages. Table 1 shows these production stages and the structures representing these production stages.

A double bottom block is built by coming together the production stages mentioned in Tab. 1. In the first phase of the

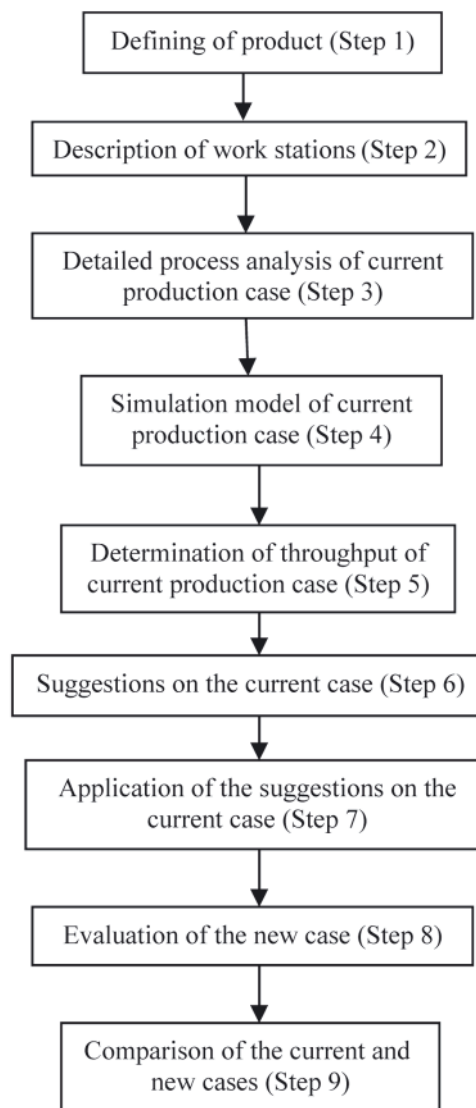


*Fig. 1. Application steps of the study*

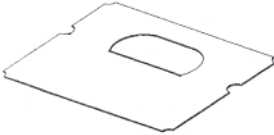
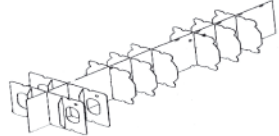
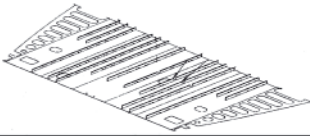
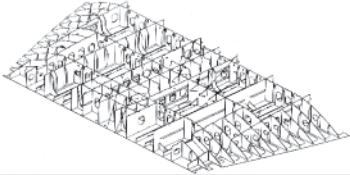
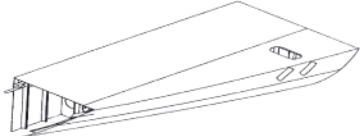
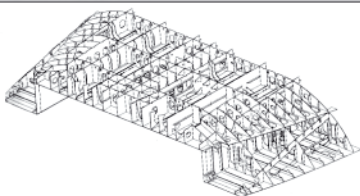
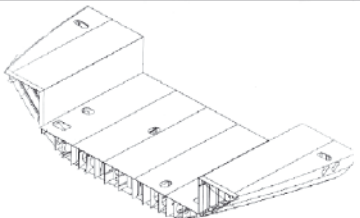
double bottom production, single section parts (A) and single plate parts (B) are fabricated. These parts are cut from the plates and profiles which have standard-dimensions and they have specific dimensions after cutting process. Then, they are fitted and minor assembly is built (C). Two or more minor assemblies constitute sub assembly (D). Flat plates are sub-merged welded and flat plate assembly (E) is fabricated. When the profiles are fillet welded on flat plate assembly, the flat plane assembly (F) is built. Minor and sub assemblies are welded on the flat plane assembly (F) and major sub assembly (G) is manufactured. Curved panel assembly (H) is manufactured on pin jigs. In block assembly area, sub unit assembly (J) and curved panel assembly are mounted and welded, finally a double bottom block (K) is built.

There are also some outfitting equipments in double bottom block just like manholes, bottom plugs, zinc, vertical ladder and doubling plates. These outfitting equipments are mounted into block structure's body. Tab. 2 shows these outfitting materials.

### *Descriptions of work stations (Step 2)*

Ship production is extremely hard job since it includes a great deal of process. A ship is manufactured by performing thousands of work activities. In order to manufacture a ship, various types of workstations are needed. Every workstation

Tab. 1. Production stages of a double bottom block and structures

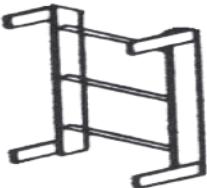
Production Stage	Definitions of production stages	Structures representing production stage
A	Single section part	
B	Single plate part	
C	Minor assembly	
D	Sub assembly	
E	Flat plate assembly	
F	Flat panel assembly	
G	Major sub assembly	
H	Curved panel assembly	
J	Sub unit assembly	
K	Unit assembly	

has a task for ship production. Tab. 3 shows the work stations which have function in double bottom block production.

In edge cutting station (I1), the edge cutting operation of ship hull plates is carried out. Edge cutting operation is the contour cutting of flat plates. And the plates which are subject to edge cutting constitute the panel structure. The edge cleaning operation of the ship hull plates, which are cut in edge cutting station (I1), is carried out in edge cleaning and sequencing

station (I2). There are some materials and slags on the edge surfaces of the plates after edge cutting. Using a grinding machine, these materials and slags remove from the edge surfaces of the plates. In I2 station, the plates are also sequenced in accordance with the process turn. The hull plates are welded and the panel structure is produced in panel production station (I3). In panel cutting station (I4), the panel which is manufactured in panel production station (I3) is subject to

Tab. 2. Outfitting materials used in double bottom block

Outfitting name	Outfitting structure
Manhole	
Bottom plug	
Zinc	
Vertical ladder	
Doubling plates	

Tab. 3. The work stations in the production process of the double bottom block

Station no	Station name
I1	Edge cutting
I2	Edge cleaning and sequencing
I3	Panel production
I4	Panel cutting
I5	Profile spot welding
I6	Profile TIG welding
I7	Section spot welding
I8	Section TIG welding
I9	Grinding
I10	Profile cutting
I11	Profile bending
I12	Nest cutting
I13	Pre-fabrication
I14	Jig
I15	Plate bending (Press)
I16	Block assembly

counter cutting in accordance with its dimensions. The profiles are assembled on the panel by spot welding in profile spot welding station (I5). The profiles are welded by TIG welding in profile TIG welding station (I6). The minor and sub assemblies are joined on the flat panel assembly by spot welding in section spot welding station (I7). The minor and sub assemblies are welded on the flat panel assembly by TIG welding in section TIG welding station (I8). Grinding station (I9) is the last station of the panel line. In this station, the grinding operations of the flat panel and major sub assemblies are performed. The cutting operations of the profiles are performed in profile cutting station (I10). Standard-dimensioned profiles, which are sent

to profile cutting station, are cut with specific dimensioned profiles. The bending operations of the profiles are performed by box machine in profile bending station (I11). The bending profiles are used in curved panel. Nest cutting station (I12) is the heart of the shipyard production system. In this station, single plate assemblies are manufactured. Minor and sub assemblies are produced in pre-fabrication station (I13). Curved panel assemblies are produced in jig station (I14). Jig structure consists of curved jigs. The curved panels are lied down the jig structure and the curved profiles are welded on this curved plates. In plate bending station (I15), the bending operations of the plates, coming from nest cutting station, are performed. Therefore, the flat plates are transformed to the curved plates. The structures and parts produced in previous work stations are sent to block assembly station (I16) and the block structure is formed by assembling the corresponding parts. Fig.2 shows the work flows between work stations.

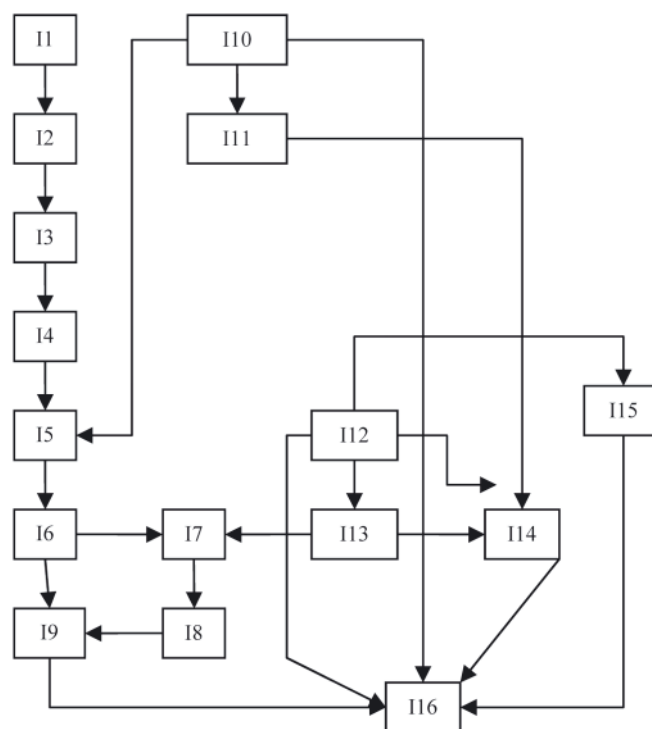


Fig. 2. Work flow in the shipyard production system

### Detailed process analysis of current production case (Step 3)

In this step, the comprehensive process analysis of the work stations are carried out. Every work station has a considerable number of work activities. At the beginning of the detailed process analysis, the work activities are determined and then the durations of each work activity are achieved. Because there are over 2500 work activities, the process analysis of only panel production and panel cutting stations are presented here.

#### Process analysis of panel production station (I3)

In panel production station, panel structure is fabricated by submerged arc welding. Fig. 3 shows the general arrangement of the panel production station. In the first step, the plates are fixed to panel line by using conveyor fixing mechanism. Then, they are sent to tolerance plate's welding area where the tolerance plates are welded with tack welding. Submerged arc welding operation starts from the tolerance plates because the welding becomes more stabilized. After that, the plates are transferred to submerged arc welding machine with conveyor.

Tab. 4. Detailed process analysis of panel production station (I3)

Activity no.	Activity description	Repetition number of activity	Activity duration (min.)
1	The overhead crane goes to the flat plate to be transported	11	4.125
2	The overhead crane comes down to the flat plate surface	12	5.746
3	The overhead crane holds the flat plate	12	1.997
4	The overhead crane lifts the flat plate	12	5.746
5	The overhead crane transports the flat plate	12	4.5
6	The overhead crane takes down the flat plate	12	5.4
7	The overhead crane leaves the flat plate surface	12	0.996
8	The overhead crane goes up the flat plate surface	12	5.4
9	The operator walks to the start point of the conveyor line	11	2.2
10	The worker walks to the conveyor line plate fixed mechanism.	12	0.864
11	The operator fixes the plate on the conveyor line	12	3.996
12	The worker runs the conveyor line	46	3.818
13	The operator walks to the welding tolerance plates	20	1.1
14	The conveyor transports the plate to the tolerance plate welding area	12	1.042
15	The alignment of the plate on the tolerance plate welding area	8	1.307
16	The operator brings the tolerance plates to the flat plate	20	1.1
17	The operator puts the tolerance plates near the corners of the flat plates	40	5.32
18	The worker walks to spot welding machine	2	0.086
19	The worker runs the spot welding machine	2	0.166
20	The operator sets up the spot welding machine	50	8.32
21	The operator fixes the tolerance plates on the corners of the flat plates with spot welding	40	38
22	The operator walks to the other corner of the flat plate	20	3.46
23	The operator goes to the TIG welding machine	22	2.066
24	The conveyor transports the flat plate to the TIG welding area	12	1.414
25	The worker walks to the TIG welding machine in order to check the position of the flat plate	12	1.536
26	The worker checks out the position of the flat plate	12	18
27	The operator runs the TIG welding machine	12	16.992
28	The flat plate is fixed to the TIG welding machine with clamps	12	9
29	The worker checks out whether the plate is fixed on the TIG welding machine conveniently or not.	12	60
30	The worker brings the spot welding machine near the TIG welding machine	10	0.72
31	The operator comes down to the plates for spot welding	10	0.53
32	The spot welding operation of the plates prior to TIG welding	10	115.358
33	The worker goes to the torches of the TIG welding machine	10	0.32
34	The operator sets up the TIG welding machine before TIG welding process.	10	41.664
35	TIG welding of the plates	10	272.19
36	The conveyor transports the panel outside the TIG welding station.	10	1.728

Here, the plates are welded with submerged arc welding and they are then sent to buffer area. As a result, flat plate assembly (production stage E) is fabricated. Table 4 illustrates the detailed process analysis in panel production station.

#### Process analysis of panel cutting station (I4)

Counter cutting of the panel is performed in this station. Fig. 4 shows general arrangement of panel cutting station. The

panel fabricated in I3 gets to Buffer Area 2. Then, the panel is transferred to panel cutting machine with conveyor. Panel cutting machine performs counter cutting operation. But, before this, blasting operation is fulfilled. Then, automatic marking operation is done. Therefore, the alignments of the piece parts can be easily performed. After that, the counter cutting operation is carried out. Finally, the panel is transferred to Buffer Area 1. Detailed process analysis of panel cutting station is illustrated in Table 5.

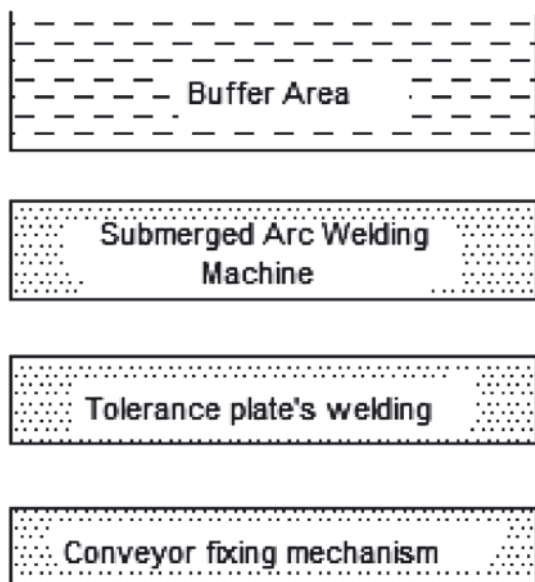


Fig. 3. General arrangement of panel production station (13)

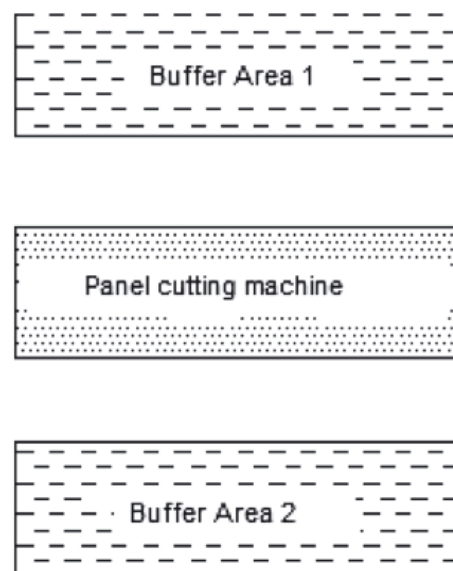


Fig. 4. General arrangement of panel cutting station (14)

Tab. 5. The process analysis of panel cutting station (14)

Activity no.	Activity description	Repetition number of activity	Activity duration (min.)
1	The operator transports the panel to the panel cutting station	2	1.334
2	The operator goes to bring the cutting program CD	2	2
3	The operator takes the cutting program CD	2	1
4	The operator goes back the cutting station with CD	2	2
5	The operator loads the Program CD to the cutting machine	2	2
6	The cutting machine moves on the counter line of the panel	2	7.811
7	The cutting machine signs the reference points on the panel	2	3.906
8	The cutting machine loads the reference points on itself.	2	2
9	The operator runs the panel cutting machine	2	0.5
10	Blasting and marking processes	2	139.937
11	Cutting process	2	101.457
12	The worker takes the marking pen	2	2
13	Manuel marking process	2	17.583
14	Taking the outfitting parts and bringing them to the cutting station.	12	3
15	The workers put the outfitting parts on the panel.	12	9
16	The worker runs the spot welding machine	12	1.992
17	Spot welding process	12	15.83
18	The worker runs the grinding machine	12	1.992
19	Grinding process after the spot welding process	6	7.334
20	The worker runs the TIG welding machine	6	1.992
21	TIG welding process	6	126.48
22	Grinding process after the TIG welding process	6	7.49
23	The conveyor transports the panel outside the panel cutting station	2	1.066

In the same way, the detailed process analysis is performed for the other work stations. Because there are over 2500 work activities, it is impossible to present here. After the work activities and their durations are determined, the completion times of the work stations are calculated by considering the serial and parallel work activities. In Table 6, the completion times of the work stations are given. For instance, the process time of edge cutting station is 190 minutes. In other words, the edge cutting process of the plates, which constitute the panel of the double bottom block, takes 190 minutes.

Tab. 6. Station completion times of the current case

Station name	Completion time (min.)
Edge cutting	190
Edge cleaning and sequencing	203
Panel production	622
Panel cutting	356
Profile spot welding	380
Profile TIG welding	414
Section spot welding	501
Section TIG welding	660
Grinding	99
Profile cutting	410
Profile bending	350
Nest cutting	653
Pre-fabrication1	448
Pre-fabrication2	632
Jig	1522
Plate bending (Press)	1317
Block assembly	2196

**Simulation model of current production case (Step 4)**

In this step, simulation model of the current production system is created. Fig. 5 depicts the simulation model of the current case and Tab. 7 shows the modules which are used in simulation model.

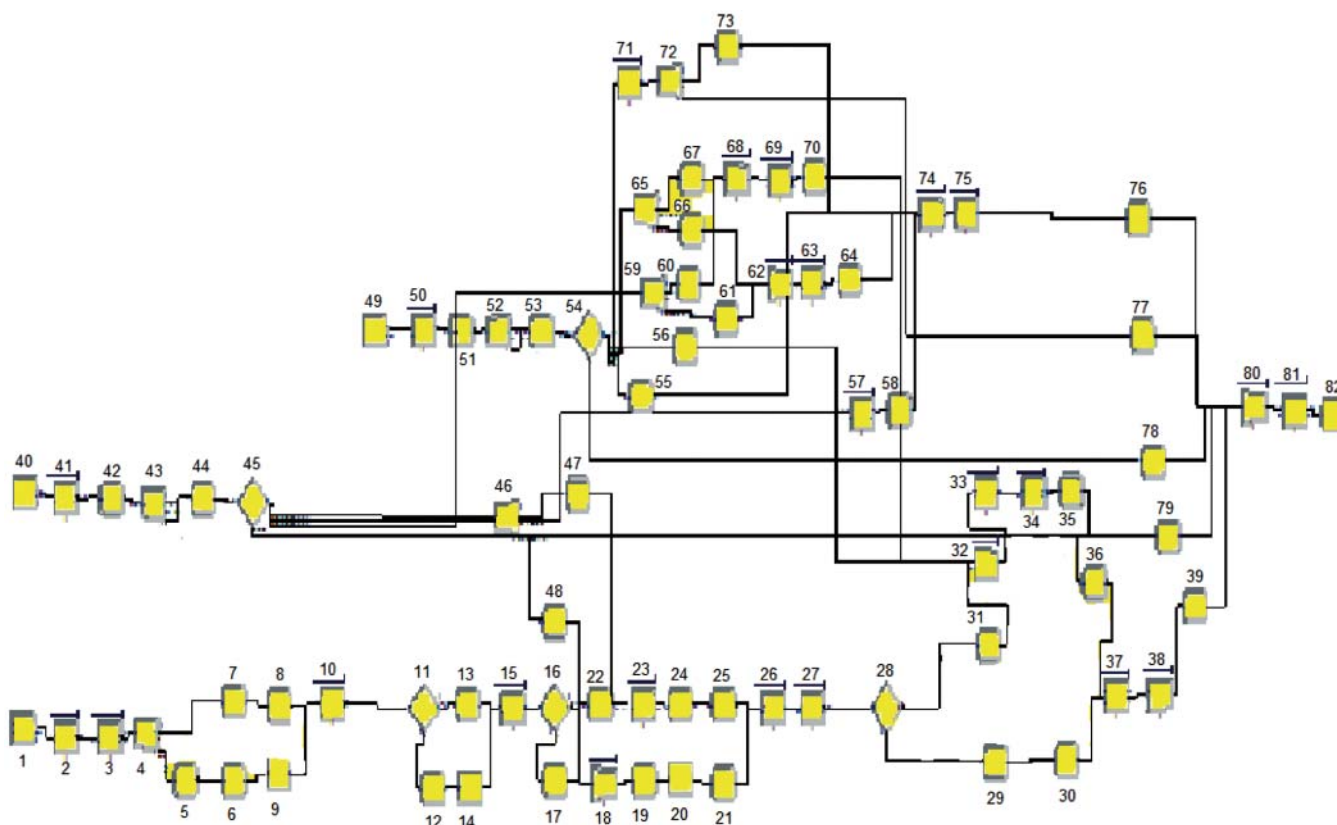


Fig. 5. Simulation model of the current case

Tab. 7. Definition of module numbers

Module no.	Module name	Module no.	Module name	Module no.	Module name
1	Create1	29	Assign13	57	Process of profile bending (I11 station)
2	Process of plate edge cutting (I1 station)	30	Assign14	58	Assign 27
3	Process of plate edge cleaning	31	Assign15	59	Separate 5
4	Separate1	32	Batch3	60	Assign 28
5	Assign1	33	Process of section spot welding(I7 station)	61	Assign 29
6	Assign2	34	Process of section TIG welding (I8 station)	62	Batch 5
7	Assign3	35	Assign16	63	Process of pre-fabrication1
8	Assign4	36	Assign17	64	Assign 30
9	Delay1	37	Process of grinding (I9 station)	65	Separate 6
10	Process of panel production (I3 station)	38	Batch4	66	Assign 31
11	Decide1	39	Assign18	67	Assign 32
12	Assign5	40	Create2	68	Batch 6
13	Assign6	41	Process of profile cutting (I11 station)	69	Process of pre-fabrication1
14	Delay2	42	Assign19	70	Assign 33
15	Process of panel cutting (I4 station)	43	Separate 2	71	Process of plate bending (I15 station)
16	Decide2	44	Assign20	72	Separate 7
17	Assign7	45	Decide4	73	Assign 34
18	Batch1	46	Separate 3	74	Batch 7
19	Assign8	47	Assign 21	75	Process of jig (I14 station)
20	Delay3	48	Assign 22	76	Assign 35
21	Assign9	49	Create 3	77	Assign 36
22	Assign10	50	Process of nest cutting (I12 station)	78	Assign 37
23	Batch2	51	Assign 23	79	Assign 38
24	Assign11	52	Separate 4	80	Batch 8
25	Assign12	53	Assign 24	81	Process of block assembling (I16 station)
26	Process of profile spot welding (I5 station)	54	Decide 5	82	Dispose
27	Process of profile TIG welding (I6 station)	55	Assign 25		
28	Decide3	56	Assign 26		

In ARENA simulation model, various modules are employed to create the simulation model of the production system. Tab. 8 represents the modules and their definitions.

Tab. 8. Description of modules

Module name	Description
Create	Describes the arrival time and quantity of the materials entering into the production system
Process	Describes the work stations in the production system
Assign	Makes assignments the products leaving any work station and it is also used in assembly operations
Decide	This module orients the products to the work stations where they will go to
Batch	Used in assembly operations. It combines the products for assembly operation
Separate	Divides the main product into sub products. It is usually used for cutting operations
Dispose	Shows the exit of the production system

### ***Determination of throughput of current production case (Step 5)***

After the simulation model is created, the model is run along 720 hours. The current case has a capacity of producing 18 double bottom blocks at the end of the operation time of 720 hours. In other words, the current case can produce a double bottom block in 2400 minutes.

### ***Suggestions on the current case (Step 6)***

In the current production line, the assemblies of the outfitting and piping are carried out in the block assembly station. After the completion of the steel works, the outfitting assembly and then the piping assembly are carried out. Therefore, all these operations are done in serial way, which means more work load and longer lead times. If we can carry out the outfitting and piping operations in earlier work stations and distribute the work load, we can reduce the work load and the completion time of the block assembly station. By doing this, the waiting time in front of the block assembly area is lowered and the lead time of the double bottom block may be shorter. Tab. 9 depicts the suggestions on the current case.

Tab. 9. The suggestions on the current case

No. of suggestions	Workstation	Description of suggestions
1	Panel cutting	The welding operations of the manholes on tanktop panel were carried out. These welding operations are one side welding. In this way, the one side welding operations of the manholes will be finished
2	Panel cutting	The one side welding operations of the bottom plugs (two pieces) on hull panel
3	Panel cutting	The welding operations of the zincs (six pieces) on hull panel were carried out and finished
4	Pre-fabrication	The assemblies of vertical ladders (three pieces) were carried out on the sections
5	Pre-fabrication	The assemblies of the zincs (thirty-two pieces) were carried out
6	Pre-fabrication	Assemblies of pipe systems (twenty-six) on the module
7	Pre-fabrication	Manufacturing the module in pre-fabrication station (I13) in order to assemble the piping systems
8	Jig	Assembly of pipe systems (nine) on the curved panel assembly in jig station
9	Block assembly	Assembly of one vertical ladder when the block is upside down
10	Block assembly	Completing of the welding operations of two bottom plugs when the block is upside down
11	Block assembly	Completing of the welding operations of four manholes when the block is in flat position
12	Block assembly	Assembly of twenty doubling plates when the block is in flat position
13	Block assembly	Assembly of two bilge wells when the block is in flat position
14	Block assembly	Assembly of four zincs when the block is in flat position
15	Block assembly	Carrying out the outfitting and steel operations in parallel way in the block assembly station
16	Block assembly	In the block assembly station (I16), in the steel operations, there are fourteen TIG welding and spot welding workers in the current case. In the new case, the quantity of the TIG welding and spot welding workers are sixteen for steel operations. The TIG welding and spot welding operations are carried out by the same workers. And also, two spot welding and TIG welding machines which are on idle are added to the station

### Application of the suggestions on the current case (Step 7)

In this phase, the suggestions given in Step 6 are applied in the current simulation model in Fig. 5. Panel cutting, section spot welding, pre-fabrication, jig and block assembly stations were influenced by the suggestions on the current case and the completion times of these work stations are calculated again. Table 10 shows the completion times of each work stations in new case.

Tab. 10. Station completion times of the new case

Station name	Completion time (min.)
Edge cutting	190
Edge cleaning and sequencing	203
Panel production	622
Panel cutting	460
Profile spot welding	380
Profile TIG welding	414
Section spot welding	284
Section TIG welding	660
Grinding	99
Profile cutting	410
Profile bending	350
Nest cutting	653
Pre-fabrication1	621
Pre-fabrication2	632
Jig	1634
Plate bending (Press)	1317
Block assembly	1073

### Evaluation of the new case (Step 8)

In the evaluation of the new case, Arena simulation program will be used. The new case manufactures 24 double bottom blocks at the end of 720 hours. That means the new case can produce a double bottom block in 1800 minutes.

### Comparison of the current and new cases (Step 9)

Fig. 6 shows the quantity of the double bottom block manufactured in both cases at the end of 720 hours. While the current case produces 18 double bottom blocks, the new case produces 24 double bottom blocks.

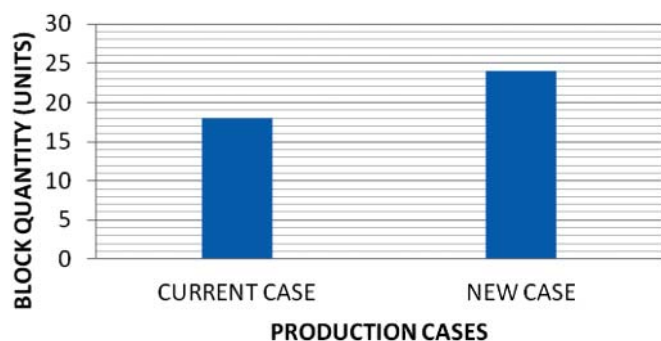


Fig. 6. Block quantity manufactured in the current and new cases

Fig. 7 shows the cycle times of the double bottom block for both cases. While a double bottom block is produced in 2400 minutes in the current case, in the new case, a double bottom block is produced in 1800 minutes.

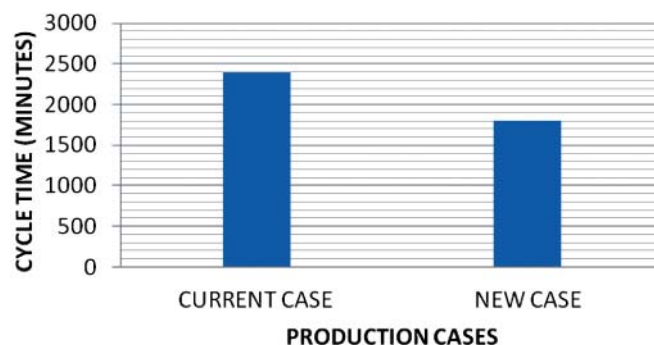


Fig. 7. Cycle times of the double bottom block for the current and new cases

It should be noted here that, no extra expenditures are paid during the transition from the current case to the new case. All the changes on the current case were performed by using the possibilities of the shipyards without purchasing any workers or equipments. Table 11 presents the need of additional equipment and manpower.

Tab. 11. Need of resources after changing

Suggestion no.	Work Station	Additional equipment	Additional manpower
1	Panel cutting	No need	No need
2	Panel cutting	No need	No need
3	Panel cutting	No need	No need
4	Pre-fabrication	No need	No need
5	Pre-fabrication	No need	No need
6	Pre-fabrication	No need	No need
7	Pre-fabrication	No need	No need
8	Jig	No need	No need
9	Block assembly	No need	No need
10	Block assembly	No need	No need
11	Block assembly	No need	No need
12	Block assembly	No need	No need
13	Block assembly	No need	No need
14	Block assembly	No need	No need
15	Block assembly	No need	No need
16	Block assembly	No need	No need

### CONCLUSIONS

In this study, some improvement suggestions with regard to outfitting and piping assembly operations were carried out on the shipyard production system. The improvements were applied on the block assembly station that was a bottleneck. The main changes on the current case were the pre-outfitting assembly operations and pre-piping assembly operations. According to simulation work, in the current case, the system can manufacture 18 blocks at the end of 720 hours. After the changes were applied on the current case, the new production case can produce 24 blocks at the end of 720 hours. So, the changes on the current case provide an improvement rate of 33% without additional expenditure. In other words, when the assembly operations of the outfitting and piping are carried

out in earlier work stations, the throughput increases. The pre-outfitting and pre-piping assembly operations provide less cycle time. The authors strongly recommend the shipyards to perform outfitting and piping assembly operations in earlier stations instead of block assembly area since the cycle time of the block is considerably decreased.

## BIBLIOGRAPHY

1. Frankel E.G.: *Impact of technological change on shipbuilding productivity*, Journal of Ship Production, 1, 3, 174-183, 1985.
2. Inozu B., et al.: *New horizons for shipbuilding process improvement*, Journal of Ship Production, 22, 2, 87-98, 2006.
3. Eker E.: *The application of the process improvement concept on the paint works*, MSc Thesis, ITU Institute of Science, Istanbul, 1999.
4. Hardwick M., Kassel B., Crump B. and Garret S.: *Improving shipyard manufacturing processes using STEP-NC*, Journal of Ship Production, 21, 3, 170-176, 2005.
5. DiBarra C.: *5S-A tool for culture change in shipyards*, Journal of Ship Production, 18, 3, 143-151, 2002.
6. Odabasi A.Y., Alkaner S., Olcer A. and Sukas N.: *Reengineering of small and medium-sized ship production facilities: An example for Turkish Shipbuilding industry*, Journal of Ship Production, 13, 1, 8-15, 1997.
7. Odabasi A.Y., et al.: *Development and evaluation of Marmara Shipyard's expansion program*, Contract Report, Istanbul, 1993.
8. Larson T., and Tice J.: *Lean and EMS Integration Workshop*, Environmental Technologies, Ship Production Panels, USA, 2005.
9. Lamb T.: *Simulation-based performance improvement for shipbuilding processes*, Journal of Ship Production, Vol. 22, No. 2, May, pp.49-65, 2006.
10. Shin J.G.: *A modeling and simulation of production process in subassembly lines at a shipyard*, Journal of Ship Production, Vol.20, No.2, May, pp.79-83, 2004.
11. Shin J.G.: *A concept and framework for a shipyard layout design based on simulation*, Journal of Ship Production, Vol.25, No.3, August, pp.126-135, 2009.
12. Alkaner S.: *The Modelling and Analysis of Ship Production with Simulation: Case Study*, PhD Thesis, ITU Institute of Science, Istanbul, 1998.
13. Greenwood A.G., Hill H.W.: *Simulation Optimization Decision Support System for Ship Panel Shop Operations*, Proceedings of the 2005 Winter Simulation Conference, pp. 2078-2086, 2005.
14. Kelton W.D., Sadowski R.P. and Sturrock D.T.: *Simulation with Arena*, Third edition, McGraw-Hill, 1998.
15. Fafandjel N., et al.: *Procedure for measuring shipbuilding process optimization results after using modular outfitting concept*, Urednistvo Casopisa Strojartvo, 50, 3, 141-150, 2008.
16. Yu H. and Ishida K.: *The evaluation of the effectiveness of modular outfitting of engine room machines*, Fourth International Conference on Marine Technology, 23-25 May, Poland, 391-399, 2001.
17. Baade R., et al.: *Modular outfitting*, Journal of Ship Production, 14, 3, 170-179, 1998.

---

Murat Ozkok, Assist. Prof.  
Department of Naval Architecture and Marine Engineering,  
Karadeniz Technical University,  
61530 Camburnu/Trabzon, TURKEY  
Phone: +90 462 752 2805,  
Fax: +90 462 752 2158,  
e-mail: muratozkok@ktu.edu.tr

I. Hakki Helvacioğlu, Assoc. Prof.  
Faculty of Naval Architecture and Ocean Engineering,  
Istanbul Technical University,  
34469, Maslak/Istanbul, TURKEY  
Phone: +90 212 285 6391,  
Fax: +90 212 285 6454,  
e-mail: ismailh@itu.edu.tr

# On the ship course-keeping control system design by using robust feedback linearization

Zenon Zwierzewicz, Assoc. Prof.  
Maritime University of Szczecin, Poland

## ABSTRACT



*In the paper the problem of ship autopilot design based on feedback linearization method combined with the robust control approach, is considered. At first the nonlinear ship model (of Norrbinn type) is linearized with the use of the simple system nonlinearity cancellation. Next, bearing in mind that exact values of the model parameters are not known, the ensuing inaccuracies are taken as disturbances acting on the system. Thereby is obtained a linear system with an extra term representing the uncertainty which can be treated by using robust,  $H_{\infty}$  optimal control techniques. The performed simulations of ship course-changing process confirmed a high performance of the proposed controller despite the assumed significant errors of its parameters.*

**Key words:** feedback linearization; robust control; differential games; ship autopilot design

## INTRODUCTION

The feedback linearization (FL) method [9, 10, 11, 13] consists in such transformation of a given nonlinear system which results in a new, linear time-invariant one. Here, by the transformation we mean the application of a proper control law combined with possible change of the system coordinates. Once a linear system is obtained, a secondary control law (or sub-control) should be designed to ensure that the overall closed-loop system performs according to the specifications.

In the simplest case of the system the FL method is reduced to the ordinary cancellation of nonlinearity by means of a properly selected control function.

One of the main drawbacks of FL method relates to inaccuracies arising during cancellation of system nonlinearities. The thereby obtained transformed system is in fact not perfectly linear and, moreover, these imperfections may often prevent the use of efficient techniques of linear systems synthesis. An effective way to solve this problem consists in combination of feedback linearization method with the robust control techniques. In this paper  $H_{\infty}$  optimal control theory within the state space framework is applied, i.e. the problem is considered from position of differential games theory [4, 5, 8, 16]. In this view the model uncertainties are considered as an action of adversary player (or opposing nature) while our part is to invent a control strategy that is the best in terms of some given quality criterion (cost functional). In other words we are trying to minimize the cost assuming the 'worst-case action' of our opponent player (disturbances). Such an approach allows devising a controller which taking into consideration system

parametric uncertainties, guarantees at the same time a good process performance.

In the paper, besides presenting a relevant portion of the above stated theory, its usefulness to ship course-keeping (or changing) problem is considered.

It is known that the PID (proportional-integral-derivative) controllers traditionally used in the field still have many shortcomings.

A disadvantage of a PID controller is that it can provide optimal performance only at the operating point for which it is designed. The ship parameters vary significantly with operating conditions such as e.g. forward speed of the vessel. Under the varying operating conditions, it is tedious and difficult to determine properly the fixed parameters of the controller that results in good performance. Furthermore, the PID autopilots can cause difficulties when the ship makes large maneuvers involving non-linear dynamic behaviour. To avoid the problems of fixed structure PID autopilots, adaptive autopilots were introduced in the 1970s and have remained a major area of research until now [2, 17].

An alternative and promising research direction is the autopilot design from position of robust control theory for nonlinear systems. Therefore the main motivation of this paper is a proposal of the robust ship autopilot design which, based on recent  $H_{\infty}$  theory, is able to finely cope with above mentioned inconveniences.

The paper is divided into five sections and ended with conclusions. The second section presents the system class definitions, basic concepts as well as the transformation of considered system into standard differential game form. In

the third section a course-keeping problem and the Norrbin's ship model structure are given. In the fourth section the two cases of robust ship autopilot design are presented (with and without load disturbances taken into account). The last, fifth section includes a short description of simulation tests and their results.

## BASIC CONCEPTS AND DEFINITIONS

Let us consider a nonlinear system in Brunovsky form [11]:

$$\begin{aligned} \dot{x}_1 &= x_2 \\ \dot{x}_2 &= x_3 \\ &\vdots \\ \dot{x}_n &= f(\mathbf{x}, \boldsymbol{\theta}^f) + g(\mathbf{x}, \boldsymbol{\theta}^g)u \end{aligned} \quad (1a)$$

$$y = x_1 \quad (1b)$$

where:

$\mathbf{x} \in \mathbf{R}^n$  – the state vector,  
 $\boldsymbol{\theta}^f \in \mathbf{R}^k, \boldsymbol{\theta}^g \in \mathbf{R}^l$  – vectors of system parameters,  
 $u \in \mathbf{R}$  – the control input,  
 $y \in \mathbf{R}$  – the system output.

In the case of exact system model, i.e. under assumption that the nonlinear functions  $f$  and  $g$  of the model (1a) are known (and  $g(\mathbf{x}, \boldsymbol{\theta}^g) \neq 0, \forall \mathbf{x} \in \mathbf{R}^n$ ) the insertion of the simple output feedback linearizing controller [9, 10, 13, 18]:

$$u = \frac{-f(\mathbf{x}, \boldsymbol{\theta}^f) + v}{g(\mathbf{x}, \boldsymbol{\theta}^g)} \quad (2)$$

in the system (1a) results in exact cancellation of both nonlinearities ( $f$  and  $g$ ), which yields:

$$y^{(n)} = v \quad (3)$$

To find the control  $v(t)$  stabilizing this linear system a standard pole location technique can be used. If  $v$  is chosen as:

$$v = -\mu_r y^{(r-1)} - \dots - \mu_1 y \quad (4)$$

and the coefficients  $\mu_i$  are such that  $\Gamma(s) = s^r + \mu_r s^{(r-1)} + \dots + \mu_1$  is a Hurwitz polynomial in the Laplace variable  $s$ , then the output  $y(t)$  and its derivatives converge to zero asymptotically, because the closed-loop dynamics is reduced to the equation:

$$y^{(r)} + \mu_r y^{(r-1)} + \dots + \mu_1 y = 0 \quad (5)$$

which, by virtue of the choice of coefficients  $\mu_i$  is asymptotically stable. Let's notice that also the internal stability i.e. the state  $x \rightarrow 0$  as  $t \rightarrow \infty$  is obtained.

As the true system parameters  $\boldsymbol{\theta}^f, \boldsymbol{\theta}^g$  are unknown and only some their estimates  $\hat{\boldsymbol{\theta}}^f, \hat{\boldsymbol{\theta}}^g$  are at our disposal the nonlinear functions of the system (1a) are  $\hat{f}(\mathbf{x}, \hat{\boldsymbol{\theta}}^f) + \hat{g}(\mathbf{x}, \hat{\boldsymbol{\theta}}^g)u$  and the control law (2) takes now the form:

$$u = \frac{-\hat{f}(\mathbf{x}, \hat{\boldsymbol{\theta}}^f) + v}{\hat{g}(\mathbf{x}, \hat{\boldsymbol{\theta}}^g)} \quad (6)$$

Since the insertion of the control (6) into the system (1a) no longer guarantees exact cancellation and thereby a resulting system linearity (like in the former case (2)) we will try to solve this problem from position of differential games. To transform our system into a suitable form we perform the following calculations.

Adding to and subtracting from the last equation of the system (1a) the sub-control  $v$  we get:

$$\dot{x}_n = \underbrace{f - \hat{f} + (g - \hat{g})u}_w + v \quad (7)$$

where the formula  $v = \hat{f} + \hat{g}u$  obtained from (6) was also used here.

Now denoting  $w = f - \hat{f} + (g - \hat{g})u$  and treating  $w$  as system disturbances we may rewrite the equations (1a) into the general matrix form [3].

$$\dot{\mathbf{x}} = \mathbf{A}\mathbf{x} + \mathbf{B}_v \mathbf{v} + \mathbf{B}_w \mathbf{w} \quad (8a)$$

$$\mathbf{y} = \mathbf{C}_y \mathbf{x} + \mathbf{D}_{yv} \mathbf{u} \quad (8b)$$

$$\text{where: } \mathbf{A} = \begin{bmatrix} 0 & 1 & 0 & \dots & 0 \\ 0 & 0 & 1 & \dots & 0 \\ \vdots & & & \ddots & \vdots \\ 0 & & & & 1 \\ 0 & 0 & \dots & 0 & 0 \end{bmatrix}, \mathbf{B}_v = \mathbf{B}_w = \begin{bmatrix} 0 \\ 0 \\ \vdots \\ 0 \\ 1 \end{bmatrix} \quad (9)$$

$$\mathbf{D}_{yv}^T \mathbf{C}_y = \mathbf{0}, \mathbf{D}_{yv}^T \mathbf{D}_{yv} = \mathbf{I}$$

Let's observe that for optimization purposes a new output, (8b), is defined.

The matrices  $\mathbf{C}_y$  and  $\mathbf{D}_{yv}$  should be so selected as to achieve the proper weighting in the following cost functional:

$$\begin{aligned} J_\gamma(\mathbf{x}, v, w) &= \|\mathbf{y}(t)\|_2^2 - \gamma^2 \|\mathbf{w}(t)\|_2^2 = \\ &= \int_0^\infty (\mathbf{y}^T(t)\mathbf{y}(t) - \gamma^2 \mathbf{w}^T(t)\mathbf{w}(t)) dt \end{aligned} \quad (10)$$

where  $\gamma > 0$  is a properly chosen constant (see below) called the performance bound.

The last two conditions of (9) are assumed to avoid cross terms in the functional (10) so that to get an equivalence to the corresponding Lqr criterion, i.e.:

$$\mathbf{Q} = \mathbf{C}_y^T \mathbf{C}_y, \mathbf{R} = \mathbf{D}_{yv}^T \mathbf{D}_{yv} = \mathbf{I} \quad (11)$$

(compare (33), (34)).

We have defined a differential game of two players where each of them is trying to influence the system by proper (profitable for him) choice of his strategy –  $v$  and  $w$ , respectively.

We (as the first player) are trying to minimize (10) with respect to  $v$  while the disturbances (the second player) is assumed to maximize the cost (10).

Assuming the commutativity of min-max operators as well as that the optimal strategies  $v^*, w^*$  of both parties exist we have:

$$\min_v \max_w J_\gamma(\mathbf{x}, v, w) = J_\gamma(\mathbf{x}, v^*, w^*) \quad (12)$$

Let's observe that minimization of the maximized, by the second player, cost (10) refers to the situation where we are doing our best (optimally stabilizing the system output) assuming the worst-case realization of system disturbances.

One can prove [3] that if for a given  $\gamma > 0$   $w^*$  maximizing the cost (10) exists, this fact can be interpreted in terms of the condition:

$$\|G_{yw}(K)\|_\infty < \gamma \quad (13)$$

where:

$K$  – applied controller which denotes boundedness of the infinity norm of the closed-loop transfer function  $G_{yw}$  from the disturbances  $w(t)$  to the output  $y(t)$ . This guarantees also the system  $L_2$ -gain stability (from  $w$  to  $y$ ) [1].

Minimization of (10) with respect to  $v$ , under assumption that the minimal bound  $\gamma$  of is obtained, allows in turn to find the optimal controller  $K^*$ .

The explanations can be summarized into the following condition:

$$\min_{K \in \mathcal{K}} \|G_{yw}(K)\|_{\infty} = \|G_{yw}(K^*)\|_{\infty} = \gamma^* \quad (14)$$

where:

- $\gamma^*$  – the smallest  $\gamma$  in the condition
- $\mathcal{K}$  – a set of available controllers.

The formulas for suboptimal strategies are [3, 1]:

$$\begin{aligned} v(t) &= -\mathbf{B}_v^T \mathbf{P}(t) \mathbf{x}(t) \\ w(t) &= \gamma^{-2} \mathbf{B}_w^T \mathbf{P}(t) \mathbf{x}(t) \end{aligned} \quad (15)$$

where matrix  $\mathbf{P}(t)$  is a solution of the  $H_{\infty}$ -like algebraic Riccati equation (RE),

$$\begin{aligned} \mathbf{P}\mathbf{A} + \mathbf{A}^T \mathbf{P} - \mathbf{P}(\mathbf{B}_v \mathbf{B}_v^T - \gamma^{-2} \mathbf{B}_w \mathbf{B}_w^T) \mathbf{P} + \\ + \mathbf{C}_y^T \mathbf{C}_y = \mathbf{0} \end{aligned} \quad (16)$$

such that:

$$\mathbf{A} - (\mathbf{B}_v \mathbf{B}_v^T - \gamma^{-2} \mathbf{B}_w \mathbf{B}_w^T) \mathbf{P} \quad (17)$$

is stable, i.e. all of the eigenvalues of this matrix have negative real parts.

In practice, to solve the above formulated problem, we have to use some iterative procedure which consists in repeating the required calculations for different values of  $\gamma$  in order to choose the smallest one. For the properly selected  $\gamma$  (i.e. for  $\gamma = \gamma^*$ ) the strategies (15) are optimal.

## COURSE-KEEPING PROBLEM AND THE NORRBIN'S SHIP MODEL STRUCTURE

The problem of course-keeping is a task of designing an automatic control aid (autopilot) which is able, by using appropriate rudder actions, to control the ship motion as to maintain a pre-assigned constant heading. This problem is often considered as consisting of two sub-problems. The first one concerns the ship controlling along the straight line at small course deviations. The second problem concerns the proper ship control during large manoeuvres, i.e. the problem of quality of transition process as a reply for a course step-change.

In order to synthesize a course-keeping controller we apply the following Norrbin's [7, 12] ship model general structure:

$$T\dot{\psi} + F(\dot{\psi}) = k\delta \quad (18)$$

where:

- $\psi$  – actual ship course angle (heading)
- $\delta$  – rudder deflection angle as a control variable
- $T, k$  – unknown model parameters
- $F(\cdot)$  – unknown function with assumed structure

In the 'classical' approach to ship control the structure of the nonlinear function  $F$  is (according to Norrbin model) often assumed in the form of a polynomial of the third order. Generally it may be assumed as follows:

$$F(\dot{\psi}) = a_3 \dot{\psi}^3 + a_2 \dot{\psi}^2 + a_1 \dot{\psi} + a_0 \quad (19)$$

For the ship with hull symmetry we have  $a_2 = 0$ . The bias term  $a_0$  is frequently taken as null, being conveniently treated as an additional rudder-offset which can be made null by the adequate selection of the integral action in the autopilot design.

The most commonly used structure has therefore the form:

$$F(\dot{\psi}) = a_3 \dot{\psi}^3 + a_1 \dot{\psi} \quad (20)$$

Now, assuming that the structure of the function  $F$  has been predetermined the coefficients  $a_i$  are usually identified during sea trials [12]. After some ship-circulation tests we apply regression analysis to the obtained data ( $\dot{\psi}$  in function of  $\delta$ ), for each of the mentioned structures separately, and then we search for the best fitting solution.

Since each of the tests should be performed for prescribed sailing conditions, e.g. different ship load, trim and velocity it follows that the problem of sufficiently general model building is a laborious and expensive task. For this reason in practice linear models are preferred [14] as being simpler for identification as well as we have, in this case, a number of linear synthesis methods at our disposal. For several control tasks however, especially for strongly nonlinear objects, the linear models are insufficient. The control algorithm obtained from such model leads not only to the deterioration of control performance but may also produce an unpredictable destabilization of system. Due to the above mentioned facts we propose an approach which, while dealing with nonlinear models, avoids, at the same time, to cope with the demanding identification task.

## ROBUST SHIP AUTOPILOT DESIGN

In this section, based on the above given theoretical facts as well as on the presented Norrbin's model structure, we formulate and then solve the problem of robust ship course-keeping control synthesis. It is assumed, for simplicity (but without loss of generality), that the desired (reference) course value equals to zero:  $\psi_d = 0$ .

### The case without additional load disturbances

To apply the above mentioned theory let us first define the course-keeping problem as a differential game. To this end we rewrite the Norrbin's model (18) in the state space form:

$$\begin{aligned} \dot{\psi} &= r \\ r &= \Phi(r) + c\delta \end{aligned} \quad (21)$$

where:

$$\Phi = -F(\cdot)/T,$$

$$c = k/T$$

$r$  – course turning rate (angular velocity).

According to (20) the function  $\Phi$  is:

$$\Phi(\dot{\psi}) = b_3 \dot{\psi}^3 + b_1 \dot{\psi} \quad (22)$$

where:

$$b_i = a_i/T, \quad i = 1, 3$$

To make use of simple feedback linearization method we apply (compare (6)) the controller:

$$\delta = \frac{-\hat{\Phi} + v}{\hat{c}} = \frac{-(\hat{b}_3 \dot{\psi}^3 + \hat{b}_1 \dot{\psi}) + v}{\hat{c}} \quad (23)$$

Now, following the procedure given in section 2, we can write Eq. (21) in the form:

$$\dot{r} = v + \underbrace{\{(\hat{b}_3 - b_3) \dot{\psi}^3 + (\hat{b}_1 - b_1) \dot{\psi} + (c - \hat{c})\delta\}}_w \quad (24)$$

or simply as follows:

$$\begin{aligned} \dot{\psi} &= r \\ \dot{r} &= v + w \Leftrightarrow \begin{bmatrix} \dot{\psi} \\ \dot{r} \end{bmatrix} = \begin{bmatrix} 0 & 1 \\ 0 & 0 \end{bmatrix} \begin{bmatrix} \psi \\ r \end{bmatrix} + \begin{bmatrix} 0 \\ 1 \end{bmatrix} v + \begin{bmatrix} 0 \\ 1 \end{bmatrix} w \end{aligned} \quad (25)$$

where  $w$  denotes errors caused by the model parameter uncertainty (considered here as a control strategy of the opposing nature).

The system output may be assumed as follows:

$$y = \begin{bmatrix} y_1 \\ y_2 \end{bmatrix} = \begin{bmatrix} \lambda & 0 \\ 0 & 0 \end{bmatrix} \begin{bmatrix} \psi \\ r \end{bmatrix} + \begin{bmatrix} 0 \\ 1 \end{bmatrix} v = \begin{bmatrix} \lambda \psi \\ v \end{bmatrix} \quad (26)$$

where the constant  $\lambda$  is a criterion weight.

The matrices which define the system in question are as follows:

$$A = \begin{bmatrix} 0 & 1 \\ 0 & 0 \end{bmatrix}, \quad B_v = B_w = \begin{bmatrix} 0 \\ 1 \end{bmatrix}, \quad C_y = \begin{bmatrix} \lambda & 0 \\ 0 & 0 \end{bmatrix}, \quad D_{yv} = \begin{bmatrix} 0 \\ 1 \end{bmatrix} \quad (27)$$

Let's note that by the proper choice of the output matrices  $C_y$ ,  $D_{yv}$ , a desired cost criterion (compare (11)) is obtained.

To find the proper numerical solution  $P(t)$  of Riccati-like equation (16) we can use Matlab function `care` [6] for different values of the constant  $\gamma > 0$ . As we want to select  $\gamma$  to be minimal (provided the solution RE exists) we have to apply this procedure repeatedly. This way we get the proper control strategy (see (15)) which will be used later in the process simulation.

### The case with added load disturbances

During the routine work of the autopilot (i.e. under specified steady-state conditions, e.g. straight route mode) besides modelling errors we have also to take into account the load disturbances. The disturbances lead to the steady heading error which can be typically compensated by integral action introduced to the control system.

To cope with the steady-state error we will consider in this section the problem of robust regulator design equipped with integral action.

Let us first define an extra error in the form of integral of the course error:

$$e = \int_0^t \psi \, dt \quad (28)$$

Based on the model (25) we define the augmented system by adding the error equation (28) (written in differential form):

$$\begin{aligned} \dot{\psi} &= r \\ \dot{r} &= v + w + d \\ \dot{e} &= \psi \end{aligned} \Leftrightarrow \begin{bmatrix} \dot{\psi} \\ \dot{r} \\ \dot{e} \end{bmatrix} = \begin{bmatrix} 0 & 1 & 0 \\ 0 & 0 & 0 \\ 1 & 0 & 0 \end{bmatrix} \begin{bmatrix} \psi \\ r \\ e \end{bmatrix} + \begin{bmatrix} 0 \\ 1 \\ 0 \end{bmatrix} v + \begin{bmatrix} 0 \\ 1 \\ 0 \end{bmatrix} w + \begin{bmatrix} 0 \\ 0 \\ 1 \end{bmatrix} d \quad (29)$$

where  $d$  are constant or slowly varying load disturbances.

The complementary output equation is:

$$y = \begin{bmatrix} y_1 \\ y_2 \\ y_3 \end{bmatrix} = \begin{bmatrix} \lambda & 0 & 0 \\ 0 & 0 & 0 \\ 0 & 0 & 1 \end{bmatrix} \begin{bmatrix} \psi \\ r \\ e \end{bmatrix} + \begin{bmatrix} 0 \\ 1 \\ 0 \end{bmatrix} v = \begin{bmatrix} \lambda \psi \\ v \\ e \end{bmatrix} \quad (30)$$

Thus the matrices that define our system are as follows:

$$A = \begin{bmatrix} 0 & 1 & 0 \\ 0 & 0 & 0 \\ 1 & 0 & 0 \end{bmatrix}, \quad B_v = B_w = \begin{bmatrix} 0 \\ 1 \\ 0 \end{bmatrix}, \quad C_y = \begin{bmatrix} \lambda & 0 & 0 \\ 0 & 0 & 0 \\ 0 & 0 & 1 \end{bmatrix}, \quad D_{yv} = \begin{bmatrix} 0 \\ 1 \\ 0 \end{bmatrix} \quad (31)$$

Let's notice that during controller synthesis process the disturbances  $d$  are not directly taken into account. However, thanks to above presented system structure, any appearance of disturbances during system operation leads to controller counteraction which prevents steady-state error.

## COURSE-CHANGING PROCESS SIMULATIONS

The standard method of assessing the control system quality is based on analysis of the transition process as a response to the step input. Thus in the following simulations we will test the ship behaviour after step change of the course set-point under different controller structures as well as various criteria data.

### Ship simulation model

According to [15] we assume, as the actual parameters of the ship model (21), the dynamic manoeuvring parameters of the m/s *Compass Island*. The units of time, length and angle are one minute, one nautical mile and one radian, respectively. The parameters were determined as follows:

$$\begin{aligned} b_3 &= -0.62 \text{ min}, \quad b_1 = -1.064 \text{ min}^{-1}, \\ b_2 &= b_0 \cong 0, \quad c = 3.553 \text{ rad/min} \end{aligned} \quad (32)$$

The parameters are, of course, not known to the control system designer thereby during the process simulations we will take another set of their values – possibly, substantially different.

It is assumed also that the ship's velocity during the steady-state control process phase is constant  $u = 0.25$  nm/min and that all the time we have constant propelling force.

The ship has the following characteristics: the maximum rudder angle is 35 deg., gross register tonnage of 9214 RT, deadweight of 13498 t, length of 172 m., draught of 9.14 m, one propeller, and maximum speed of 20 kn. Let's note that the assumed parameters make the ship directionally stable [12, 14] but we can get similar results for the ship which is directionally unstable (e.g. for the opposite sign of the coefficient  $b_1$ , i.e.  $b_1 = -1.064 \text{ min}^{-1}$ ).

### Simulation results

In order to examine the performance of the robust controller in question a corresponding Lqr regulator [3] has also been tested for comparison. The matching criteria matrices for the two cases were chosen the same.

As an approximate counterpart values to the actual ship parameters (32) (unknown for designer) we assume:

$$\begin{aligned} \hat{b}_3 &= -1 \text{ min}, \quad \hat{b}_1 = -2 \text{ min}^{-1}, \\ \hat{b}_2 &= \hat{b}_0 \cong 0, \quad \hat{c} = 2 \text{ rad/min} \end{aligned}$$

The parameters are essential for the controller design as they contain some uncertain data of the ship's dynamics.

The remaining numerical data are as follows:

$$\gamma^* = 1.05, \quad \lambda = 2$$

and

$$Q = \begin{bmatrix} \lambda^2 & 0 \\ 0 & 0 \end{bmatrix}, \quad R = 1 \quad (33)$$

where the criteria matrices  $Q$  and  $R$  refer to the corresponding Lqr problem. Let's notice that the matrices are exactly the same as those which occur in the matching robust case (compare (26)).

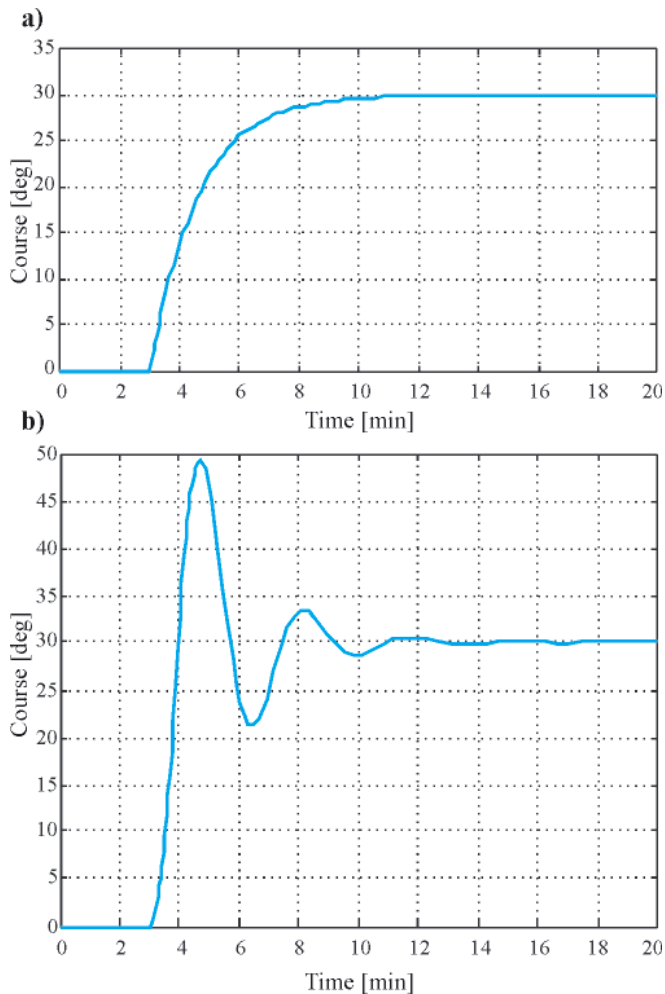


Fig. 1. Ship headings versus time for: a) robust controller, b) Lqr regulator (30° turning)

The following figures show the situation where the ship is moving for 3 min with steady speed (0.25 nm/min) along a straight line and then we apply a 30-degree step heading change command (in the case given in Fig. 3 and 4a disturbing torque is additionally applied).

The graphs presented in Fig. 1 and 2 show respectively the plots of headings and rudder deflections versus time for: a) robust controller, b) Lqr regulator.

In Fig. 3 and 4 are presented corresponding plots but for the case where the controllers are provided with integral action.

Let's notice that despite the fact that the order of parameter errors is here about 100% the robust controller performance (Fig. 1a) is very good. On the other hand the corresponding Lqr controller operates close to the stability margin (see Fig. 1b).

Moreover, according to the author experience, the plant-model parameter errors for the robust controller can be made substantially higher without noticeable process performance degradation.

Fig. 3 and 4 show corresponding graphs, however, with the difference that the controllers: robust and Lqr one are now equipped with integral action. The intensity of the constant load disturbances  $d$  acting on the ship, in the form of torque, corresponds to the compensating deflection of the rudder by 11 deg (see Fig. 4).

The numerical data for this case are as follows:

$$\gamma^* = 1.2, \lambda = 7$$

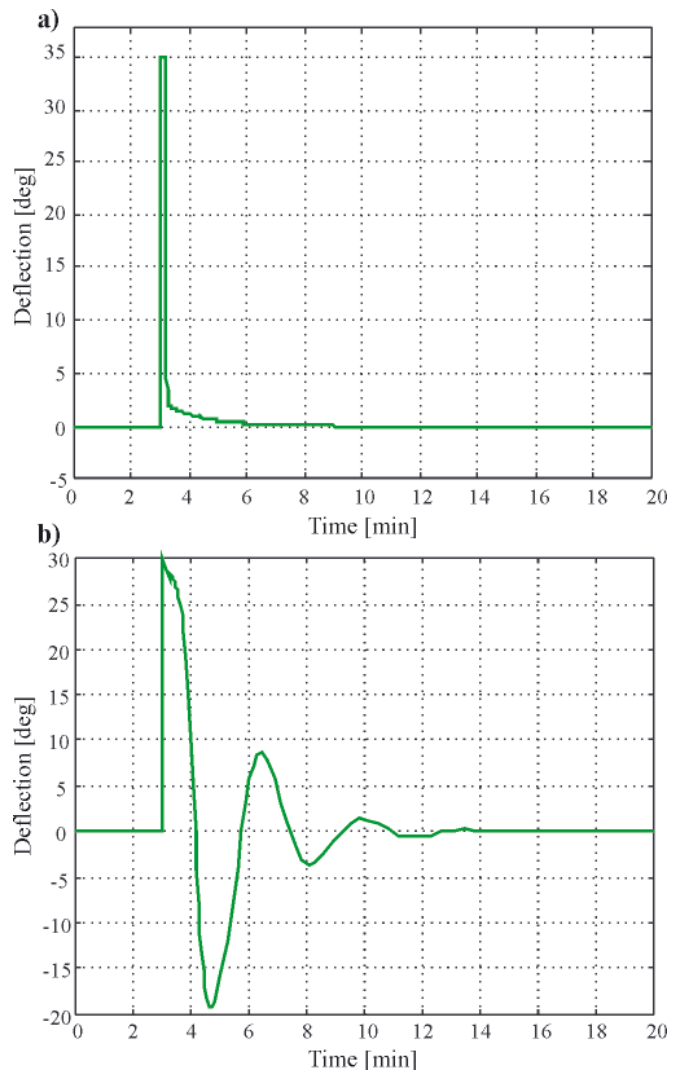


Fig. 2. Rudder deflections for: a) robust controller, b) Lqr regulator (30° turning)

and

$$\mathbf{Q} = \begin{bmatrix} \lambda^2 & 0 & 0 \\ 0 & 0 & 0 \\ 0 & 0 & 1 \end{bmatrix}, \mathbf{R} = 1 \quad (34)$$

where the criteria matrices  $\mathbf{Q}$  and  $\mathbf{R}$  refer, as before, to the corresponding Lqr problem.

As it can be seen, also in this case the robust controller performance is still better than its Lqr counterpart.

Let's observe that the plant-model mismatch disturbances  $w$  are diminishing with the progress of a transient phase of the process regulation (compare (24)). Thus the proper effect of the integral action is manifesting itself during the system steady-state, i.e. just after the process transient phase.

By manipulating the criteria weighting  $\lambda$  we can adjust the required trade-off between precision of the output variable (psi) in relation to the control effort (v) and/or the integral of course error (e).

Taking e.g.  $\lambda = 7$  we highly penalize the course error in relation to the control effort  $v$  as well as to the integral error  $e$ . To increase the number of degrees of freedom in this respect we could introduce some additional weighting related to the

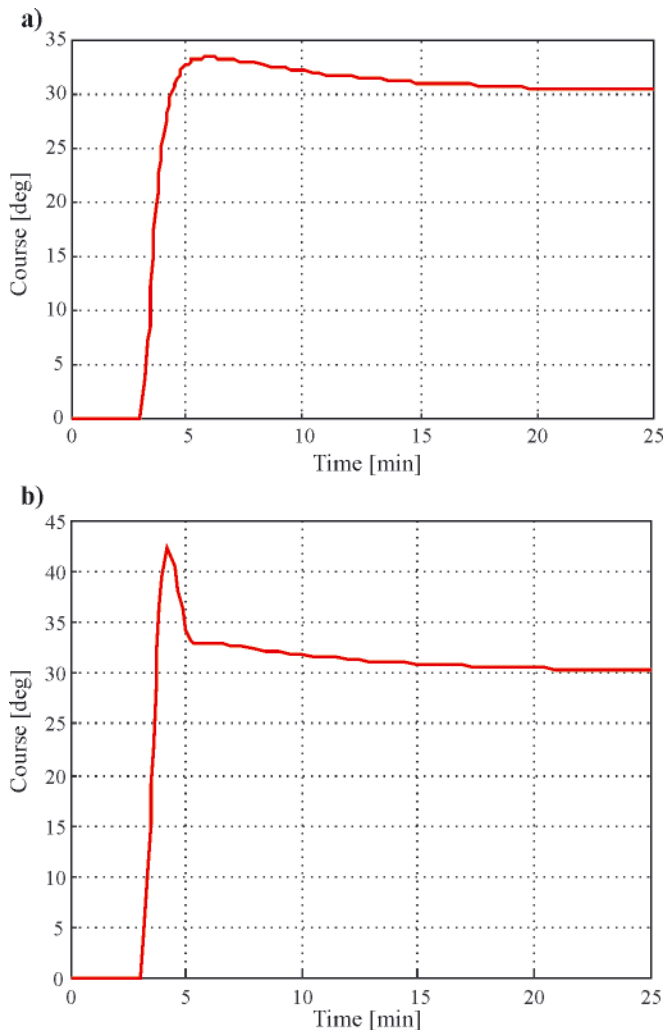


Fig. 3. Ship headings versus time for controllers with integral action: a) robust controller; b) Lqr regulator (30° turning)

state variable  $e$ . High penalization of this variable results in a rapid decrease of the course steady-state error, however, at the cost of increasing the course overshoot.

## CONCLUSIONS

The paper describes a proposition of a novel technique for robust control system design, which can be used to the ship motion control.

The technique seems to be very attractive for designing the ship autopilot albeit it requires additional research which should take into account different types of ship nonlinear models (e.g. including a steering gear) as well as consider various sailing conditions (in this phase of research the disturbances from waves has been deliberately omitted). It is worth noting that the modern adaptive PID controllers only partially solve the problem of ship model parameter changes. They can tune (as a rule) their gains only in response to the ship velocity changes while the number of factors responsible for the ship dynamic variations is much greater (e.g. ship load). The factors, when not taken into account by the controller, may lead to the degradation of steering process performance. Therefore, each new design proposal in this respect should attract attention.

The presented paper is focused on the properly formulated theory rather than on the practical engineering issues and is devised as a theoretical introduction to more practice-oriented engineering research.

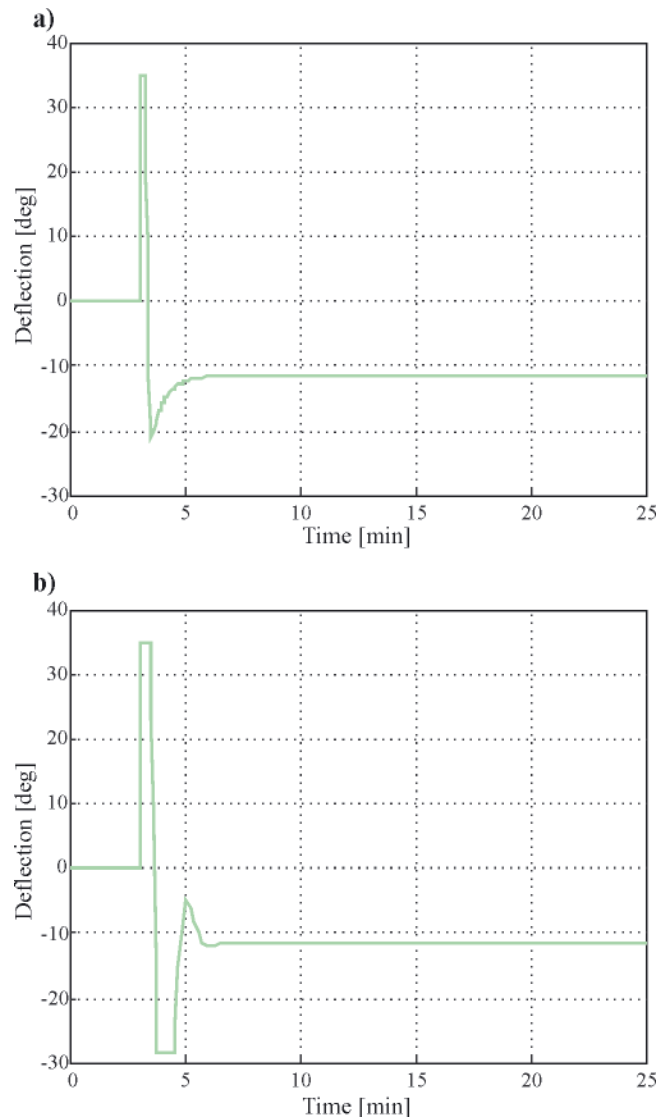


Fig. 4. Rudder deflections for controllers with integral action: a) robust controller; b) Lqr regulator (30° turning)

## BIBLIOGRAPHY

1. Abu-Khalaf M., Huang J., Lewis F. L.: *Nonlinear Constrained Feedback Control*. Advances in Industrial Control. Springer, London, 2006.
2. van Amerongen J.: *Adaptive steering of ships. A model-reference approach to improved manoeuvring and economical course keeping*. Ph.D. Thesis, Delft University of Technology, 1982.
3. Burl J. B.: *Linear optimal control*. Addison-Wesley, Menlo Park, CA, 1999.
4. Basar T., Bernhard P.: *H $\infty$  - optimal control and related minimax design problems. A dynamic game approach*. Birkhäuser, Berlin 1991.
5. Basar T., Olsder G.J.: *Dynamic noncooperative game theory*. SIAM Series in Classics in Applied Mathematics, Philadelphia, 1999.
6. *Control System Toolbox User's Guide. For Use with MATLAB*. The MathWorks, Inc. 1998.
7. Fossen T. I.: *Guidance and control of ocean vehicles*. John Wiley, Chichester, USA, 1994.
8. Isaacs R.: *Differential games*. John Wiley, New York 1965.
9. Isidori A.: *Nonlinear Control Systems. An introduction*, Springer-Verlag, Berlin, 1989.
10. Khalil H.K.: *Nonlinear Systems*. Prentice Hall, Upper Saddle River, NJ, 2002.

11. Lewis F. W., Jagannathan S. and A. Yesildirak: *Neural Network Control of Robot Manipulators and Non-Linear Systems*. Taylor & Francis, 1998.
12. Lisowski J.: *Ship as an object of automatic control*. Wyd. Morskie, Gdańsk 1981 (in Polish).
13. Márquez H. J.: *Nonlinear control systems. Analysis and design*. John Wiley, NJ, 2003.
14. Morawski L., Pomirski J.: *Design of the robust PID course-keeping control system for ships*. Polish Maritime Research, No. 1, 2002.
15. de Wit C., Oppe J.: *Optimal collision avoidance in unconfined waters*. Journal of the Institute of Navigation, Vol. 3, 126, No.4, 1979/80.
16. Zwierzewicz Z.: *On some geometric aspects of differential games* (in Polish). Archives of Control Sciences, No. 3-4, 1985
17. Zwierzewicz Z.: *Ship course-keeping via nonlinear adaptive control synthesis*. Int. Journal of Factory Automation, Robotics and Soft Computing, 2007, no. 2, April, 2007, pp.102-107.
18. Zwierzewicz Z.: *Methods and algorithms of ship automatic control systems* (in Polish). Scientific publishing of Szczecin Maritime University, Szczecin 2012

---

#### CONTACT WITH THE AUTHOR

Zenon Zwierzewicz, Assoc. Prof.  
Faculty of Marine Engineering  
Maritime University of Szczecin  
Wały Chrobrego 1-2  
70-500 Szczecin, POLAND  
e-mail: iciao@am.szczecin.pl

# A novel method for archiving multibeam sonar data with emphasis on efficient record size reduction and storage

**Marek Moszynski**, Assoc. Prof.  
**Andrzej Chybicki**, Ph.D.  
**Marcin Kulawiak**, Ph.D.  
**Zbigniew Lubniewski**, Ph.D.  
Gdansk University of Technology, Poland

## ABSTRACT

*Over the past few years considerable advances in sonar technology, spatial positioning capabilities and computer processing power have lead to significant improvements in mapping, imaging and technologies of seafloor exploration. Recently, modern multibeam echosounder systems (MBES) capable of recording backscatter data for the whole water column, not just for the seabed, have become available thus providing data allowing for visualization and analysis of objects other than the seabed such as single fish, fish schools or pollution. Unlike bathymetric sonars, which only capture the seafloor, multibeam systems produce very large amounts of data during surveys. Because of this, storing the data collected during hydrographic or scientific cruises becomes a crucial problem. In this context, the paper proposes a new approach for efficient reduction and storage of MBES records. The results of a sample implementation of the algorithm being tested on several different sets of MBES data are also discussed.*

**Key words:** sonar; compression; storage; reduction; efficiency

## INTRODUCTION

Modern multibeam echosounder systems (MBES) are capable of recording backscatter data for the whole water column, which allows for analysis and visualization of not only the seabed, but objects such as fish schools and single fish as well. They produce very large amounts of data during surveys, as it has been shown eg. by Buelens *et al.* (2005). Current trends in sonar development involve the use of innovative transducer materials as well as application of sophisticated processing techniques including focusing algorithms that dynamically compensate for the curvature of the wavefront in the nearfield and thus allow narrower beam widths (higher lateral resolution) at close ranges. Future developments will probably focus on “hybrid”, phase-comparison/beam-forming sonars, the development of broad-band “chirp” multibeam sonars, and perhaps synthetic aperture multibeam sonars (Demkowicz & Bikonis, 2006). Not long ago, Buelens *et al.* (2006) considered storage and compression as one of the most important computational challenges in processing of MBES data. However, since Ferguson’s and Chayes’s (1995) proposal of a binary file format for multibeam sonar data storage, there has been little development in the field of efficient MBES data processing which would allow for fast, semi-real-time sharing of the results between diverse groups of interest such as fishermen, hydrographers or researchers

(Chybicki 2008). Apart from works of Wu and Zielinski (1997), not much attention has been given to research of algorithms for storing and archiving MBES data that would allow for efficient browsing, analysis and visualization of collected information.

Even the prospect of having a common file format in which the same data sets can be shared between researchers and hydrographers offers an interesting new perspective, leading to savings in instrumentation and survey costs. Efficient MBES data storage algorithms can also make Remotely Operated Vehicles (ROV’s) and particularly Autonomous Underwater Vehicles (AUV’s) to become more widely adopted as platforms for seafloor mapping systems.

This paper presents the concept of a MBES data reduction and storage algorithm, developed by the authors for RESON Inc., along with the results of its sample implementation.

## MATERIALS AND METHODS

MBES data, just like every other type of information, can be encoded using well-known methods. However, given the nature of MBES, a specialized approach could yield substantially better results. During the presented research, the authors designed and utilized a modification of Huffman coding (1952) for reduction of MBES record sizes according to the rules of information theory (1948), as described in the following section.

## Entropy coding

Entropy coding is a lossless data compression method based on information probability schemes. This area of knowledge was first mathematically described by Claude E. Shannon. In 1948 he defined the basics of information theory in which he proposed concepts of measuring the amount of information. He assumed that a set of possible events  $S = \{s_1, s_2, \dots, s_n\}$  is called the alphabet if every element  $x_i$  is a symbol used to construct the communicate. He also assumed that the probability of every event is known as  $p(x_i) = p_i$ . The set of probabilities is described as  $P = \{p_1, p_2, \dots, p_n\}$  assuming that for every  $I(p_i) > 0$  and  $\sum_i p_i = 1$ . In this case, the function:  $I(x_i) = -\log_k(x_i)$  for  $k > 0$  and  $k \neq 1$  is called the self-information associated with event  $x_i$ .

According to Shannon (1948), self-information is the function for measuring the information brought by the particular event  $x_i$ , which is reversely proportional to the probability of the event.

The self-information thesis was extended by the definition of entropy which says that the function defined as:

$$H(p_1, p_2, \dots, p_n)$$

is equal to:

$$H(S) = -\sum p_i \log_k(p_i) \quad (1)$$

with the set of  $n$  independent events  $S = \{s_1, s_2, \dots, s_n\}$  and the set of corresponding probabilities  $P = \{p_1, p_2, \dots, p_n\}$ . Entropy is the mean auto-information of the set of particular events and, when assuming a binary source, can also be considered as the smallest average number of bits required for a symbol to be encoded, as shown by Balakrishnan et al. (2007) and Titchener (2000).

## Huffman coding

The first optimized method of compression coding based on the information theory was given by David Huffman (1952). The term refers to the use of a variable-length code table for encoding a source symbol (such as a character in a file) where the variable-length code table has been derived in a particular way based on the estimated probability of occurrence for each possible value of the source symbol.

Huffman coding uses a specific method for assigning the  $n$ -bit representations for each entry symbol, known as a prefix code. The method consists of replacing commonly used symbols with shorter representations and less commonly used symbols with longer representations. To achieve this goal Huffman coders create a prefix-free binary tree of non-overlapping bit-sequences, where the length of each sequence is inversely proportional to the likelihood of the symbol to be encoded.

Huffman binary code is *biunique*, meaning that the code is *uniquely decodable* and the sum of the probabilities associated with all symbols is always less than or equal to one. If the sum of probabilities is strictly equal to one, the code is termed a *complete* code. In general, a Huffman code need not be unique, but it is always one of the codes minimizing the complete code length.

Huffman coding is a particularly good compression method for datasets with non-linear distribution, and can be applied to many different types of data such as voice, sound, text and others. The Huffman algorithm is currently one of the most popular and efficient compression methods, and it can work in linear time if input probabilities (also known as *weights*) are sorted. It has been shown (eg. by Larmore, 1986) that when the

actual symbol frequencies agree with those used to create the code, no other mapping of individual source symbols to unique strings of bits will produce a smaller average output size.

Although Huffman coding is optimal for a symbol-by-symbol coding with a known input probability distribution, its efficiency has since been surpassed by several compression algorithms developed later. Huffman coding is also used as one of the stages for more complex compression techniques, eg. Cosine Transform based compression methods such as JPEG (Hashemian, 2003), Wavelet Transform Compression methods such as JPEG 2000 (Chang *et al.*, 2006) or Deflate/Inflate algorithms (Khademi & Krishnan, 2006). These coding techniques often have better compression capability although they are characterized by greater computing complexity and larger amount of memory that needs to be allocated during data compression and decompression.

## MBES and it's data structure

Multibeam sonars are a type of sonar systems widely used for surveillance and sensing in seas, oceans and other water containers (Mayer *et al.*, 2007). They provide a wide swath survey of the ocean floor at each ping by pulsing the bottom with a series of soundings normal to the track of the vessel and recording the reflected echoes in an orientation parallel to the vessel.

A typical multibeam sonar system consists of several elements, including transducer, Digital Signal Processor (DSP) and workstation, as shown in Fig. 1. The transducer, which uses linear or cylindrical arrays of receivers and projectors mounted at appropriate angles to each other (typically in so called the "Mills cross" arrangement, where the receive array lies in the athwart ship direction and the transmit array lies in the fore-aft direction) is responsible for ping generation and registration of backscattered acoustic wave signal. The registered data is transmitted to the DSP where the beamforming (based on sum-delay or Fourier transform algorithms), bottom detection (amplitude or phase detection algorithms), georeferencing, calibration and stabilization processes are performed. For each receive beam, the bottom echo from the intersection of the transmit and the receive beam footprint is detected. The entire system is managed by



Fig. 1. The overview of multibeam sonar system structure

the workstation, which is a PC unit operating under Windows or Linux. The workstation also enables storing and archiving of processed data.

The minimum and maximum depth values for data acquisition depend on sonar model and vary between a few meters (min) to over 1000 m (max). Nominal beamwidth ranges from  $0.5^\circ$  to  $1.5^\circ \times 0.5^\circ$  to  $1.5^\circ$  and the frequency of performing the transmit-receive cycle (ping-rate) is 40 Hz. The commonly applied operating frequency of multibeam systems is between 200 kHz and 400 kHz. Most multibeam systems offer integrated modules capable of acoustical imaging, mapping and data storage. The data recorded by these systems is stored in binary files defined by vendors. Although there are several formats of MBES data storage, their syntactic contents are similar due to the common architecture of multibeam systems.

The echo arrival time and the angle of the receive beam provide information for bathymetry, and the backscattering strength is used for seabed imaging (Shah & Talukdar, 1999). The process of forming beams is called beamforming and has been widely described in literature e.g. by Rñhovde (1999) or Thorner (1990). In this context, sea-bottom charts and images are formed by appropriate processing and combining data from many consecutive swaths.

The result of surveys made with the use of MBES systems is usually stored in two basic configurations:

- a) The data is processed and logged by dedicated operating software like QUINSy, HYPACK, PDS 2000 or other. In this case the results of surveys are kept in dedicated databases or database files.
- b) The raw records retrieved from MBES system are logged as a binary file in order to perform further analysis.

In both of these configurations the MBES data is received as a set of binary records containing various information delivered by the multibeam system, such as bathymetry, water-column data, beam geometry data and sonar configuration data. Additionally, external sensors data such as CTD probe, GPS, Compass, Gyro and others may be also included. The exact structure of the dataset depends on the particular multibeam sonar model, survey purpose, configuration and connected external sensors. Nevertheless, the following characteristics are common for every multibeam sonar system:

- The multibeam system must be connected to a workstation in order to collect and process the acquired data and present the results;
- Data is delivered as a set of binary datagrams (records) via a connection between the sonar processor and the workstation;
- The MBES produces several types of datagrams, each containing different types of information such as GPS data, bathymetry data, external sensors data (i.e. heave, pitch, roll) and water column data;
- No compression of MBES records is performed either by the sonar hardware or the specialized software.

Although collecting water-column data is not mandatory during multibeam hydrographic cruises, it delivers a lot of additional information about the monitored marine environment. It is also used by diverse groups of researchers as an important component of survey results, delivering acoustic information about various underwater objects, as shown by Gerlotto *et al.* (1999) and Mayer *et al.* (2002) and for seafloor characterization and classification (Lubniewski, 2010). The water column data represents a set of signals acquired from multibeam sonar sensors in one sonar ping. The set of beamforming functions depends on the sonar specification. The datasets presented in

the paper were acquired by RESON Seabat 7125 multibeam system which utilizes standard sum-delay beamforming. Two different visualizations of the water-column data acquired from this device are shown in Fig. 2. In this sonar the water-column is available as a two-dimensional binary array where the value of point defined by indices  $m$  and  $n$  is the 16-bit integer value of beam numbered  $m$  and sample numbered  $n$  (Marcus, 2007). The presented research was conveyed with the use of eight different datasets acquired by means of the RESON Seabat 7125 MBES. The overall characteristics of this data are shown in Tables 1 and 2.

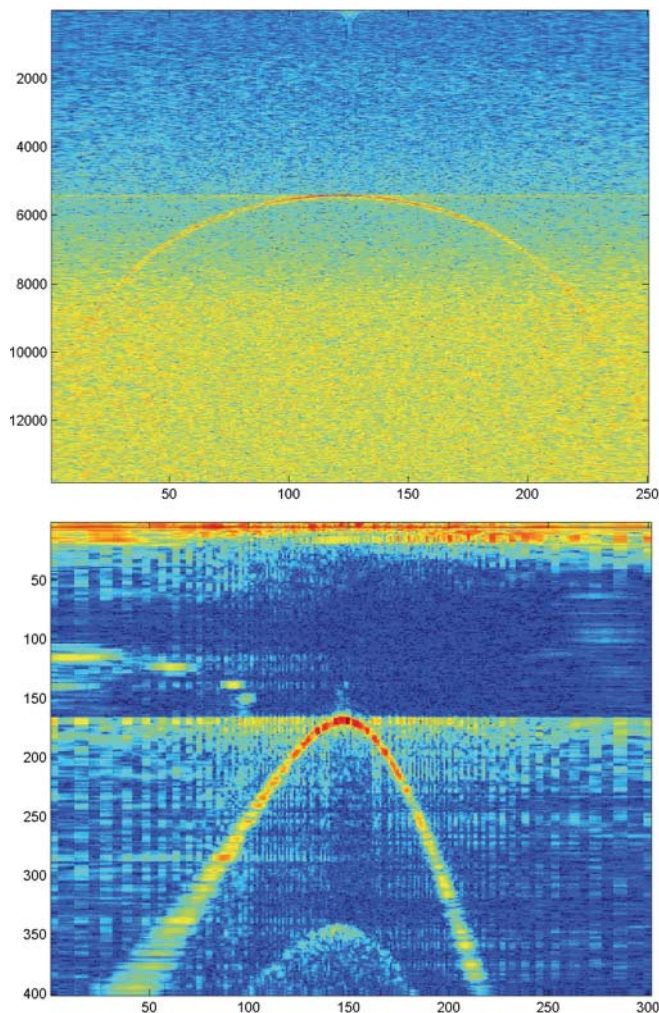


Fig. 2. Sample water-column data acquired by RESON 7125 Seabat Multibeam System.

In order to explain the importance of efficient water-column data processing, a more detailed description needs to be given. Although the tested system generates 256 beams, in some multibeam systems the maximum number of beams can reach 3520 per one sonar head. The number of registered samples for individual beams depends on the depth and probing frequency and can reach up to 32 thousands, as shown e.g. by Van Buren and Blue (1990), Xiaofeng and Wenjun (1998) or Foote *et al.* (2003). Since each value is stored as a 16-bit float or integer, the size of water column data can easily exceed 95% of all data collected by a multibeam system, as shown in Table 1. This is particularly apparent when the data is stored in linear scale, as it is the case in the datasets utilized in the presented work.

In literature the value of water-column datagram samples is calculated according to the sonar equation:

$$EL = SL + TS - 2TL$$

In other words: Received echo level (EL) is equal to transmitted source level (SL) plus target strength (TS) minus two-way transmission loss (2·TL) expressed in dB. The two-way transmission loss is:

$$2TL = 2 \alpha R + 40 \log R \text{ (re } R_0=1\text{m)}$$

where  $\alpha$  is absorption coefficient (dB/m) and R is slant range (m).

In a water column datagram, the received echo level is adjusted for system dependent parameters in addition to being amplified with a range dependent TVG function:

$$A_{WC} = EL - SL - 10 \log \Omega_{TX} \cdot \Omega_{RX} + 2 \alpha R + 40 \log R + C \quad (2)$$

where  $\Omega_{TX}$  and  $\Omega_{RX}$  are along-track (transmit) and across-track (receive) beam widths respectively (expressed in radians). These values are dependent on actual sonar model and operating parameters. For instance, in the RESON 7125 MBES which was used as a source of data during the presented work, the parameter  $\Omega_{RX}$  was equal to  $0.5^\circ$  and  $\Omega_{TX}$  equaled  $1^\circ$ . The parameter C represents gain selection of MBES transceiver used to adjust the signal level to system dependent parameters.

In the presented formulas the echo levels calculations are expressed in dB. Also, the transducers accuracy used in the RESON 7125 MBES system is lower than 0.5 dB, as shown eg. by Van Buren and Blue (1990), Xiaofeng and Wenjun (1998), or Foote *et al.* (2003). This is the reason why some MBES manufacturers (eg. Kongsberg) apply conversion from linear scale to dB scale with 0.5dB re 1 $\mu$ P precision. That has been also applied during the presented research.

In this context, the objectives of this work are to achieve improved data reduction ratio and offer reduced time of processing in comparison to standard archiving tools.

### The proposed algorithm

The developed algorithm is a modification of static Huffman codes dedicated for multibeam sonar data. It aims to:

- enable efficient coding/decoding of large binary files containing MBES data;
- lay foundations for a standard file format for compressed MBES data;
- deliver an efficient archiving tool for online processing of particular MBES records, fulfilling the following requirement:
  - compression time of every record produced by MBES system must be shorter than the time of creating it by the sonar system;
  - program memory use must be unrelated to the size of compressed files, and be possibly small.

The algorithm aims to improve MBES data processing speed in comparison to standard Huffman coders by assuming that the histograms of records and probabilities for particular symbols (byte values) to be encoded are similar within individual datagram types. Using this knowledge, the algorithm composes several Huffman trees based only on the first datagram of particular type delivered by the MBES system.

According to (1), the entropy of a dataset (datagram) is the minimum average number of bits that can represent an encoded symbol using binary prefix code, which can be expressed as:

$$E_{\text{pattern}} = - \sum_{i=0}^{256} p_i \log_2(p_i)$$

where  $p_i$  is the probability corresponding to symbol i that can also be defined as  $n_i/N$  where  $n_i$  is the number of bytes

containing value i in first pattern datagram and N is the total number of bytes. The latter is usually constant for every datagram type, as shown by Marcus (2007). According to Huffman theory,  $\log_2(p_i)$  represents the number of bits required to encode symbol i. In this case,  $E_{\text{pattern}}$  is the entropy of the pattern datagram, which defines the Huffman tree. Once a tree is created for the analyzed type of datagram, the calculated Huffman structure is applied for encoding the rest of the records of particular type. In this case the entropy, calculated for a consecutive record is defined as:

$$E = - \sum_{i=0}^{256} (p_i + \Delta p_i) \log_2(p_i) \quad (3)$$

where  $\Delta p_i$  is the difference of probability between the probability symbol i in the pattern datagram and the current datagram, and  $\sum_{i=0}^{255} \Delta p_i = 0$ .

To make data uniquely decodable, additional information about the compressed records, such as the type of compressed datagram and its original and compressed sizes, must be saved to the result file.

Fig. 3 depicts the entropy of the water-column data calculated by (3) on five sample datasets. As shown in the diagram, the entropy difference of at least 30 consecutive datagrams is approximately constant. Thus, assuming that the entropy is the lower bound for Huffman coding algorithm, compression ratio shouldn't vary much between consecutive swaths. It is also worth mentioning that in some cases an increase of entropy was observed after several pings, which is a result of on-device gain adjustment when forming beam geometry data. This will have a considerable impact on the presented results.

It may be noticed that the number of datagram types produced by the MBES system is constant and, according to technical specification, does not exceed 20-25 in most cases. This issue is described in detail by Marcus (2007) and Van Buren & Blue (1990). The entropy characteristics shown in Fig. 3 allow the algorithm to assume that the consecutive records of the same type generated by the MBES system are similar in content. Thus, all consecutive datagrams of the same type are encoded using the same Huffman tree which was generated for the first datagram. Because the Huffman tree is generated only once for each datagram type, the algorithm is granted a considerable increase in performance without negative influence on compression ratio. This mechanism is depicted in Fig. 4.

As it has been said in the preceding section, in some MBES systems (e.g. RESON 7k series) the water-column data is stored in linear scale, which causes unnecessary waste of storage space. In order to further optimize the size of the resulting data, its precision has been made a user-controlled parameter which can be set in the range of 0.1-1 dB. For best data reduction efficiency without losing information relevant for visualization or analysis of the water-column data, the parameter must be set in such a way as to match the accuracy of the MBES system. During the tests, this parameter was set to 0.5 dB, which is more than the native precision of the RESON 7125 MBES, as shown eg. by Van Buren and Blue (1990), Xiaofeng and Wenjun (1998), or Foote *et al.* (2003).

An additional advantage of this approach is the fact that the proposed compressed file format enables access and decompression of particular records without exigency of decoding the whole dataset, while maintaining the efficiency of decompression. In this case, the only elements that must be read from the compressed file are the appropriate Huffman tree and the position of the compressed data. Reading the structure

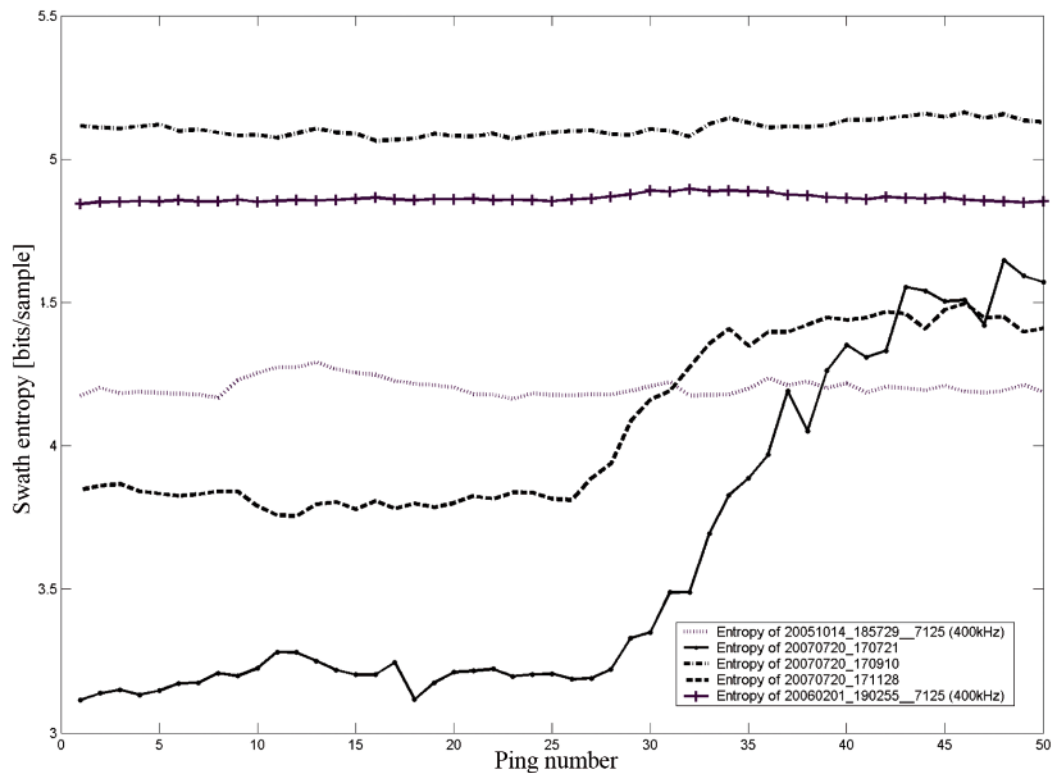


Fig. 3. Entropy of consecutive water-column records according to (3)

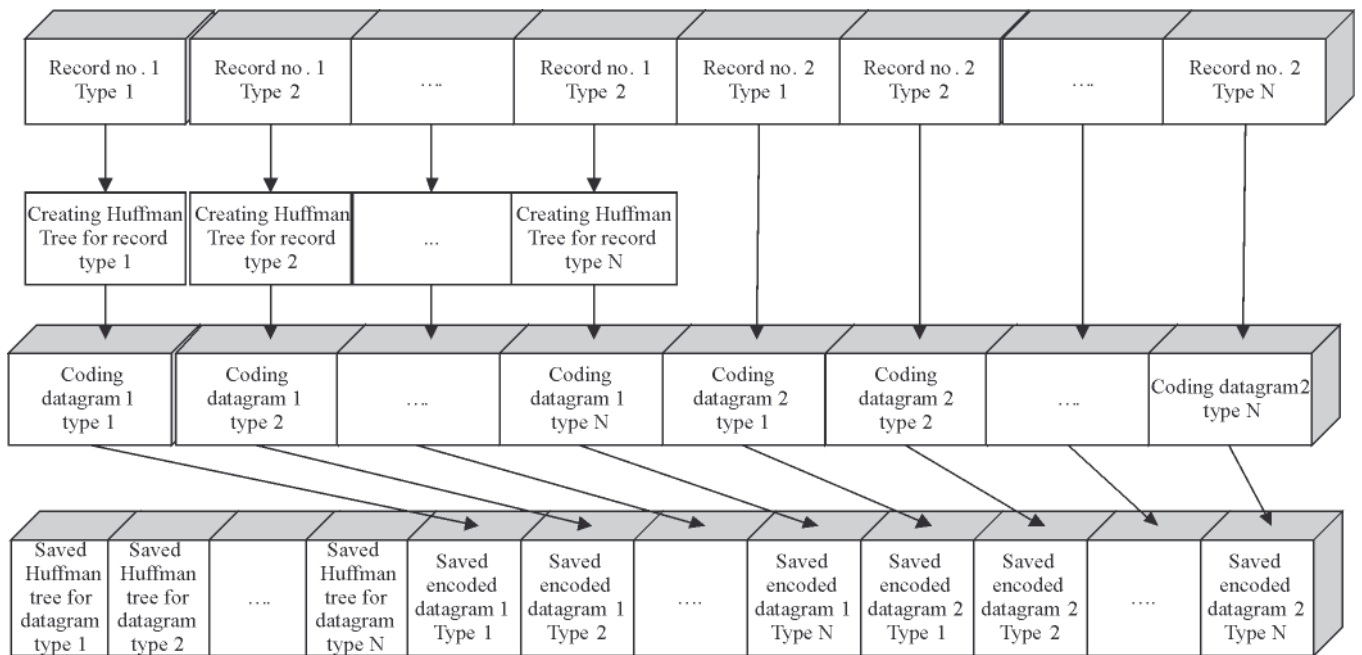


Fig. 4. Block diagram of the proposed online compression algorithm

of the compressed file and retrieving the information such as the total number of datagrams, original size of particular datagrams and their types is also possible without the need of decoding the whole compressed dataset. That is particularly useful when processing files bigger than 500 MB. In this case the decompression process would last considerably longer when using standard archiving tools.

## RESULTS

A sample application of the proposed algorithm for multibeam data processing was implemented using C++ programming language. The software processes binary files containing 7k series multibeam sonar records. This section

contains the results of testing the software as well as the information on the testing methodology and input datasets.

### Testing methodology and input data characteristics

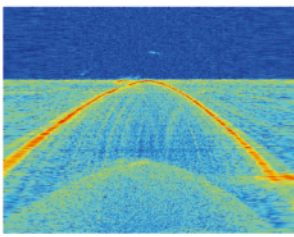
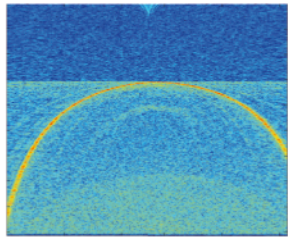
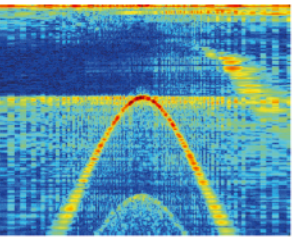
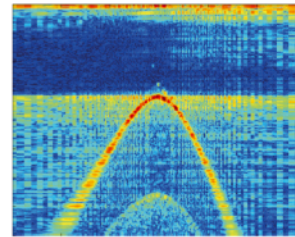
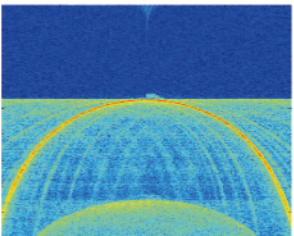
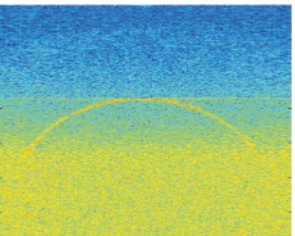
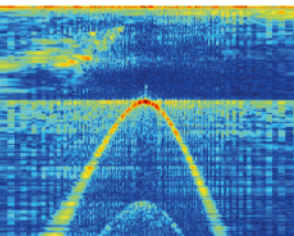
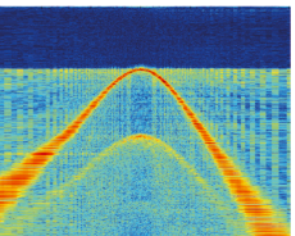
The basic acceptance criteria for the proposed method are: time of compression of particular datagram types, time of processing of whole dataset, and compression ratio.

Tables 1 and 2 show the information on the datasets used for testing the compression algorithms. The files were acquired during scientific or research surveys in an area of Santa Barbara, California, USA, which is characterized by relatively flat and homogenous bathymetry. The data was

Tab. 1. Description of sample datasets acquired during research in the area of Santa Barbara, California, USA

Dataset name	Percentage of water-column data in entire dataset	Operating frequency [kHz]	Sample rate [kHz]	Result file size[MB]
20060719_204657__7125 (400kHz).s7k	85.72%	396	34	557
20051014_185729__7125 (400kHz).s7k	83.09%	396	34	589
20070720_170910.s7k	82.77%	100	6	1 100
20070720_171128.s7k	82.82%	100	6	477
20060201_190255__7125 (400kHz).s7k	83.07%	400	34	601
20070315_184108.s7k	97.96%	396	34	127
20070720_170721.s7k	82.84%	100	6	937
20070831_185543.s7k	87.87%	100	6	1046

Tab. 2. Acoustic parameters of water-column data processed during the tests

20060719_204657__7125 (400kHz).s7k	20051014_185729__7125 (400kHz).s7k	20070720_170910.s7k	20070720_171128.s7k
			
Number of pings: 146 Number of samples = 1595 Number of beams = 512 Range selection [m] = 35 Power selection [dB] = 218 Gain selection [dB] = 30	Number of pings: 274 Number of samples = 1829 Number of beams = 256 Range selection [m] = 40 Power selection [dB] = 207 Gain selection [dB] = 43	Number of pings: 1013 Number of samples = 401 Number of beams = 301 Range selection [m] = 50 Power selection [dB] = 185 Gain selection [dB] = 83	Number of pings: 429 Number of samples = 401 Number of beams = 301 Range selection [m] = 50 Power selection [dB] = 200 Gain selection [dB] = 25
20060201_190255__7125 (400kHz).s7k	20070315_184108.s7k	20070720_170721.s7k	20070831_185543.s7k
			
Number of pings: 278 Number of samples = 1839 Number of beams = 256 Range selection [m] = 40 Power selection [dB] = 220 Gain selection [dB] = 30	Number of pings: 9 Number of samples = 1595 Number of beams = 512 Range selection [m] = 300 Power selection [dB] = 220 Gain selection [dB] = 19	Number of pings: 843 Number of samples = 401 Number of beams = 301 Range selection [m] = 50 Power selection [dB] = 175 Gain selection [dB] = 40	Number of pings: 137 Number of samples = 806 Number of beams = 301 Range selection [m] = 100 Power selection [dB] = 220 Gain selection [dB] = 10

acquired using maximum pinging frequency of 40 Hz. It is important to note that the surveys were made under various conditions, with varying place of measurement, depth, bottom type, sonar frequency, probing frequency, etc. This is to clearly show that the research was based on a broad range of datasets, which cover a lot of the possible MBES survey configurations.

Table 1 clearly shows that appropriate methods of processing water-column data are the key to reducing the size of MBES records. This means that an efficient and fast algorithm for processing water-column data will guarantee optimal results of processing the entire file. Table 2 presents the information on acoustic parameters and sample visualizations for every water-column dataset processed during the tests. The images display raw frames of data without any form of post-processing such as fanshape correction.

### Measured efficiency of the algorithm

The presented results were obtained on a standard desktop PC equipped with an Athlon X2 3600 + CPU paired with 1 GB of RAM, running Windows XP SP3. For each dataset, Table 3 lists the time of compression for water-column records compared with the time in which the records were generated by the sonar system. Additionally the compression ratio acquired with the use of the proposed method and that acquired by the standard ZIP compression tool are also presented. The time of compression of the remaining elements of a record (bathymetry, position etc.) is usually about 1-2 ms and is always shorter than the time of record generation.

The proposed method can be also applied as an archiving tool for MBES data. Currently, the most commonly used tools for

archive volume reduction are the well known file compression tools such as ZIP, RAR or the newly developed 7-ZIP. These tools do not utilize the information about the character of MBES data and consider the input simply as a series of bytes. Table 4 presents a comparison of the proposed archiving tool with other standard data compression applications based on the total time of archiving the whole dataset.

## DISCUSSION

As shown in Table 4, the proposed method offers superior archiving speed in all test cases, being on average 68% faster than the next best ZIP algorithm, while offering up to 111% smaller output file size. In most cases the proposed tool also offers greatest reduction of the input file size, with two exceptions (test cases no. 6 and 7) where 7-ZIP performs 15% better, but at a cost of up to 829% longer processing time. There is also one special case where 7-ZIP offers 91% better results. This is due to statistical change of datagram contents during the survey where the pattern datagram doesn't describe the content of records registered at later stages of the survey. In this case additional analysis of the data is required to update Huffman trees describing the statistical information about the content of the records (as seen previously in Fig. 3). Even though the proposed algorithm fails to produce the smallest file size in this test case, it is 384% faster than 7-ZIP.

To better understand the origins of the obtained results, a more in-depth analysis of the data used in test cases no. 6 and 7 is required. Figures 5 and 6 show the differences between the contents of consecutive water-column datagrams in the problematic surveys, in the form of images representing the actual data and corresponding histograms.

Tab. 3. Compression ratio yielded with proposed methods of particular water-column datagrams compared to time of generation of the records by RESON 7125 MBES system

Dataset name	Average water-column record compression time [ms]	Time of generation of water-column record [ms]	Compression ratio	ZIP compression ratio
20060719_204657__7125 (400kHz).s7k	80	150-200	0.28-0.32	0.48
20070315_184108.s7k	350-400	450-500	0.31-0.33	0.79
20070720_170721.s7k	15-20	100-120	0.19-0.21	0.41
20070831_185543.s7k	20-25	300-350	0.32-0.35	0.53
20051014_185729__7125 (400kHz).s7k	40	70-80	0.26-0.27	0.47
20070720_170910.s7k	12	120-130	0.32-0.33	0.66
20070720_171128.s7k	11-12	120-130	0.23-0.28	0.45
20060201_190255__7125 (400kHz).s7k	42-43	70-80	0.30-0.31	0.52

Tab. 4. Compression ratios and the time of archiving of selected compression tools in comparison to the proposed method

Test case	Dataset name	Result file size[MB]	ZIP ratio/time [s]	7-ZIP ratio/time[s]	RAR ratio/time [s]	Proposed methods ratio/time [s]
1	20060719_204657__7125 (400kHz).s7k	557	0.65 / 155	0.50 / 295	0.54 / 220	0.31 / 65
2	20070315_184108.s7k	589	0.79 / 35	0.63 / 73	0.69 / 42	0.31 / 12
3	20070720_170721.s7k	1 100	0.51 / 255	0.23 / 11 min.	0.44 / 380	0.44 / 172
4	20070831_185543.s7k	477	0.48 / 80	0.40/195	0.41 / 110	0.19 / 29
5	20051014_185729__7125 (400kHz).s7k	601	0.63/178	0.48 / 380	0.57 / 182	0.28 / 90
6	20070720_170910.s7k	127	0.53 / 305	0.40 / 13 min.	0.46 / 430	0.49 / 234
7	20070720_171128.s7k	937	0.52 / 125	0.40 / 13 min.	0.46 / 170	0.46 / 94
8	20060201_190255__7125 (400kHz).s7k	1046	0.66 / 170	0.54 / 340	0.61 / 225	0.31 / 82

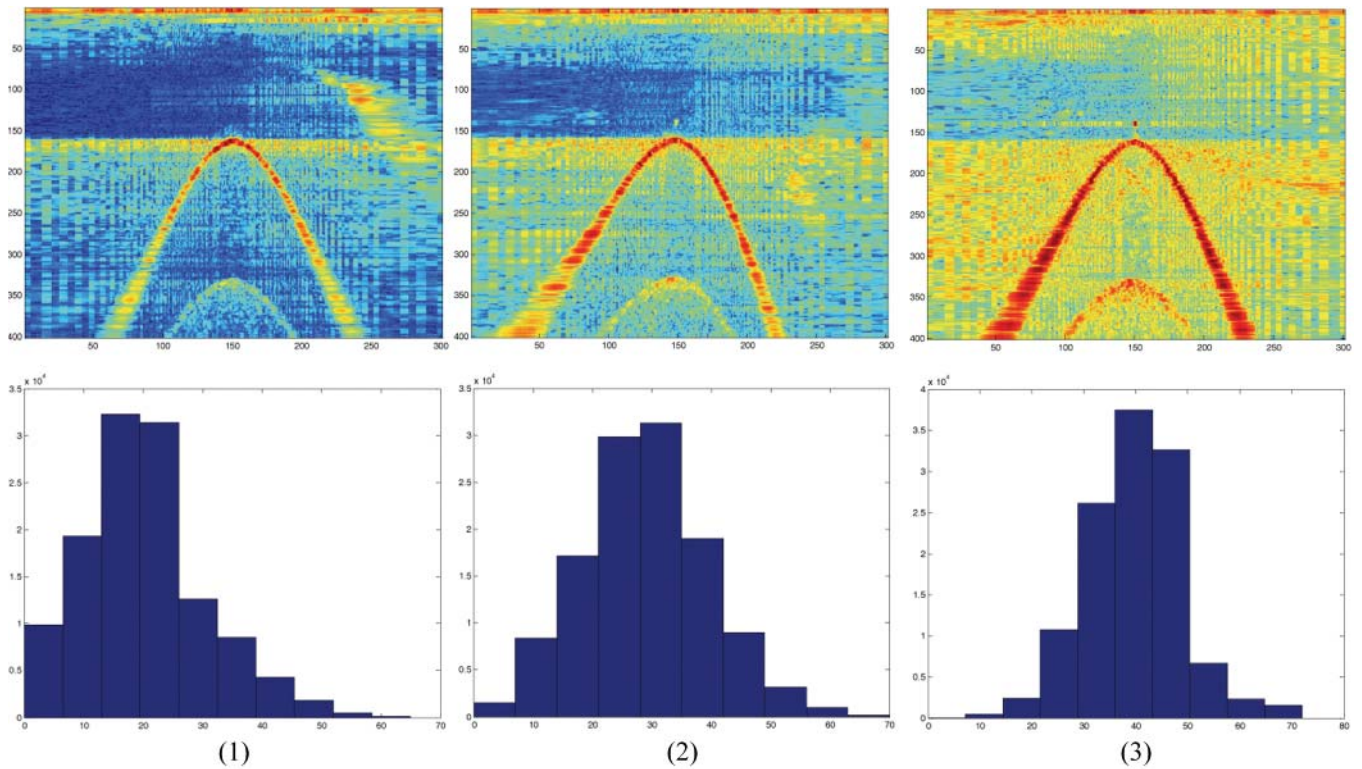


Fig. 5. Water column data and corresponding histogram for consecutive records in 20070720\_170910. Left – ping no. 1, middle – ping no. 150, right – ping no. 300

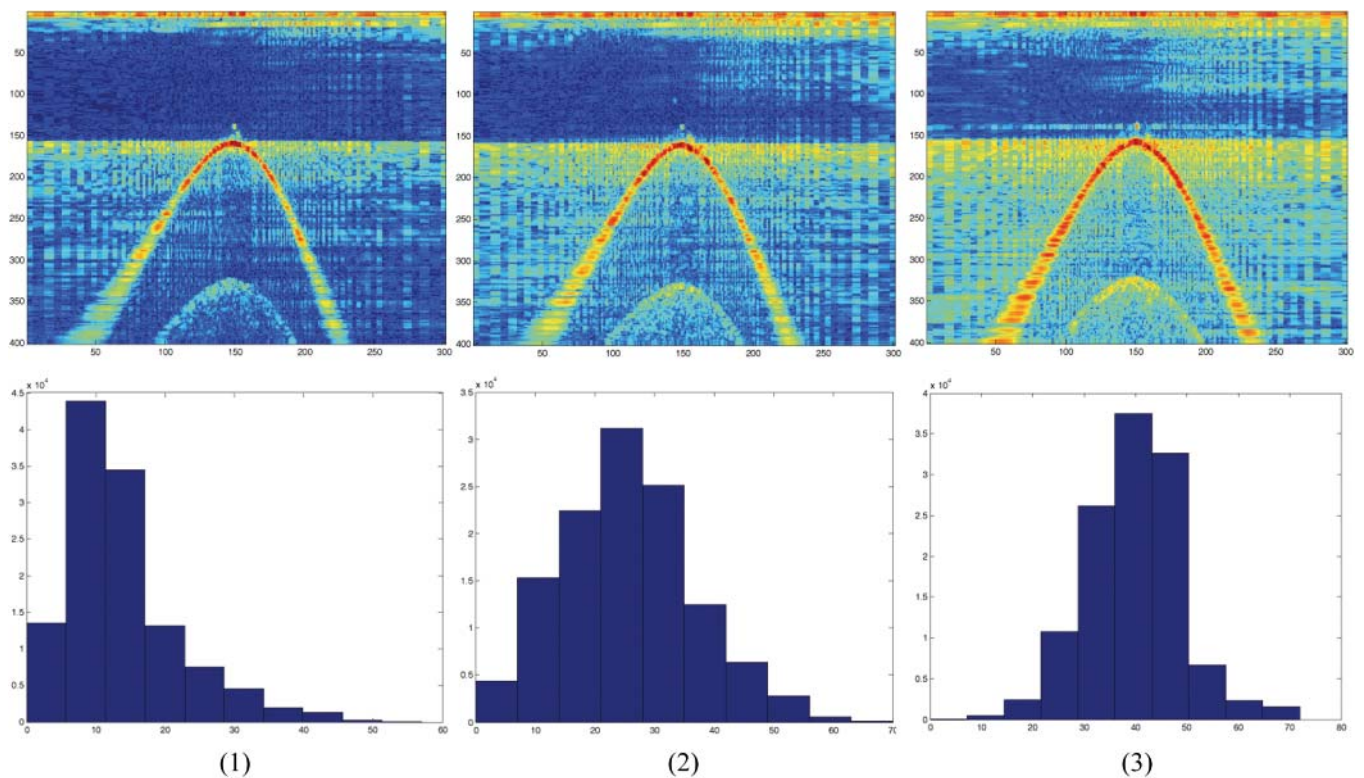


Fig. 6. Water column data and corresponding histograms of records in 20070720\_171128. Left – ping no. 1, middle – ping no. 100, right - ping no. 220

According to (2), such parameters as TVG, gain, and power of the sonar, as well as others that can be automatically or manually adjusted during the survey, influence the statistical parameters of the data contents and thus can make compression less effective. The change of gain as a function of ping number in the two problematic datasets is shown in Fig. 7. A modification of the algorithm that would automatically update the Huffman trees when the compression of consecutive records becomes less effective is an important issue to consider, especially for

dataset structures similar to those of 20070720\_170910 and 20070720\_171128.

What is also important is the fact that the time of processing particular datagrams is shorter than the time interval between delivering consecutive records by the MBES system. Therefore, the proposed method can be used as on-the-fly record size reduction tool in routine research or commercial surveys, or efficient archiving tool for bigger multibeam sonar data warehouses.

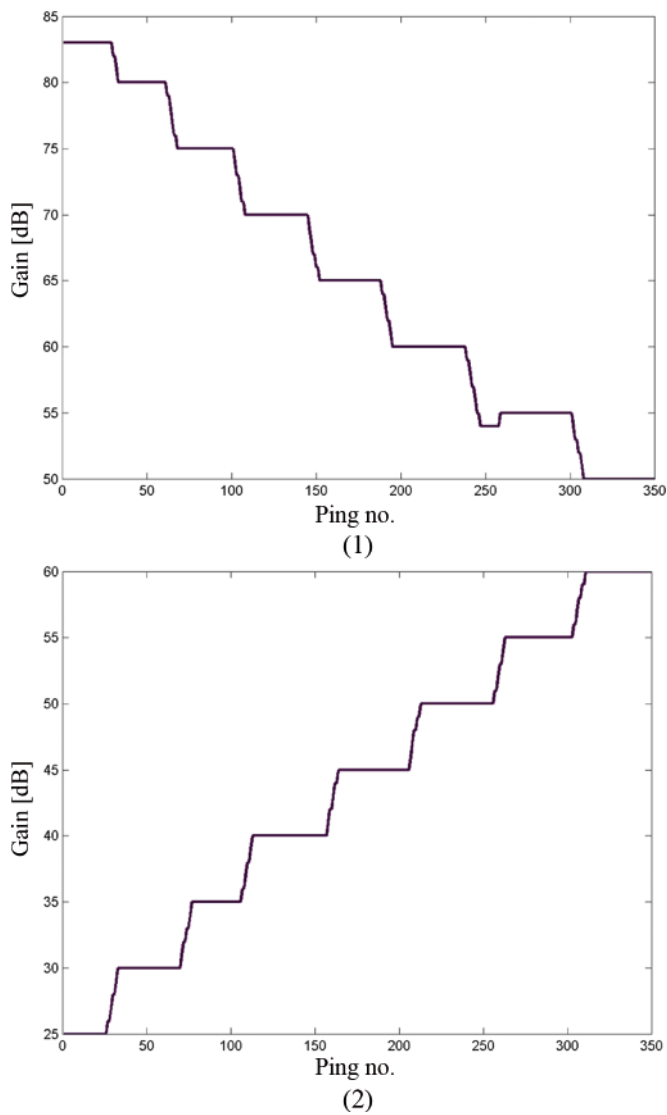


Fig. 7. Gain selection presented as a function of ping no. in 20070720\_170910 (left) and in 20070720\_171128 (right)

An additional advantage of the presented algorithm is that it is dedicated to processing MBES data, and thus it allows unique identification of the type of processed information. As a consequence, the proposed compressed file format enables selective access to data such as individual datagrams and their types without the need of decoding the whole compressed dataset. This ascertains considerable time savings in comparison to standard archiving tools, in particular for larger datasets.

The versatility of the algorithm allows its application to on-the-fly MBES data processing. The presented performance results were obtained on a standard PC-class computer. Implementing and running the algorithm on a dedicated processor such as a CUDA-enabled GPU provides a substantially different level of performance, opening a new range of possible applications of the algorithm. Preliminary research shows that utilizing a GPU allows the algorithm to achieve semi-real-time compression of water column data. This in turn allows the compressed frames to be dynamically visualized in three dimensions via a Web-based Geographic Information System. A sample visualization of animated MBES swath in 3D is shown in Fig. 8.

Because the contents of every MBES frame have been already processed, they may be easily analyzed according to the paradigms of Geovisual Analytics. Application of online analysis algorithms enables extraction of water-column data such as pelagic fish schools on-the-fly as well as their visualization in 3D context alongside digital terrain data

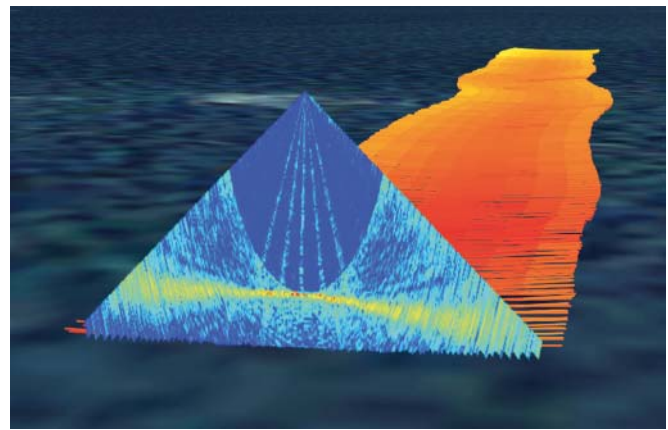


Fig. 8. A three-dimensional visualization of processed sonar data

such as bathymetry (Kulawiak 2010). Fig. 9 shows a three-dimensional visual analysis of processed water column data in the context of a standard two-dimensional map via WebGL. For this purpose, GPS location data from the vessel is used to localize the collected MBES information in geographical context in the form of a marker on a two-dimensional map constructed with the use of HTML5. The contents of the data are then visualized inside the marker popup cloud on a three-dimensional canvas. The water-column data is streamed from the server in compressed form, which enables its dynamic visualization on the client. The data presentation has been set up to exclusively depict the ocean bottom as well as objects floating below the water surface. Changes in the shape of the bottom have been reflected by different colors of the three-dimensional model. The backscatter objects in water column data are colored in white.



Fig. 9. Three-dimensional geovisual analysis of water-column backscatter data

The proposed modification of Huffman coder, optimized for storing and compressing MBES records, enables its application in devices which process MBES data in real-time, while its efficiency rivals that of well-established compression tools like ZIP and RAR. However, the presented study of multibeam sonar data reduction and storage methods has been conveyed in a field that has not yet been properly explored. This will likely change as the amounts of data collected during research, as well as commercial surveys, will continuously increase. Properly designed MBES data processing algorithms may result in opening up new worlds of interactive exploration to a multitude of users. Despite their preliminary nature, the presented results show great promise of fast and efficient MBES data reduction, storage and retrieval. Some important factors influencing the compression ratio such as TVG, gain, and bottom type are yet to be considered. The presented MBES data reduction and storage

techniques can become a powerful tool for users of MBES systems, used as an efficient archiving tool for researchers, hydrographers, ecologists, fishers and commercial groups of interest, such as dredging industry or pipeline inspection and chart production companies.

## Acknowledgements

Authors of the paper wish to thank Pawel Pocwiardowski, Ph.D. from RESON Inc. for the effort that he put into the presented research.

## BIBLIOGRAPHY

- Balakrishnan, K. J. & Touba, N. A.: *Relationship Between Entropy and Test Data Compression*, IEEE Transactions on Computer-Aided Design of Integrated Circuits and Systems, 26 (2) 2007: 386 - 395.
- Buelens, B., Williams, R., Sale, A., Pauly, T.: *Model Inversion for Midwater Multibeam Backscatter Data Analysis*, Oceans 2005 - Europe, 1: 431 - 435.
- Buelens, B., Williams, R., Sale, A., Pauly, T.: *Computational Challenges in Processing and Analysis of Full-Watercolumn Multibeam Sonar Data*. In: Proceedings of the Eighth European Conference on Underwater Acoustics, 12-15 June 2006. Carvoeiro, Portugal.
- Chang, Y.-W., Truong, T.-K., Chang, Y.: Direct mapping architecture for JPEG Huffman decoder, Communications, IEE Proceedings, 153 (3) 2006: 333 - 340.
- Chybicki, A., Moszynski, M., Pocwiardowski, P.: *Compression algorithms for multibeam sonar records*, *Hydroacoustics*, vol. 11, 2008, pp. 55-63, 25th Symposium on Hydroacoustic (SHA'25), Jastrzebia Góra, Poland, 25-28 May, 2008.
- Demkowicz, J. & Bikonis, K.: *Combined Spline Wavelet Decomposition for 3D Seafloor Imaging from Multibeam Sonar Echoes*, *Acta Acustica United with Acustica*, 92, 2006: 1-187.
- Ferguson, S. & Chayes, D. A.: *Use of Generic Sensor Format to Store Multibeam Data*, *Marine Geodesy*, 18 (4) 1995: 299-315.
- Foote, K. G., Chu, D., Hammar, T. R., Baldwin, K. C., Mayer, L. A., Hufnagle, L. C., Jech, J. M.: *Protocols for calibrating multibeam sonar*, *Journal of the Acoustical Society of America*, 114 (4) 2003: 2307-2308.
- Gerlotto, F., Soria, M., Freon, P.: *From two dimensions to three: the use of multibeam sonar for a new approach in fisheries acoustics*, *Canadian Journal of Fisheries and Aquatic Science*, 56 1999: 6-12.
- Hammerstad, E.: *Advanced multibeam echosounder technology*, *Sea Technology*, 36 1995: 67-69.
- Hashemian, R.: *Direct Huffman coding and decoding using the table of code-lengths*, *Information Technology: Coding and Computing [Computers and Communications] Proceedings: 237-241, 2003.*
- Huffman, D. A.: *a Method for the Construction of Minimum-Redundancy Codes*, Proceedings of the I.R.E.: 1098-1102, 1952.
- Khademi, A. & Krishnan, S.: *Comparison of JPEG 2000 and Other Lossless Compression Schemes for Digital Mammograms*. pp. 3771-3774. In: Engineering in Medicine and Biology Society, 2005 IEEE-EMBS 2005 27th Annual International Conference. 17-18 Jan. 2006, Shanghai, China.
- Kulawiak, M., Chybicki, A., Moszynski, M.: *Web-based GIS as a tool for supporting marine research*, *Marine Geodesy* 33 (2 & 3) 2010: 135-153.
- Larmore, L. L.: *Height restricted optimal binary trees*, *SIAM Journal of Computing*, 16 1986: 1115-1123.
- Lubniewski, Z., Stepnowski, A., Chybicki, A.: *Seafloor characterisation combined approach using multibeam sonar echo signal processing and image analysis*. p. 131-137. In: Proceedings of 10th European Conference on Underwater Acoustics ECUA 2010, Istanbul, Turkey.
- Marcus, J.: *SeaBat 7K Data Format Definition for Ifremer*, Revision: B, Reson Inc, 2007.
- Mayer, L., Li, Y. & Melvin, G.: *3D visualization for pelagic fisheries research and assessment*, *ICES Journal of Marine Science*, 59, 2002: 216-225.
- Mayer, L. A., Raymond, R., Glang, G., Richardson, M. D., Traykovski, P., Trembanis, A. C.: *High-Resolution Mapping of Mines and Ripples at the Martha's Vineyard Coastal Observatory*, *IEEE Journal of Oceanic Engineering*, 32 (1) 2007: 133-149.
- Rñnhovde, A.: *High Resolution Beamforming of SIMRAD EM3000 Bathymetric Multibeam Sonar Data*, MSc Thesis, University of Oslo, Norway, 1999, 121 pp.
- Shah, G. S. & Talukdar, K. K.: *a study of enhanced signal processing on multibeam bathymetric data*, *OCEANS'99 MTS/ IEEE Riding the Crest into the 21st Century*, 2 (2) 1999: 904-909.
- Shannon, C. E.: *a mathematical theory of communications*, *Bell Systems Technical Journal*, 27, 1948: 379-423.
- Thorner, J. E.: *Approaches to sonar beamforming*. p. 69 - 78. In: Proceedings of the 1990 IEEE Southern Tier Technical Conference. April 1990, Binghamton, NY, USA.
- Titchener, M. R.: *a measure of information*, p 353 - 362. In: Data Compression Conference 2000 Proceedings DCC 2000, 28-30 March 2000. Snowbird, USA.
- Van Buren, A. L. & Blue, J. E.: *Calibration of underwater transducers at NRL*, *Journal of the Acoustical Society of America*, 86 (S1) 1990: S60.
- Wu, L. & Zielinski, A.: *Lossless Compression of Hydroacoustic Image Data*, *IEEE Journal of Oceanic Engineering*, 22 (1) 1997: 93-101.
- Xiaofeng, J. & Wenjun, Y.: *Transient calibration of underwater acoustic transducers Measurement*, *Science and Technology*, 9 (11) 1998.

## CONTACT WITH THE AUTHORS

Marek Moszynski, Assoc. Prof.  
 Andrzej Chybicki, Ph.D.  
 Marcin Kulawiak, Ph.D.  
 Zbigniew Lubniewski, Ph.D.  
 Faculty of Electronics, Telecommunications  
 and Informatics  
 Gdansk University of Technology  
 Narutowicza 11/12  
 80-233 Gdansk, POLAND  
 e-mail: marmo@pg.gda.pl  
 e-mail: andrzej.chybicki@eti.pg.gda.pl  
 e-mail: marcin.kulawiak@eti.pg.gda.pl

# Possibilities for Motorways of the Sea development in the eastern part of the Adriatic Sea

Bojan Beškovnik, Ph.D.

Intereuropa, Global logistics service, Ltd. Co., Slovenija

## ABSTRACT



*This article presents a wider perspective on possibilities of Motorways of the Sea development in the Adriatic Sea, with a special emphasis on the eastern coast of the Adriatic Sea. A complete overview of Motorways of the Sea development has been presented, and key elements influencing the development of Motorways of the Sea were analysed. It has been ascertained that there exist a lot of bottlenecks in the connection to the transport infrastructure in South East Europe. Superannuated port infrastructure, unsuitable inland connections, and nonexistent IT tools for electronic data exchange between all participants in the logistics chain hinder dynamic development of Motorways of the Sea. All these elements were thoroughly analysed, and a proposal for a macro transport strategy suitable for South East Europe has been exposed. It has been accentuated that there is a future for Motorways of the Sea introduction but all described bottlenecks have to be further analysed and removed in a short period of time, to stimulate private sector for financial investments.*

**Key words:** Motorways of the Sea; port infrastructure; intermodality; inland connections; South East Europe; Adriatic Sea

## INTRODUCTION

Today, intermodality and the use of sea transport route is an important topic of European transport policy. Consequently, these fields are subjects of detailed analysis and are included in the European development plans. Establishing intermodality and developing Motorways of the Sea to obtain sustainable passenger and cargo mobility are essential goals for the European Commission. Such a policy is not new, as it was developed in early nineties of last century, when a green paper on the impact of transport on the environment was released by the European Commission. In addition, a white paper on the common transport policy was presented in 1992, where the industry was called to support co-modality between different transport modes, especially between sea and rail transport, and to establish efficient transport services using intermodal nodes within the EU network.

The idea and the concept of MoS were firstly developed in June 1992 when Viamare S.p.A. introduced the first initiative to shift road transport to the sea. It was a sea line between Genoa and Termini Imeri in Sicily that was the starting point of today's common European strategy called Motorways of the Sea (MoS). According to Paixao [1], Bagchus and Kuipers [2] presented the concept "autostrade del mare" for the cargo shift from the road to the sea in the Portugal and Netherlands Corridor. This MoS concept started a dynamic development in

Europe, as Grimaldi introduced the service between Genoa and Palermo, and the International Association of Turkish hauliers introduced a RO-RO (roll on-roll off) service between Turkey and Italy. Different services were established in the next years, first a RoPax (roll on-roll off and passenger) service between Ancona and Patras, followed by different services in the Baltic and North Sea region.

Increased industrial interests stimulated the European Commission to highlight the MoS as a European concept to decrease the use of road transport, and consequently decrease the air pollution and traffic congestion in the European territory. Psaraftis [3] says that MoS will concentrate flows of freight on specific sea routes with the aim to establish new viable, regular and frequent maritime links between Member States, reduce road congestion, and improve the access to peripheral EU countries. For this reason the MoS concept has been promoted as an intra-community strategy and a cross-border project between all EU states. Special emphasis was put on ports with their infrastructure and hinterland connections, especially the railway network connections. European Commission recognised that MoS should be developed under a long-term transport strategy. Thus, different studies and project were launched and financially supported. Baird [4] recognises that from an academic standpoint these projects also contributed towards the development of an analytical framework to determine the feasibility of MoS.

Some EU countries already developed MoS services for regular sailing from their ports. A big challenge is foreseen for the region of South East Europe, especially for the Adriatic Sea region. This was also recognised by previous research studies done by Haralambous [5] and Tilling [6]. Consequently, new research activities are necessary to stimulate the development of MoS in South East Europe and in the Adriatic Sea.

## THE MOS CONCEPT

### *Development of MoS in EU transport network*

The MoS were developed on a European Short Sea Shipping platform, as they are involving different operators and logistics players in a unique transport chain. The MoS concept was placed by EU as a strategic transport policy for the second time in 2001. Previously the European Commission worked on the 'European Marine Motorways' project under the Transport Research and Technological Development Program of the 4th Framework. Within this program, commercial viability of conventional and high-speed RO-RO services was studied in order to find an alternative to freight road transport.

With a white paper on transport policy presented by European Commission in 2001 some important principles regarding the implementation of MoS were incorporated into a strategic European document. The use of European inland waterways to support more balanced usage of transport modes and to develop intermodality placed a special focus on port organization and infrastructure in use. In addition, European Commission suggested that the industry prioritises ports with good hinterland rail connections and supports the creation of important intermodal points in the Mediterranean, Atlantic and North Sea coasts.

On this base, the study to define four MoS regions was carried out by the High Level Group, chaired by Karel van Miert and supported by European Commission [7]. According to the study presented in June 2003, the following four regions were proposed and later on accepted by the European Commission:

- Motorway of the Baltic Sea (linking the Baltic Sea with Central and Western Europe, including the route through the North Sea/Baltic Sea Canal);
- Motorway of the Sea of Western Europe (leading from Portugal and Spain via the Atlantic Arc to the North Sea and the Irish Sea);
- Motorway of the Sea of South East Europe (connecting the Adriatic Sea to the Ionian Sea and the Eastern Mediterranean, including Cyprus);
- Motorway of the Sea of South West Europe (western Mediterranean, connecting Spain, France, Italy, Malta and linking South East Europe and also the Black Sea).

According to the experience from the Short Sea Shipping development, a lot of bottlenecks were identified. These are: complicated customs procedures, a lot of paper work, different operational and commercial documents in use, administrative procedures, expensive services' implementation, mostly insufficient critical mass of cargo to be shifted in a short period, etc. During the last decade a lot of bottlenecks were eliminated, resulting in better starting conditions to establish and promote MoS. The European Commission played a crucial role in these actions, especially in reducing administrative barriers and in simplifying customs formalities on the entire transport route.

The major unsettled problems are still connected to the ports, their infrastructures and the railway networks, which

are especially in eastern and southern Europe underdeveloped. Such infrastructure hardly supports cargo's expectation for fast and cost effective services. In addition, the economy in the region is underdeveloped. This was ascertained also by Midelfart-Knarvik *et al.* [8], as they say that the MoS of the Baltic Sea and the MoS of Western Europe offer greater potentials in MoS development; as they can be supported by higher industrial distribution at a European level and by better trade relations. Moreover, Paixao [1] says that not all ports will be MoS gateways, only 87.2% of port authorities surveyed in a research of EU ports are predisposed to become MoS interfaces.

### *Key elements influencing development of MoS*

It is of crucial importance to identify key elements that influence the development of MoS, because they have a deep impact on strategic decisions of shippers and intermodal operators. Based on the analyse of the European Marine Motorways project (EMMA) under the 4<sup>th</sup> Framework Program, Baird [9] exposes six main elements influencing adoption of MoS in EU transport framework. These elements are:

- Price – MoS transport price versus actual road transport;
- Service schedule – minimum service schedule of MoS should be a daily service to compete with actual road service;
- Reliability – regular departures of vessels, with no weather influences;
- Transit time – MoS should secure 24 to 48 hours door-to-door services to compete with actual road service;
- Efficiency in port – factors as handling speed, cargo security, 24-hour working in the port should be secured to maintain low-cost transport and service schedules;
- On-board facilities – a range of services for drivers should be secured to accompany the cargo and to be included in the total transport costs.

The price of transport services provided by MoS is a sensitive factor, because shippers or cargo owners might decide to shift their cargo from road transport to a MoS service, just in case the "all in" price is competitive. According to the United Kingdom Marine Motorways study performed by Napier University and Partners [10], a price of a RO-RO door-to-door service consists of the following three groups of costs:

- 50% for the sea RO-RO transport;
- 42% for road transport from door to port services and vice versa;
- 8% for cargo handling.

From the MoS price perspective it has to be emphasised that the price of inland transport is still very crucial in total costs for MoS services. Even if we shift cargo from road to the sea, over 40% of all costs will be generated by inland services. Almost one tenth of all costs are produced by cargo handling. This poses very important pressure to the ports, in order to increase efficiency in every sphere of their organisation. Maintaining service schedule, service reliability and total door-to-door transit time are key elements to be secured by MoS. Shinghal and Fowkes [11] say that high frequency is a central attribute when customers are determining mode choice.

In addition to the above six key elements, three important factors should be also mentioned. The first one is the degree of the developed hinterland infrastructure. The second one is the location of port terminals or hinterland intermodal terminals, and the third one is an IT connection between all participators in the logistics chains.

The efficiency of ports, port services and especially port-hinterland connections are important elements for MoS [12]. The issue of developed or modernised hinterland infrastructure is for sure a big challenge for the underdeveloped regions and economies. Even if a super fast RO-RO service is introduced between the two ports, the problem of superannuated inland infrastructure can eliminate the advantage of fast sea service. The location of ports or hinterland intermodal terminals influences the transfer of cargo from different transport means. Ports or intermodal terminals must be positioned out of urban centres and massive traffic, to guarantee congestion-free access between sea and inland transport. Special transport corridors should be introduced to speed up the transfer of intermodal transport units out of the port or terminal systems. This must be supported by uniformed IT programs and connections, and by simplified documentation procedures.

Based on all described key elements influencing the development of MoS services in the European transport network it can be stressed out that intermodality plays a crucial role in MoS development. The MoS can be more easily introduced in the areas where intermodal transport is already present and frequently used. Paulauskas and Bentzen [13] accentuate that a few parallel and independent transport routes that exclude any negative technical, political or economical influence are needed to develop MoS. Moreover, IT platforms and IT tools between port authorities, port operators, financial institutions, cargo owners, logistics operators etc. should be uniformed to simplify logistics processes in the door-to-door cargo delivery.

For sure the financial perspective of supporting MoS development has to be considered too, as MoS implementation is directly connected to the financial support of the national economy of an interested state, or European funds. Of course, financial investments from the private sector are of significant importance, too. Beside this issue, the primary focus is on the infrastructure, which has to be previously secured. Only in this way will shippers and operators support the modal shift offered by MoS.

## **TRANSPORT CHARACTERISTICS OF EAST MEDITERRAN AND ADRIATIC SEA**

The region of South East Europe is becoming very interesting research matter from the transport and logistics perspective. This is mainly connected with the analysed possibilities of further economical development and investment possibilities performed by global manufacturing and logistics companies. The region of Balkans is therefore presenting an opportunity to partly cover manufacturing necessities for the western economies, as in the era of global crisis transport costs have become an important issue of total price reduction. Far East production established in last decades is moving closer to the final consumer markets. Eastern Europe was recognized as an important alternative. These possibilities were already recognized by Fiat, Bosch, Continental, IKEA etc.

South East Europe is attracting developed economies, but investments in massive manufacturing need a support from the transport and logistics sector in order to ensure “just in time” and “just in sequence” production and distribution of products to the final consumers. Consequently, the development of transport infrastructure and new transport concepts will play a significant role in future development of the region.

Transport concepts like MoS can significantly support increased cargo flows of raw materials in import and finished product in export from the Balkans. The MoS will also fulfil higher transport quality expectations from the investors and logistics operators. Analysing the existing transport

infrastructure and procedural bottlenecks can speed up the economy and industry to prioritise the settlement of the mentioned tasks.

### ***Analysing and removing existing bottlenecks***

Bottlenecks influencing the development of MoS in South East Europe were analysed in different research papers [5, 6, 14, 15]. With the S.W.O.T analyse Haralambous [5] exposed six main weaknesses of MoS in South East Europe. These are:

- Inadequate port infrastructure to support intermodality in all states,
- Problematic port-hinterland connections, mainly with railway routes,
- Insufficient railway infrastructure in all parts, delay in the realisation of the TEN railway projects in South East Europe,
- Over-aged vessel fleet shipping in the area, unable to support fast modal shift,
- Lack of synergy among states and economies,
- Absence of large Trans-national logistic operators that could play the leading role for uniting interested actors.

In addition, Haralambous [5] says that threats, such as congestion in core ports and lines, dependences of regional economies, mostly on road transport, and the risk of failure of viable schemes after the end of funding, due to high investment and operational costs, are influencing the development of MoS. Consequently, it can be stated that transport infrastructure and services directly related to it are presenting the main bottleneck.

Tilling [6] also sees the main bottleneck in the underdeveloped infrastructure and complete transport sector, and exposes that drastic reform in the transport industry is still advocated as the only chance of the survival and economic growth of the South East European countries, as the capacity of countries to maintain the existing infrastructure and operational services is practically non-existent.

Beside the superannuate infrastructure, an important bottleneck is foreseen in the field of cargo information exchange between ports, shipping lines and other logistics operators. The lack of used IT tools in the entire logistics chain definitely hinders the MoS development. This field should be thoroughly analysed, and a detailed action plan appropriate for South East Europe should be prepared shortly.

As far as other bottlenecks are concerned, a severe doubt appears inevitable, as some economies and important companies are significantly depending on road transport and they might lose significant profit from shifting from road to sea or MoS. Consequently, strong resistance to change traditional transport routes and modes is being predicted. For this reason, it is important that the economy and industry recognise long term benefits of MoS implementation.

### ***Main possible routes of MoS***

Possible routes of MoS are developed according to market needs. Capacity utilization is an important element that should be considered. Beside this element the industry should consider also following elements: trade imbalance and variations in demand, competitive situation, state of the market, and types of customers and cargo [16].

Taking into account possible route characteristics different studies proposed a range of MoS corridors for South East Mediterranean and the Adriatic Sea. A study carried out for the “East Med MoS Master Plan” [17] funded by the

European Commission – DG TREN proposed nine main MoS corridors. Five corridors are important for the cargo flow in the Adriatic Sea. These corridors are: Igoumenitsa-Koper, Venice-(Igoumenitsa)-Patra-(Korinthos), Igoumenitsa-Ancona-Koper, Venice-Koper-Ploce and Malta-Venice.

Just three MoS corridors include ports on the eastern coast of the Adriatic Sea. In all three corridors Koper port plays an important role. Meanwhile, from a range of other ports just port of Ploce is proposed for the line with Venice port.

The Corridor Igoumenitsa-Koper should be an alternative to the strong road transport between south Europe and central Europe. Markets as Hungary, Austria and other central European countries should shift an important part of a daily truck line to the MoS. A yearly traffic of 400 000 to 600 000 tons has been foreseen till the year 2015. This MoS corridor organized by RO-RO service should be an alternative to the existing X. Pan-European Corridor and should use V. Pan-European Corridor to link Koper port with the hinterland destinations by rail, as already almost 70% of all cargo is transported from the port by rail.

The described MoS corridor will face troubles to attract significant cargo flow, because the length of the journey from Greece to Slovenia via X. Pan-European Corridor is approximately 1 450 km. It can be foreseen that only one third of the actual road transport might be transferred to MoS service. Consequently, the total annually shifted traffic could reach up to 600 million ton/km.

The second proposed corridor Igoumenitsa-Ancona-Koper is almost the same corridor as the previous one, but important cargo flow from central part of Italy should be collected by RO-RO service for central Europe, the Balkans, and for the western part of Greece. The study “East Med MoS Master Plan” shows that from Ancona to Koper and vice versa over 2 million tons of goods should be shifted to MoS by 2015. Main countries interested in such service should be Slovenia, Croatia and Hungary, as they have strong import and export goods flow with the central part of Italy.

The MoS corridor Venice-Koper-Ploce should be mainly established to connect the northern and central part of Italy to the Balkans, especially markets of Croatia and Serbia. With this RO-RO service around 800 000 to 1.3 million tons of goods might be shifted from roads to the sea. This corridor might also experience troubles with shifting significant cargo flow and passengers to MoS service, because the distance by road between northern Italy and Croatia is just 500 to 600 km, and these markets are connected mainly by highways.

Beside the proposed MoS corridors, an important corridor should be additionally supported in the future. It is the RO-RO service between northern Adriatic ports (Trieste or Koper) with Albania and its port in Durres. Durres port is situated on important VIII. Pan-European Corridor and directly connects markets of FYR Macedonia, Bulgaria, Romania, Serbia and partly Greece. Although Albania is not an EU country the service should be seen as an important European intermodal link, which should offer and gain important benefits from modal shift.

## THE CASE STUDY OF THE ADRIATIC SEA REGION

The case study performed on the Adriatic Sea region concentrates mainly on the eastern coast of the Adriatic Sea. A lot of bottlenecks have been foreseen by different authors, therefore a complete analyse of all main key elements influencing the MoS development is necessary. Consequently, all main ports were analysed and compared, including the

actually used infrastructure and IT tools or programs used by terminal operators. In addition, the inland infrastructure and hinterland terminals were analysed to formulate a strategy of faster MoS development in the Eastern Mediterranean and in the Adriatic Sea. Moreover, it becomes very important to set up a macro strategy for MoS development for a longer period, in order to attract financial support from the private sector.

### Port infrastructure and superstructure

Port systems are one of the important elements in MoS development. They should cut down all waste operations, extra costs on door-to-door transportation, and perform lean modal shift. Problems of agile port operations have been deeply analysed and discussed by Vis and de Koster [18], Steenken et al. [19], and Notteboom et al. [20]. Paixao and Marlow [21] propose that ports must adopt a completely new logistic approach and agility to cope with new trends on the global market.

It has been realised that there exist big differences between the ports and their terminals in sense of technical equipment, handling capacities and infrastructure. But it is valid for all these marine systems that are faced with more and more intermodal units to be handled in short time and at low cost. It is essential for operators to reduce unproductive time and to offer effective processes in order to be in line with constantly increasing competition among ports or terminals.

According to the research of all main ports on the eastern coast of the Adriatic Sea, the infrastructure and superstructure is very poor. All maritime ports, except Koper and Piraeus, are underdeveloped on the sea side as well as on the land side. The dedicated intermodal infrastructure practically does not exist. In Tab. 1 basic infrastructure data for container and RO-RO terminals were collected. The data for Piraeus port were not included as this port is not representative due to well developed infrastructure and important role for containerised and RO-RO traffic in the Mediterranean.

All five analysed ports together have just 10 specialised RO-RO ramps. In most cases, the quay or berths for RO-RO and container vessel are the same. Among these ports only Koper has suitable infrastructure to support efficient MoS services. Other ports can also be a gateway for MoS, but their infrastructure and superstructure cannot assure efficient modal shift which MoS should offer to the cargo owners. Beside the infrastructure, the superstructure of the maritime ports is also superannuated and actually cannot support higher volumes of intermodal cargo. Ports as Ploce, Bar and Durres do not have specialised container berth cranes. Almost the same situation is on the yard, where container gantry cranes are not in use. All handlings of intermodal units are performed by reachstackers or forklifts.

Tab. 1. Basic port infrastructure data for container and RO-RO terminals

Port	Quay length [m]	Draught [m]	RO-RO ramps	Yard capacity [m]
Bar	770	12	1	65 000
Durres	700	10	4	30 000
Koper	1 400	11.4	4	1 135 000
Ploce	300	13.8	1	38 000
Rijeka	460	11	0	135 500

Moreover, it has to be jeopardising that in the South East Europe region there are no functioning modern hinterland intermodal terminals. This has been acknowledged also by

Šakalys and Palšatis [22], as they came to the conclusion that a very small quantity of inland terminals exist in Southern and Eastern Europe, and they operate with limited handling equipment and on limited land area. The only operating railway stations that can accommodate containers and other intermodal units are situated in capital cities such as Belgrade, Zagreb, Ljubljana, Sarajevo, etc. These terminals do not use modern handling technologies, the degree of automation is very low, and static and dynamic capacities cannot secure optimal handling processes.

Obviously the actual port infrastructure and superstructure on the eastern coast of the Adriatic Sea is not in a position to fulfil all key elements of MoS development. On the one hand, port systems cannot be cost effective, and on the other, they cannot maintain requested service schedules and so important transit times. The reliability of such MoS would be under a big question.

### *Inland connections and infrastructure*

Intermodal transport and appropriate infrastructure is an important element of MoS development. It can be expressed as a basic platform to develop MoS, and it is directly linked with the health of the regional economy. Stronger economy uses intermodal transport advantages in order to achieve stronger long-term development. Consequently, such economies are directly investing in intermodal infrastructure. The comparison between Western European infrastructure with South Eastern one shows that the last one is underdeveloped and superannuates.

The difference is not as big in road infrastructure as it is in railways. States of South East Europe invested in highways

development between the capital cities. Highway connections with the maritime ports are practically nonexistent, except Koper port and to some extent the ports of Rijeka and Durres.

The MoS for the South East Europe should be developed with connection to the rail transport. The railway should be used as the key transport solution between maritime terminals and hinterland hub terminals. Consequently, the road transport should be used only on shorter transport routes up to 150 km and on direct to door deliveries. Unfortunately, the use of the rail transport in South East Europe drastically decreased in the last decade, and at the same time the railway infrastructure was not modernised accordingly. As shown in Tab. 2, the total length of railway lines in South East Europe is 13 276 km and was reduced by over 200 km in the analysed countries. Meanwhile, in the same period Western Europe increased them, especially in Spain and Germany.

The length of the road network in South East Europe is about 182 600 km. Just 3 910 km or 2.14% of all road networks are highways, where just Greece and Croatia are above this low average. Consequently, it can be stressed out that such an infrastructure does not allow high transport speed and cannot secure high security standards.

Beside the fact that the road network is not developed and does not permit high transport speed, it must be accentuated that the rail network is even more superannuated. As analysed in Tab. 3, on an average the rail network represents just 6.8% of total inland transport network. Furthermore, the railway transport speed is in average below 40 km/h, in some sections even below 20 km/h.

The analysis can be summarized that inland connections are not supporting modern logistics concepts. This can have positive and negative impacts on the development of MoS.

*Tab. 2. Total length of railway lines (km) [23]*

	2001	2002	2003	2004	2005	2006	2007	2008	2008/2001
<b>Belgium</b>	3 454	3 518	3 521	3 536	3 544	3 560	3 568	3 513	101.7
<b>Czech Rep.</b>	9 523	9 600	9 602	9 612	9 614	9 597	9 588	9 586	100.6
<b>Germany</b>	35 986	35 803	41 531	-	38 206	-	41 209	37 798	105.1
<b>Spain</b>	12 310	12 298	-	12 873	12 839	13 008	13 368	13 353	108.5
<b>Sweden</b>	11 021	11 095	11 037	11 050	11 017	11 020	10 972	11 022	100
<b>Netherlands</b>	2 809	2 806	2 811	2 811	5 231	2 797	2 801	2 888	102.8
<b>Slovenia</b>	1 228	1 228	1 228	1 228	1 228	1 228	1 228	1 228	100
<b>Croatia</b>	2 726	2 726	2 726	2 726	2 726	2 722	2 722	2 722	99.8
<b>Macedonia</b>	699	699	-	699	699	699	699	699	100
<b>Bulgaria</b>	4 320	4 317	4 316	4 259	4 154	4 146	4 143	4 144	95.9
<b>Romania</b>	11 015	11 002	-	11 053	10 948	10 789	10 777	10 785	97.9
<b>Greece</b>	2 377	2 383	2 414	2 449	2 576	2 509	2 551	2 552	107.4

*Tab. 3. Total length of roads and railway lines in South East Europe*

	Roads [km]	Highways [km]	Roads/Highways [%]	Rail [km]	Road/rail [%]
<b>Albania</b>	18 000	170	0.94	447	2.48
<b>Bosnia&amp;Her.</b>	22 900	0	0.00	1 031	4.50
<b>Croatia</b>	28 400	1 340	4.72	2 722	9.58
<b>Greece</b>	17 000	1 030	6.06	2 552	15.01
<b>Macedonia</b>	9 570	190	1.99	699	7.30
<b>Montenegro</b>	5 174	0	0.00	250	4.83
<b>Serbia</b>	42 690	560	1.31	4 347	10.18
<b>Slovenia</b>	38 873	620	1.59	1 228	3.16

On the one hand, superannuated inland infrastructure calls for MoS, in order to shift cargo from inland transport to potentially better and faster sea transport. On the other hand, inland transport infrastructure is in worse conditions close to the ports, as some of them are still not connected with the highways. Consequently, road door-to-door services are preferred.

### *IT systems and documentation procedures*

Modern information technologies and systems are very important tools to enhance the integration of intermodal operations and to speed up the modal shift at intermodal points. Efficient data exchanges between all logistics operators and cargo owners are especially important to establish just one IT data network, with uniformed quantity and quality of information flow. European Union and European Commission recognised this important goal a decade or two ago. The main aim is to support research which addresses practical problems of implementing the latest information technologies in intermodal logistic organisation, and help to break barriers by introducing cutting-edge technologies to the system, standards and services [24].

Different EU projects analysed actual needs of the industry to work in a real-time logistics information network. Important projects were INTRARTIP, MARNET, ITESIC, INFOLOG, etc, which provided proposals for full information network architecture, consisting of a uniformed information platform and standardised solutions to integrate Electronic Data Interchange (EDI) in the entire logistics chain. Services like MoS need up-to-date booking services, tracking and tracing management, paperless working processes, simplified administrative services, etc.

Unfortunately, ports and hinterland terminals do not use uniformed IT systems, which should be easily connected through standardised information platform. Among the analysed ports and terminals only ports of Koper and Piraeus have integrated an EDI system that to some extent simplifies information exchange between shipping lines, ports and the inland transport operator. Ports of Rijeka, Ploce, Bar and Durres do not use modern IT platforms to simplify data exchange between logistics providers. Moreover, in Durres port all the procedures and direct orders to the port are still managed through hard copy documents, which can be hand over manually or as scanned documents by e-mail system. The same procedure is in practice also with other authorities as customs, phytosanitary inspections, police etc.

IT communication is one of the key elements influencing MoS development, and the present situation in the ports and hinterland terminals in South East Europe is not satisfactory for fast MoS development. A two-pillar action plan should be made in a short time to remove the barriers of interoperability between different information systems. Firstly, ports must integrate an EDI practice in their processes, even if they are inhomogeneous with other operators. And secondly, a centralised communication node should be developed. Such a node should connect and integrate shipping lines, their agents, logistics providers, forwarders and cargo owners into a main 'umbrella' module. Consequently, an IT platform should be successfully implemented, improving cargo information exchange and securing on-line cargo tracing and tracking. Thus, the needs and expectations from MoS should be provided.

### *A need for macro transport strategy*

Based on the described findings, it is necessary that the region of South East Europe makes a common strategy on

developing intermodality in the region and on how MoS should be developed in a long term. According to the research, a short-term strategy would not bring necessary actions to actively develop MoS in the Balkans. In this situation two approaches are possible – a bottom-up or a top-down approach. Rodrigue et al. [25] says that with a top-down approach direct and fast actions can be implemented, but these actions should be executed by the governments or Port authorities. These actions should not be focused on road charges only as they may not achieve the desired shift from road to sea operations, particularly in countries where the economic and social impacts of road freight movement outweigh its external impacts and costs [26].

Parantainen and Merilainen [27] say that a bottom-up approach is the best way of developing concrete projects. Projects should be based on realistic estimates of transport volumes and create permanent and economically feasible transport chains. This is also valid for MoS, because the development of MoS should be done on a project base. It can be anticipated that with the bottom-up approach the industry can efficiently enter the sector of intermodality and modal shift. With such approach, the industry must present its expectations and needs to governmental institutions and dynamically co-create a macro transport development strategy in the region. With this it is possible to influence governmental investments in transport infrastructure and future legislation in the transport sector. The industry must press the Port authorities to introduce EDI platforms and to reduce documentation processes in business cooperation with the ports and hinterland terminals. Clark et al. [28] expose that legal restrictions can negatively affect port performance and the transport system as a whole. Thus, the industry must be active also in this very important field of transport regulation.

Given the analysed infrastructure, superstructure, and current data exchange procedures in South East Europe it is necessary to develop a long-term transport policy for this European region. With a macro transport strategy an innovative environment should be established. According to Haralambous [5], the intermodal chain must provide free flow without any bottlenecks, physical or operational, and has to be a credible choice. The concentration on cargo flow is recommended to ensure viability, but also the promotion of ports from Maritime transport servers to intermodal nodal points that provide fast and low cost services, and optimum connections to land high level infrastructure are prerequisites for the success.

Therefore, the MoS development mainly has to focus on infrastructure modernization to stimulate intermodality and, at the same time, the key elements and goals of modern, lean and green logistics should be considered accordingly.

## **CONCLUSION**

The MoS initiative is an important goal supported and coordinated by the European Commission. The main goal is to reduce congestion on European roads, to shift cargo and passengers from land transport to the sea, to reduce external costs from the extent use of road transport, and to achieve long-term economic growth in the Community. Based on the above, the MoS concept has been promoted as an intra-community strategy, with special emphasis on ports, their infrastructure and hinterland connections, especially railway network connections.

The MoS are very important "tools" also for the region of South East Europe. Global companies recognised Eastern Europe as an important alternative for Far East production. But investments in massive manufacturing need a support

from the transport sector, in order to secure “just in time” and “just in sequence” production and distribution. The MoS can significantly support increased cargo flows of raw materials in import and finished product in export from the Balkans, but also need modernised port infrastructure as well as inland connections.

The situation in South East Europe, especially in the Balkans, does not offer a short-term solution for massive MoS implementation. Firstly, the economy is very poor, especially in the era of global crisis. Secondly, the transport infrastructure and superstructure is superannuated, and without actual funds it is impossible to realise important investments, neither by the states nor private sector.

The only adequate intermodal points are the ports of Koper and Piraeus, which invested in infrastructure and superstructure during the last decades. These ports can be an important gateway for MoS. Although they are well equipped and organised, the main bottleneck remains the inland connection by rail. Port of Koper is suffering from congestion on the rail transport, as over 70% of goods are transported from the port by rail. Other ports as Rijeka, Ploce, Bar and Durres do not have adequate infrastructure to importantly support MoS. Their main problem is also that they do not use uniformed IT systems, which should connect shipping lines, shipping agents, forwarders and other operators in a unique IT chain.

Undoubtedly, the MoS have a future in South East Europe and in the Adriatic Sea. But it is necessary to develop a long-term transport policy for this European region to further analyse all described bottlenecks, in order to remove them shortly. In this way, a private sector should be importantly stimulated for direct financial investments. Consequently, a bottom-up approach of MoS development should be established. According to the past experience with MoS implementation, this is the only appropriate way to have long active MoS services.

## BIBLIOGRAPHY

- Paixao A.C.: *Motorway of the sea port requirements: the viewpoint of port authorities*. International Journal of Logistics: Research and Applications, Vol. 11, No. 4, 2008, p. 279–294.
- Bagchus R.C. and Kuipers, B.: *Autoestrada del Mare*. In: European ShortSea Shipping, Proceedings from the First European Research Round Table Conference on Short Sea Shipping, London, England, 1993.
- Psarafitis H.N.: *EU Ports Policy: Where Do We Go from Here?*. Maritime Economics & Logistics Vol. 7, 2005, p. 73–82.
- Baird A.J.: *Investigating the feasibility of fast sea transport services*. Maritime Economics & Logistics, Vol. 6, 2004, p. 252–269.
- Haralambous G.: *The contribution of the “Sea Motorways” to the European transport Policy*. European Conference of Transport Research Institutes – YRS05, Hague, 2005.
- Tilling C.: *The EU common transport policy for south-east Europe – what makes it a factor of cohesion and sustainability?*. South East Europe Review, Dusseldorf, 2006.
- European Commission: *Priority projects for the trans-European transport network up to 2020*. High-Level group report, Luxembourg, 2003.
- Midelfart-Knarvik K.H., Overman H.G., Redding S.J., Venables A.J.: *The Location of European Industry*. Economic Papers Number 142. Luxembourg, 2000.
- Baird A. J.: *The Economics of Motorways of the Sea*. Maritime Policy Management, Vol. 34, No. 4, 2007, p. 287-310.
- Napier University & Partners: *UKMM – United Kingdom Marine Motorways Study, Future Integrated transport (FIT) Link Programme*. Department for Transport and Engineering & Physical Science Research Council (EPSRC), Edinburgh, 2002.
- Shinghal N. and Fowkes T.: *Freight mode choice and adaptive stated preferences*. Transport Research Part E, Vol. 38, 2002, p. 367-378.
- Ng A.K.Y.: *Competitiveness of short sea shipping and the role of port: the case of North Europe*. Maritime Policy & Management, Vol. 36, No. 4, 2009, p. 337-352.
- Paulauskas V. and Bentzen K.: *Sea Motorways as a Part of the Logistics Chain*. Transport, Vol. 23, No. 3, 2008, p. 202-207.
- Trujillo L. and Medda F.: *Road Freight Market Distortion and the Viability of SSS*. Second annual conference on competition and regulation in network industries, Brussels, 2009.
- Paraschiv D.M., Popa I., Caragin A.R., Tartavuela R.I.: *Evolution of Strategic Supply Chain in Central and Eastern Europe in Turbulent Times – Focus Romania*. The 8th International Conference on Logistics and SCM Research, Bordeaux, 2010.
- Styhre L.: *Strategies of capacity utilisation in short sea shipping*. Maritime Economics & Logistics, Vol. 11, No. 4, 2009, p. 418-438.
- European Commission: *Elaboration of the East Mediterranean Motorways of the Sea master plan*. East Mediterranean master plan of the Motorways of the Sea, Brussels, 2009.
- Vis I.F.A. and De Koster R.: *Transvesselment of Containers at a Container Terminal: an Overview*. European Journal of Operational Research, Vol. 147, No. 1, 2003, p. 1-16.
- Steenken D., Voss S., Stahlbock R.: *Container Terminal Operation and Operation Research – a Classification and Literature Review*. OR Spectrum, No. 26, 2004, pp 3-49.
- Notteboom T.E. and Rodrigue J.P.: *Port Regionalization: Towards a New Phase in Port Development*. Maritime Policy and Management, Vol. 32, No. 3, 2005, p. 297-313.
- Paixao A. C. and Marlow P. B.: *Fourth generation ports-a question on an agility?*. International Journal of Physical Distribution and Logistics Management, Vol. 33, No. 4, 2003, p. 335-376.
- Šakalys A. and Palšatis R.: *Development of intermodal transport in new European Union states*. Transport, Vol. 21, No. 2, 2006, p. 148-153.
- Eurostat, 2010, [http://appsso.eurostat.ec.europa.eu/nui/show.do?dataset=rail\\_if\\_tracks&lang=en](http://appsso.eurostat.ec.europa.eu/nui/show.do?dataset=rail_if_tracks&lang=en)
- European Commission: *Motorways of the Sea – Modernising European Short Sea Shipping Links*. Luxembourg, 2006.
- Rodrigue J. P., Slack B., Comtois C.: *Green Logistics (The Paradoxes of)*. in: Brewer A.; Button, K.; Hensher, D. The handbook of Logistics and supply-chain management, London, 2001.
- Medda T. and Trujillo L.: *Short-sea shipping: an analysis of its determinants*. Maritime Policy & Management, Vol. 37, No. 3, 2010, p. 285-303.
- Paratainen J. and Merilainen A.: *The Baltic Sea Motorway – Recent Development and Outlook for the Future*, Journal of Maritime Research, Vol. 4, No. 2, 2007, p. 21-30.
- Clark X., Dollar D., Micco A.: *Port efficiency, maritime transport costs, and bilateral trade*. Journal of Development Economics, Vol. 75, 2004, p. 417-450.

## CONTACT WITH THE AUTHOR

Bojan Bešković, Ph.D.  
Intereuropa, Global logistics service, Ltd. Co.  
Vojkovo nabrežje 32,  
SI-6000 Koper, SLOVENIJA  
e-mail: bojan.beskovnik@intereuropa.si



The Ship Handling Research and Training Centre at Ilawa is owned by the Foundation for Safety of Navigation and Environment Protection, which is a joint venture between the Gdynia Maritime University, the Gdansk University of Technology and the City of Ilawa.

**Two main fields of activity of the Foundation are:**

- Training on ship handling. Since 1980 more than 2500 ship masters and pilots from 35 countries were trained at Ilawa Centre. The Foundation for Safety of Navigation and Environment Protection, being non-profit organisation is reinvesting all spare funds in new facilities and each year to the existing facilities new models and new training areas were added. Existing training models each year are also modernised, that's why at present the Centre represents a modern facility perfectly capable to perform training on ship handling of shipmasters, pilots and tug masters.
- Research on ship's manoeuvrability. Many experimental and theoretical research programmes covering different problems of manoeuvrability (including human effect, harbour and waterway design) are successfully realised at the Centre.

The Foundation possesses ISO 9001 quality certificate.

**Why training on ship handling?**

The safe handling of ships depends on many factors - on ship's manoeuvring characteristics, human factor (operator experience and skill, his behaviour in stressed situation, etc.), actual environmental conditions, and degree of water area restriction.

Results of analysis of CRG (collisions, rammings and groundings) casualties show that in one third of all the human error is involved, and the same amount of CRG casualties is attributed to the poor controllability of ships. Training on ship handling is largely recommended by IMO as one of the most effective method for improving the safety at sea. The goal of the above training is to gain theoretical and practical knowledge on ship handling in a wide number of different situations met in practice at sea.

For further information please contact:

**The Foundation for Safety of Navigation and Environment Protection**

Head office:  
36, Chrzanowskiego Street  
80-278 GDAŃSK, POLAND  
tel./fax: +48 (0) 58 341 59 19

Ship Handling Centre:  
14-200 ILAWA-KAMIONKA, POLAND  
tel./fax: +48 (0) 89 648 74 90  
e-mail: [office@ilawashiphandling.com.pl](mailto:office@ilawashiphandling.com.pl)  
e-mail: [office@portilawa.com](mailto:office@portilawa.com)